# Bond Behaviour of Corroded and CFRP Repaired RC Beams Subjected to Monotonic and Repeated Loading

by

Rania Al-Hammoud

A thesis
presented to the University of Waterloo
in fulfillment of the
thesis requirement for the degree of
Doctor of Philosophy
in
Civil Engineering

Waterloo, Ontario, Canada, 2012

©Rania Al-Hammoud 2012

# AUTHOR'S DECLARATION

I hereby declare that I am the sole author of this thesis. This is a true copy of the thesis, including any required final revisions, as accepted by my examiners.

I understand that my thesis may be made electronically available to the public.

# Abstract

All reinforced concrete (RC) design theories are based on the assumption that concrete exhibits a perfect bond with the steel reinforcement. The bond between steel and concrete is essential to the transfer of the load applied from the concrete to the steel reinforcement. When steel bars are corroded, the concrete cracks, and the strength of the bond between the steel bars and the concrete is decreased. Structures such as bridges and marine structures are prone to corrosion. These structures are usually also subjected to repeated loading. Repeated loading can initiate cracks in the concrete surrounding the steel bars that propagate as the number of load cycles increases leading to the destruction of the concrete-steel interface and slip of the steel bars inside the concrete. The combined effect of corrosion and repeated loading reduces the service life of RC structures.

This study investigated the effect of anchorage length and confinement from supports, stirrups and carbon fibre reinforced polymer (CFRP) on the bond behaviour of corroded and uncorroded reinforced concrete beams subjected to monotonic and repeated loading. Fifty-seven large-scale reinforced concrete beams (152*254*2000 mm) were tested for the purpose of this study. The variables were stirrup spacing (75 mm and 150 mm), anchorage length (200 mm, 350 mm and 650 mm), corrosion level (mild corrosion and high corrosion level), repair condition (wrapped or unwrapped with FRP sheets in the anchorage zone) and the fatigue load range.

From this study, it was found that the resistance to bond stresses (forces) between the steel and concrete were provided mainly by the concrete keys. The bond stresses increased with the number of the concrete keys engaged. The factors that affected the number of concrete keys engaged were: confinement from the supports, confinement from the stirrups, confinement due to wrapping with FRP sheets and change in anchorage length.

Decreasing the stirrup spacing from 150 mm to 75 mm increased the number of concrete keys engaged thus increasing the bond capacity and changed the mode of failure under monotonic loading from splitting to pullout. The beams with the first stirrup spacing (150 mm c/c) when tested under repeated loading failed by bond fatigue while the beams with the

second stirrup spacing (75 mm c/c) failed by flexure at the end of a debonded region that started from the support. The failure mechanism is discussed for each case.

The change in anchorage length from 200 mm to 350 mm increased the static and fatigue bond capacity of the beams by 60% and 12.5% respectively. The debonding for this group of beams (200 mm and 350 mm anchorage length) subjected to monotonic loading started from the pocket and propagated towards the support while the debonding for the 350 mm anchorage length beams subjected to repeated loading started at the location of a crack that widened while fatiguing the beam and propagated towards the support. The change in anchorage length from 350 mm to 650 mm did not affect the monotonic bond capacity of the beams since in this case, debonding was initiated from the supports and the change in anchorage length had little effect.

The confinement with FRP sheets caused the concrete keys at both the top and bottom of the bar to be crushed and increased the bond stress of the wrapped beams. The bond strength of the beams repaired with CFRP sheet was governed by the strength of the FRP sheets for all anchorage lengths and corrosion levels. The CFRP repair of the 200 mm anchorage length set of beams increased the capacity of the uncorroded beams by 80% and the capacity of the corroded beams by about 25% under static and repeated loading compared to the control (uncorroded and unrepaired) beam. The CFRP repair of the 350 mm anchorage length set of beams changed the mode of failure from bond to flexure.

The fatigue life for the beams varied linearly on a logarithmic scale with the load range applied with a shallow slope. Corroding the 200 mm anchorage length set of beams to a mild corrosion level decreased their fatigue strength by 34% compared to the control beams. Corroding the 350 mm anchorage length set of beams to a mild corrosion level did not affect the fatigue strength for the single beam that failed in bond.

Finally a probabilistic approach was used to allow the design engineers to estimate the design fatigue life for similar beams with 95% probability for a given normalized stress ratio.

## Acknowledgements

I would like to thank my family for their great support through the years of my research. Majdi without your support and continuous encouragement I wouldn't have been able to finish my thesis. Mom and dad without the ambitious drive you implanted in me to pursue a higher degree, I wouldn't have even started.

I would also like to express my appreciation and gratitude to my thesis supervisors, Professor Khaled Soudki and Professor Tim Topper, for their encouragement, guidance, and support in my research. They gave me valuable insight and motivation for this work. Professor Soudki, you were an advisor and a friend, you helped relief the stress that came from the lab, and you were always encouraging to the best. You were always there to guide and help through your tough busy schedule. Professor Topper, you were my father whom I miss from back home. You were always there to help, motivate, encourage and push to the limit. You were always there with me, in the lab, in the office, giving me all the time needed, and explaining as many times as needed. You were so patient. Thanks for everything.

I would also like to thank Professor Mahash Pandey for his help and advice regarding the reliability chapter. Professor Pandey, you were able to find the time within your busy schedule to sit with me, discuss the details of what reliability analysis could be done and include in my thesis. Your comments were highly valuable for this thesis.

I would also like to acknowledge and thank all the technicians and staff of the Department of Civil Engineering at the University of Waterloo, all the Undergraduate research assistant and co-op students who helped with this research, and all my colleagues in the FRP Research Group for their support and useful discussion.

I would like to extend my gratitude to the PhD Committee, Prof. Hamid Jahed, Prof. Wei-Chau Xie, Prof. John Straube and the external Prof. Mark Green for the time invested in reading and reviewing my thesis towards the completion of my degree.

This work is supported in part by research funding from ISIS Canada (Intelligent Sensing for Innovative Structures), a Network of Centers of Excellence, the Ministry of Training-

Colleges and Universities (OGSST Scholarship), Sika Canada for the donation of CFRP composites, Hogg Ready Mix for the donation of the concrete, and Micron Optics for their support with the Fibre Optic Sensors reading equipment. Their contributions are greatly appreciated.

# Dedication

This thesis is dedicated to my family, my mother, my father, my brother, my sister, my husband (Majdi) and my three kids (Yazan, Zaman and Taym).

# Table of Contents

AUTHOR'S DECLARATION ii
Abstract iii
Acknowledgements v
Dedication vii
Table of Contents viii
List of Figures xi
List of Tables xix
Chapter 1 Introduction 1
1.1 General 1
1.2 Research Motivation 2
1.2.1 Research Needs 2
1.2.2 Research Objectives 3
1.3 Thesis Organization 4
Chapter 2 Literature Review and Research Needs 5
2.1 General 5
2.2 Background 5
2.2.1 Corrosion 5
2.2.2 Bond in Reinforced Concrete 8
2.2.3 Fibre Reinforced Polymer Composite 11
2.3 Effect of Repeated Loading on the Steel to Concrete Bond Behaviour 13
2.4 Effect of Corrosion on the Bond Behaviour 14
2.1 Effect of Confinement on the Bond Behaviour in Reinforced Concrete Beams 17
2.1.1 The Effect of Confinement from the Supports and Stirrups 17
2.1.2 The Effect of FRP Confinement on Bond Behaviour under Static Load 18
2.1.3 Effect of FRP Confinement on the Bond Behaviour under Repeated Loading 22
Chapter 3 Experimental Program 24
3.1 Introduction 24
3.2 Test Program 24
3.2.1 Group 1 Beams 24
3.2.2 Group 2 Beams 27
3.3 Design of Specimens 28

3.4 Concrete Placement ..... 31
3.5 FRP Strengthening ..... 33
3.6 Material Properties ..... 34
3.6.1 Concrete ..... 34
3.6.2 Steel ..... 35
3.6.3 FRP System ..... 36
3.7 Induced Corrosion ..... 36
3.8 Evaluation of Corrosion ..... 38
3.9 Testing ..... 38
3.9.1 Instrumentation ..... 38
3.9.2 Beam preparation for testing ..... 41
3.9.3 Loading procedure ..... 41
Chapter 4 Experimental Results_ Group 1 Beams ..... 44
4.1 Introduction ..... 44
4.2 The confinement effect of the supports ..... 44
4.3 Static capacity of the control beams ..... 47
4.3.1 Beams with Stirrup Configuration “A” ..... 47
4.3.2 Beams with stirrup configuration B ..... 53
4.4 Stress and Strain Behaviour of a Cracked and an Uncracked Section ..... 57
4.5 Effect of Corrosion ..... 58
4.6 Effect of stirrups and supports on monotonic behaviour ..... 65
4.7 Fatigue Tests ..... 70
4.7.1 Stirrup configuration A ..... 70
4.7.2 Stirrup Configuration B ..... 78
4.7.3 Fatigue Life Discussion for Stirrup Configurations A and B ..... 83
4.8 Concluding Remarks ..... 85
Chapter 5 Experimental Results_ Group 2 Beams ..... 87
5.1 Introduction ..... 87
5.2 Corrosion Results ..... 87
5.3 Static Test Results ..... 95
5.3.1 Set 1 Beams ..... 95
5.3.2 Set 2 Beams ..... 113

5.4 Fatigue Beam Results ..... 125
5.4.1 Set 1 Beams – Fatigue Behaviour ..... 125
5.4.2 Set 2 Beams – Fatigue Behaviour ..... 148
5.5 The effect of bonded length ..... 154
5.5.1 Monotonic Behaviour ..... 154
5.5.2 Fatigue Behaviour ..... 155
5.6 Concluding Remarks ..... 157
5.6.1 General Conclusions ..... 157
5.6.2 Set 1 beams ..... 158
5.6.3 Set 2 beams ..... 159
Chapter 6 Reliability of Fatigue Life ..... 160
6.1 Estimation of the pdf parameters using the S-N relationship ..... 160
6.2 Estimation of the Mean and Design Fatigue Lives ..... 171
6.3 Conclusion ..... 176
Chapter 7 Conclusions and Recommendations for Future Work ..... 177
7.1 Summary of Conclusions ..... 177
7.2 Recommendations for Future Studies ..... 181
Appendix A Beam Design ..... 182
Appendix B Calculation of the Induced Corrosion Level ..... 185
Appendix C Experimental Mass Loss Calculation ..... 187
Appendix D Strain behaviour for Beams from Group 2- Set 1 ..... 190
Appendix E Strain Profile for Group 2- Set 2 unrepaired beams that failed in bond ..... 201
Appendix F Fatigue Slip Behaviour for Group 2 – Set 2 unrepaired beams that failed in bond ..... 205
Bibliography ..... 208

# List of Figures

Figure 2.1 Micro-cell versus macro-cell corrosion (Badawi, 2003) ..... 5
Figure 2.2 Bond mechanism of deformed reinforcement in concrete due to (a) adhesion, (b) bearing and (c) friction. ..... 9
Figure 2.3 Bond stress components (ACI Committee 408, 2003). ..... 9
Figure 2.4 The stress strain behaviour of FRP. ..... 12
Figure 2.5 Variation of bond strength with corrosion (FIB, 2000). ..... 16
Figure 2.6: General bond stress-slip law (Harajli, Hamad, & Rteil, 2004). ..... 20
Figure 2.7 Benefits of using FRP laminates in repairing corroded structures ..... 21
Figure 3.1Beams with stirrup configuration A; 150 mm spacing between stirrups in the shear zone. All dimensions are in mm. ..... 25
Figure 3.2 Beams with stirrup configuration A*; 125 mm spacing between stirrups in the shear zone. All dimensions are in mm. ..... 25
Figure 3.3 Beams with stirrup configuration B; 75 mm spacing between stirrups in the shear zone. All dimensions are in mm. ..... 27
Figure 3.4 Longitudinal and cross-sectional details for the beams in group 2-Set 1 (All dimensions are in mm). The dashed part of the steel reinforcement represents the unbonded length. ..... 29
Figure 3.5 Longitudinal and cross-sectional details for the beams in group 2- Set 2 (All dimensions are in mm). The dashed part of the steel reinforcement represents the unbonded length. ..... 29
Figure 3.6 The fabricated cage for beams from group 2 - Set 2. ..... 29
Figure 3.7 Cage for a beam from group 1 stirrup configuration A. ..... 31
Figure 3.8 Schematic drawing of the 200 mm anchorage length beam, showing the salted concrete region as a hatched area. ..... 32
Figure 3.9 General view of the cages in the formwork before casting. ..... 33
Figure 3.10: Beam with 200 mm anchorage length wrapped with CFRP sheets. ..... 34
Figure 3.11 A repaired beam turned upside-down. ..... 34
Figure 3.12: A schematic drawing of (a) the corrosion chamber setup with the beams divided in sets in series, (b) the electrical connections for the accelerated corrosion setup. ..... 37
Figure 3.13: Encapsulated strain gauge. ..... 40

Figure 3.14: Details of fibre optic sensors. ..... 40
Figure 3.15 Schematic drawing of the test setup for group 1 beams. ..... 42
Figure 3.16: Test setup for group 2 beams. ..... 43
Figure 4.1 Load versus mid-span deflection curve for Beam M-A-100-0-1. ..... 45
Figure 4.2 Beam M-A-100-0-spiral cage in form. ..... 46
Figure 4.3 Beam M-A-100-0-3, the supports were in contact with the bottom of the beam only at two points. ..... 47
Figure 4.4 Beam M-A-100-0-U load versus mid-span deflection curve. ..... 48
Figure 4.5 Load versus slip from free end for Beam M-A-100-0-U. ..... 49
Figure 4.6 Load versus mid-span deflection curve for Beam M-A*-100-0-U. ..... 51
Figure 4.7 Load versus slip behaviour from free end for Beam M-A*-100-0-U. ..... 51
Figure 4.8 Cracks in the anchorage zone of Beam M-A*-100-0-U. ..... 52
Figure 4.9 Concrete on top of the reinforcing bar after failure for Beam M-A*-100-0-U. The beam is turned upside-down. ..... 52
Figure 4.10 Load versus mid-span deflection for Beam M-B-100-0-1. ..... 54
Figure 4.11 Strain profile for Beam M-B-100-0-1. ..... 55
Figure 4.12 Load versus slip for Beam M-B-100-0-2. ..... 56
Figure 4.13 Dissection of Beam M-B-100-0-2 after failure showing the crushing of the concrete keys above the reinforcing bar. The beam is upside-down. ..... 56
Figure 4.14 Strain profile showing the different curves that a strain value in the steel bar might reach for a specified load. ..... 58
Figure 4.15 Corrosion cracks before testing of Beam M-A-100-5 from (a) side 1, (b) side 2 and (c) bottom side of beam. The widths of the corrosion cracks are shown in mm. .... 60
Figure 4.16 Load versus mid-span deflection for Beam M-A-100-5. ..... 60
Figure 4.17 Strain profile along the reinforcing bar of Beam M-A-100-5. ..... 61
Figure 4.18 Load versus slip behaviour for Beam M-A-100-5. ..... 61
Figure 4.19 Corrosion cracks for Beam M-B-100-5 from (a) side and (b) bottom faces. Note corrosion cracks were noticed only from one side of the beam. The crack widths are recorded in mm. ..... 62
Figure 4.20 Load versus mid-span deflection curve for Beam M-B-100-5. ..... 64

Figure 4.21 Strain profile for Beam M-B-100-5 along the length of the reinforcement in the anchorage zone. Notice that strain 3 was malfunctioned after reaching 80 kN load. ..... 64
Figure 4.22 Strain profile for Beam M-A-100-0-1. ..... 66
Figure 4.23 Strain profile at maximum load for the static beams with stirrup configuration A. The stirrup is represented by a vertical line. ..... 67
Figure 4.24 Shear forces at the location of the stirrups at maximum load for the static beams with stirrup configuration A. ..... 68
Figure 4.25 Typical concrete keys crushing close to the support for beams with stirrup configuration A. This picture is taken from Beam M-A-100-0-3 after failure. The beam is turned upside-down. ..... 68
Figure 4.26 Strain profile for Beam M-B-100-0-2. ..... 69
Figure 4.27 Concrete keys crushed along the anchorage zone for Beam M-B-100-0-2. This beam is turned upside-down. ..... 69
Figure 4.28 Slip versus percentage of fatigue life for Beam F-A-66-0. ..... 71
Figure 4.29 Slip versus percentage of fatigue life for Beam F-A-64-0. ..... 72
Figure 4.30 Slip versus percentage of fatigue life for Beam F-A-60-0. ..... 72
Figure 4.31 Strain versus percentage of cycles of fatigue life for beam F-A-66-0. ..... 74
Figure 4.32 Strain versus percentage of fatigue life for beam F-A-64-0. ..... 74
Figure 4.33 Strain versus percentage of fatigue life behaviour for beam F-A-60-0. ..... 75
Figure 4.34 Beam F-A-64-0 close to failure in the testing frame showin the concrete close to the support spalling. ..... 76
Figure 4.35 Beam F-A-64-0 after failure and removing the reinforcing bars. The beam was turned upside-down. ..... 77
Figure 4.36 Beam F-A-60-0 after failure and removing the reinforcing bars. The beam was turned upside-down. ..... 77
Figure 4.37 Strain profile for beam F-A-66-0. The stirrups locations along the anchorage length of the beam are marked on the graph. ..... 79
Figure 4.38 Beam F-A-66-0 after failure and reinforcing bars removed. The beam is turned upside-down. ..... 79
Figure 4.39 Strain profile for beam F-B-97-0 along with the stirrup locations. ..... 81

Figure 4.40 Beam F-B-97-0 after failure and removing the reinforcing bars. The beam was turned upside-down. ..... 81
Figure 4.41 Slip versus percentage of fatigue life behavior for beam F-B-97-0. ..... 82
Figure 4.42 The anchorage zone for Beam F-B-97-0 after failure in the testing frame. ..... 82
Figure 4.43 Fatigue life curve for beams with stirrup configurations A and B. ..... 84
Figure 5.1 Variation of the mass loss results versus the induced current exposure time in days. ..... 88
Figure 5.2: (a) cracks due to corrosion; (b) corroded bar extracted from beam F-200-R-h-88. ..... 88
Figure 5.3 Schematic drawing of the corrosion cracks for Beam M-200-R-h. The corrosion crack widths are measured in mm. ..... 91
Figure 5.4 Schematic drawing of the corrosion cracks for the beams from set 1 (200 mm anchorage length) corroded to a high corrosion level and tested for fatigue (Set 1 – Group R-h). The crack width measurements are given in mm. ..... 92
Figure 5.5: Schematic drawing of the corrosion cracks for Beam M-350-R-h. The corrosion crack widths are measured in mm. ..... 93
Figure 5.6: Schematic drawing of the corrosion cracks for the beams from set 2 (350 mm anchorage length) corroded to a medium corrosion level and tested for fatigue (Set 2 – Group U-m). The crack width measurements are given in mm. ..... 93
Figure 5.7: Schematic drawing of the corrosion cracks for the beams from set 2 (350 mm anchorage length) corroded to a high corrosion level and tested for fatigue (Set 2 – Group R-h). The crack width measurements are given in mm. ..... 94
Figure 5.8: intact concrete taken from the anchorage zone from below the steel bar. ..... 96
Figure 5.9: Beam M-200-R-n after failure and removing the bar from the anchorage zone. The beam was turned upside-down. ..... 97
Figure 5.10: Load versus midspan deflection for the beams from Set1-Group M. ..... 98
Figure 5.11 Strain profile for Beam M-200-R-m. ..... 99
Figure 5.12 Strain profile for bar 1 in Beam M-200-U-n-2. ..... 100
Figure 5.13: Load Slip behaviour for Beam M-200-U-n-2. ..... 101
Figure 5.14 Load versus slip behaviour for Beam M-200-R-n. ..... 102
Figure 5.15 Load versus slip behaviour for Beam M-200-U-m. ..... 102

Figure 5.16 Load versus slip for Beam M-200-R-m..... 104
Figure 5.17 Beam M-200-R-m after failure..... 104
Figure 5.18 Schematic drawing showing bar dimensions for M-20 bars used to reinforce the beams in the current study. All dimensions are in mm..... 105
Figure 5.19 Beam M-200-U-n-2 after failure and removing the reinforcing bars to examine the concrete keys. The beam was turned upside down..... 105
Figure 5.20 Beam M-200-U-m after failure and removing the reinforcing bars to examine the concrete keys. The beam was turned upside down..... 106
Figure 5.21 Beam M-200-R-n after failure and removing the reinforcing bars to the concrete keys. The beam was turned upside down..... 106
Figure 5.22 Bond Stress versus load for Beam M-200-U-n-2..... 108
Figure 5.23 A section of Set1 beams along with the locations of the strain gauges along the length of the bar..... 109
Figure 5.24 Average bond stress along the length of the bar versus slip for Beam M-200-U-n-2..... 109
Figure 5.25 Beam M-200-U-n-2 after failure..... 110
Figure 5.26 Bond stress versus applied load behaviour for Beam M-200-R-n..... 111
Figure 5.27 Bond stress versus load for Beam M-200-R-m..... 112
Figure 5.28 Cracks in the bonded length of Bream M-350-U-n along (a) side of the beam and (b) bottom of the beam..... 114
Figure 5.29 Beam M-350-U-n turned upsode down showing concrete crushed close to the pocket on top of the bar..... 114
Figure 5.30 Flexural failure of Beam M-350-R-m..... 115
Figure 5.31 Load versus mid-span deflection for the beams from Set 2 - Group M..... 116
Figure 5.32 Strain profile for Beam M-350-U-n..... 117
Figure 5.33 Strain Profile for Beam M-350-U-m..... 118
Figure 5.34 Strain profile for Beam M-350-R-n..... 119
Figure 5.35 Strain profile for Beam M-350-R-m..... 119
Figure 5.36 Strain profile for Beam M-350-R-h..... 120
Figure 5.37 Final failure of Beam M-350-R-h by crushing of concrete. Part of the FRP ruptured close to the pocket..... 120

Figure 5.38 Load versus slip behaviour for Beam M-350-U-n. ..... 121
Figure 5.39 Load versus slip behaviour for Beam M-350-U-m. ..... 122
Figure 5.40 Load versus slip behaviour for Beam M-350-R-n. ..... 123
Figure 5.41 Load versus slip behaviour for Beam M-350-R-m. ..... 123
Figure 5.42 Load versus slip behaviour for Beam M-350-R-h. ..... 124
Figure 5.43 Bond stress versus load behaviour for Beam M-350-U-n. ..... 125
Figure 5.44 (a) the cracks after failure in the bonded region of beam F-200-U-n-70-1. (b) intact concrete above the bar in Beam F-200-U-n-70-2. The beam was turned upside-down. ..... 128
Figure 5.45: (a) upper concrete above bar and (b) lower concrete below the bar in beam F-200-U-m-43. ..... 129
Figure 5.46 Load range versus fatigue life for Beams Corroded to a mild corrosion level from set 1 along with flexural analysis. ..... 130
Figure 5.47 Gundrilled holes in the reinforcements for the beams with 200mm anchorage length. ..... 131
Figure 5.48 Beam F-200-R-m-72 failed by bar rupture in the pocket. ..... 131
Figure 5.49 FRP rupture close to the pocket in Beam F-200-R-h-80. ..... 132
Figure 5.50 Concrete Keys crushed along the anchorage zone for Beam F-200-R-h-80. The beam was upside down and the reinforcing bars removed. ..... 133
Figure 5.51: Variation in load range with life for Set 1 beams failing in fatigue of bond. ..... 134
Figure 5.52 Slip versus percentage of fatigue life behaviour for Beam F-200-U-n-70-1. ..... 136
Figure 5.53 Slip versus percentage of fatigue life for Beam F-200-U-m-43. ..... 136
Figure 5.54 Slip versus percentage of fatigue life behaviour for Beam F-200-R-m-90. ..... 137
Figure 5.55 Slip versus percentage of fatigue life behaviour for Beam F-200-R-m-96. ..... 137
Figure 5.56 Slip versus percentage of fatigue life behaviour for Beam F-200-R-h-80. ..... 138
Figure 5.57 Strain Profile at different percentages of the fatigue life for Beam F-200-U-n-70-2. ..... 141
Figure 5.58 Strain profile at different percentages of the fatigue life for Beam F-200-U-n-60. ..... 141
Figure 5.59 Strain Readings from FBG sensors along the length of the beam for Beam F-200-U-m-44. ..... 142

Figure 5.60 Strain Readings from encapsulated strain gauges along the length of the beam from Beam F-200-U-m-44. ..... 142
Figure 5.61 Strain profile for Beam F-200-R-m-90. ..... 144
Figure 5.62 Strain profile for Beam F-200-R-m-96. ..... 145
Figure 5.63 Strains on the FRP wrapping sheet versus percentage of fatigue life for Beam F-200-R-m-90. ..... 146
Figure 5.64 Strains on the FRP wrapping sheet versus percentage of fatigue life for Beam F-200-R-m-96. ..... 147
Figure 5.65 Strain profile of the bar with percentage of fatigue life for Beam F-200-R-h-80. ..... 147
Figure 5.66 Strains on the FRP wrapping sheet versus percentage of fatigue life for Beam F-200-R-h-80. ..... 148
Figure 5.67 Failure mode for Beam F-350-U-n-74. ..... 150
Figure 5.68 Stirrup rupture in Beam F-350-U-n-80. ..... 150
Figure 5.69 Bar rutpture in Beam F-350-R-m-126. ..... 151
Figure 5.70 Failure of Beam F-350-R-m-140 by concrete crushing. ..... 151
Figure 5.71 Strain Profile for Beam F-350-U-n-74. ..... 152
Figure 5.72 (a) Schematic drawing of beam with diagonal crack, (b) a section of the beam at the crack. ..... 152
Figure 5.73 Schematic drawing showing the location of the strain gauges in the beams with 350 mm anchorage length. ..... 153
Figure 5.74 Slip versus percentage of fatigue life for Beam F-350-U-n-74. ..... 153
Figure 5.75 Fatigue life with respect to load range applied for Beams from Group 2- Set 2 failing in bond. ..... 155
Figure 5.76 Fatigue with respect to load range applied for Beams from group 2, Set 1 and Set 2. ..... 156
Figure 6.1 The Weibull pdf for Set 1 - Group U-n for the different stress ratios. ..... 165
Figure 6.2 The Weibull pdf for Set 1 - Group U-m for the different stress ratios. ..... 166
Figure 6.3 The Weibull pdf for Set 1- Group R-h for the different stress ratios. ..... 167
Figure 6.4 The Weibull pdf for Set 2 - Group U-n for the different stress ratios. ..... 168
Figure 6.5 Reliability function for Set 1 - Group U-n for the different stress ratios. ..... 169

Figure 6.6 Reliability function for Set 1- Group U-m for the different stress ratios. ..... 169
Figure 6.7 Reliability function for Set 1 - Group R-h for the different stress ratios. ..... 170
Figure 6.8 Reliability function for Set 2 - Group U-n for the different stress ratios. ..... 170
Figure 6.9 Stress ratio versus fatigue life for the test data and predicted data from Set 1 - Group U-n. ..... 174
Figure 6.10 Stress ratio versus fatigue life for the test data and predicted data from Set 1 - Group U-m. ..... 174
Figure 6.11 Stress ratio versus fatigue life for the test data and predicted data from Set 1 - Group R-h. ..... 175
Figure 6.12 Stress ratio versus fatigue life for the test data and predicted data from Set 2 - Group U-n. ..... 175

# List of Tables

Table 2.1 Tensile properties of FRP laminates (ACI Committee 440.2, 2002)..... 13
Table 3.1 Test matrix - Group 1..... 26
Table 3.2 Test matrix for Group 2 - Set 1 Beams (Anchorage length = 200 mm) ..... 30
Table 3.3 Test matrix for Group 2- Set 2 Beams (Anchorage length = 350 mm) ..... 31
Table 3.4: The 28-day compressive strength of concrete for the different casts ..... 35
Table 3.5: Mechanical properties of the CFRP system..... 36
Table 3.6: Sikadur 30 tensile properties (as supplied by the manufacturer)..... 41
Table 4.1 Results of fatigue beams from group 1. ..... 70
Table 5.1: Actual mass loss for beams from Set 1 (200 mm anchorage length). ..... 90
Table 5.2: Actual mass loss for beams from Set 2 (350 mm anchorage length). ..... 91
Table 5.3 Fatigue lives for Beams from Set 1. ..... 126
Table 5.4 Recorded slip for the different percentages of the fatigue life of the unrepaired beam (F-200-U-m-44)..... 143
Table 5.5 Fatigue lives for beams from Set 2. ..... 149
Table 6.1: Weibull parameters values for each group with the different stress ratios..... 163
Table 6.2: Weibull parameters for selective stress ratios. ..... 164
Table 6.3 Mean and Design Fatigue Lives for different probabilities of failure for beams from Set 1 - Group U-n. ..... 172
Table 6.4 Mean and Design Fatigue Lives for different probabilities of failure for beams from Set 1 - Group U-m. ..... 172
Table 6.5 Mean and Design Fatigue Lives for different probabilities of failure for beams from Set 1- Group R-h. ..... 173
Table 6.6 Mean and Design Fatigue Lives for different probabilities of failure for beams from Set 2 - Group U-n. ..... 173

# Chapter 1
# Introduction

## 1.1 General

All reinforced concrete design theories are based on the assumption that concrete exhibits a perfect bond with the steel reinforcement. The bond between steel and concrete is essential to the transfer of the load applied from the concrete to the steel reinforcement. The bond between steel and concrete is originally due to adhesion, friction and bearing forces (ACI Committee 408, 2003). Once slip is initiated, the major forces affecting the bond strength become the bearing forces of the bar lugs on the concrete keys (ACI Committee 408, 2003). The major factors that affect the bond resistance are: concrete strength, concrete cover, bar spacing, bar geometry and surface conditions, and confinement (ACI Committee 408, 2003). Confinement can be either active by the reinforced concrete beam being in direct contact with a support or passive due to the presence of internal stirrups (FIB, 2000).

Corrosion severely decreases the service life of reinforced concrete structures. Corrosion of reinforcing steel results in corrosion products of increased volume resulting in cracking of the concrete surrounding the bars. Corrosion is common in North America due to the widespread use of de-icing salts. The salts combine with oxygen from the air and the humidity from rain and/or snow to cause reinforcement bars inside concrete members to rust. Repairing the corrosion deteriorated structures is costly. According to Zhang and Mailvaganam (2006), rehabilitation of reinforced concrete structures consumes more than 50% of every dollar spent on construction.

When steel bars are corroded, the concrete cracks, and the strength of the bond between the steel bars and the concrete is decreased. This increase in the number of cracks and their widths leads to an increase in the deflection and a decrease in the load carrying capacity of the reinforced concrete element and may lead to a sudden or brittle failure (FIB, 2000).

Structures such as bridges and marine structures are prone to corrosion. These structures are usually subjected to repeated loading. As the live load to dead load ratio has increased, the effect of repeated loading has started to govern the design for the serviceability limit state (ACI Committee 215, 1974). Repeated loading can initiate cracks in the concrete surrounding

the steel bars that propagate as the number of load cycles increases leading to the destruction of the concrete-steel interface and slip of the steel bars inside the concrete. Repeated loading often causes serious damage to a structure under service loads that are far below the ultimate loads (Mor, Gerwick, & Hester, 1992; ACI Committee 408, 1992).

The present study investigated the effect of anchorage length, corrosion and confinement from supports, stirrups and fibre reinforced polymer (FRP) sheets on the bond behaviour of reinforced concrete beams under monotonic and repeated loading. FRP reinforcement has emerged as an alternative to traditional methods for the repair and strengthening of concrete structures. Its use is of interest to rehabilitation engineers because of its high strength to weight ratio, high fatigue resistance and the fact that it does not corrode (ACI Committee 440, 2007).

## 1.2 Research Motivation

### 1.2.1 Research Needs

Based on the literature review, it is clear that there are several gaps regarding the understanding of the fatigue bond behaviour of corroded reinforced concrete beams repaired with CFRP sheets.

The bond between reinforcing steel and concrete is an important parameter in determining the fatigue strength and the serviceability conditions of a flexural reinforced concrete member. Despite its importance, the study of bond behaviour under repeated loading has not been given sufficient attention. Most of the experimental research done on bond under repeated loading was conducted using pull-out specimens which are known to give unrealistic bond behaviour and non-conservative bond strength values. Structures such as bridges and marine structures are prone to corrosion. These structures are usually subjected to repeated loading. Many researchers have studied the effect of corrosion on reinforced concrete beams. However, most of those studies focused on the flexural strength of the beams. Very few researchers have studied the effect of corrosion on the bond behaviour between the reinforcing steel and the concrete under repeated loading.

FRP has proven to be successful as a strengthening method for concrete structures under monotonic loads; however, little research was done to study the effect of repeated loading on

the bond behaviour of corroded reinforced concrete beams and FRP repaired corroded reinforced concrete beams.

The lack of experimental data has left designers with little knowledge in understanding the performance of the steel to concrete bond, especially with corroded steel reinforcement and repeated loading. Such data are needed to assess the performance of RC structures under repeated service loads as well as in predicting the residual strength of these structures.

### 1.2.2 Research Objectives

This study was designed to increase our knowledge of the bond behaviour of corroded reinforced concrete beams subjected to repeated loading. The main purpose of this investigation was to analyze the effect of anchorage length and confinement from supports, stirrups and FRP on the bond behaviour of corroded reinforced concrete beams under monotonic and repeated loading. The specific objectives are as follows:

- Analyze the effect of the different variables (stirrup spacing, support confinement, FRP confinement and anchorage length) on the mechanics of bond.
- Analyze the effect of different corrosion levels on the bond behaviour of beams under repeated loading.
- Critique the effect of stirrups on the bond behaviour of reinforced concrete beams under static and repeated loading.
- Critique the effect of combined confinement from direct support and stirrups on the bond behaviour under monotonic and repeated loading.
- Critique the effect of anchorage length on the bond behaviour of reinforced concrete beams under static and repeated loading.
- Analyze the effect of FRP wrapping on the bond behaviour of corroded and uncorroded beams under repeated loading.
- Quantify the effect of FRP sheets as a repair system to restore the bond strength under monotonic loading.
- Apply the probability density function that best describes the variation in the fatigue life of the beams.

- Analyze the design fatigue life corresponding to a given bond stress ratio with 95% probability.

## 1.3 Thesis Organization

The thesis is divided into seven chapters. Chapter 1 introduces the topic of the research study. Chapter 2 provides the background of the different aspects studied in this thesis which include corrosion, bond in reinforced concrete and fibre reinforced polymer composites. The chapter also provides a review of the part of the literature that relates to this study which leads to the research needs and objectives. In Chapter 3, the experimental program for this research is presented along with the material properties, the specimen details, the corrosion technique and the test set-up. The beams are divided into two groups, group 1 studied the effect of confinement from stirrups and supports, while groups 2 studied the effect of anchorage length on the different aspects discussed earlier. The results from group 1 beams are presented, discussed and analyzed in Chapter 4. The results from group 2 beams are presented, discussed and analyzed in Chapter 5. Chapter 6 presents an analysis for the reliability of the fatigue life. The parameters of the Weibull probability density function (pdf) that best fits the fatigue life data were estimated using the S-N relationship obtained from the experimental data. Then the pdf was used to estimate the mean and design fatigue lives for different stress ratios and probabilities of failure. Finally, Chapter 7 presents the conclusions from the present work and provides recommendations for future work.

# Chapter 2
# Literature Review and Research Needs

## 2.1 General

This chapter provides background material on the subject of the corrosion of steel reinforcement, bond between the steel reinforcement and the concrete, and the use of fibre reinforced polymers. A review of the available literature concerning the effect of repeated loading, corrosion and confinement on the bond behaviour is presented.

## 2.2 Background

### 2.2.1 Corrosion

Concrete is characterized by its high pH value (12.5 – 13.5). This aids in forming a passive film around the reinforcing steel. This passive film is composed primarily of a relatively thin layer of a form of iron oxide that protects the metal from corrosion by limiting the oxidation of iron. The initiation of corrosion occurs when the protective passive film is broken by either carbonation or by the presence of chloride ions. This may occur over the whole length of the steel reinforcement or part of it.

Once corrosion is initiated, it requires an anode and cathode that are electrically connected and form ions due to a chemical reaction. The aqueous pore solution of the concrete matrix allows the released ions to transfer from the cathode to the anode. The anode and cathode may be on the same bar or on separate bars at a finite distance from each other. These two cases define the two types of corrosion: Micro-cell corrosion and macro-cell corrosion (Figure 2.1).

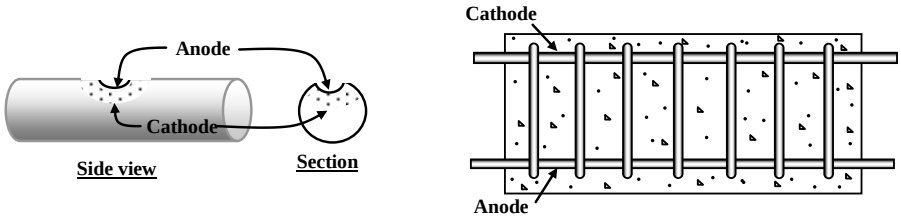


**Figure 2.1 Micro-cell versus macro-cell corrosion (Badawi, 2003)**

The anodic reaction that takes place at the steel bar where ions are produced is given by:

$$Fe \rightarrow Fe^{2+} + 2e^{-}$$ **Equation 2-1**

The electrons are consumed at the cathode by the following reaction:

$$\frac{1}{2}O_2 + H_2O + 2e^{-} \rightarrow 2(OH)^{-}$$ **Equation 2-2**

The released hydroxyl ions at the cathode travel through the electrolyte to react with the ions at the anode producing rust. The process of rust formation is described by several chemical reactions that occur in the presence of oxygen and moisture ($H_2O$). These reactions result in the formation of a rust product ($Fe_2O_3$) around the bar. In the anhydrate form, $Fe_2O_3$ occupies approximately two times the volume of the original steel. However, when hydrated ($Fe_2O_3.H_2O$), the ferric oxide may occupy up to ten times the volume of the original steel (Broomfield, 1997).

The increase in volume causes tensile stresses in the concrete that lead to longitudinal cracking and spalling of the concrete. This damage facilitates the contact with oxygen, moisture and chlorides and increases the rate of bar corrosion by ten times or more (Bentur, Diamond, & Berke, 1997). Concrete cracking also leads to deterioration of the bond between the steel and the concrete.

In addition, corrosion causes a loss in bar section that in combination with loss of bond between the steel and concrete leads to a reduction of the concrete member's load carrying capacity, and an increase in deflection.

#### 2.2.1.1 Chloride Induced Corrosion

There are three theories that explain the effects of chloride ions on steel corrosion (ACI Committee 222, 2001): The oxide film theory where a breakdown of the protective passive film occurs over part of the steel reinforcement due to a reaction of chloride ions with the steel, the adsorbtion theory and the transitory complex theory. Chloride ions reach the reinforcing steel by penetrating the concrete via pore water channels and cracks in the concrete. Chloride ions may also act as a catalyst to speed up the corrosion reaction.

The source of the chloride ions varies widely. They are found in the de-icing salts used on bridges in cold areas, in some chemical admixtures, in marine environments, and even in aggregates that contain chlorides.

There is a minimum chloride ion concentration required to initiate corrosion of a steel reinforcing bar. This minimum required chloride ion concentration is referred to as the corrosion chloride threshold. This threshold value is influenced by several factors such as the resistivity of the concrete, the water-cement ratio of the concrete and atmospheric conditions. In general, the corrosion chloride threshold value ranges from 0.6 – 0.9 $kg/m^3$ of concrete (ACI Committee 222, 2001).

#### 2.2.1.2 Accelerated Corrosion Technique

The highest corrosion rate recorded in service is between 10 and 25 $\mu A/cm^2$ (FIB, 2000). At this rate of corrosion, tests in a laboratory environment would take years. Therefore, researchers have used an accelerated corrosion technique. This technique is based on the fact that corrosion process is activated by chloride salts and accelerated by electrical polarization of the steel reinforcement. Although the induced current technique could produce different chemical products than the ones expected in the field; however the expected physical effect from both rust products would be similar in terms of stresses and corrosion cracks.

To initiate the corrosion process, salt is either added to the concrete mix or the test specimen is wholly or partially submerged in a salted solution. To accelerate the corrosion process, the steel reinforcement is connected to the positive terminal of an external power supply so that a positive electrical potential is applied to the steel. Thus, the steel is encouraged to release $Fe^{+2}$ ions. Researchers have used external copper or stainless steel plates, or an internal stainless steel bar to act as cathode during the corrosion process. It should be noted that although current densities as high as 10,400 $\mu A/cm^2$ were used in experiments, however it is recommended that a maximum current density of 200 $\mu A/cm^2$ be applied to avoid an increase in strain response and crack width (El Maadawy & Soudki, 2003).

### 2.2.2 Bond in Reinforced Concrete

In reinforced concrete structures, forces are transferred to the reinforcing steel through the surrounding concrete. The transfer of forces from the concrete to the steel (and vice versa) is made possible by a force transfer between the two materials referred to as bond. For smooth reinforcing bars, a measure of bond is the strength magnitude of the shear stresses along the surface between the concrete and the embedded steel bar at which bond fails. The higher the failure surface shear stress (or the maximum resistance to relative motion or slippage under stress), the more effective will be the interaction that transfers force between the concrete and the steel.

Bond in reinforced concrete structures is made up of three components (Figure 2.2):

- Chemical adhesion between concrete and steel
- Friction due to the presence of small irregularities on the bar's surface
- Mechanical interaction between the ribs of the deformed bar and the surrounding concrete

Deformed bars have superior bond properties due to mechanical interlocking between the concrete and the steel. This does not mean that friction and chemical adhesion are negligible for deformed bars, but they are of secondary importance. Therefore, the primary bond mechanism restraining the relative slip between a deformed bar and the surrounding concrete is the forces due to bearing of the bar ribs against the concrete. The force due to friction between the steel and the concrete at the bar rib adds vectorially to the component of bond acting perpendicular to a rib (Figure 2.3). The vertical component of the resultant bond force is a radial pressure which induces circumferential tensile stresses in the surrounding concrete. The maximum horizontal component of the resultant bond force at bond failure is the effective bond strength. If the concrete cover on the ribs or the spacing between the anchored bars is small, then the radial pressure which is the vertical component of the bond force will cause splitting failure (Figure 2.3).

If the cover and spacing between the bars is large enough or if sufficient transverse reinforcement is provided, a splitting failure cannot develop and a pullout failure will occur or the bar will yield. In a pullout failure, the concrete between the deformations is sheared off

from the surrounding concrete. The bond strength in a pullout failure is dependent on the strength of concrete in direct shear.

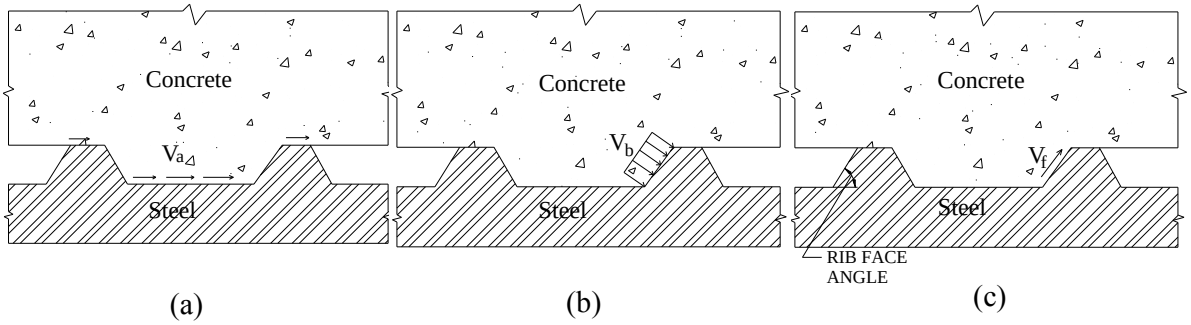


**Figure 2.2 Bond mechanism of deformed reinforcement in concrete due to (a) adhesion, (b) bearing and (c) friction.**

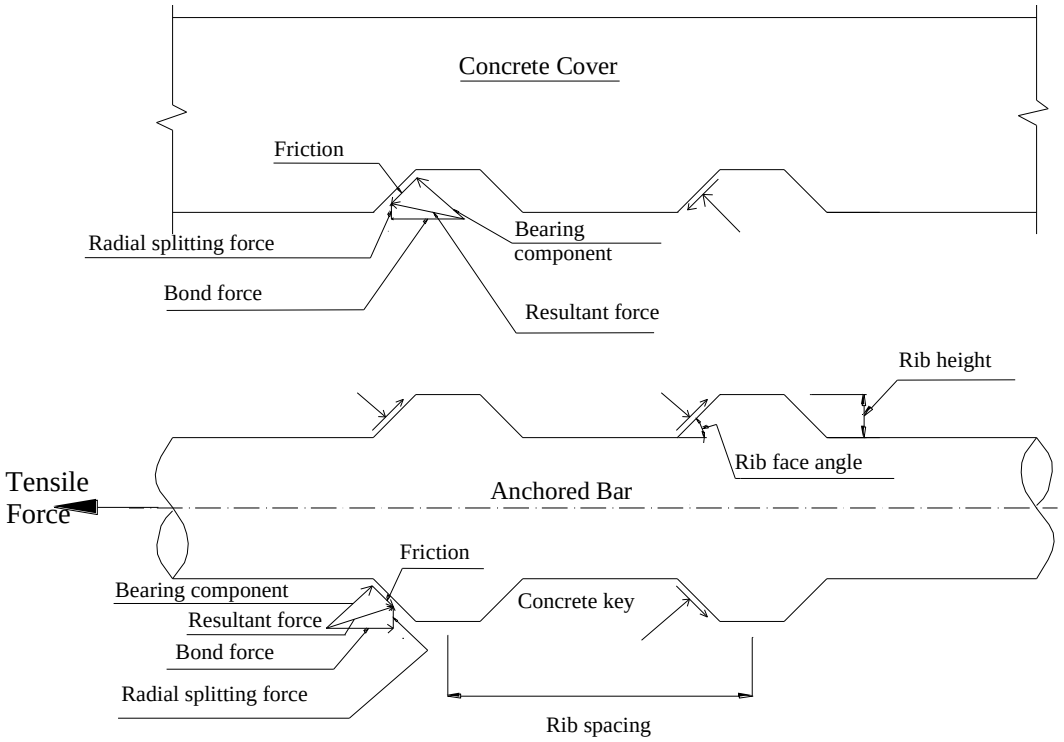


**Figure 2.3 Bond stress components (ACI Committee 408, 2003).**

It has been well established in research studies that variables affecting the bond strength of deformed or ribbed bars include the bar size and surface conditions, the depth of concrete cover, the spacing between embedded bars, the bonded length of the bar, the concrete strength, the confinement of the concrete (due to transverse reinforcement or FRP

surrounding the bars), and the position of the bars when the concrete is cast (ACI Committee 408, 2003).

Bar Size

The bond force increases with an increase in bar size for a given development length. Larger bar size requires a larger bonded length to yield the bar. Therefore, it is preferable to use smaller size bars than larger bars having the same area (ACI Committee 408, 2003).

Concrete cover and bar spacing

The larger the bar cover and spacing the better the bond strength until another failure mode is provoked. If the bar cover and spacing is very large a pull-out failure or a failure by yielding of the bar can be expected, instead of the splitting failure that occurs when the cover and/or the bar spacing is small. Splitting cracks usually develop through the smallest cover. In most structures, if a bond failure develops, it would be due to splitting (ACI Committee 408, 2003).

Bonded length of the bar

The bond capacity increases with an increase in the bonded length. This increase is not proportional to the length due to the non-uniform nature of bond forces. For splice and pull-out specimens, the loaded end of the bonded length transfers most of the bond forces to the concrete. The non-loaded or free end has little effect on the transfer of the bond force. When a splitting failure occurs, a crack develops at the surface of the concrete. The energy needed to initiate the crack, increases with an increase of the bonded length but at a slower rate (ACI Committee 408, 2003).

Concrete strength

The bond force between the steel bars and the concrete is dependent on the concrete tensile properties. The bond strength traditionally has been related to $(f'_c)^{1/2}$, where $f'_c$ is the compressive strength of the concrete. This is due to the fact that the tensile strength of concrete is directly proportional to the square root of the concrete compressive strength. However, recent studies on bond strength have shown that relating the bond strength to $(f'_c)^{1/4}$ would give a better representation. This is because of the fact that the bond strength is dependent on the concrete fracture energy in addition to the concrete tensile strength (ACI

Committee 408, 2003). Concrete cracks develop when the loading energy is greater than the concrete fracture energy. Those cracks would decrease the bond between the steel bars and the concrete. Therefore, the higher the fracture energy is, the higher the bond strength. In general, it has been found that as the concrete strength increases, the bond strength increases but at a lower rate (ACI Committee 408, 2003).

Amount of transverse confinement

Confinement in the form of transverse reinforcement, steel stirrups or fibre reinforced polymer (FRP) confines the concrete over the bonded length and hence impedes the propagation of splitting cracks (ACI Committee 408, 2003; Hamad & Rteil, 2006). This causes an increase in the bond force between the steel bars and the concrete. As the area of transverse confinement increases, the confining force increases which may result in a pullout failure rather than splitting failure (ACI Committee 408, 2003).

Bar casting position

It was observed by several researchers (Brettmann, Darwin, & Donahey, 1986; Jeanty, Mitchell, & Mirza, 1988) that the top reinforcement bars have a lower bond strength than the bottom reinforcement bars. This is attributed to the fact that settlement occurs in the lower part of the concrete causing water and air bubbles to accumulate underneath the upper bars. This decreases the contact surface area between the steel bars and the concrete, hence decreasing the bond (ACI Committee 408, 2003).

### 2.2.3 Fibre Reinforced Polymer Composite

The use of fibre reinforced polymer (FRP) composites in civil engineering has recently emerged as an alternative to the traditional methods used for rehabilitation or reinforcement of structures. FRPs are of interest to rehabilitation engineers because of their high-strength to weight ratio, high fatigue resistance, ease of installation and the fact that they do not corrode (ACI Committee 440, 2007). However, FRPs exhibit linear elastic behaviour up to failure with no yielding in contrast to steel reinforcement (Figure 2.4).

FRP products for reinforcing concrete structures are manufactured in different forms such as bars, fabric, 2D and 3D grids, and plates. FRP is a composite that consists of high tensile

strength fibres within a polymer matrix joined at the macroscopic level (ACI Committee 440, 2007).

Table 2.1 provides some properties of available FRP systems. Fibres are the load-carrying components of FRP composites. In general, they are characterized by very small diameters and very high length to diameter ratios. Fibres can be organic, inorganic, synthetic or metallic. The fibres most commonly used in construction are carbon, aramid and glass. Carbon fibres have the best mechanical properties and highest cost among these three types of fibres. They have excellent resistance to fatigue, creep, and heat.

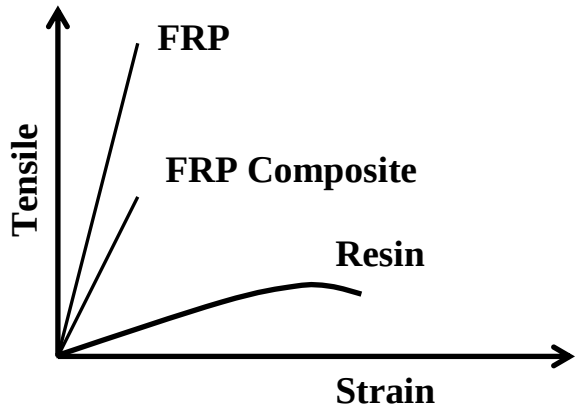


**Figure 2.4 The stress strain behaviour of FRP.**

The main function of the matrix (also called the resin) is to support, protect, and separate the fibres. The matrix binds the fibres together, and transmits and distributes the externally applied stresses to the fibres. The matrix also provides protection for the fibres from surface damage due to mechanical abrasion or a chemical reaction with the environment. The matrix helps prevent the propagation of a crack from one fibre to another, hence delaying a catastrophic failure. A common characteristic of the matrix that gives composite materials their high strength to weight ratio is their low density. This is one of their most attractive characteristics.

FRP materials that have been used in the rehabilitation of concrete structures are laminates, strips, and prestressing rods.

**Table 2.1 Tensile properties of FRP laminates (ACI Committee 440.2, 2002).**

| Resin | Tensile strength (MPa) | Tensile modulus (GPa) | Rupture Strain (%) |
|---|---|---|---|
| **GFRP** | 520-1400 | 20-40 | 1.5-3.0 |
| **CFRP** | 1020-2080 | 100-140 | 1.0-1.5 |
| **AFRP** | 700-1720 | 48-68 | 2.0-3.0 |

## 2.3 Effect of Repeated Loading on the Steel to Concrete Bond Behaviour

The bond between reinforcing steel and concrete is an important parameter in determining the fatigue strength and the serviceability conditions of a flexural reinforced concrete (RC) member. Despite its importance, the study of bond behaviour under repeated loading has not been given sufficient attention. Repeated loading causes failure of a beam by bond at lower loads than the static bond capacity of the beam. Microcracks in the concrete around the bars propagate as the number of cycles increases. This leads to the destruction of the concrete-steel interface leading to slip of the bar (FIB, 2000; Mor, Gerwick, & Hester, 1992; ACI Committee 215, 1974).

Most of the experimental research done on bond under repeated loading was conducted using pull-out specimens. This type of specimen has several drawbacks, the major one is that the concrete stress field around the steel bar is in compression, which is different from that encountered in most reinforced concrete members (ACI Committee 408, 2003). Very few experiments were done on bond-beam specimens. The main conclusions of these experiments can be summarized as follows (Verna & Stelson, 1962; Bresler & Bertero, 1968; Perry & Jundi, 1969; Rehm & Elingehausen, 1979; Balazs, Fatigue of bond, 1991; Balazs & Koch, 1992; Koch & Balazs, 1992; Balazs, 1998) (Plizzari, Lundgren, & Balazs, 2002; Oh & Kim, 2007; Rteil, Soudki, & Topper, 2011)

- Specimens that failed in bond under static loading failed in bond under repeated loading.
- Bond failure was accompanied by splitting cracks and a decrease in the load carrying capacity.

- Bond behaviour under repeated loading was affected by concrete strength and bonded length.
- Initially, the bond stresses were highest at the loaded end(s), and then the bond stresses redistributed shifting the highest bond stress towards the free end due to external and internal concrete cracking as the number of cycles increased.
- The slip of a reinforcing bar was influenced by the bond length and the peak load applied.
- The slip increased with the number of cycles in three stages: first it increased at a decreasing rate, then the rate stabilized until the cyclic slip reached the value of the slip corresponding to monotonic failure, then the slip rate continuously increased until failure occurred.
- The slip rate increased when the maximum applied load increased or the bonded length decreased.
- If repeated loading induced no failure to bond specimens, then the static bond strength capacity of those specimens was not affected (that is the beam will continue to follow the monotonic envelope).

## 2.4 Effect of Corrosion on the Bond Behaviour

Corrosion leads to a reduction in the cross-sectional area of the reinforcing steel which is used as a measure of the severity of corrosion. However, in service the maximum loss rate of reinforcing steel cross-sectional area is about 50 $\mu m / yr$. (Broomfield, 1997) states that "less than 100 $\mu$m of steel section loss is needed to start cracking and spalling of the concrete". This means that corrosion often damages the bond between the steel and the concrete long before the reduction of the cross-sectional area of the bars becomes critical. The deterioration of bond is often critical for the serviceability of reinforced concrete structures (ACI Committee 222, 2001; Broomfield, 1997).

The volume of rust produced from the corrosion process is much greater than the volume of steel from which it is produced. This leads to the formation of minute cracks on the concrete surface and the appearance of rust products. The cracks run parallel to the corroded reinforcing steel. If these cracks are not dealt with at an early stage, their width will increase

causing more oxygen and water to migrate through them to the steel. This leads to a more rapid corrosion of the reinforcing steel which in turn leads to a more severe cracking of the RC element and a loss of the bond between the reinforcing steel and the concrete as well as a further reduction in the cross-sectional area of the reinforcing steel to an extent that the RC structure becomes a safety hazard (Broomfield, 1997).

Research on the effect of corrosion on the flexural strength of reinforced concrete beams has shown that corrosion leads to a decrease in the yield and ultimate capacity of the structure as well as an increase in the maximum midspan deflection (Al-Hammoud, Soudki, & Topper, 2011; Masoud, Soudki, & Topper, 2005). However in the research work in which both the anchorage zone and the flexural zone were corroded, the failure changed from concrete crushing (flexural failure) to bond splitting. This leads to the conclusion that in corrosive environments, bond splitting is more likely than flexural failure (Uomoto, Tsuji, & Kakizawa, 1984; Okada, Kobayashi, & Miyagawa, 1988; Tachibana, Maeda, & Kajikawa, 1990; Kawamura, Maruyama, Yoshida, & Masuda, 1995; Almusallam, Al-Gahtani, Aziz, & Rasheeduzzafar, 1996; Rodriguez, Ortega, & Casal, 1997; Mangant & Elgarf, 1999; El Maadawi & Soudki, 2005). Hence it is important to study the effect of corrosion on bond.

Experimental studies reported in the literature on the effect of corrosion on the bond behaviour of reinforced concrete beams under monotonic loading showed that at a low corrosion rate (about $0.04 mA/cm^2$) the bond strength initially increased as corrosion increased so long as the section was not cracked (Figure 2.5) (FIB, 2000).This increase was attributed to the fact that the corrosion rust product produced before cracking would cause a rough surface around the bar hence increasing the friction force on the interface between the reinforcing steel and the concrete (FIB, 2000). As the corrosion increased further, the bond strength decreased slightly but remained at levels higher than for the uncorroded beams. Once the concrete cracked due to corrosion, the bond stresses between the reinforcing steel and the concrete decreased below the level for the uncorroded beam and the slip of the reinforcing bar relative to the concrete increased (Al-Sulaimani, Kaleemullah, & Basunbul, 1990; Cabrera & Ghodoussi, 1992; Clark & Saifullah, 1993; Rodriguez, Ortega, & Casal, 1994; Almusallam, Al-Gahtani, Aziz, & Rasheeduzzafar, 1996; Mangant & Elgarf, 1999; Auyeung, Chung, & Balaguru, 2000; FIB, 2000; Fang, Lundgren, Chen, & Zhu, 2004). This decrease in the bond strength was attributed to a decrease in the interlock between the ribs

and the concrete due to a severe deterioration of the ribs; the increase in the width of the longitudinal cracks that reduced the concrete confinement; and the large amount of rust flakes around the bar that lubricated it and hence decreased the friction force between the reinforcing steel and the concrete (FIB, 2000).

It should be noted that a decrease in the bond leads to a decrease in the load carrying capacity of a reinforced concrete structure, an increase in the deflection of the structure and an increase in the slip between the reinforcing steel and the concrete (ACI Committee 408, 2003).

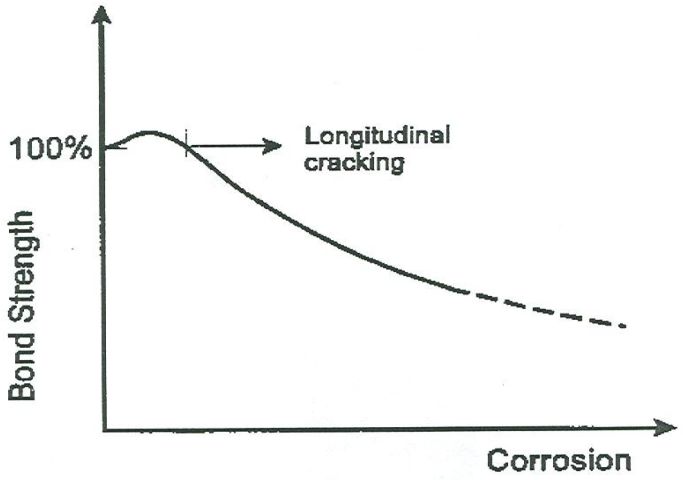


**Figure 2.5 Variation of bond strength with corrosion (FIB, 2000).**

Lundgren et al. proposed a 1-D model to predict the stress-slip response of corroded reinforced concrete beams. The model was un-conservative for beams exposed to high corrosion level and with a low transverse reinforcement (Lundgren, Kettil, Hanjari, Schlune, & San Roman, 2012).

Despite the fact that many structures that are prone to corrosion are subjected to repeated loading, such as bridges and marine structures, little research has been done in this field. (Rteil, 2007; Rteil, Soudki, & Topper, 2011) studied the effect of corrosion on the bond behaviour of reinforced concrete beams under repeated loading. The following conclusions were drawn:

- The widths and number of the cracks initiated at the level of the steel bar in the anchorage zone increased with an increase in the number of cycles applied to the beam.

- The propagation rate of the horizontal cracks was divided into three stages. Stage I during the first 20% of the fatigue life of a beam during which the propagation rate was high and then it decreased to a steady value during stage II which consumed 60-70% of the beam's fatigue life. The rate then increased during stage III which occupied the last 10-20% of the beam's fatigue life.
- Failure was by concrete splitting where the bottom cover was pushed away preserving the concrete keys intact except for the corrosion effect.
- The fatigue strength of the beams decreased due to corrosion.
- The peak value of the bond stress moved from the loaded end of the bonded length to the free end during cyclic loading until failure occurred. This shift in bond stress was possibly due to the loading configuration.
- The slip increased at a slow rate until about 90% of the beam's life after which it increased exponentially. The initial and final slip increased with an increase in the level of corrosion.
- The initial slip increased with the maximum applied load.
- The slip at the loaded end was higher than the slip at the free end of the steel bonded length.

(Rteil, Soudki, & Topper, 2011) used a fatigue slip-growth analysis approach to calculate the life of a specimen failing in fatigue of bond. This approach depends on the initial and final slip, maximum load applied, and the level of corrosion.

## 2.1 Effect of Confinement on the Bond Behaviour in Reinforced Concrete Beams

### 2.1.1 The Effect of Confinement from the Supports and Stirrups

Confinement can be either active by the reinforced concrete beam being in direct contact with a support or passive due to the presence of internal stirrups (FIB, 2000).

Several researchers have studied the effect of confinement on the bond behaviour of steel in reinforced concrete. It was concluded that transverse reinforcement increases ductility of

the bond and reduces the rate of load drop post-peak (Zuo & Darwin, 2000). Guizani and Chaallal (Guizani & Chaallal, 2011) showed that the confinement from stirrups had a greater effect than the concrete cover and bar spacing on bond failure. The effect of the stirrups on confining the splitting crack was considered the main important bond factor (Guizani & Chaallal, 2011). Once splitting cracks widen, the stirrups take the force at the crack preventing the crack from opening further and confining the concrete (Giuriani, Plizzari, & Schumm, 1991). After splitting of the cover occurs, confinement from stirrups becomes essential for the bond strength (Bamonte & Gambarova, 2007). The stirrups are most effective for the bond behaviour of bar diameters bigger than 14 mm and when the bar slip is high (Giuriani, Plizzari, & Schumm, 1991). Beams with stirrups showed almost no reduction in bond stress due to corrosion compared to beams without stirrups (Hanjari, Coronelli, & Lundgren, 2011).

In addition to passive confinement from the stirrups, active confinement from direct contact with the supports plays an important role on the bond behaviour of steel-concrete interface as in the case of reinforced concrete beam-column joints (FIB, 2000). This confinement prevents splitting cracks from arriving to the surface until the concrete keys are crushed and the bar fails in a pull out mode (FIB, 2000).

Most of the studies done on bond used a small anchorage length and the authors discussed mainly the effect of confinement on cracking. In this research study a longer anchorage length was used (33 $d_b$) and the effect of combined confinement from direct support and stirrups was studied under monotonic and repeated loading. Also the effect of a mild corrosion level combined with confinement effect was discussed.

### 2.1.2 The Effect of FRP Confinement on Bond Behaviour under Static Load

#### 2.1.2.1 Uncorroded Specimens

Only recently has FRP reinforcement been used as a method of repairing and strengthening the bond between steel and concrete in reinforced concrete beams.

Several researchers (Kono, Inazumi, & Kaku, 1998; Hamad, Rteil, & Soudki, 2004; Hamad, Rteil, Selwan, & Soudki, 2004; Hamad, Rteil, Soudki, & Harajli, 2004; Harajli, Hamad, & Rteil, 2004; Hamad, Hage Ali, & Harajli, 2005; Hamad & Rteil, 2006) and (Rteil,

2007) have studied the effect of FRP confinement on the bond behaviour of beam specimens under static loading. They all concluded that FRP confinement increased the bond capacity of the beam. They also concluded that confinement improved the post failure ductility of the reinforced concrete beam; in that FRP confinement lowered the drop in the load rate after failure compared to unconfined specimens.

(Hamad, Rteil, Soudki, & Harajli, 2004) proposed an equation, similar to the one in ACI for confinement by steel stirrups, to calculate the additional bond stress due to FRP confinement:

$$u_{tr,f} = \frac{f_{fe} A_{tr,f}}{16.6 s_f n_b d_b} \qquad \textbf{Equation 2-3}$$

where $u_{tr,f}$ is the additional bond strength due to the presence of the FRP sheets, $f_{fe}$ is the effective stress in the FRP sheets, $A_{tr,f}$ is the total cross-sectional area of FRP sheets normal to the plane of splitting within spacing $s_f$, $n_b$ and $d_b$ are the number and diameter of the steel bars being spliced or developed, $s_f$ is the spacing between FRP sheets, for a continuous sheet $s_f$ = the width of the sheet.

(Harajli, Hamad, & Rteil, 2004) also reported that FRP reinforcement was better than stirrups in providing confinement because the external confinement was more effective in restraining splitting crack growth in the concrete. (Harajli, Hamad, & Rteil, 2004) proposed a bond stress-slip law. The bond stress-slip behaviour for splitting was divided into four stages. In the initial stage the stiffness of the bond stress-slip response is assumed to be similar to that of a pullout failure since the response is associated with adhesion and friction (Figure 2.6). As tensile cracks start to develop, a second stage starts and continues until the maximum bond stress is reached. This stage is characterized by a softer response than that observed for pullout tests. In stage three, there is a sudden drop in the bond stress that ends when the bond forces reach equilibrium with the post splitting concrete tensile strength $u_{ps}$. In the fourth stage, the bond resistance deteriorates gradually with increasing slip until the bond drops to zero when the widening of the concrete splitting cracks results in complete failure of the bond (Figure 2.6). When concrete confinement is provided the internal crack growth is restricted, leading to finer splitting cracks, hence increasing the resistance of the concrete

matrix after splitting. Accordingly, (Harajli, Hamad, & Rteil, 2004), proposed the following equation to calculate the maximum bond stress accounting for confinement:

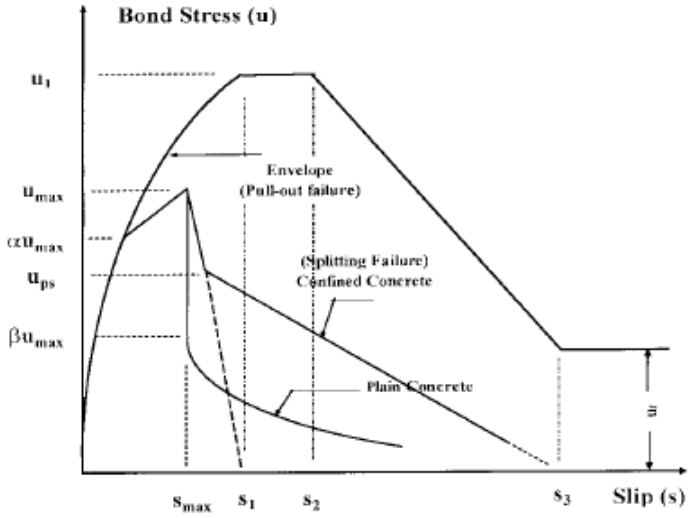


**Figure 2.6: General bond stress-slip law (Harajli, Hamad, & Rteil, 2004).**

$$u_{\max}(MPa) = 0.78\sqrt{f'_{c(MPa)}}\left(\frac{c+K_c}{d_b}\right)^{2/3} \le u_1 \qquad \textbf{Equation 2-4}$$

where $K_c(mm) = \left(7.0A_{tr}/sn\right)$ for concrete confined with ordinary transverse steel

$= \left(28.0r_e A_{FRP}/sn\right)$ for concrete externally confined with fibre reinforced polymer sheets,

$$r_e = \frac{E_{FRP}}{E_s}$$

$A_{tr}$ = area of ordinary transverse steel in a spacing s

$A_{FRP}$ = area of FRP sheets within a spacing s

$f'_c$ = concrete compressive strength (MPa)

The post-splitting bond resistance is given by:

$$u_{ps} = u_{\max}(0.5 + K_{cs}) \le u_{\max} \qquad \textbf{Equation 2-5}$$

where $K_{cs} = \left( {}^{7.5A_{tr}}\!/\!_{snc} \right)$ for concrete confined with ordinary transverse steel

$= \left( {}^{22.0r_e A_{FRP}}\!/\!_{snc} \right)$ for concrete externally confined with fibre reinforced polymer sheets,

#### 2.1.2.2 Corroded Specimens

When externally bonded FRP laminates are used to repair corrosion damaged RC elements, wrapping a corroded element with FRP laminates may reduce the corrosion activity because a FRP wrap acts as a low-permeability barrier to the further ingress of water and oxygen into concrete, which is required for corrosion reactions to continue (Debaiky, Green, & Hope, 2000; Soudki & Sherwood, 2000; Khoe, Sen, & Bhethanabotla, 2012). The physical confinement may impede the dispersion of corrosion products and thus stifle the corrosion reaction itself. Wrapping a concrete section with FRP laminates provides external confinement that resists the internal displacement caused by the expansion of the corrosion products and thus decreases corrosion and bond splitting cracks (Soudki & Sherwood, 2000). Hence, the structural strength of corroding reinforced concrete beams is improved if they are repaired with FRP laminates (Soudki, Rteil, Al-Hammoud, & Topper, 2007). Figure 2.7 summarizes the benefits of using FRP laminates in the repair of corroded RC elements.

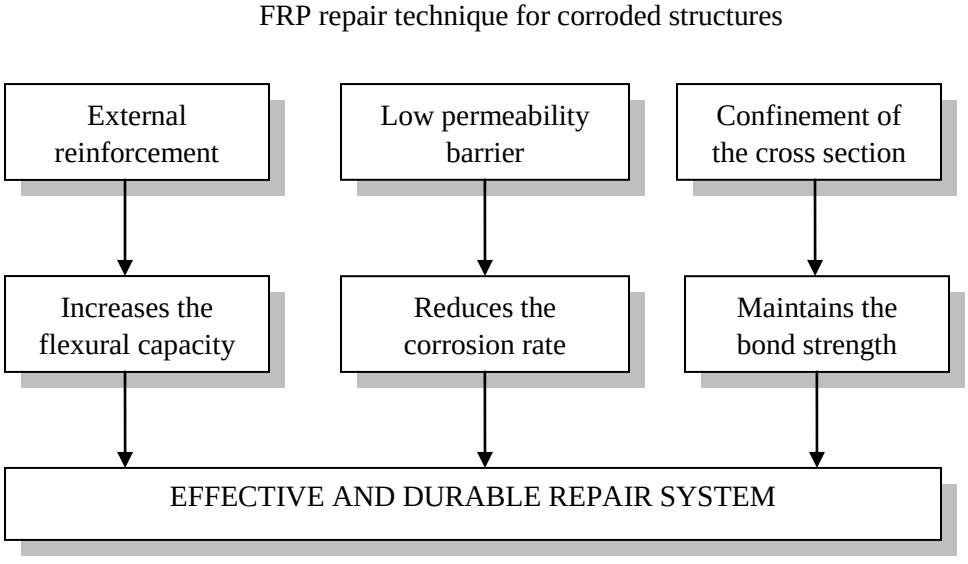


**Figure 2.7 Benefits of using FRP laminates in repairing corroded structures**

(Soudki & Sherwood, 2003) were the first to study the effect of FRP confinement on the bond behaviour of reinforced concrete beams subjected to corrosion. (Soudki & Sherwood, 2003; Craig & Soudki, 2005) tested pullout and bond anchorage specimens. The studies showed that wrapping the specimens with FRP sheets increased the bond strength of the specimens. The bond strength of FRP wrapped specimens was doubled compared to unwrapped specimens in the case of a high corrosion level (about a 10% mass loss). The effect of FRP wrapping on corrosion was more noticeable in specimens with a smaller concrete cover than a thick concrete cover because the greater thickness of the latter already delayed the onset of corrosion compared to the former. CFRP wrapped specimens had a higher slip-initiation load due to the confinement of corrosion cracking that the FRP sheets provided. This increased the transverse stiffness of the specimens to displacements due to bond-splitting forces and hence reduced the slip of the bar. In both studies, the use of CFRP sheets to confine the corroded bond regions changed the mode of failure. In the pullout specimens, the mode of failure changed from bar-bond splitting in unwrapped specimens to bar pullout or bar rupture in FRP wrapped specimens. In the beam specimens, the mode of failure changed from bond splitting to flexure failure (steel yielding).

(Papakonstantinou, Balaguru, & Auyeung, 2011) concluded that CFRP increased the bond strength of corroded reinforced concrete pull-out specimens and reduced the corrosion related bond-slip. The increase in the corrosion level had little effect on the bond strength of the confined reinforced concrete (Papakonstantinou, Balaguru, & Auyeung, 2011).

### 2.1.3 Effect of FRP Confinement on the Bond Behaviour under Repeated Loading

To the author's best knowledge, few papers have been published concerning the effect of FRP on the bond behaviour of corroded and uncorroded specimens under repeated loading. (Soudki, Rteil, Al-Hammoud, & Topper, 2007; Rteil, Soudki, & Topper, 2007; Rteil, Soudki, & Topper, 2007; Rteil, Soudki, & Topper, 2007) reported that wrapping corroded beams with FRP sheets decreased the width and number of longitudinal cracks compared to the unwrapped beams. Corrosion caused an average reduction of 18% in the fatigue strength of the wrapped beams compared to the non-corroded wrapped beams. However, comparing the corroded wrapped beams to the uncorroded un-wrapped beams, the fatigue strength increased on average by 30%. The increase in the fatigue strength of the wrapped un-corroded beams

compared to the unwrapped un-corroded beams was 32%. (Rteil, 2007) reported that for the first 4 to 8 % of the wrapped beams' life, the slip increased at a decreasing rate. After that, the slip continued to increase at a slow rate until the last 10% of the beams' life when the slip rate increased exponentially.

# Chapter 3
# Experimental Program

## 3.1 Introduction

The experimental program in this study consisted of testing fifty-seven reinforced concrete bond beams that were divided into two groups. The purpose of the beams in group 1 was to study the effect of confinement from the supports and the stirrups on the monotonic and fatigue bond behaviour. Group 2 beams were designed to study the effect of anchorage length on the bond behaviour of steel to concrete interface of beams subjected to static and repeated loading.

## 3.2 Test Program

### 3.2.1 Group 1 Beams

Sixteen large scale beams (254mm*152mm*2000mm) were tested in this group. The beams were divided into two sets. Set 1 consisted of 10 beams tested monotonically to failure. Set 2 consisted of 6 beams tested under repeated loading until failure by fatigue. Table 3.1 shows the different beams with their related nomenclature.

The variables in set 1 were: corrosion level, support conditions and stirrup configuration. Two different corrosion levels were considered (0% corrosion, and a low corrosion level about 4.5 % mass loss). Three support conditions were used to study the confinement effect of the supports on the bond behaviour of the steel reinforcement in these beams. Cast-in 16 mm threaded anchors were placed in the concrete beams to fix the supports at the end of the beams. The supports were fixed to the cast-in anchors from the end with the following three conditions: leaving a gap between the bottom of the beam and the support, keeping the support in contact with the bottom of the beam at two points only, or fixing the support so that it was in contact with the beam across its full width. Three different stirrup configurations in the anchorage zone were used: stirrup configuration A with a 150 mm spacing between stirrups, stirrup configuration A* with a 125 mm spacing between stirrups and stirrup configuration B with a 75 mm spacing between stirrups. Figure 3.1, Figure 3.2

and Figure 3.3 show the schematic drawings of the beams with stirrup configurations A, A* and B, respectively.

The variables in set 2 were: stirrup configuration and the fatigue load range. Two stirrup configurations were used: A and B. In stirrup configuration A, the spacing between stirrups was 150 mm, and in stirrup configuration B, the spacing was 75 mm. Figure 3.1 and Figure 3.3 show the schematic drawing of the beams with stirrup configuration A and B from this set. For each stirrup configuration, three different load ranges were applied.

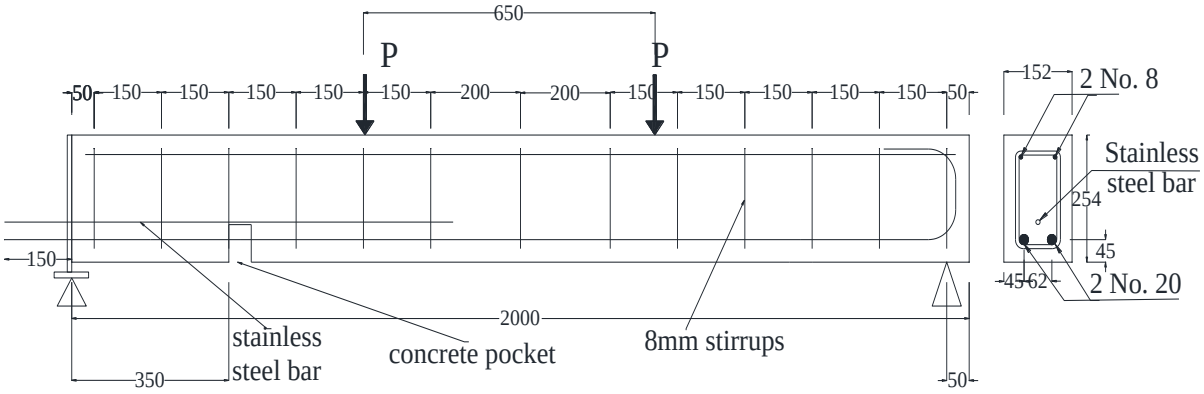


**Figure 3.1Beams with stirrup configuration A; 150 mm spacing between stirrups in the shear zone. All dimensions are in mm.**

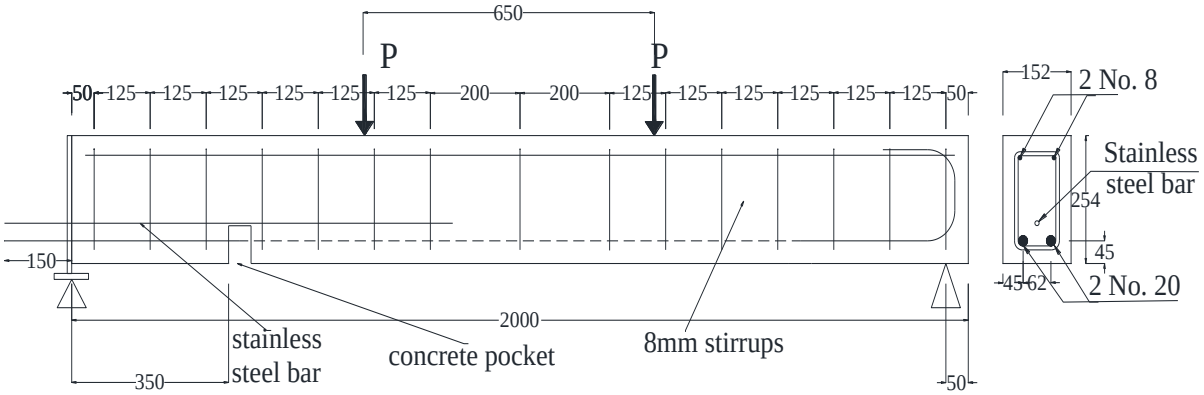


**Figure 3.2 Beams with stirrup configuration A*; 125 mm spacing between stirrups in the shear zone. All dimensions are in mm.**

**Table 3.1 Test matrix - Group 1**

| Set | Beam Notation | Type of Load | Load Range (kN) | Stirrup spacing (mm) | Support Conditions | Corrosion Level (%) |
|---|---|---|---|---|---|---|
| 1 | M-A-100-0-1 | Monotonic | 100 | 150 | Not in contact* | 0 |
| | M-A-100-0-2 | Monotonic | 100 | | complete contact† | 0 |
| | M-A-100-0-3 | Monotonic | 100 | | Partial contact‡ | 0 |
| | M-A-100-0-Spiral | Monotonic | 100 | | Not in contact | 0 |
| | M-A-100-0-U | Monotonic | 100 | | complete contact | 0 |
| | M-A-100-5 | Monotonic | 100 | | Complete contact | 5 |
| | M-A*-100-0-U | Monotonic | 100 | 125 | complete contact | 0 |
| | M-B-100-0-1 | Monotonic | 100 | 75 | Not in contact | 0 |
| | M-B-100-0-2 | Montonic | 100 | | Complete contact | 0 |
| | M-B-100-5 | Montonic | 100 | | Complete contact | 5 |
| 2 | F-A-66-0 | Fatigue | 66 | 150 | Complete contact | 0 |
| | F-A-64-0 | Fatigue | 64 | | | |
| | F-A-60-0 | Fatigue | 60 | | | |
| | F-B-97-0 | Fatigue | 97 | 75 | Complete contact | 0 |
| | F-B-91-0 | Fatigue | 91 | | | |
| | F-B-83-0 | Fatigue | 83 | | | |

* The supports are not touching the bottom soffit of the beam.
† The support is completely touching the beam across the width.
‡ The support is only touching the beam at 2 points to minimize the effect of confinement.

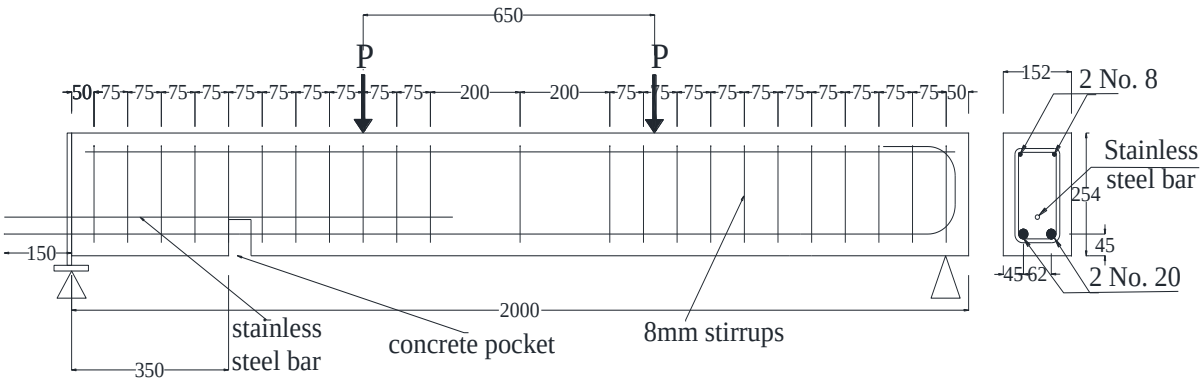


**Figure 3.3 Beams with stirrup configuration B; 75 mm spacing between stirrups in the shear zone. All dimensions are in mm.**

### 3.2.2 Group 2 Beams

This group consisted of testing forty-one reinforced concrete bond beams. The variables were: the anchorage length (200 mm or 350 mm), the type of load applied (monotonic or repeated loading), the repeated load range, the severity of corrosion (no corrosion, mild corrosion and severe corrosion levels), and whether a carbon fibre reinforced polymer (CFRP) repair method was used or not. The forty-one beams were divided into two sets depending on the anchorage length. Set 1 had 24 beams with a 200 mm anchorage length. Set 2 had 17 beams with a 350 mm anchorage length. Figure 3.4 and Figure 3.5 show the details for the beams of Set 1 and Set 2, respectively. The beams within each set were divided into five groups, the first group consisted of beams tested monotonically to failure, and the other five groups were tested under repeated loading and divided depending on the corrosion level and the wrapping condition. The primary variable within each group was the applied load range (see Table 3.2 and Table 3.3).

A nomenclature for the beams was chosen and is explained in the following. The first letter was used to identify the type of loading applied. M was used for monotonic loading and F was used for fatigue or repeated loading. Next the anchorage length was identified, 200 represented a 200 mm anchorage length and 350 represented a 350 mm anchorage length. A second letter was then used to identify the type of repair. The symbol U was used for unrepaired beams and R was used for beams repaired by wrapping CFRP sheets following corrosion exposure. The level of corrosion in terms of severity was given by the next letter. The severity of corrosion varied from no corrosion (n), to a mild corrosion level (m), and to a

high corrosion level (h). The mild corrosion level was on average a 5% theoretical mass loss while the high corrosion level was on average a 15% theoretical mass loss. Next was a number that gave the applied load range in kN. The minimum load in the load cycle was kept constant at 10 kN for all the beams tested under fatigue loading. The maximum load was varied in order to get a reasonable distribution of fatigue lives (between 10,000 and 1,000,000 cycles).

### 3.3 Design of Specimens

The fifty-seven beams in this study were all the same size with a rectangular cross-section (254 x 152 mm) and a length of 2000 mm. Each beam was reinforced with two 20M deformed bars with a 40 mm clear cover on the bottom and the sides. Two 8 mm smooth bars were used in the compression zone at a distance of 44 mm from the top of the beam and a distance of 40 mm from the sides. The shear reinforcement consisted of 8 mm stirrups at a spacing of 125 mm in the shear zone and a spacing of 200 mm in the flexure zone to prevent shear failure except for beams with stirrup configuration A* and B where the stirrup spacing in the shear zone was 150 mm and 75 mm respectively. A hollow 8 mm stainless steel bar, Grade 304, was placed at a distance of 80 mm from the bottom of the beam only for the beams that were subjected to corrosion. The stainless steel bar was used as an anode in the accelerated corrosion process (see section 3.7). The stainless steel bar and the two 20M deformed bars were extended 150 mm from one end of the beam to provide for the electrical connections necessary for accelerated corrosion. The 20M deformed bars were bent from the other end to form a standard hook to ensure that bond failure occurred at the instrumented end of the beam. The excel sheet showing the design of the beams is shown in

In order to provide the required anchorage length in the beams of group 2, a low density polyethylene (LDP) tube was placed over the reinforcing bar in the un-bonded zones, in the middle of the beam and at 175 mm from the end of the beam (Figure 3.6). Also, a pocket (152 x 75 x 50 mm) at the end of the specified anchorage length was provided to allow for easy instrumentation of the tension steel to measure the slip and strain (Figure 3.4 and Figure 3.5). A similar pocket was provided in the beams of group 1 at a distance of 350 mm from the support (Figure 3.7). Blocks of high-density (HD) foam were taped around the tension reinforcement before casting to create these pockets (Figure 3.6).

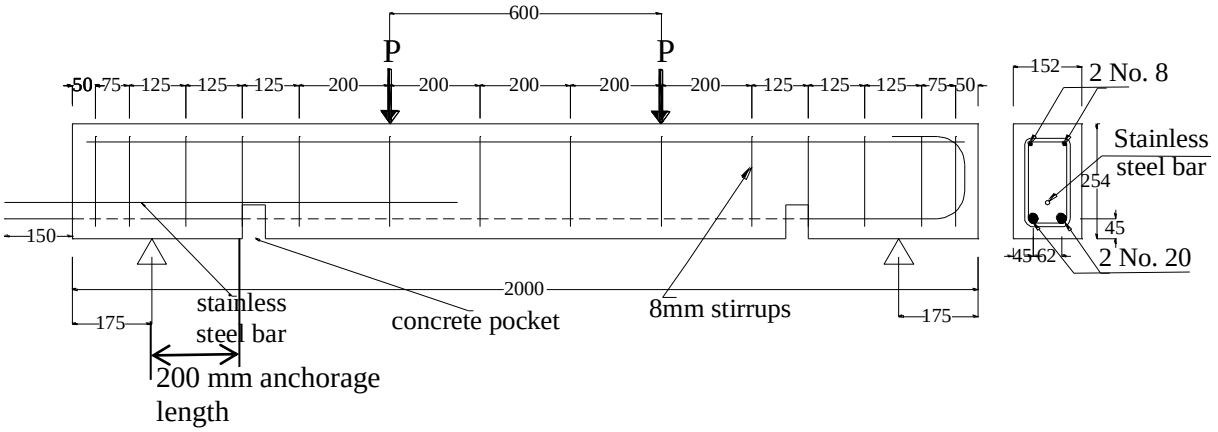


**Figure 3.4 Longitudinal and cross-sectional details for the beams in group 2-Set 1 (All dimensions are in mm). The dashed part of the steel reinforcement represents the unbonded length.**

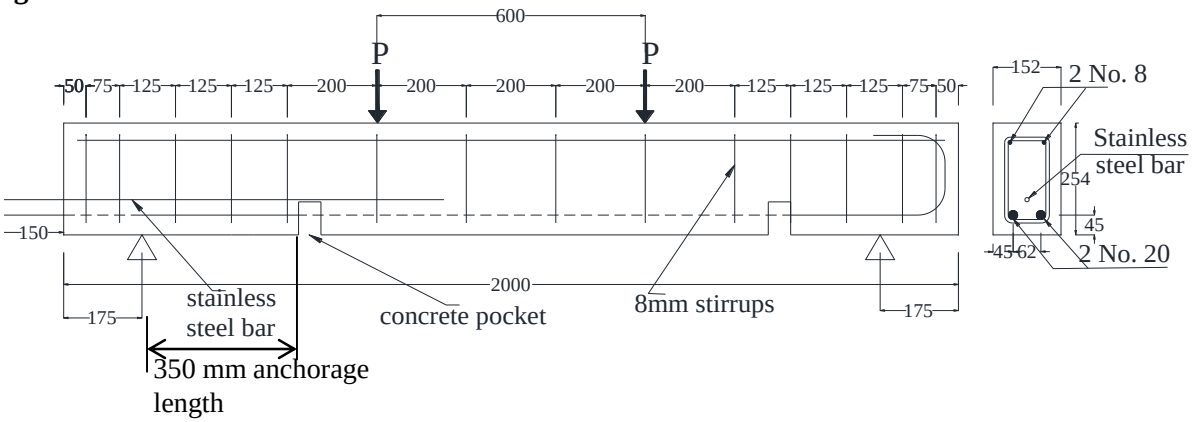


**Figure 3.5 Longitudinal and cross-sectional details for the beams in group 2- Set 2 (All dimensions are in mm). The dashed part of the steel reinforcement represents the unbonded length.**

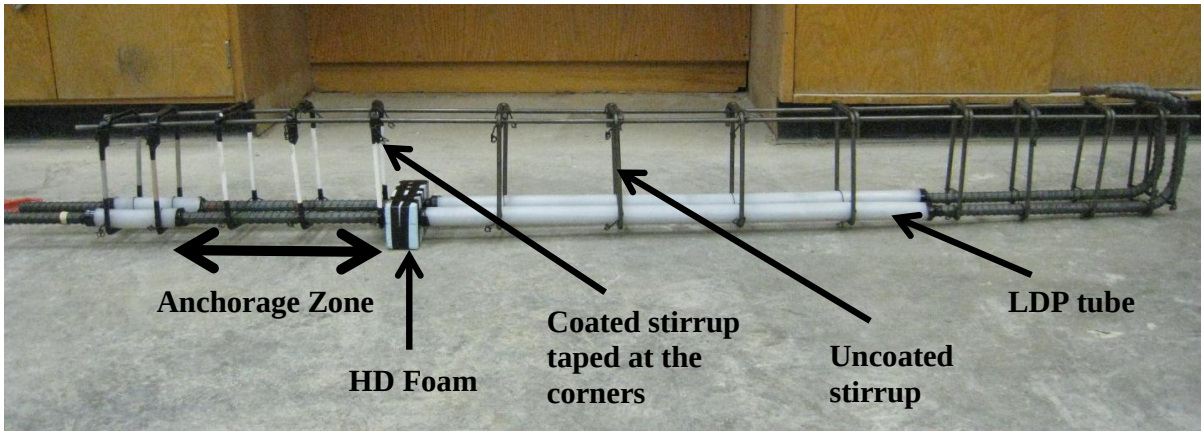


**Figure 3.6 The fabricated cage for beams from group 2 - Set 2.**

**Table 3.2 Test matrix for Group 2 - Set 1 Beams (Anchorage length = 200 mm)**

| Group | Beam Notation | Type of Load | Max. Load Applied (kN) | Load Range (kN) | Corrosion Level | CFRP Repair |
|---|---|---|---|---|---|---|
| M | M-200-U-n-1 | Monotonic | 99.73 | 99.73 | No | No |
| | M-200-U-n-2 | | 90.7 | 90.7 | No | No |
| | M-200-R-n | | 172.7 | 172.7 | No | Yes |
| | M-200-U-m | | 73.74 | 73.74 | Mild | No |
| | M-200-R-m | | 123.7 | 123.7 | Mild | Yes |
| | M-200-R-h | | 119.6 | 119.6 | High | Yes |
| U-n | F-200-U-n-60 | Fatigue | 70 | 60 | No | No |
| | F-200-U-n-66 | | 76 | 66 | | |
| | F-200-U-n-68 | | 78 | 68 | | |
| | F-200-U-n-70-1 | | 80 | 70 | | |
| | F-200-U-n-70-2 | | 80 | 70 | | |
| U-m | F-200-U-m-43 | Fatigue | 53 | 43 | Mild | No |
| | F-200-U-m-44 | | 54 | 44 | | |
| | F-200-U-m-45 | | 55 | 45 | | |
| | F-200-U-m-46 | | 56 | 46 | | |
| | F-200-U-m-48 | | 58 | 48 | | |
| R-m | F-200-R-m-72 | Fatigue | 82 | 72 | Mild | Yes |
| | F-200-R-m-80 | | 90 | 80 | | |
| | F-200-R-m-90 | | 100 | 90 | | |
| | F-200-R-m-96 | | 106 | 96 | | |
| R-h | F-200-R-h-75 | Fatigue | 85 | 75 | High | Yes |
| | F-200-R-h-80 | | 90 | 80 | | |
| | F-200-R-h-88 | | 98 | 88 | | |
| | F-200-R-h-96 | | 106 | 96 | | |

In order to protect the stirrups and compression steel from corrosion in the anchorage zone, the stirrups in the anchorage were coated with a chemical resistant epoxy coating called TRU-GLAZE 4508, manufactured by DEVOE COATINGS. The corners of the stirrups were also taped with electric insulation tape (Figure 3.6).


**Figure 3.7 Cage for a beam from group 1 stirrup configuration A.**

**Table 3.3 Test matrix for Group 2- Set 2 Beams (Anchorage length = 350 mm)**

| Group | Beam Notation | Type of Load | Max. Load Applied (kN) | Load Range (kN) | Corrosion Level | CFRP Repair |
|---|---|---|---|---|---|---|
| M | M-350-U-n | Monotonic | 151.06 | 151.06 | No | No |
| | M-350-R-n | | 178.3 | 178.3 | No | Yes |
| | M-350-U-m | | 118.10 | 118.1 | Mild | No |
| | M-350-R-m | | 184.5 | 184.5 | Mild | Yes |
| | M-350-R-h | | 174.74 | 174.74 | High | Yes |
| U-n | F-350-U-n-70 | Fatigue | 80 | 70 | No | No |
| | F-350-U-n-74 | | 84 | 74 | | |
| | F-350-U-n-80 | | 90 | 80 | | |
| | F-350-U-n-90 | | 100 | 90 | | |
| U-m | F-350-U-m-70 | Fatigue | 80 | 70 | Mild | No |
| | F-350-U-m-82 | | 92 | 82 | | |
| R-m | F-350-R-m-126 | Fatigue | 136 | 126 | Mild | Yes |
| | F-350-R-m-135 | | 145 | 135 | | |
| | F-350-R-m-140 | | 150 | 140 | | |
| R-h | F-350-R-h-110 | Fatigue | 120 | 110 | High | Yes |
| | F-350-R-h-122 | | 132 | 122 | | |

## 3.4 Concrete Placement

The beams from group 1 were cast in 4 batches. In the first batch, 11 beams were cast. Those are the non-corroded beams and hence no salted concrete was added. In the second batch, 2 beams were cast with salted concrete placed in the region adjacent to the support (350 mm x 152 mm x 100 mm) to study the effect of corrosion. Unsalted concrete was placed in the rest

of the beam. Another 3 beams were then cast in 2 different batches to examine the effects of spiral confinement, debonding and changing stirrup spacing. These are all discussed later in Chapter 4. The beams from group 2 were cast in three batches due to formwork and space availability. The first cast consisted of 9 beams and the second and third casts consisted of 16 beams each. Salted concrete was placed in the anchorage zone of the beam to accelerate corrosion of the two 20M deformed bars in this region. The salted concrete occupied a space of 200 mm long and 100 mm deep from the beam soffit for Group 2-Set 1 beams and 350 mm long and 100 mm deep from the beam soffit for Group 2-Set 2 beams and the corroded beams in Group 1. Unsalted concrete was placed in the rest of the beam. Ready mix concrete was used for casting the beams.

Figure 3.9 shows the steel-reinforcing cage inside the casting forms. During casting, rigid plastic dividers of a 100 mm depth were placed in the forms at the end of the anchorage zone (200 mm length or 350 mm length) to separate the salted concrete from the unsalted concrete. Salted concrete was poured into the anchorage zone between the end of the beam and the plastic divider (Figure 3.8). The unsalted concrete was then poured so as to fill the rest of the area to a height of 100 mm, after which the plastic dividers were removed. Then the rest of the beam was filled with unsalted concrete. Hand-held vibrators were used during concrete placement. Standard concrete cylinders (100 x 200mm) were prepared according to CSA-A23.2 (2009).

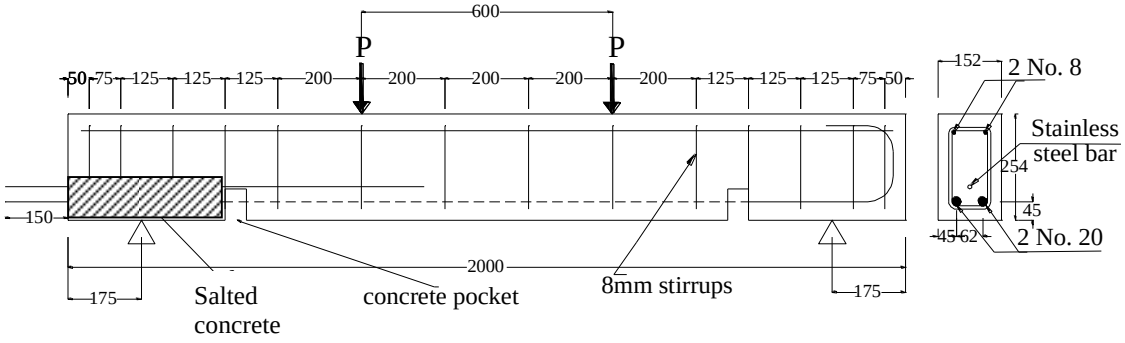


**Figure 3.8 Schematic drawing of the 200 mm anchorage length beam, showing the salted concrete region as a hatched area.**

**Figure 3.9 General view of the cages in the formwork before casting.**

## 3.5 FRP Strengthening

A single layer of U-CFRP sheet was used to confine the beam in bond. This sheet was wrapped along the anchorage zone of the beam. The fibre orientation for this U-CFRP sheet was perpendicular to the steel reinforcement in the anchorage zone. Two different widths of the fibre U-wraps were used: 200 mm (for the beams with 200 mm anchorage length) and 350 mm (for the beams with 350 mm anchorage length). The length of the U-CFRP sheet for both widths was 650 mm. Details of the wrapping are shown in Figure 3.10. All the beams had the same repair scheme.

The CFRP sheets were applied according to the manufacturer's recommendations. The concrete surfaces were ground and then cleaned to get rid of corrosion staining on the surface and any grease or foreign particles. The edges of the beam's cross-section were then rounded with a grinder to a diameter of at least 10 mm. The corrosion cracks in the beams were then sealed with Sikadur-31, Hi-Mod Gel. The beams were then left to cure for 24 hours, after which their surfaces were ground again to get rid of the extra cured epoxy. Then the epoxy resin was placed on the concrete surface after which the CFRP sheets were bonded to the

beam. Additional epoxy was applied on top of the CFRP sheets. Pressure was then applied by a roller on the CFRP sheet that was placed on the beam to ensure that the epoxy impregnated into the CFRP sheet. This should lead to a good bond between the CFRP sheet and the concrete surface of the beam. Figure 3.11 shows a repaired beam turned upside down.

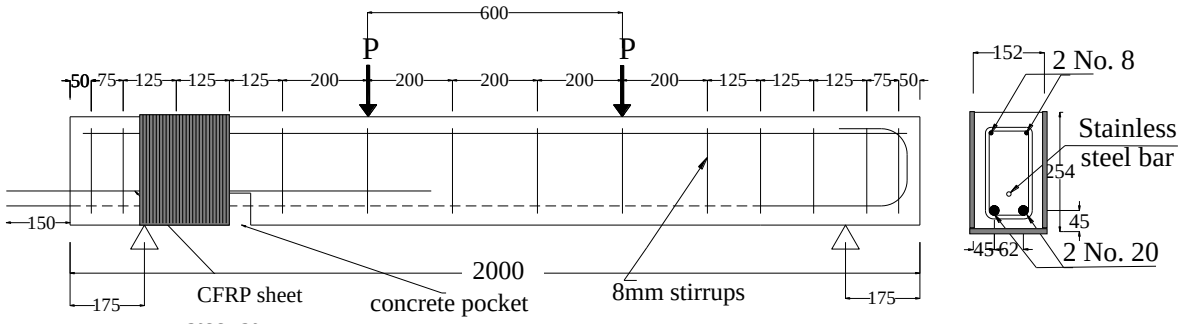


**Figure 3.10: Beam with 200 mm anchorage length wrapped with CFRP sheets.**

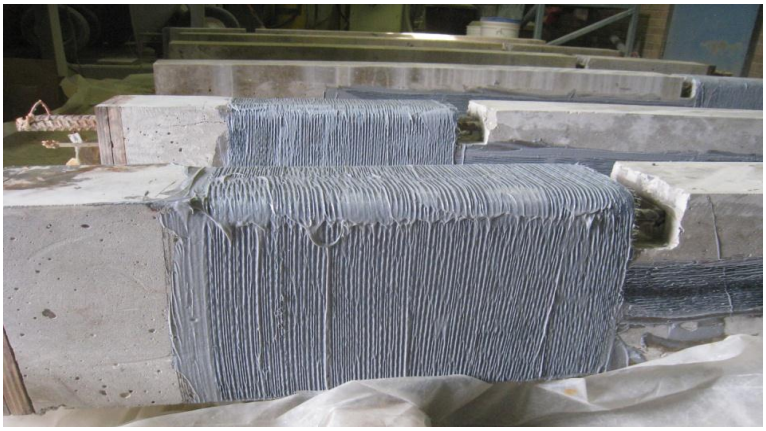

**Figure 3.11 A repaired beam turned upside-down.**

## 3.6 Material Properties

### 3.6.1 Concrete

Ready mix concrete was supplied by Hogg Ready Mix. The specified concrete strength was 35 MPa. The concrete mixture proportions for all beams were (per cubic meter): 290kg of Portland cement, 90 kg of slag, 640 kg of fine aggregates, 1190 kg of coarse aggregates (19 mm maximum aggregate size), 325ml/100kg of water reducer, 250ml/ 100 kg of retarder and 160 litres of water leading to a water cement ratio of 0.42.

For the first cast from group 2 that consisted of 9 beams a 1 cubic meter volume of ready mix concrete of the above proportions was ordered. For the second and third casts from group 2 that consisted of 16 beams each, a truck with a 2 cubic meter volume of ready mix concrete with the above proportions was used. In each cast a 0.1 cubic meter volume of concrete was removed from the truck in order to add salted water to the mix. This concrete was mixed in a small batching equipment with 3.8 kg of water and 1.4 kg of salt (NaCl). Due to the size of the batching equipment, the mixing was done in 3 installments. This led to a concrete mix with a water-cement ratio of 0.52. The 1.4 kg of salt (NaCl) resulted in 2.15% of chloride ($Cl^-$) by weight of cement. For the rest of the concrete in the truck of the first cast from group 2 (0.9 $m^3$) 34.2 kg of water was added resulting in a w/c ratio of 0.52. For the rest of the concrete in the truck in the second and third casts from group 2 (1.9 $m^3$ in each cast) 55.1 kg of water was added resulting in a w/c ratio of 0.52.

The 28-day compressive strength of the salted and unsalted concrete for the different casts is given in Table 3.4. The average compressive strength of at least three cylinders was considered in the strengths provided by Table 3.4. In the first cast of group 2 beams, the salted concrete had a lower strength than the unsalted concrete due to leftover water from cleaning the mixer before use. In the second and third casts of group 2 beams, the mixer was dried using a towel before each use.

**Table 3.4: The 28-day compressive strength of concrete for the different casts**

| | Group 1 Beams (MPa) | Group 2- First Cast (MPa) | Group 2- Second Cast | Group 2 - Third Cast |
|---|---|---|---|---|
| Salted Concrete | 37.0 ± 0.50 | 35.9 ± 1.34 | 46.5 ± 0.41 | 43.5 ± 0.23 |
| Unsalted Concrete | 37.1 ± 0.46 | 48.6 ± 4.86 | 47.0 ± 0.64 | 44.6 ± 0.73 |

### 3.6.2 Steel

The 20M deformed bars used in flexure were Grade 400 steel with guaranteed yield strength of 400 MPa. The 8 mm smooth bars had a yield strength of 340 MPa. The 8 mm hollow stainless steel bar had an outside diameter of 7.94 mm (5/16 inch) with a 0.89 mm (0.035 inch) wall thickness. The stainless steel bars were Grade 304.

### 3.6.3 FRP System

The CFRP repair system used was manufactured by SIKA Inc. The CFRP sheets were SikaWrap 230C and the epoxy resin was Sikadur 330. Table 3.5 summarizes the mechanical properties of the fibre, epoxy and the cured CFRP system used as given by the manufacturer. Sikadur 330 has two components A and B that are mixed in a ratio of 4:1 by weight. The epoxy resins were mixed using a low speed drill at 400 to 600 rpm.

**Table 3.5: Mechanical properties of the CFRP system.**

| | **Fibres** | **Epoxy** | **CFRP system** |
|---|---|---|---|
| Tensile strength (MPa) | 3450 | 30 | 715 |
| Tensile modulus (MPa) | 230000 | -- | 61012 |
| Elongation (%) | 1.5 | 1.5 | 1.09 |
| Thickness (mm) | -- | -- | 0.381 |

* Supplied by the manufacturer data sheet (SIKA, 2008)

## 3.7 Induced Corrosion

The level of corrosion damage induced in the beams varied from a 0% to a 15% theoretical mass loss. The theoretical mass loss was calculated using Faraday's law:

$$m = \frac{Ita}{ZF}$$

where, m is the mass loss (g), I is the corrosion current (A), t is the corrosion time (s), a is the atomic weight (56 g for iron), Z is the valence of the corroding metal (2 for iron) and F is Faraday's constant (96,500 A.s).

In order to achieve the required level of corrosion, an accelerated corrosion technique was applied. In this technique the corrosion process was activated by the chloride salts in the concrete and accelerated by an electrical polarization of the steel reinforcement. The amount of chlorides (2.15% by weight of cement) added to the concrete mix was sufficient to depassivate the reinforcing steel and initiate corrosion, since it was larger than the corrosion threshold value (ACI Committee 222, 2001). The beams were subjected to a constant current density of 150 $\mu A/cm^2$ using power supplies as recommended by El Maadawy & Soudki (2003). To ensure a constant current in the beams, the steel reinforcement bars of the beams were connected in series and the direction of the current was adjusted so that the tension steel

served as the anode and the stainless steel served as the cathode (Figure 3.12). This caused the main reinforcing bars to act as anodes and hence corrode in the salted zone. During corrosion the beams were placed in a special chamber where the required moisture and oxygen for the corrosion process were provided continuously. For the desired current density of 150 μA/cm$^2$, the net current in the salted zone was estimated to be 38 mA for Group 2-Set 1 beams (anchorage length = 200 mm) and 66 mA for group 1 beams and Group 2-Set 2 beams (anchorage length = 350 mm). The current is the product of the current density and the surface area of the reinforcing bars within the salted zone. Calculations for the induced corrosion level are shown in Appendix B. Since the stirrups in the salted zone were epoxy-coated, they were not included in the current calculation. The corrosion time calculated from Faraday's law was up to 52 days for a 5% mass loss and 157 days for a 15% mass loss. As reported by the literature (Al-Hammoud, Soudki, & Topper, 2011; Badawi & Soudki, 2005) the mass loss calculated from Faraday's law over-predicts the mass loss at a low corrosion level and under predicts the mass loss at a high corrosion level. Accordingly, the beams that were corroded to a 15% theoretical mass loss were corroded under the induced current technique for 204 days instead of the 157 days calculated from Faraday's law to ensure the desired mass loss.

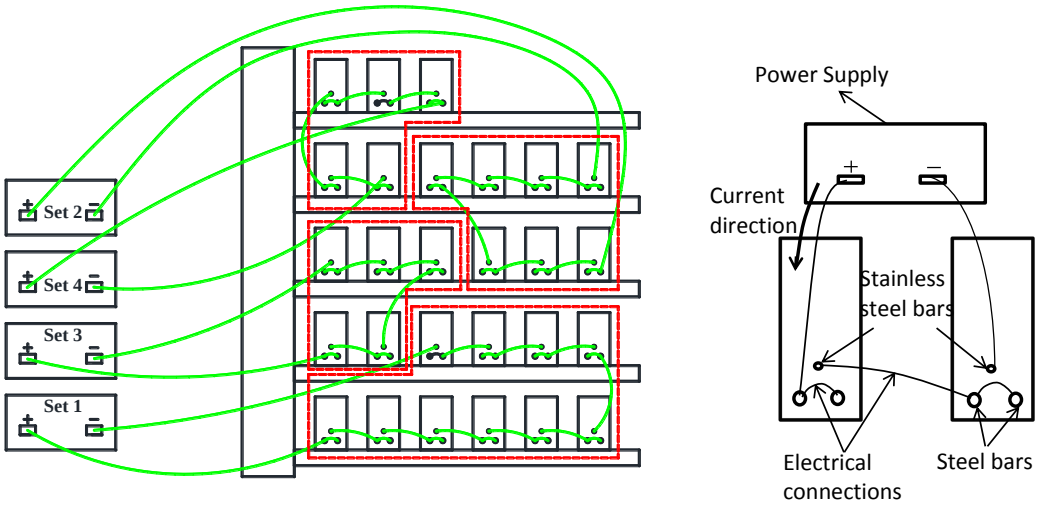


(a) (b)

**Figure 3.12: A schematic drawing of (a) the corrosion chamber setup with the beams divided in sets in series, (b) the electrical connections for the accelerated corrosion setup.**

## 3.8 Evaluation of Corrosion

The corrosion level of the steel reinforcement in the beams was determined using a mass loss analysis. The mass loss measurement was done using a destructive test described in ASTM Standard G1-03 (2011). After the beams were load tested to failure, the tensile steel reinforcement from the corroded zone was extracted. The mass loss analysis was carried on a 180 mm and 330 mm long sections of the steel reinforcement from Set 1 and Set 2 beams respectively following the procedure described in Appendix C.

To accelerate the corrosion process, the beams were placed in a special chamber ensuring a continuous mixture of moisture and oxygen and were subjected to a constant current density of 150 $\mu A/cm^2$.

## 3.9 Testing

### 3.9.1 Instrumentation

Linear variable differential transducers (LVDTs) were used to measure the slip in the bonded region of the bars relative to the concrete from the loaded end (pocket) and the free end. The LVDTs had a range of 50 mm and accuracy of 0.01 mm. An LVDT, with a range of 100 mm and accuracy of 0.01 mm, was used to measure the beam deflection at midspan.

Electrical resistance strain gauges (manufactured by Tokyo Sokki Kenkyujo Co., Japan) that had a resistance of 120 Ω and gauge lengths of 30 and 5 mm were used. The 5 mm strain gauges were placed on the steel in the pocket, and inside the steel bar in a groove along the bonded length. A groove of 6 mm width by 5 mm depth was formed in one of the 20M deformed bars in each beam from the straight end. The length of the groove formed in the bar was 575 mm for the beams in group 1 beams and group 2 - Set 1 (200 mm anchorage length) and 630 mm for the beams in group 2- Set 2 (350 mm anchorage length). Three strain gauges were installed in this groove at equal spacings (80 mm for group 2- Set 1 beams and 150 mm for group 1 beams and group 2- Set 2 beams) in the anchorage length to be tested. The epoxy SIKADUR 330 was used to fill the grooves and protect the strain gauges during casting and the corrosion exposure. Also 30 mm strain gauges were placed on the CFRP sheets used for confinement at the bonded section of the wrapped beams.

Thirty-two of the reinforcement bars from group 2 beams were gun drilled with a hole diameter of 10 mm to a depth of 550 mm. The holes were then cleaned with acetone and air pressure. Fibre optic sensors were installed in half of these bars and encapsulated strain gauges (Figure 3.13) were installed in the other half. The encapsulated strain gauges had a 1.7 mm wide strain gauge entirely coated with an epoxy resin forming an 8 mm wide encapsulation. To fit the encapsulated strain gauge in the bar the gun-drilled hole diameter had to be 10 mm. The gun-drilled hole in the bar where the FOS was installed was kept at 10 mm (although it did not need to be this wide) to allow for a comparison between the two bars in one beam (each beam had 2 bars: one with encapsulated strain gauges and one with FOS).

Fibre optic sensors and encapsulated strain gauges were used to measure the strains along the length of the bar in the corroded repaired beams from group 2. Due to corrosion, the bar surface was expected to damage the adhesion of the strain gauges placed on the surface of a bar. Accordingly, the strain gauges and fibre optic sensors were placed inside the gun-drilled bars. Sikadur 52 was used to attach the fibre optic sensors and the encapsulated strain gauges to the inside of the rebar. The fibre optic sensors used were multiplexed fibre Bragg grating (FBG) sensors and had the following characteristics: custom FBG sensor array, FBG center wavelengths: 1520nm – 1540nm – 1560nm – 1580nm (+/- 0.5 nm tolerance) 5000με Rated FBG, >50%R, <3nm BW, >15dB isolation, 1 each fusion-spliced 8m jumper (with heavy duty 3mm type buffer cladding), 1 each FC/APC.

To place the FBG sensors, a small weight was introduced at the end of the lead wire to make sure that the FBG sensors reached the bottom of the hole in the rebar. This confirms that the strain readings of the arrays were taken at the points specified along the length of the bar. The encapsulated strain gauges were placed as follows. To ensure the position of the strain gauge along the length of the bar, the wires of three encapsulated strain gauges just close to the strain gauge were glued to a 1.5 mm diameter steel rod. The steel rod was then placed in the gun-drilled hole inside the bar. The holes for both the FBG sensors and the encapsulated strain gauges were then filled with epoxy. The spacing between the arrays of the FBG sensors was 50 mm and 70 mm for the beams with anchorage zones 200 mm and 350 mm respectively (Figure 3.14). The spacing between the encapsulated strain gauges was about 80 mm and 150 mm for the beams with anchorage zones 200 mm and 350 mm respectively (Al-Hammoud, Soudki, & Topper, 2011).

Initially, the plan was to test 16 beams from group 2 with FBG sensors. While placing the FBG sensors in the gun-drilled holes, two sensors broke, and during handling the beams, another 6 sensors were damaged due to breaking of the output wire close to the edge of the bar. Hence only 8 beams had working FBG sensors.

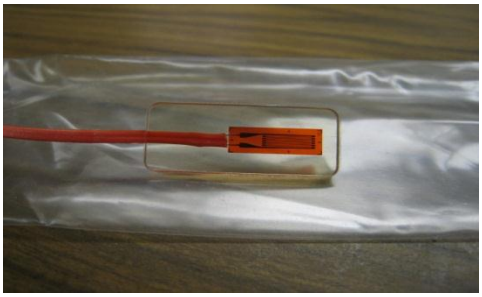

**Figure 3.13: Encapsulated strain gauge.**

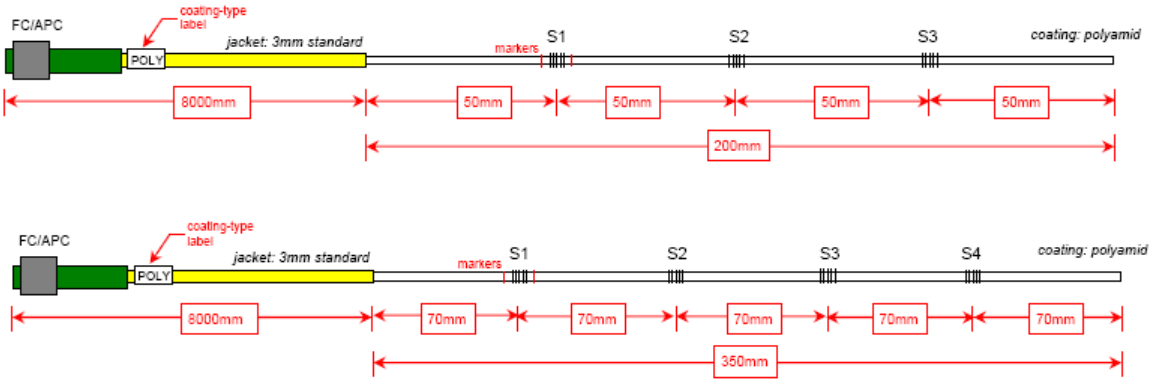


**Figure 3.14: Details of fibre optic sensors.**

The load was applied using a servo-controlled hydraulic actuator controlled by a MTS SE controller. The load was measured using a 333 kN load cell with an accuracy of 0.1 kN.

The readings of the strain gauges, the LVDTs and the load cell were recorded using a National Instrument SCXI data acquisition system at a sampling rate of 20 readings per second and saved in a computer. The readings from the multiplexed FBG sensors were recorded using a sm130 Optical Sensing Interrogator module through "ENLIGHT", Micron Optics Sensing Analysis software in another computer. The data from the two computers were then synchronized with the help of a fixed time stamp recorded on both computers.

### 3.9.2 Beam preparation for testing

The beams from the two different groups were prepared differently for testing. For the beams from group 1, the beam end supports consisted of an end plate that was fixed to the beam by bolting it to the cast-in anchors from the anchorage zone end. This end plate rested in a roller. At the other end (hooked bar end), the beam was sitting on a half circle steel plate resembling a pin.

As for the beams from group 2, two L-shaped steel plates were glued to the beam using SIKAdur 30 at the support point (Figure 3.16). The properties of Sikadur 30 are given in Table 3.6. The supports were glued to the beam so that the L-shaped plate would not touch the beam at the support point. This helped eliminate the confinement effect that would be caused by the supports under loading. Several tests were done using concrete blocks of alternate methods of attaching the steel supports to the ends of the beam. In the end the steel supports were sandblasted and a piece of corrugated thin rubber roughened with sandpaper was placed between layers of epoxy separating it from the steel plate on one side and the concrete surface on the other. The rubber caused the distribution of stress along the surface of the concrete to become more uniform.

**Table 3.6: Sikadur 30 tensile properties (as supplied by the manufacturer).**

| Type | Tensile strength (MPa) | Modulus of elasticity (MPa) | Elongation at break (%) | Number of days to reach design strength |
|---|---|---|---|---|
| Sikadur 30 | 24.8 | 4,500 | 1 | 7 |

### 3.9.3 Loading procedure

Two different types of loading were used: monotonic loading and repeated loading. For both monotonic and repeated loading, the beams were subjected to four point bending. The load was applied through a spreader steel beam that transferred the load to the beam through two point contacts that are 650 mm apart for group 1 beams (Figure 3.15) and 600 mm apart for group 2 beams (Figure 3.16). The loading system produced a constant moment region in the middle third of the beam specimen. Figure 3.15 and Figure 3.16 show the test setup for beams from group1 and group 2 respectively.

In the monotonic loading test, the beam was loaded in displacement control. The displacement was increased at a rate of 1.5mm per minute until the beam failed.

The fatigue tests were performed under load control. Load was applied manually using the set point control on the controller until the desired maximum load was reached and then the load was decreased to the mean load. Thereafter, a sine wave load cycle was applied about the mean load using the MTS 407 controller at a frequency of 1 Hz. The minimum load was set at 10 kN, so that the beam would not slip or bounce. The maximum load levels were varied to give fatigue lives of between 10,000 and 1,000,000 cycles. Those fatigue lives were chosen to produce an S-N curve covering the fatigue lives of interest to designers.

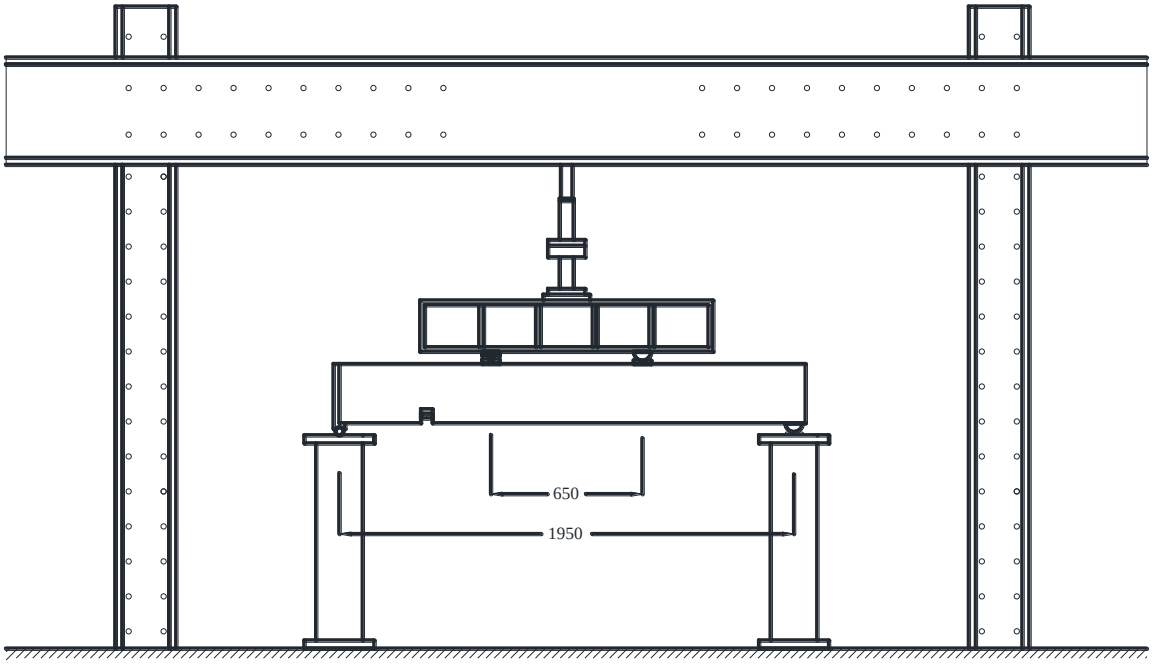


**Figure 3.15 Schematic drawing of the test setup for group 1 beams.**

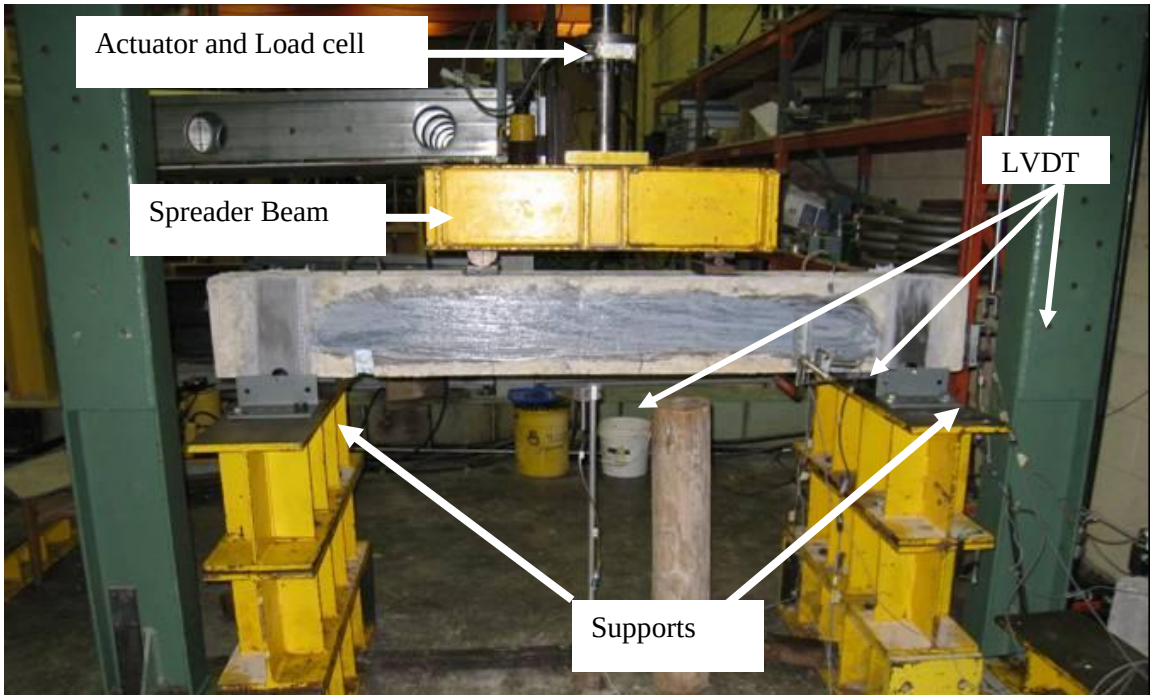


**Figure 3.16: Test setup for group 2 beams.**

# Chapter 4
# Experimental Results_ Group 1 Beams

## 4.1 Introduction

In this chapter the confinement effect from the supports and stirrups on the bond behaviour of beams under static and repeated loading are discussed. Sixteen beams were tested in group 1 for the purpose identified above and are discussed in this chapter.

## 4.2 The confinement effect of the supports

The first objective in testing beams M-A-100-0-1, M-A-100-0-2, M-A-100-0-3 and M-A-100-0-Spiral was to study the confinement effect of the supports on the bond between the steel reinforcement and the concrete. The second objective was to obtain the static capacity of the beams with stirrup configuration A. It is known that the bearing force of the supports confines the concrete around the reinforcing bar. An attempt was made to eliminate this confinement effect of the supports by using different supports. However the different support conditions investigated failed to carry the loads applied.

The beams differed in only one variable which was the support condition. In beam M-A-100-0-1, the supports were not in contact with the bottom of the beam at the start of the test, they were only fixed to the beam from the end through the cast-in anchors, hence providing no confinement to affect the bond. The ultimate load reached by this beam was 114.9 kN. The observed beam behaviour was as follows: cracks along the length of the cast-in anchors were observed at about 34kN, however the beam continued to carry load until splitting failure occurred along the cast-in anchors at 65kN causing the supports to fail. The load dropped to 47 kN and remained at this level until the mid-span displacement reached about 7.4mm and the supports touched the beam. Then the load increased again. The beam reached a maximum load of 114.9 kN and a mid-span displacement of 12.5mm with respect to the initial end level before the supports touched the beam. The slip at maximum load was about 2 mm. After the load dropped, the beam continued to carry load with increasing slip. Figure 4.1 shows the load versus mid-span displacement curve of beam M-A-100-0-1.

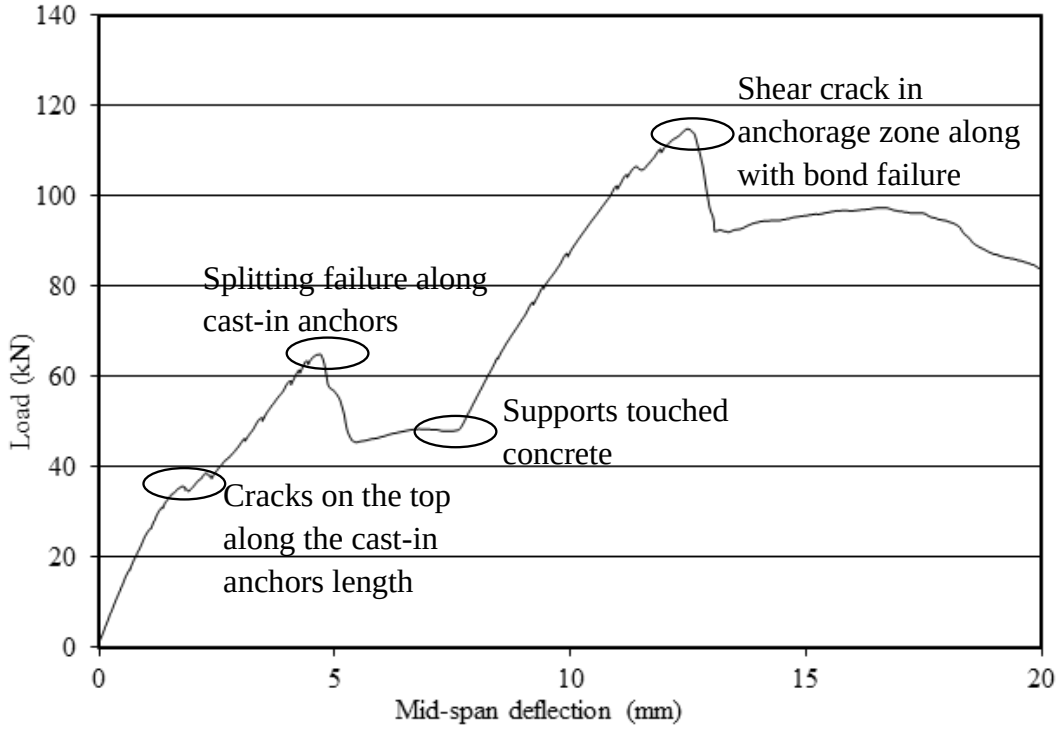


**Figure 4.1 Load versus mid-span deflection curve for Beam M-A-100-0-1.**

In Beam M-A-100-0-spiral, steel spirals (made of 6.1 mm steel rods) were added before casting around the cast-in anchors (Figure 4.2). This was done in an attempt to avoid cracking of the concrete around the cast-in anchors. Spirals reinforced the concrete in a ring diameter of 61.5mm. The support plate was connected to the end of the beam by bolting it into the cast-in anchors, and was not in contact with the beam from the bottom at the start of the test. As the beam was loaded monotonically to failure, cracking of the concrete along the bottom of the spirals surrounding the cast-in anchors started at 56 kN causing the load to drop slightly before increasing again. Shear cracks were visible at a load of 67 kN. A splitting crack along the cast-in anchors occurred at a load of 92 kN. Splitting cracks occurred along the length of the reinforcement bars in the anchorage zone at a load of 97 kN. The beam continued to carry load until it reached its maximum load of 104.2 kN at a bar slip from the free end of about 5 mm. Concrete cracked all around the cast-in anchors and the load decreased slowly with increasing slip in the bar. The increase in compression strength around the cast-in anchors due to the presence of the spirals was not enough to prevent cracking of the concrete in that section and to keep the supports from touching the beam soffit.

In beam M-A-100-0-2, the supports at the end of the beam were in complete contact with the bottom of the beam from the beginning of the test. Shear cracks appeared at a load of 84 kN from the hooked end of the beam and at a load of 101 kN from the non-hooked end (the beam end under study) accompanied by a small reduction in the load. The beam then reached a maximum load of 112 kN at a slip of 1.5mm. Then the slip in the bars continued to increase with decreasing load.

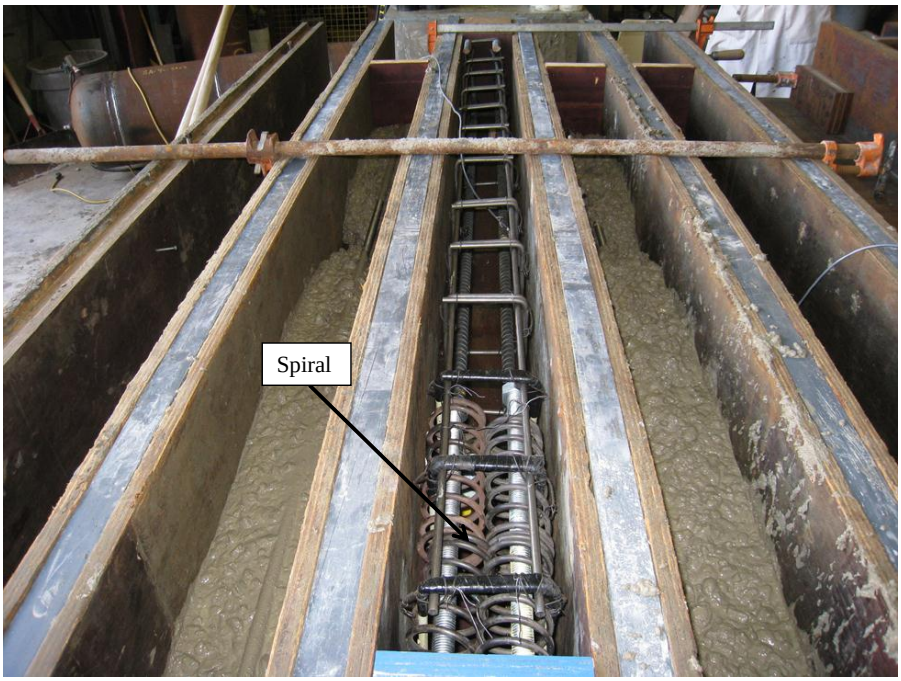


**Figure 4.2 Beam M-A-100-0-spiral cage in form.**

In beam M-A-100-0-3, the supports were in contact with the bottom of the beam only at two points (partial contact) (Figure 4.3). The maximum load reached was 96.9kN with a slip of 0.5mm. After the maximum load, the residual load capacity dropped with increasing slip.

Fixing the end support with the cast-in anchors to avoid contact of the support plate with the bottom of the beam caused the concrete to crack in the upper section. Since the methods of supporting the beam without contact at the bottom with the supports failed to achieve their objective, and no difference in the capacity of the beams with partial contact support or full contact support was noticed, the rest of the tests from this group were carried out with the supports in contact with the bottom of the beams.

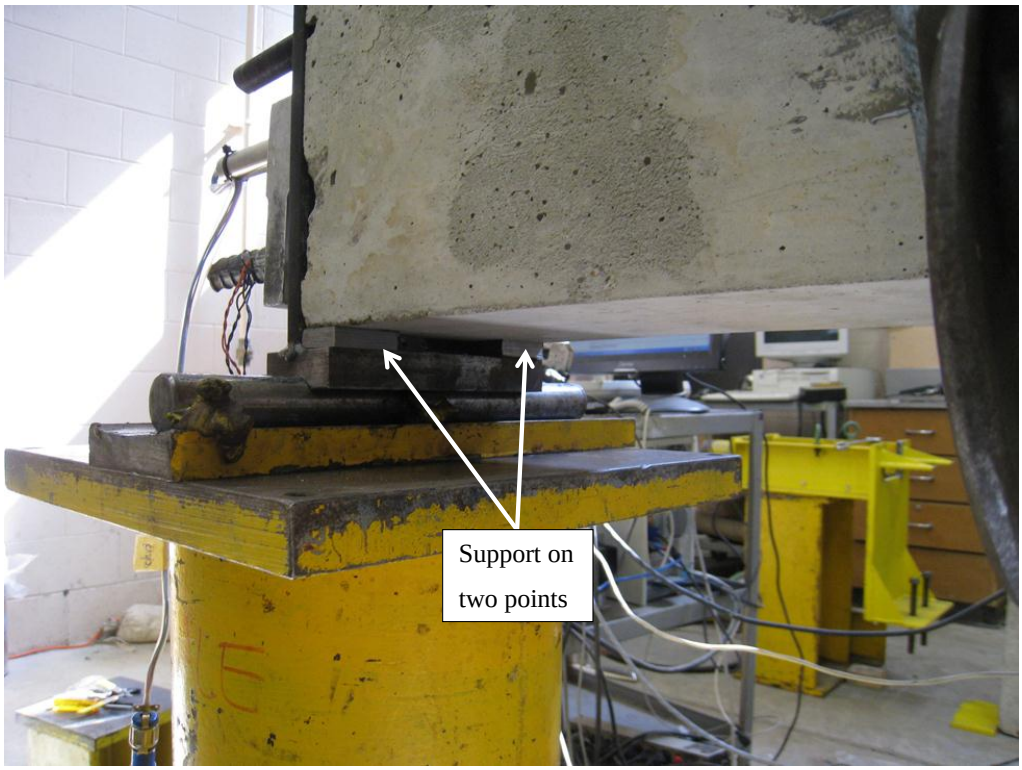


**Figure 4.3 Beam M-A-100-0-3, the supports were in contact with the bottom of the beam only at two points.**

## 4.3 Static capacity of the control beams

### 4.3.1 Beams with Stirrup Configuration "A"

Beam M-A-100-0-U had a similar configuration to beam M-A-100-0-2, the only difference was that in Beam M-A-100-0-U the reinforcement bar was unbonded except in the anchorage zone (350 mm) and the hooked bar end. This reduced the anchorage zone from 650 mm in Beam M-A-100-0-2 to 350 mm in Beam M-A-100-0-U. Figure 4.4 shows the load versus mid-span deflection curve and Figure 4.5 shows the load versus slip for Beam M-A-100-0-U.

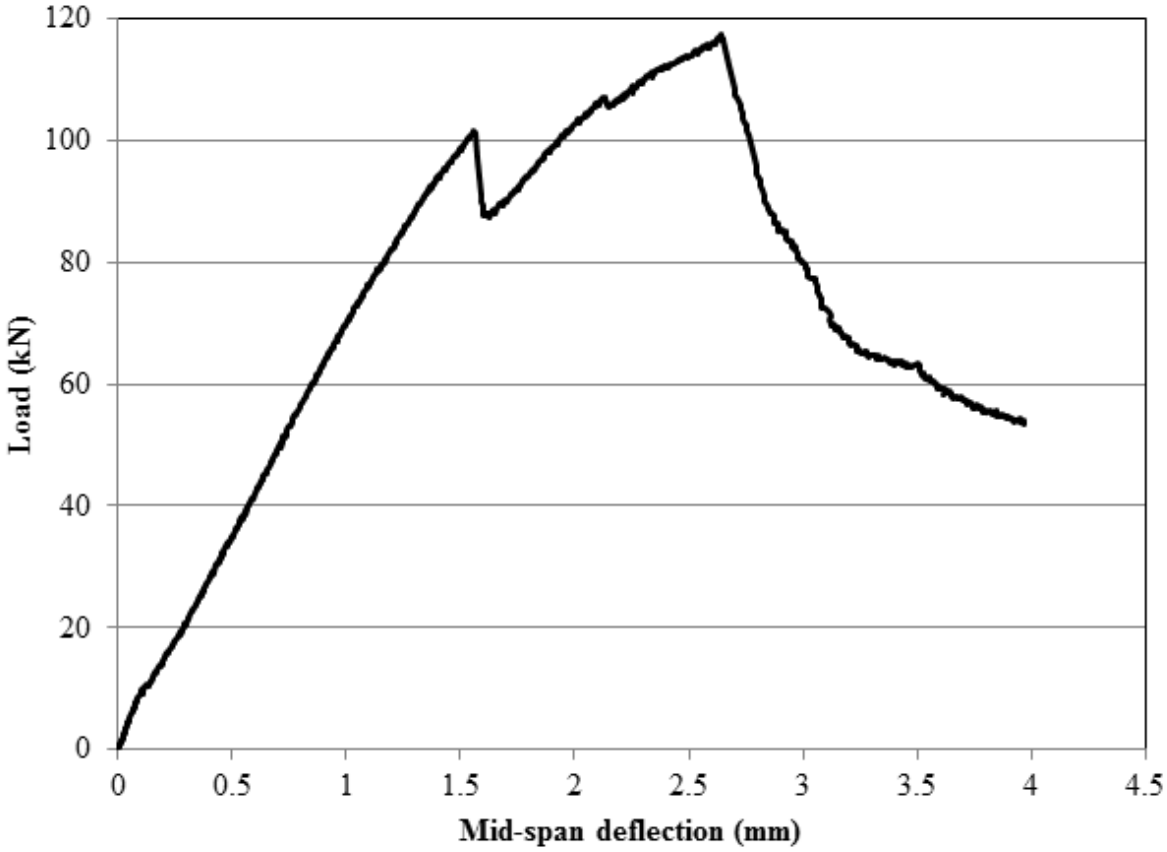


**Figure 4.4 Beam M-A-100-0-U load versus mid-span deflection curve.**

Where the reinforcement in beam M-A-100-0-U was unbonded in the constant moment region, the flexural cracks were wide but limited in number. During loading, a vertical crack appeared in the middle section of the anchorage zone (at about 170 mm from the support) reaching a height of about 70 mm and extended across the bottom of the beam. With continued loading, this vertical crack joined with a diagonal crack that formed along the side of the beam. This diagonal crack occurred at an applied load of about 100 kN and was accompanied by a drop in the load to 89 kN and by an increased slip in the bar of about 0.2 mm from the free end for both bars (Figure 4.5). The beam then continued to carry load until it reached a load of 117 kN and a free end slip of 0.9 mm after which the load decreased continuously with increasing slip. This was accompanied by a horizontal crack that propagated while the load increased along the horizontal reinforcement suggesting debonding of the steel from the concrete. Both beams, M-A-100-0-U and M-A-100-0-2, had similar

maximum bond static capacities despite the difference in anchorage zone lengths. This behaviour is discussed further in Section 4.6.

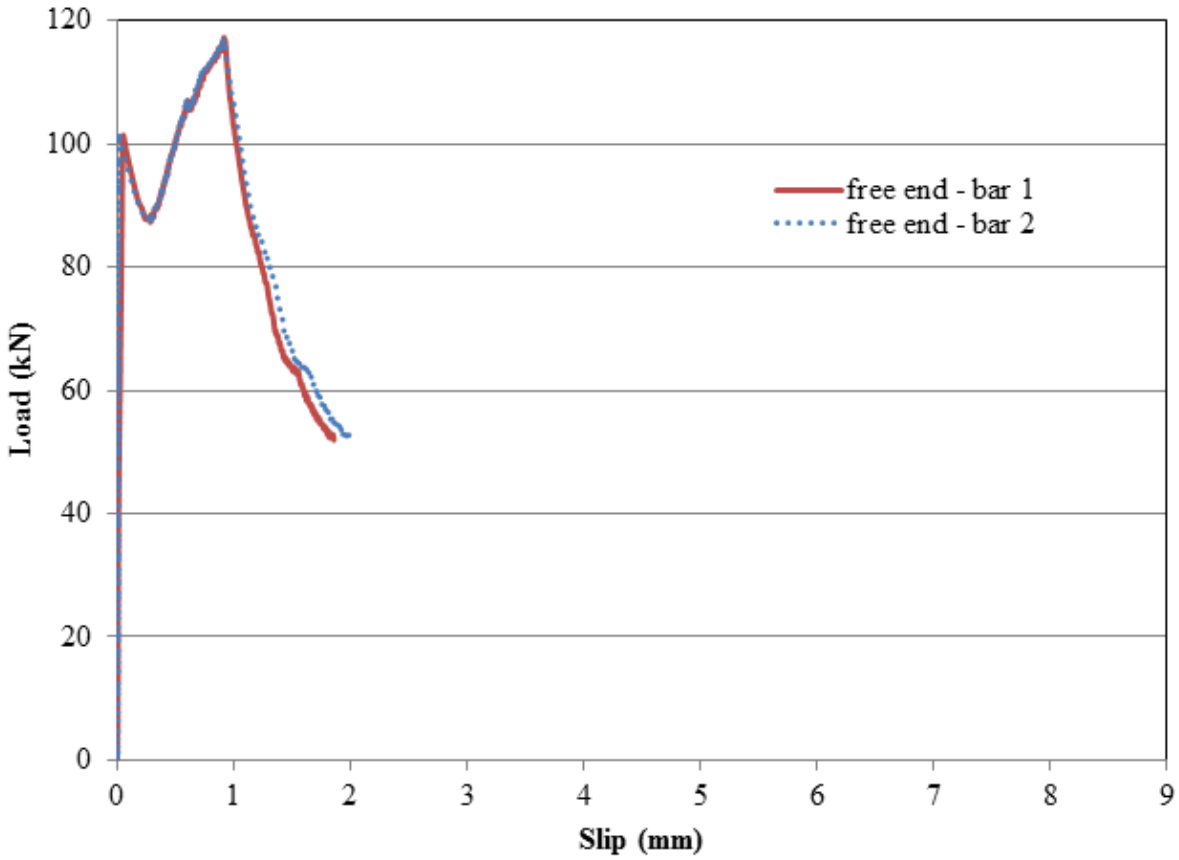


**Figure 4.5 Load versus slip from free end for Beam M-A-100-0-U.**

Diagonal cracks appeared in the beams with stirrup configuration A. Such diagonal cracks were not observed in a previous study done by Al-Hammoud, Soudki & Topper (2010). The differences between the beams in the previous study (Al-Hammoud, Soudki, & Topper, 2010) and Beam M-A-100-0-U in the current study were: 1) the stirrup spacing which was 125 mm instead of the present 150 mm spacing, 2) the bar anchorage zone was 200 mm instead of 350 mm and 3) the distance between the support and the point load varied from 525 mm for the previous study to 650 mm for the current beams. Accordingly Beam M-A*-100-0-U was fabricated with a 350 mm anchorage length and a stirrup spacing of 125 mm instead of 150 mm to investigate the reason for the difference between the above results.

Beam M-A*-100-0-U was loaded monotonically to failure. Figure 4.6 and Figure 4.7 show the load versus mid-span deflection and load versus slip curves for Beam M-A*-100-0-U.

Similar to beam M-A-100-0-U, as the load increased a vertical crack appeared at a distance of about 111 mm from the support in the anchorage zone. With increasing load this vertical crack then joined with a diagonal crack that appeared in the anchorage zone. The diagonal crack was accompanied by a drop in the load. This diagonal crack changed into a horizontal crack along the length of the bar that progressed toward the support (Figure 4.8). The beam continued to carry load until it failed at 113 kN with a recorded bar slip of 0.66 mm. The load then decreased with increasing slip until it reached a load of 60 kN at a 1.5 mm slip (Figure 4.7). The bottom concrete in the anchorage zone spalled off. The concrete around the bar was examined by dissecting the beam. The concrete keys from the bottom part of the beam remained intact. This is due to the fact that the bottom concrete spalled off eliminating any further resistance of this concrete to bar slippage. After removing the stirrups and the reinforcement, it was noted that the concrete above the bar was partially crushed in between the stirrups. The concrete was completely crushed around the middle stirrup in the anchorage zone. It was also noted that the concrete keys were completely crushed in the region above and close to the support in a manner resembling a pull-out failure (Figure 4.9).

Beam M-A*-100-0-U (stirrup spacing at 125 mm) behaved similarly to other beams in this study that had stirrup configuration “A” (stirrup spacing at 150 mm), suggesting that the presence of the diagonal shear cracks was not due to the change in stirrup spacing from 125mm to 150 mm. Increasing the anchorage length from 200 mm (Al-Hammoud, Soudki, & Topper, 2010) to 350 mm or 650 mm as presented in this group of the current study increased the capacity of the beam to above the concrete shear strength causing the concrete to crack.

The static capacity of the beams with stirrup configuration “A” was on average 112 kN.

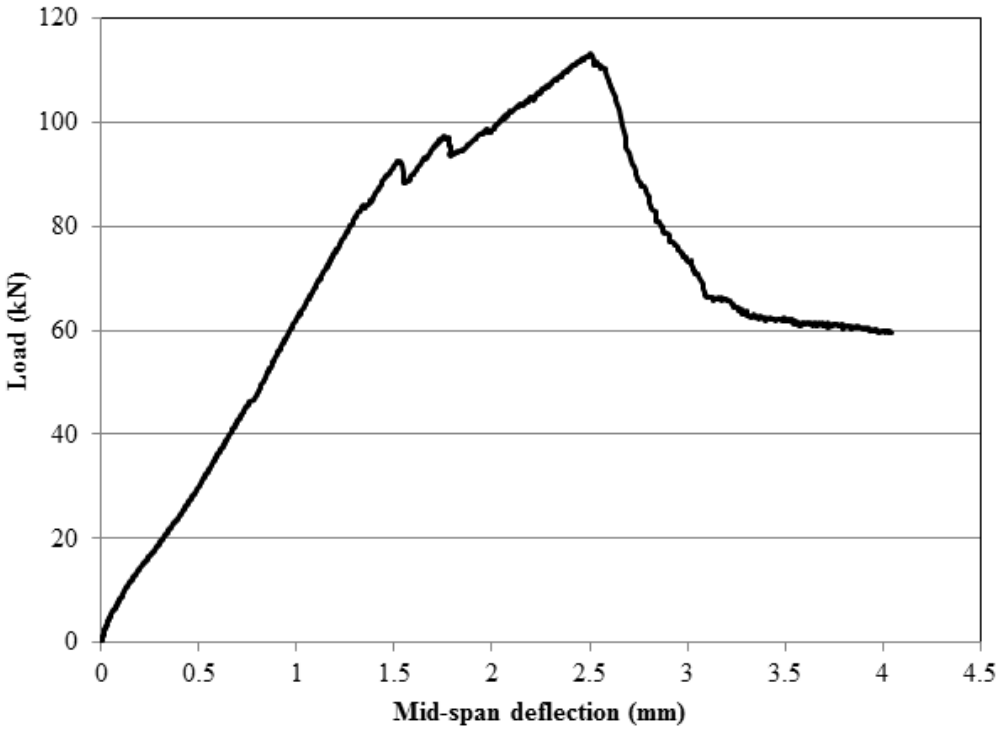


**Figure 4.6 Load versus mid-span deflection curve for Beam M-A*-100-0-U.**

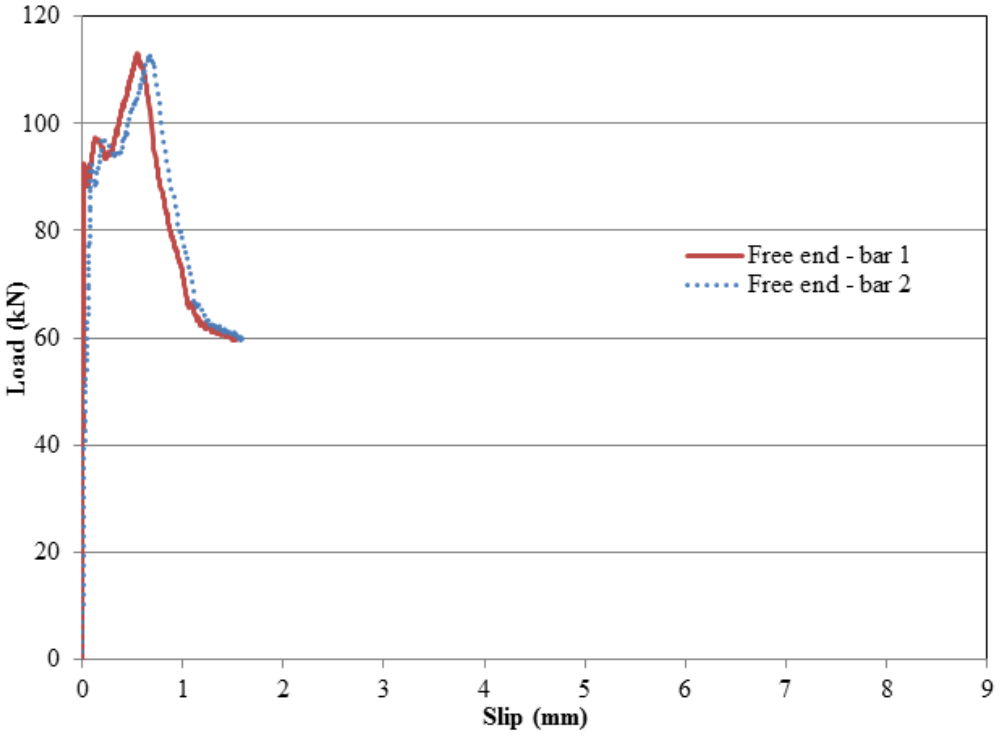


**Figure 4.7 Load versus slip behaviour from free end for Beam M-A*-100-0-U.**

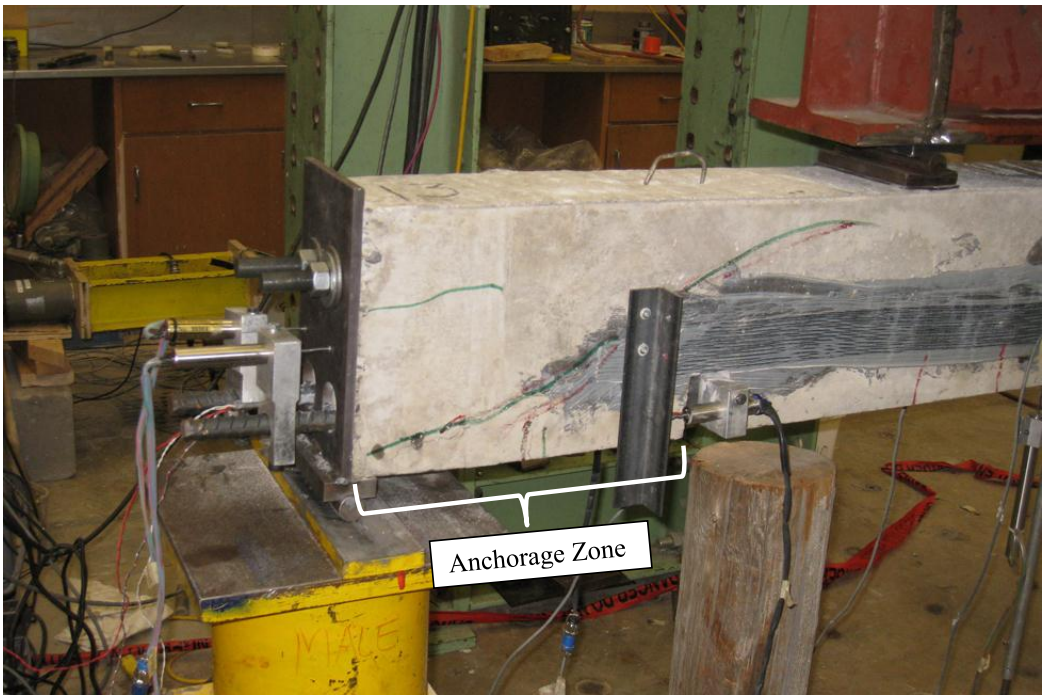


**Figure 4.8 Cracks in the anchorage zone of Beam M-A*-100-0-U.**

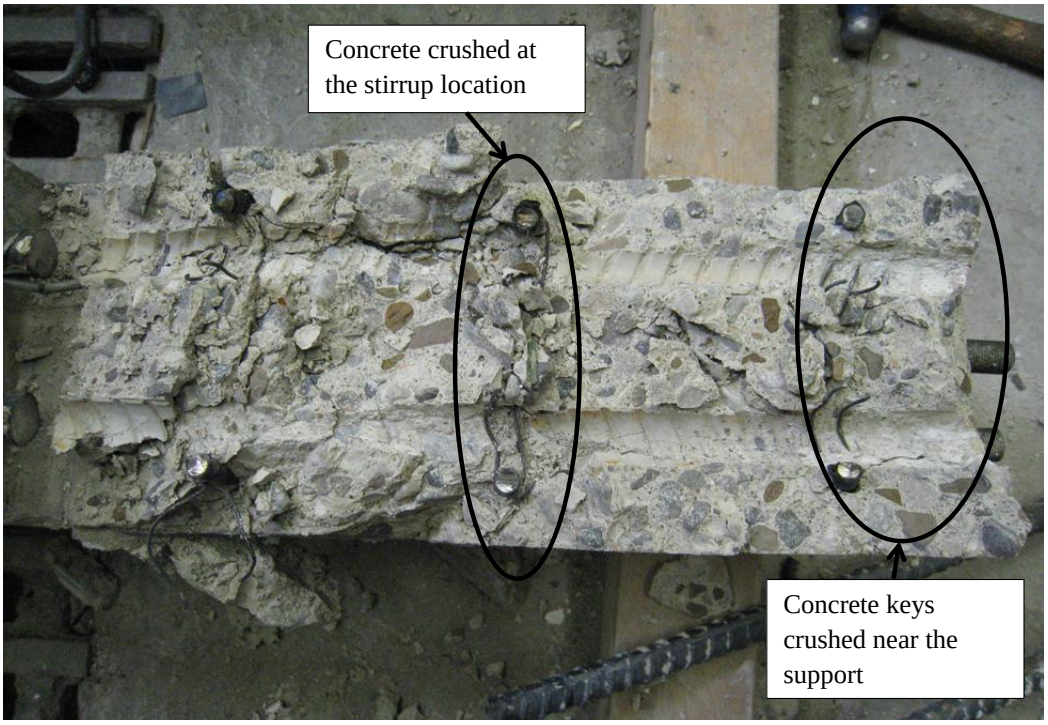


**Figure 4.9 Concrete on top of the reinforcing bar after failure for Beam M-A*-100-0-U. The beam is turned upside-down.**

### 4.3.2 Beams with stirrup configuration B

Beam M-B-100-0-1 was similar to Beam M-A-100-0-1 except for the stirrup spacing which was 75 mm (stirrup configuration B) instead of 150 mm. Beam M-B-100-0-1 was tested monotonically to failure to determine its bond static capacity. The supports were initially not in contact with the bottom of the beam; they were only fixed to the beam from the end through the cast-in anchors. Figure 4.10 shows the load versus mid-span deflection for Beam M-B-100-0-1. The observed beam behaviour was similar to Beam M-A-100-0-1 where cracks along the length of the cast-in anchors were observed at about 51 kN, however the beam continued to carry load until splitting failure occurred along the cast-in anchors at 55kN causing the supports to fail. The load dropped to 46 kN and then continued at this level until the supports contacted the beam soffit and the load increased again (Figure 4.10). The beam failed at a maximum load of 147 kN by concrete crushing in the compression zone (flexural failure). Although the final failure of the beam was by concrete crushing, there was a high slip at maximum load (about 2.0 mm) suggesting that bond failure has also occurred. Figure 4.11 shows the variation of the strain with load along the length of the bar. Two vertical cracks appeared in the anchorage zone at about 130 mm and 230 mm from the support, accompanied by an increase in the strain readings at strain location 2 at about 120 kN load. This is explained as follows: before cracking occurred in the concrete both the steel and the concrete worked together as one section in taking the tension force. After cracking the steel resisted the tension force in the beam and the stiffness of the beam at the crack location decreased. This increased the value of the strain in the bar at the location of the crack compared to the uncracked section. As the load continued to increase, a horizontal crack propagated from the support towards the closest vertical crack and the two strain gauge readings within this section became almost equal suggesting that debonding had happened in this region. In addition, at the maximum load the strain values at strain gauge locations 3 and 4 were equal suggesting that the bar was completely debonded in this section. This is explained further in Section 4.4.

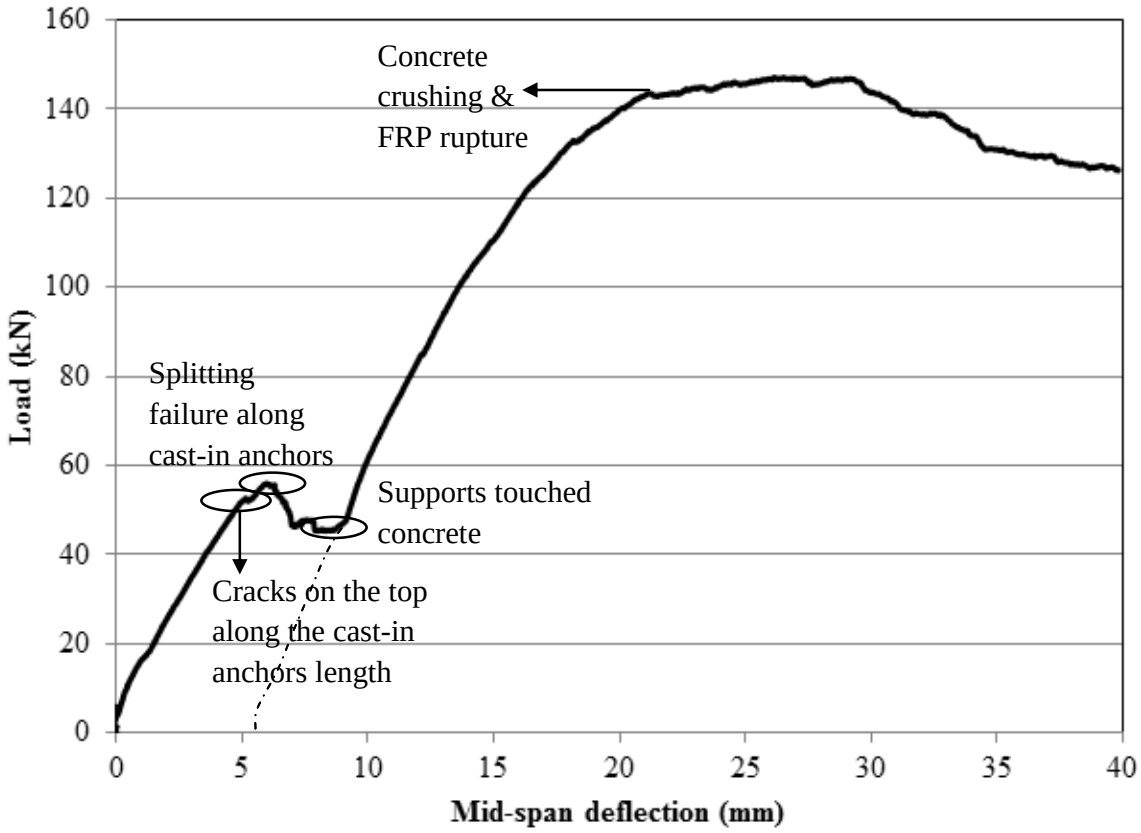


**Figure 4.10 Load versus mid-span deflection for Beam M-B-100-0-1.**

In an attempt to obtain a pure bond failure, Beam M-B-100-0-2 was strengthened by fixing a steel plate to the concrete in the compression zone and tested monotonically to failure, with the supports in contact with the soffit of the beam. The beam reached a maximum load of 145 kN with a free end slip of bar 2 of about 1.8 mm. The load then decreased slowly with increasing slip. The test was stopped when the load dropped to 64 kN with a corresponding free end slip of 8.5 mm (Figure 4.12). When the beam was dissected, it was found that the bottom part of the concrete in between the pocket and the support had spalled off leaving the concrete keys between the lugs intact. The concrete above the bar was examined after removing the bars and was found to be completely crushed along the entire 350 mm length between the support and the pocket (Figure 4.13). This type of failure was expected due to the high confinement force available from the stirrups (FIB, 2000). As the bar started to slip, the stresses introduced bearing forces normal to the steel lugs. The components of this bearing force were a horizontal force that resisted the bar slip and a vertical force that held the bar against the concrete. The stirrups kept the bar from separating from the top concrete

by resisting the vertical component of the force of the lugs on the concrete. Since the stirrups were very close (75mm spacing), there was little bending of the bar in between the stirrups. Accordingly for the bar to slip, the concrete keys had to be crushed. Decreasing the stirrup spacing from 150 mm to 75 mm, that is doubling the amount of stirrups, increased the static bond capacity on average by 30%. The stirrups held the reinforcement in place, so that the lugs on the bar crushed all the concrete keys in the anchorage zone region between the support and the pocket.

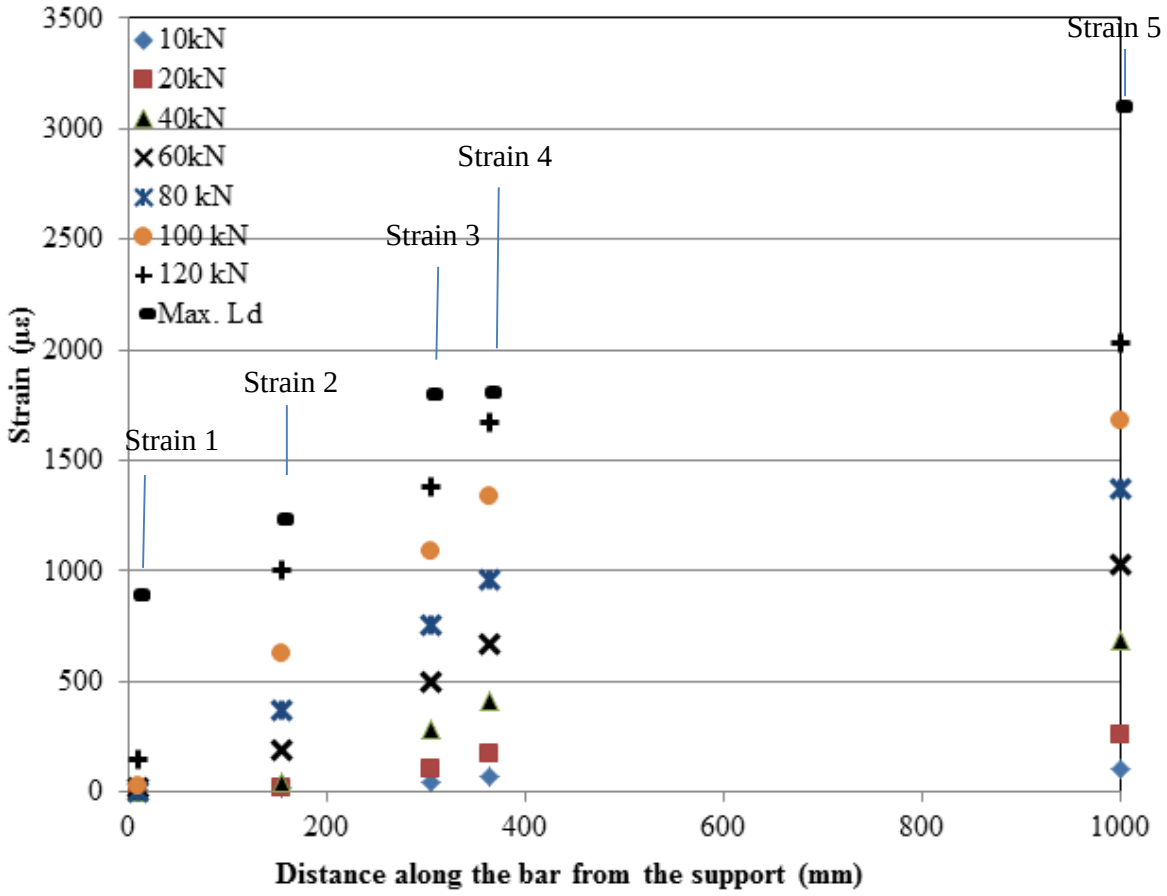


**Figure 4.11 Strain profile for Beam M-B-100-0-1.**

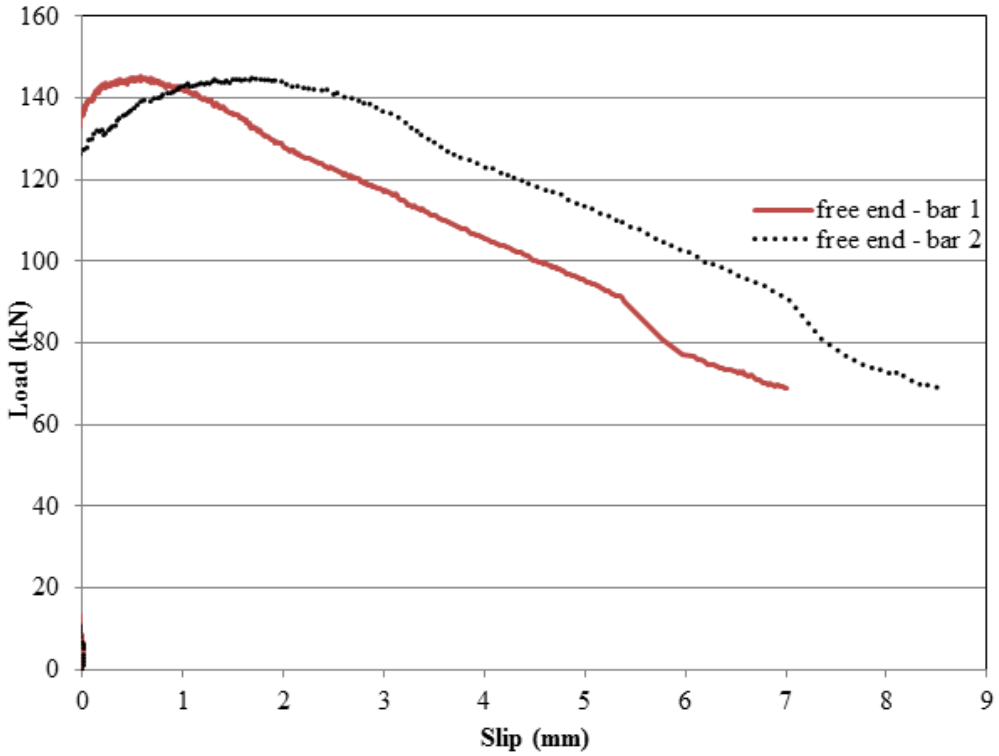


**Figure 4.12 Load versus slip for Beam M-B-100-0-2.**

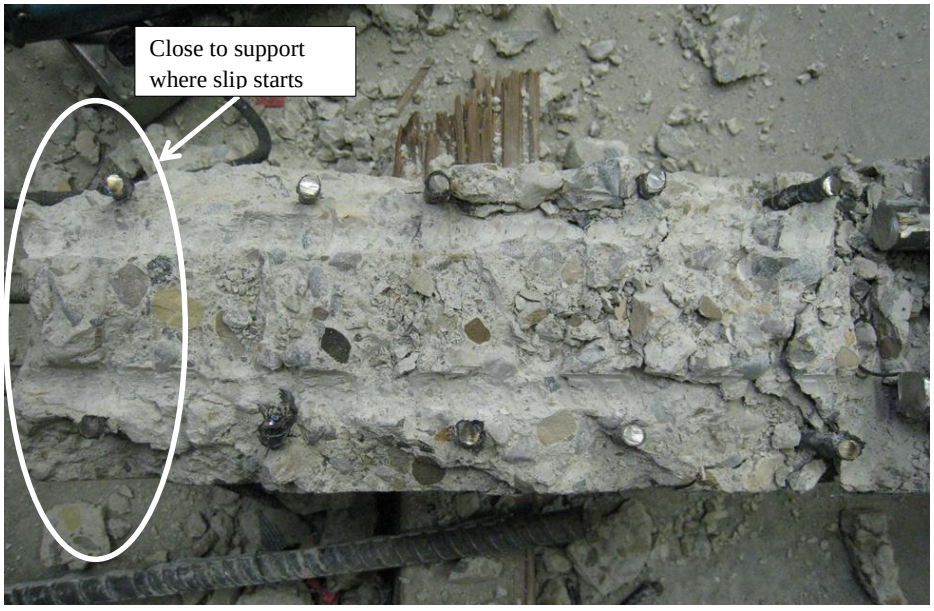


**Figure 4.13 Dissection of Beam M-B-100-0-2 after failure showing the crushing of the concrete keys above the reinforcing bar. The beam is upside-down.**

## 4.4 Stress and Strain Behaviour of a Cracked and an Uncracked Section

Observations of the strain behaviour of the steel bar in the beam help define the debonding stages of the bar and the failure location. While loading, the beam was initially uncracked and the strains were small, and the concrete resisted tensile stresses at the reinforcement level leading to a linear variation of strain versus distance from the support curve as shown by curve 1 in Figure 4.14. As the load increased, the tensile capacity of the concrete was reached and the concrete cracked. At the location of the crack, the tensile forces were taken by the steel reinforcement and the stiffness of the beam decreased leading to increased steel stresses at the location of the crack and accordingly increased strains as shown by curve 2 in Figure 4.14. In between the cracks, the concrete resisted part of the tensile forces leading to a reduced stress in the bar and accordingly a reduced strain as shown by curve 3 in Figure 4.14. The readings from the strain gauges along the length of the bar were compared to the calculated cracked and uncracked strains derived from beam theory. Four options for the strain values were possible leading to four different scenarios:

1. The strain values fell along the strain values for an uncracked section which meant the beam at the location of the strain gauge was uncracked.
2. A strain value fell on the cracked curve indicating that the beam was cracked at the location of the strain gauge.
3. The strain value fell in between the two curves suggesting that the strain gauge was located near a crack and was feeling its effect.
4. The strain value was above the cracked curve which suggested that the bar was debonded in between the strain gauge location and the point where the cracked strain versus location curve had the same value. Curve 4 shows debonding that occurred between points 1 and 2.

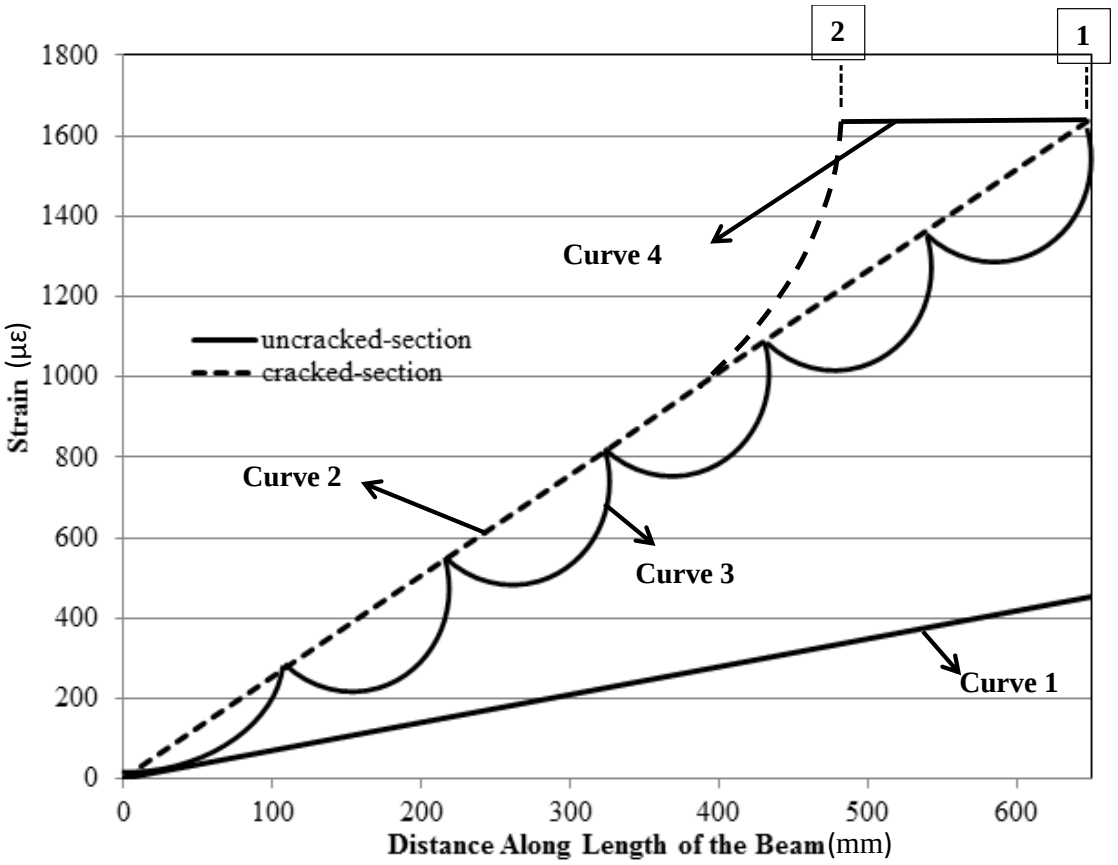


**Figure 4.14 Strain profile showing the different curves that a strain value in the steel bar might reach for a specified load.**

## 4.5 Effect of Corrosion

Beam M-A-100-5 which had stirrup configuration A (a 150 mm stirrup spacing) was corroded to a 4.5% actual mass loss. The actual mass loss was measured according to (ASTM Standard G1-03 (2011)). Figure 4.15 shows corrosion cracks just before testing of the beam. Corrosion cracks were observed along both sides of the beam at the level of the transverse reinforcement. The crack widths along the sides varied between 0.6 mm to 1.5 mm. Two hairline cracks of 0.15 mm were also observed on the bottom of the beam. This beam was tested monotonically to failure. The beam reached a maximum load of 112 kN at a displacement of 12.5 mm, after which the load started to decrease (Figure 4.16). While continuing the test after reaching the maximum load, the bottom concrete spalled off, and the section of the concrete on top of the bar close to the free end crushed and bulged out from

one side of the beam. On the other side of the beam, along the anchorage zone, the reinforcing bar was held only by the stirrups in the area close to the support and was bent in between the stirrups causing the bar to be debonded in this region. The process of debonding between the steel and the concrete can be explained with the help of the strain profiles shown in Figure 4.17. Before cracking occurred in the beam, both the concrete and the steel contributed to the tensile force, and hence the strain profile followed the linear behaviour characteristic of uncracked concrete section. Once cracks occurred, the load and the strains in the bars at the cracked sections increased. At 70 kN applied load, the strain reading from strain gauge 3 (SG3) was 638 με which was above the calculated strain at this location from a cracked section analysis (562 με). This suggested that partial debonding had occurred between this location and the pocket. At 90 kN the reading from SG4 (in the pocket) was 1416 με which was above the calculated strain from a cracked section analysis (932 με). This suggested that debonding had initiated from the pocket towards the point load. From the strain profile (Figure 4.17) it can be seen that SG3 and SG4 values continued to increase with increasing load. The variation in strain values between SG1 and SG2 at 90 kN load was negligible indicating that the bar was debonded in this section and that the bond was holding only at the support. Once the section close to the support debonded, the slip in the bar from the free end increased to 2 mm (Figure 4.18). This slip was accompanied by an increase in the bearing forces of the bar lugs that were pushing the bottom concrete away from the bar and the bar away from the top concrete. The vertical component of the bearing force was counter-acted by a vertical force in the stirrup that prevented the bar from separating from the concrete. The beam continued to support load until the concrete close to the second stirrup crushed at the maximum load of 112 kN. Then the load decreased with increasing slip from the free end as seen in Figure 4.18. This suggested that the beam had failed in bond when the bar slipped from the free end at a load of 112 kN which was approximately equal to the maximum load of the uncorroded beam. In this case corroding the beam to a 4.5 % mass loss did not cause a reduction in the static bond capacity of the beam nor did it change the failure mode.

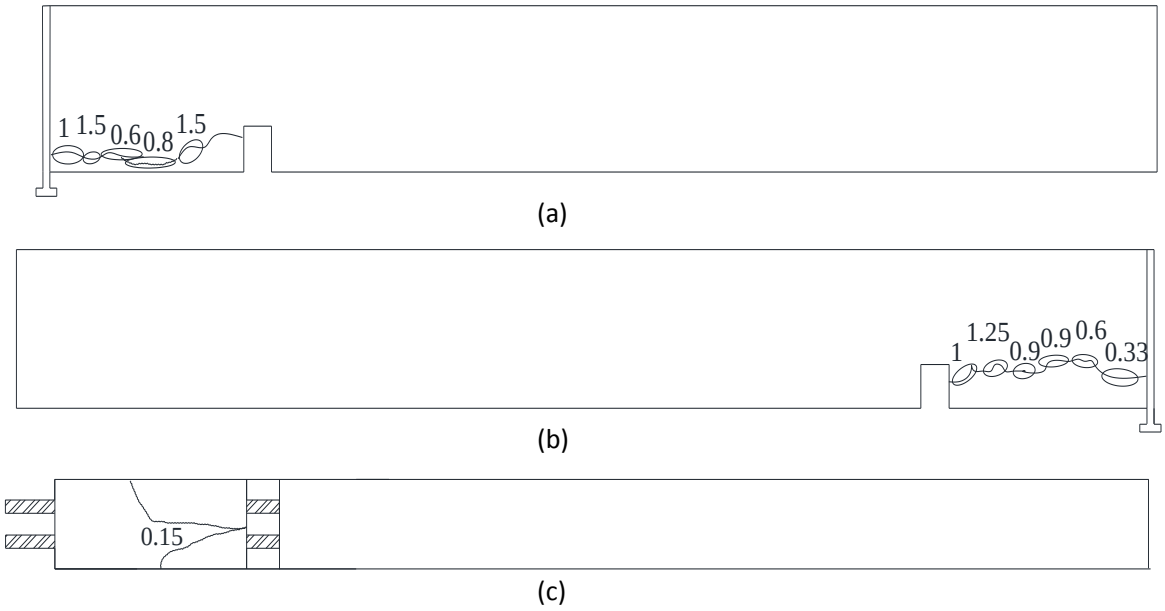


**Figure 4.15 Corrosion cracks before testing of Beam M-A-100-5 from (a) side 1, (b) side 2 and (c) bottom side of beam. The widths of the corrosion cracks are shown in mm.**


**Figure 4.16 Load versus mid-span deflection for Beam M-A-100-5.**

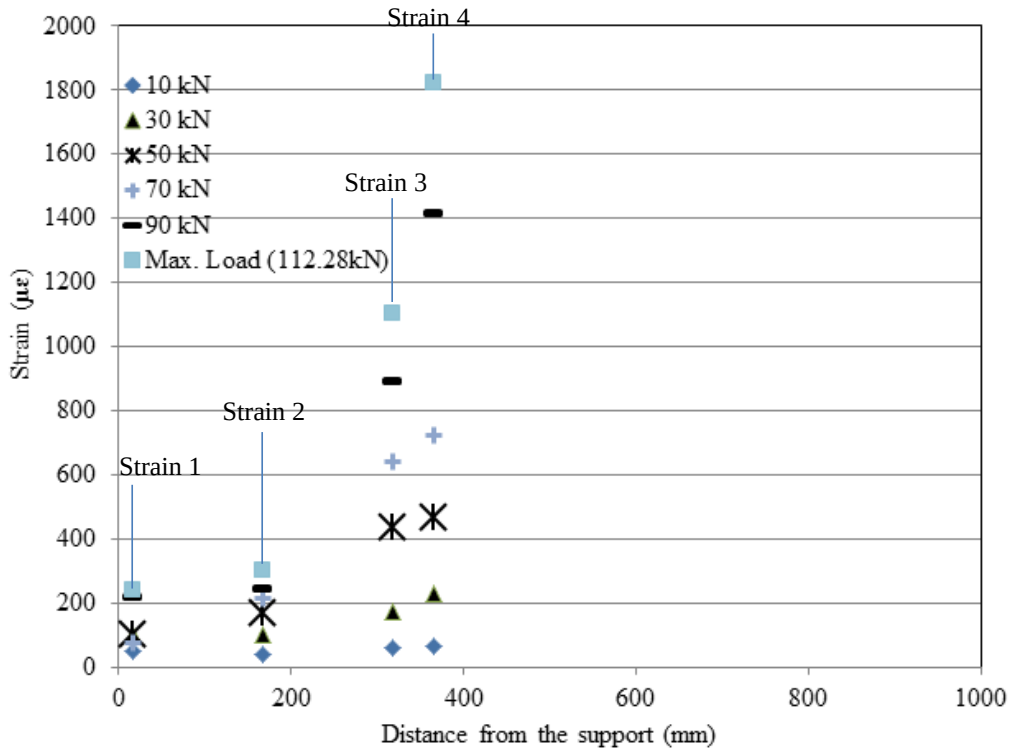


**Figure 4.17 Strain profile along the reinforcing bar of Beam M-A-100-5.**

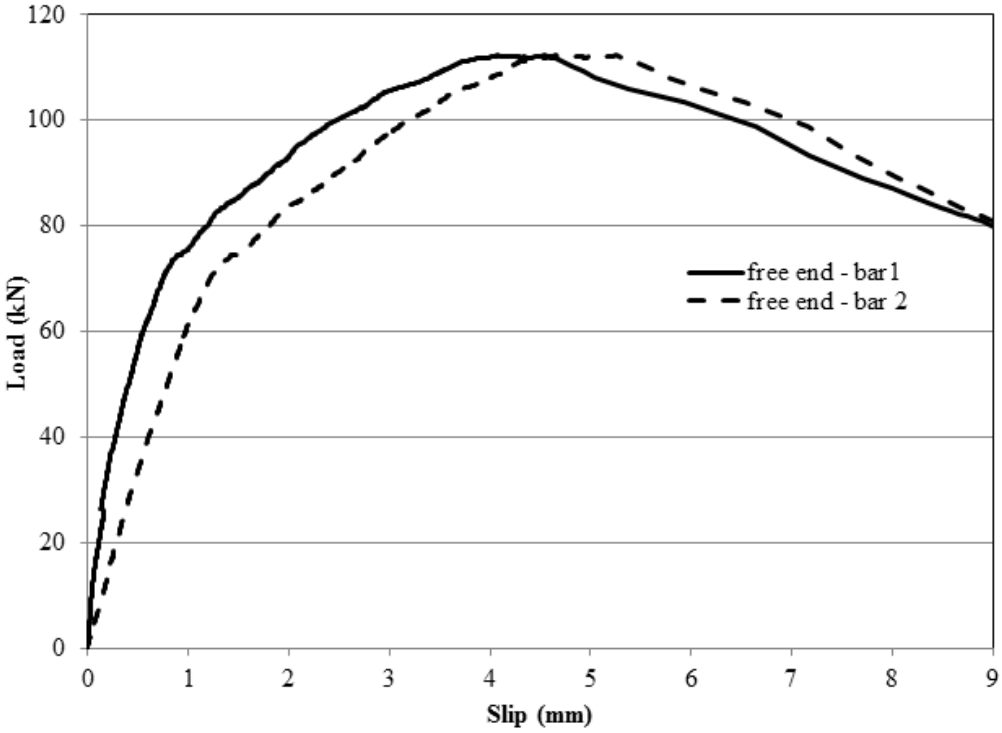


**Figure 4.18 Load versus slip behaviour for Beam M-A-100-5.**

Beam M-B-100-5 which had stirrup configuration B (75 mm stirrup spacing) was corroded to a 4.3% actual mass loss. Figure 4.19 shows the corrosion cracks for Beam M-B-100-5. The corrosion cracks appeared only on one side of the beam at the level of the transverse reinforcement and along the bottom of the beam. The crack widths along the side varied between 0.25 mm and 0.6 mm. At the bottom of the beam, the crack widths varied between 0.15 mm and 0.8 mm. The corrosion crack widths for this beam were smaller than the crack widths of the similarly corroded beam with stirrup configuration A suggesting that the increased number of stirrups confined the concrete and prevented the cracks from opening to the same degree.

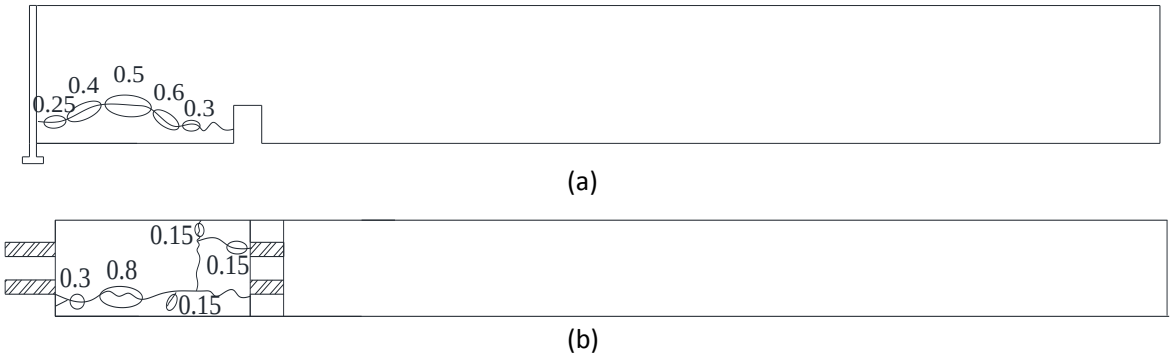


**Figure 4.19 Corrosion cracks for Beam M-B-100-5 from (a) side and (b) bottom faces. Note corrosion cracks were noticed only from one side of the beam. The crack widths are recorded in mm.**

The beam reached a maximum static load of 141.4 kN at a mid-span deflection of 12.8 mm, after which the load started to decrease (Figure 4.20). The concrete was crushed close to the free end suggesting a complete loss of bond in this region. Figure 4.21 shows the strain profile of the bar along the length of the anchorage zone. The strain values from the strain gauge readings were compared to the calculated strains from a cracked section analysis at different load levels. This helped identify the load level at which the concrete section started to debond. At a 30 kN load the concrete section close to SG1 cracked and debonding progressed towards the pocket, this was deduced from the strain value (47 με) at this point that was higher than the calculated strain value for a cracked section analysis (14 με). As the load reached 50 kN, the strain reading from SG 2 (260 με) was above the calculated strain from a cracked section analysis (212 με) which suggested that the concrete at the location of

SG2 had started debonding. The slip in the bar at the free end at this load level was about 0.5 mm. This slip increased the bearing forces on the bar lugs. The vertical components of those bearing forces were resisted by the stirrups. As debonding continued with an increasing load, the forces in the stirrups increased. When a load of 70 kN was reached, the strain reading from SG 3 (702 με) was above the calculated strain from a cracked section analysis (562 με) indicating that the concrete close to SG3 had cracked and started to debond. As the load increased, the difference in the strain values between the locations of SG 1 and SG 2 as well as between SG 4 and SG 2 increased. The increase in the strain differences meant that there was an increase in the force differences in the bar. A higher force difference between SG 1 and SG 2 and between SG 2 and SG 4 suggested higher shear forces that were the result of higher bearing forces acting on the bar as explained later in Section 4.6. The bar was pushed away from the top concrete between the stirrups but was held in place at the stirrup locations. Increased bearing forces resulted in increased forces in the stirrups that prevented the bar from moving away from the top concrete. Checking the concrete keys after failure showed that the top concrete was completely crushed at the stirrup locations before failure occurred. After failure, the bars were removed, and it was observed that the concrete above the bar was completely crushed close to the stirrup locations but that in some areas between the stirrups the concrete keys were not completely crushed. Comparing the static capacity of the corroded beam to that of a similar uncorroded beam (Beam M-B-100-0-2 with a static capacity of 145.3 kN) the reduction was only 2.7% which is within the expected variation of the test results.

It was concluded that in both the above cases, corroding the beams to mass loss of about 4.5% did not cause a significant reduction in the static bond capacity of the beam nor did it change the failure mode. This is due to the fact that the major forces affecting the bond behaviour were the confinement that was provided by the support and the stirrups was not greatly affected by the corrosion.

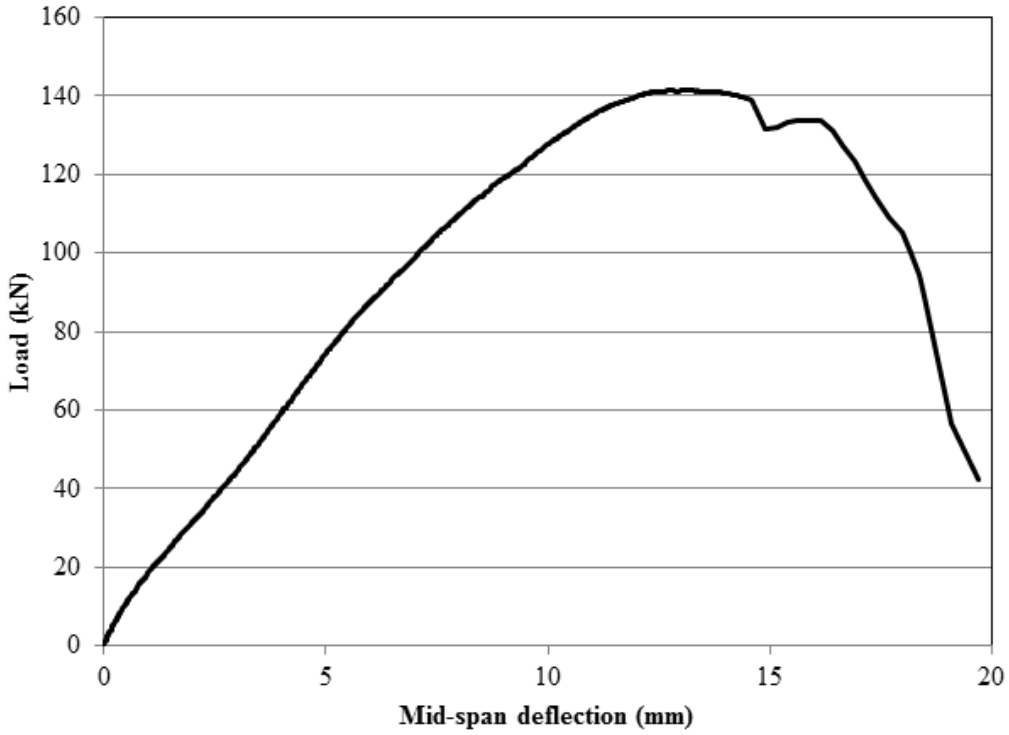


**Figure 4.20 Load versus mid-span deflection curve for Beam M-B-100-5.**

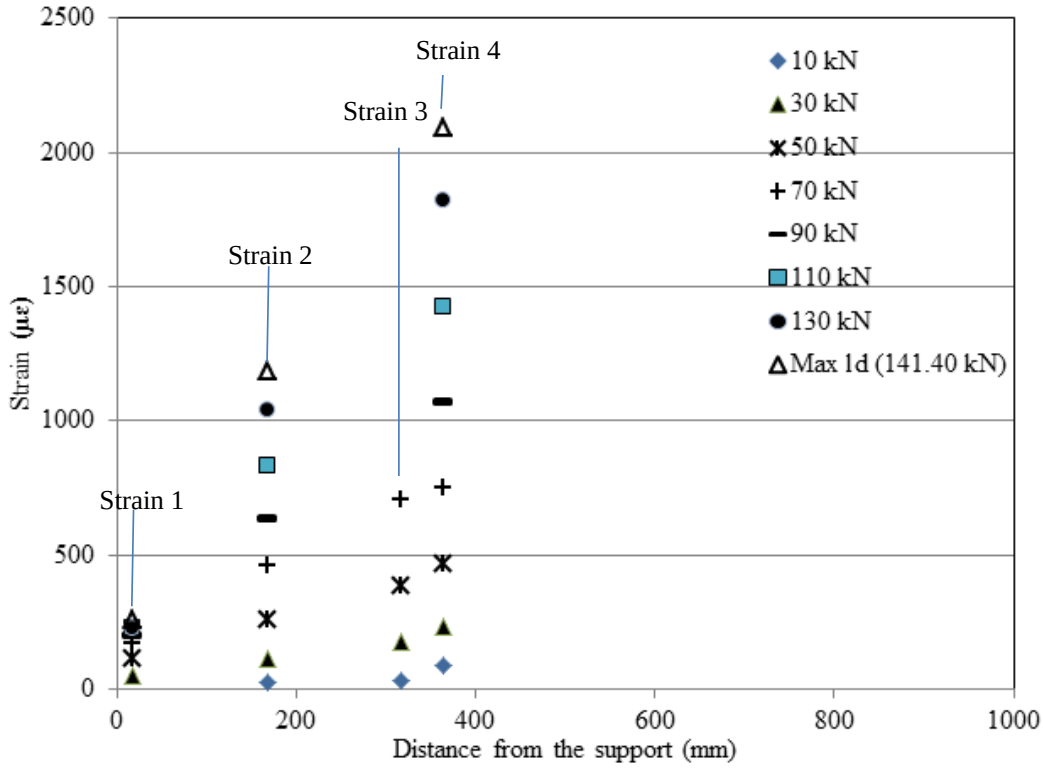


**Figure 4.21 Strain profile for Beam M-B-100-5 along the length of the reinforcement in the anchorage zone. Notice that strain 3 was malfunctioned after reaching 80 kN load.**

## 4.6 Effect of stirrups and supports on monotonic behaviour

All beams with stirrup configuration A failed in a similar manner in monotonic tests. Inspection of the failure zone in the beams revealed that the concrete keys between the stirrup locations above the bar were almost intact and were only crushed in the regions near the stirrup locations except for the area close to the support where the concrete keys were completely destroyed. The measured strains along the length of the anchorage zone in the reinforcing steel were used to analyze the failure mechanism. Figure 4.22 shows the strains in the anchorage zone of beam M-A-100-0-1 at various load levels. Bond between the reinforcing steel and concrete was originally due to adhesion, friction and bearing forces. When the bar started to slip, most of the tension forces were taken by the bearing forces of the bar lugs on the concrete keys (ACI Committee 408). The bearing force was approximately normal to the face of the lugs. The components of this force were a horizontal shear force and a vertical compression force on the concrete. The latter caused spalling of the concrete cover below the bar and a force pushing the steel reinforcement away from the top concrete (above the steel bar). If there had been no stirrups holding the bar in place, the bar would have separated from the concrete causing failure of the beam. However, the stirrups resisted these vertical forces. Figure 4.23 shows the strain profile at the maximum load for all the static beams with stirrup configuration A with the stirrup locations along the length of the beam. From the strain profile, in Figure 4.23, the values of the shear forces taken by the concrete in between two strain gauges were calculated by taking the change in strain between these strain gauges multiplied by the modulus of elasticity and the area of the steel bar ($F= E\Delta\varepsilon_s A_s$). Although the forces resisted by the stirrups were not quantified, regions with a higher shear force would have a higher bearing force and hence higher forces in the stirrups. Figure 4.24 shows the shear forces in the regions of the stirrups along with the stirrup locations. From Figure 4.24, it was clear that stirrup 1 resisted the highest forces. This was the location where slip initiated. The support plate confined the concrete around the bar in the section close to the support. This increased the stiffness of the bar to concrete connection in this section. This confinement by the support resulted in the concrete keys close to the support being crushed as the bar slipped. This was evident after the failed beam was dissected as shown in Figure 4.25. Two initial sources of bond between the steel and the concrete were the adhesion of the steel to the concrete and the mechanical interlock of

concrete keys to steel lugs. After slip initiated, the stirrups continued to stop the bars from separating from the top concrete. In between the stirrups, the concrete keys were nearly intact. This suggested that in between the stirrups the bar was pushed away from the top concrete enough that the concrete keys suffered only minor damage. The stirrups held the bar in contact with the concrete until the concrete at the stirrup locations was crushed allowing the bar to slip.

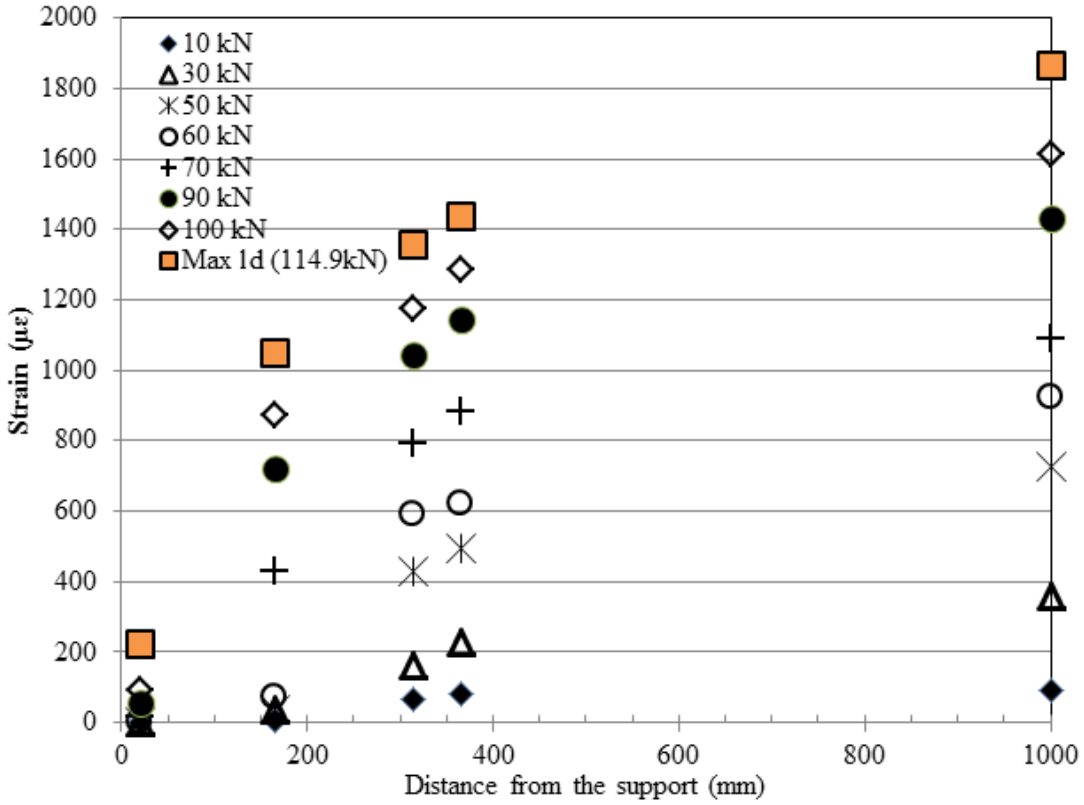


**Figure 4.22 Strain profile for Beam M-A-100-0-1.**

The failure for the beams with stirrup configuration B (75 mm stirrup spacing) was somewhat different. Debonding of the reinforcing bar from the mid-section of the beam to the pocket started early on (at about 30 kN load). This was shown by the equal strain values in SG4 and SG5 as shown in Figure 4.26. Slip was minimal at this stage but was enough to cause forces in the stirrups resisting the movement of the bar. Once slip reached the support region, the support introduced high stresses in the bar. The slip also introduced bearing forces on the bars that were resisted by the concrete keys and their vertical component was resisted by the stirrups. The stirrups held the bar in place until the concrete keys at the stirrup

locations crushed. Due to the close spacing of the stirrups the concrete keys were almost completely destroyed along the length of the anchorage zone (Figure 4.27). The close stirrup spacing did not allow the bar to bend enough to separate it from the concrete in between the stirrups and hence concrete keys along the 350 mm anchorage length resisted slip and were crushed. In conclusion, increasing the number of stirrups increased the confinement and changed the failure mode from partial splitting to almost complete pullout by crushing of the concrete keys along the whole 350 mm anchorage length.

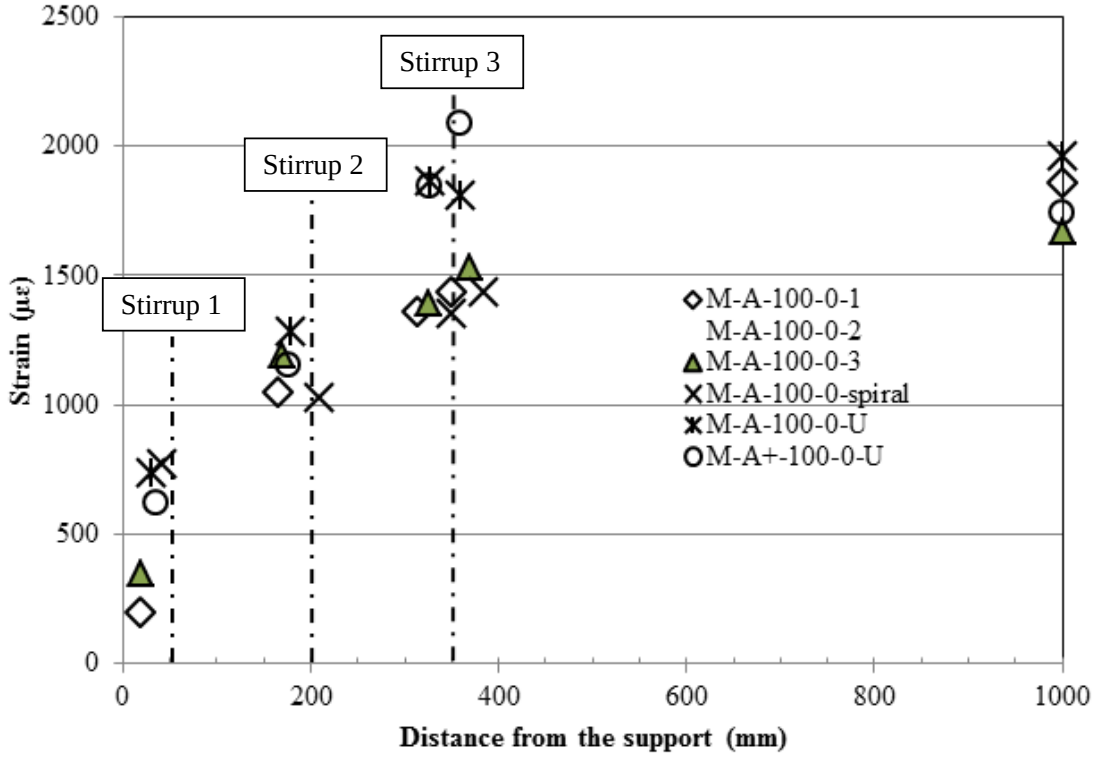


**Figure 4.23 Strain profile at maximum load for the static beams with stirrup configuration A. The stirrup is represented by a vertical line.**

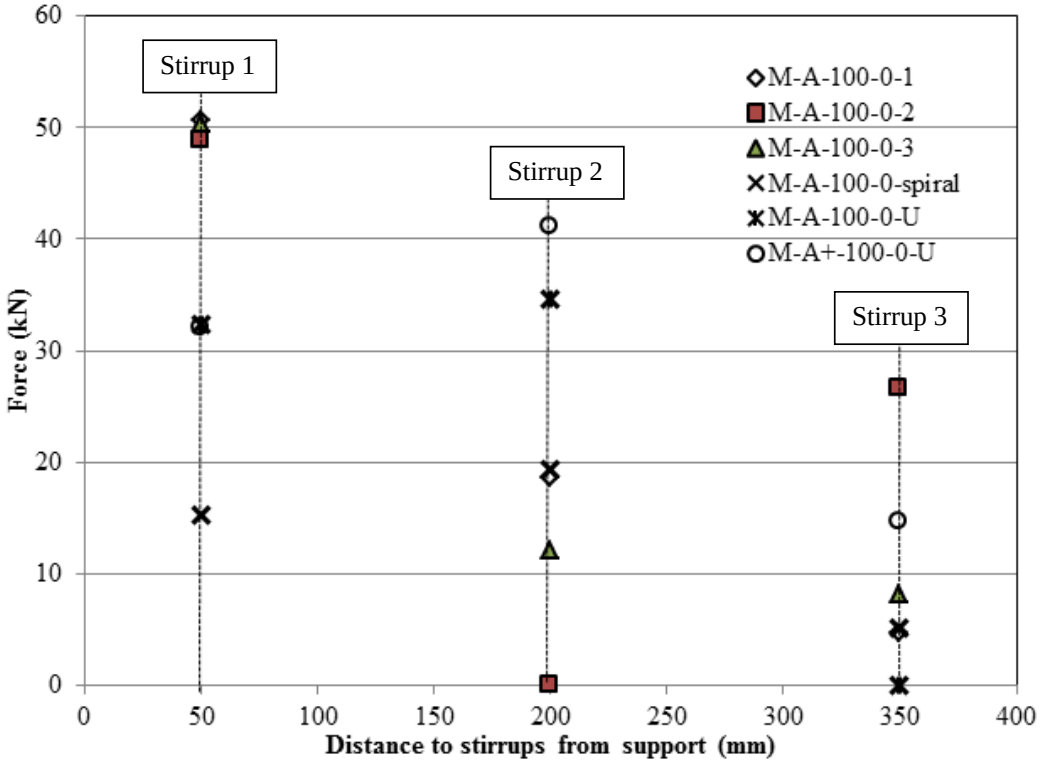


**Figure 4.24 Shear forces at the location of the stirrups at maximum load for the static beams with stirrup configuration A.**

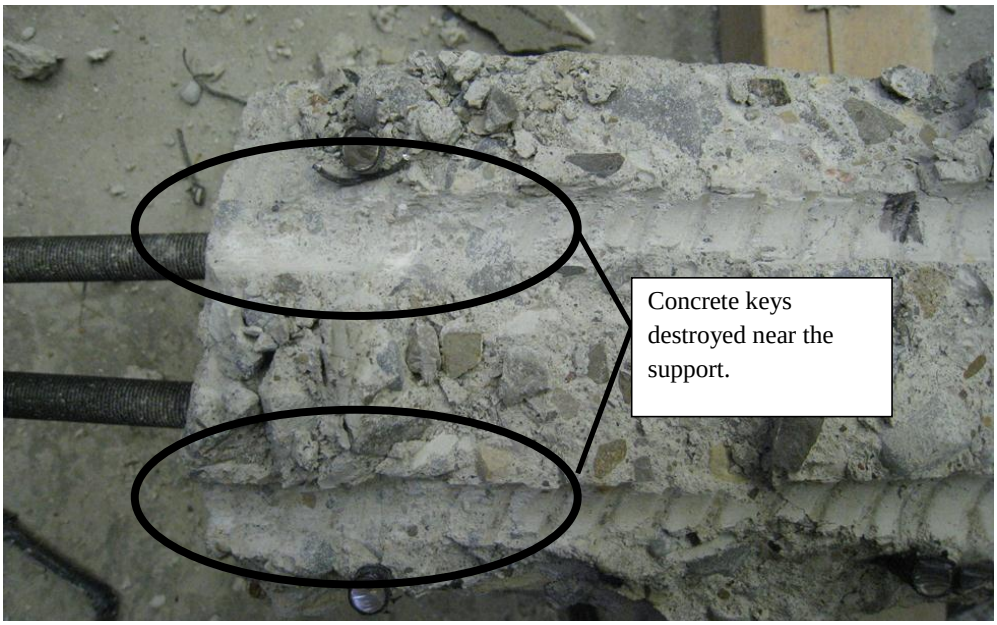


**Figure 4.25 Typical concrete keys crushing close to the support for beams with stirrup configuration A. This picture is taken from Beam M-A-100-0-3 after failure. The beam is turned upside-down.**

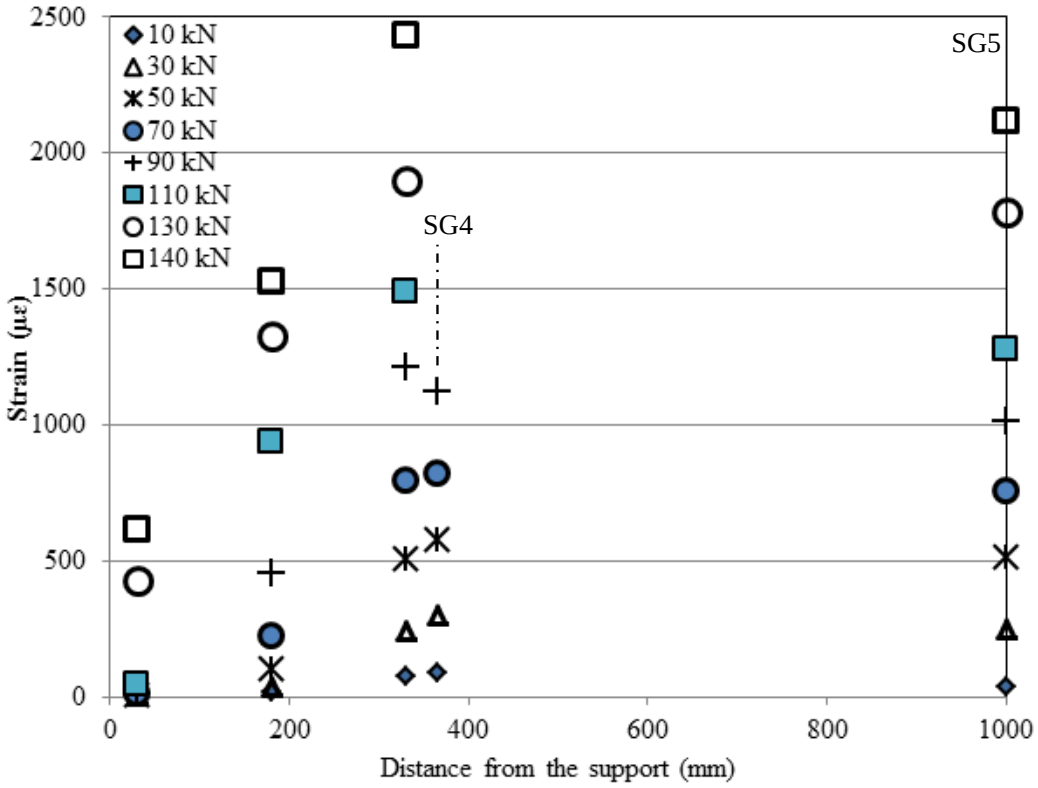


**Figure 4.26 Strain profile for Beam M-B-100-0-2.**

**Figure 4.27 Concrete keys crushed along the anchorage zone for Beam M-B-100-0-2. This beam is turned upside-down.**

## 4.7 Fatigue Tests

Six beams were tested under repeated loading. Three beams had stirrup configuration A (150 mm stirrup spacing) and three beams had stirrup configuration B (75 mm stirrup spacing). The beams were tested at different load ranges to vary the fatigue lives. The beams tested under repeated loading were first loaded manually up to the maximum load, and then the load was decreased to the mean load after which it was cycled at a frequency of 1 Hz. The minimum load was fixed for all the beams at 10 kN. Failure was defined when the beam was not able to carry the maximum load anymore. Table 4.1 gives a summary of the fatigue lives of the beams tested in the current study.

**Table 4.1 Results of fatigue beams from group 1.**

| Beam Notation | Fatigue Life (cycles) | Load Range (kN) | Maximum Load (kN) | Ratio of load range to static capacity |
|---|---|---|---|---|
| F-A-66-0 | 42,898 | 66 | 76 | 0.59 |
| F-A-64-0 | 27,407 | 64 | 74 | 0.57 |
| F-A-60-0 | 576,662 | 60 | 70 | 0.54 |
| F-B-97-0 | 7,071 | 97 | 107 | 0.67 |
| F-B-91-0 | 3,988 | 91 | 101 | 0.63 |
| F-B-83-0 | 44,707 | 83 | 93 | 0.57 |

### 4.7.1 Stirrup configuration A

The fatigue load ranges for the beams with stirrup configuration A were 66 kN for Beam F-A-66-0, 64 kN for Beam F-A-64-0, and 60 kN for Beam F-A-60-0, with respective fatigue lives of 42898 cycles, 27407 cycles and 576662 cycles. Beams F-A-66-0 and F-A-64-0 failed by bond, while beam F-A-60-0 failed in shear and flexure after a high slip of the bar occurred at the end of the beam crushing the concrete keys close to the support. The cracking pattern for the beams with stirrup configuration A was similar to that of the static beams with the same stirrup configuration. As the beam was cycled, a vertical crack appeared at about 150 mm from the support and progressed across the width of the beam from the bottom side. A diagonal shear crack then combined with the vertical crack followed by a horizontal splitting crack along the length of the bar that appeared with continued cycling of the beam.

The slip behaviour was similar for all the fatigue beams with stirrup configuration A. Slip increased during the first 10% of the fatigue life and then there was almost no increase in slip until the beams reached about 80% of the fatigue life except for Beam F-A-66-0 for which the slip increased by 1 mm from 10% to 80% of the fatigue life at a slow rate. A small increase in slip between 80% and 90% of the fatigue life was followed by a sudden large increase in the slip rate close to failure during which the slip increased from 0.5 mm to 2.3 mm at 90% of the fatigue life to between 3.8 and 6.8 mm at failure. This large slip of the bar indicated a bond failure of the beam. Figure 4.28, Figure 4.29, and Figure 4.30 show the slip versus the percentage of the fatigue life for beams F-A-66-0, F-A-64-0 and F-A-60-0 respectively.

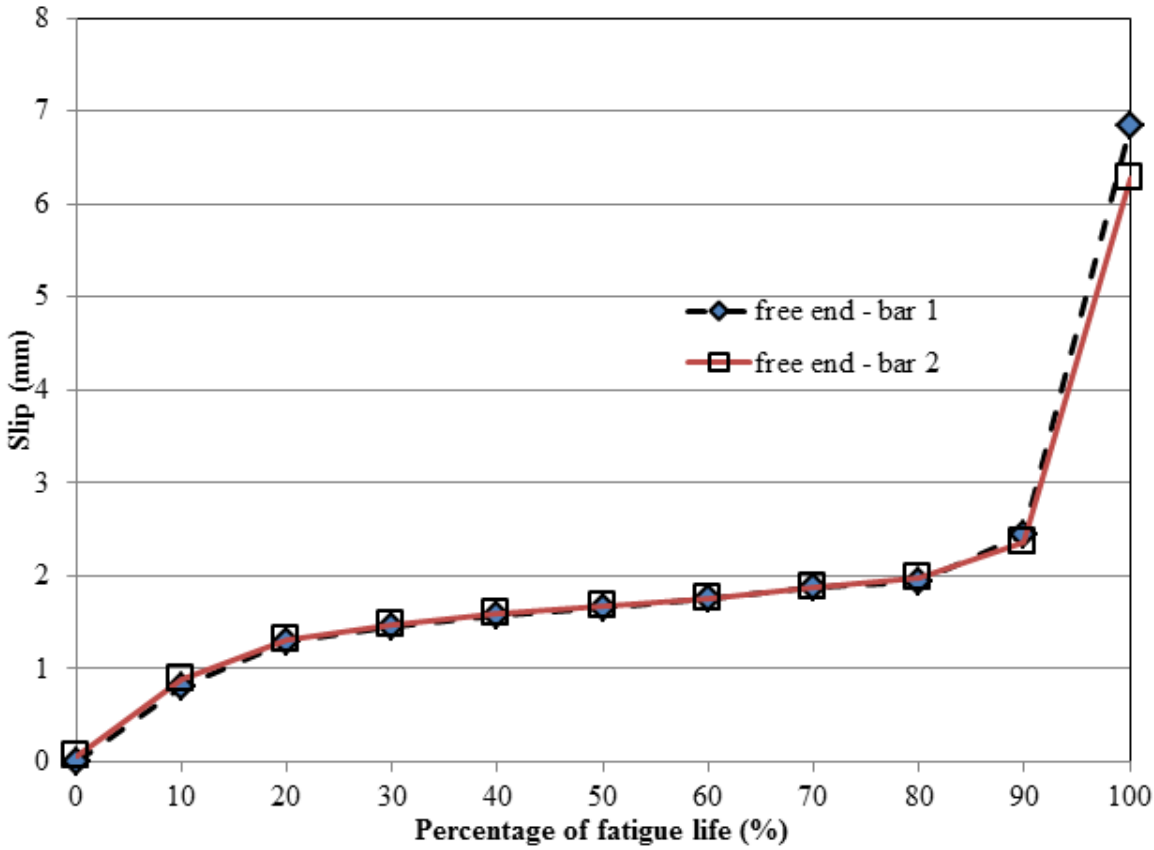


**Figure 4.28 Slip versus percentage of fatigue life for Beam F-A-66-0.**

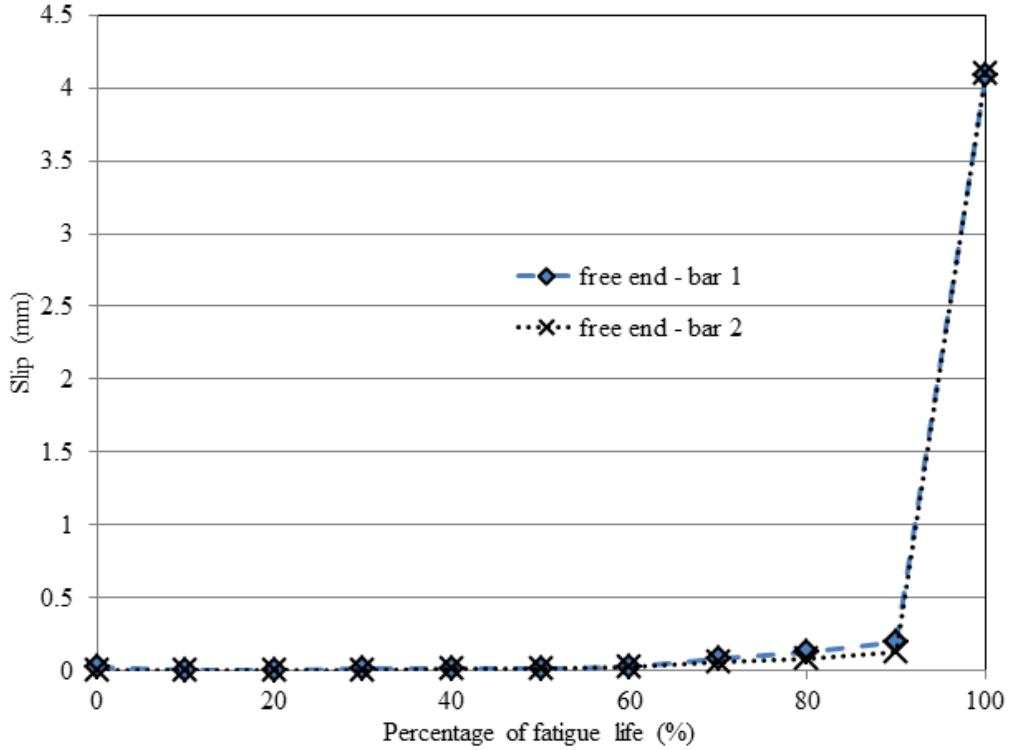


**Figure 4.29 Slip versus percentage of fatigue life for Beam F-A-64-0.**

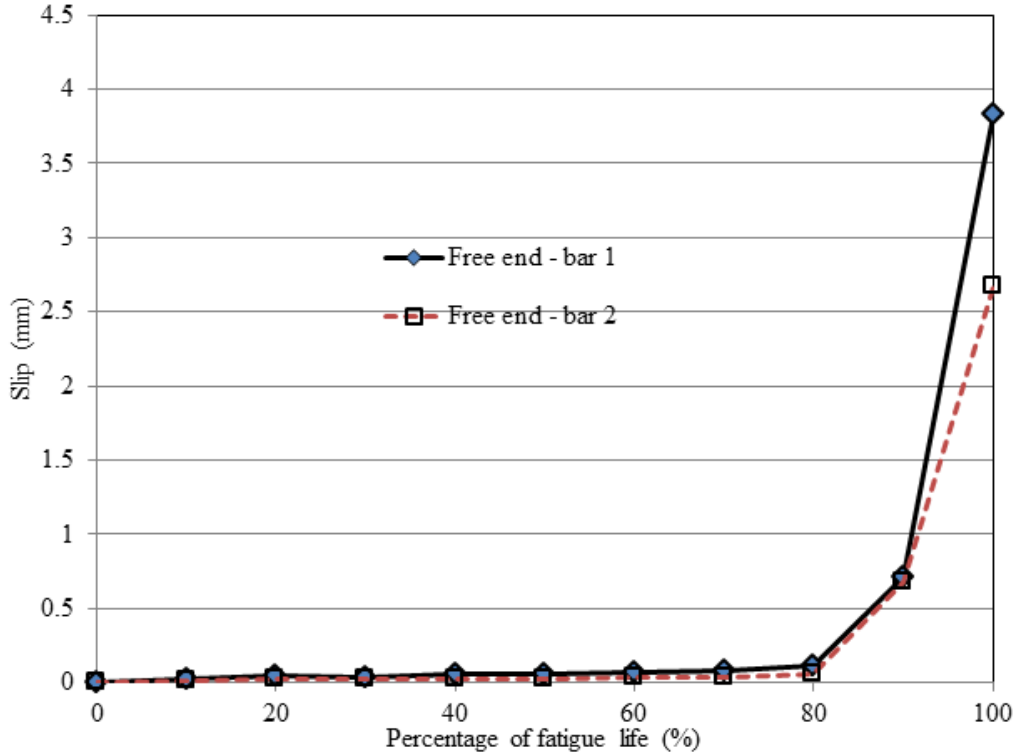


**Figure 4.30 Slip versus percentage of fatigue life for Beam F-A-60-0.**

Three strain gauges were mounted in a groove inside the bar and one strain gauge on the bar at the middle section of the beam in the constant moment region. An additional strain gauge was mounted on the steel bar in the pocket. Figure 4.31, Figure 4.32, and Figure 4.33 show the strains versus cycles for beams F-A-66-0, F-A-64-0 and F-A-60-0 respectively. Similar to the slip behaviour the strain increased during the first 10% of the fatigue life. Beams F-A-66-0 and F-A-60-0 debonded from the pocket towards the point load during the first 10% of the fatigue life. This was deduced from the values of the strain measured in the pocket that were close to the values of the strain measured in the constant moment region. Beam F-A-64-0 had partial debonding between the pocket and the loading point during the first 10% of the fatigue life. This was deduced from the fact that the values of the strain in the pocket were only slightly less than the values of the strain in the constant moment region, and greater than the strain value expected from a cracked section analysis. Then the strain values for all the three beams remained almost constant until about 80% of the fatigue life. Beyond that point, the strain profile was different for the different beams.

For Beam F-A-66-0, the strain values close to the support (SG1 and SG2) dropped to values close to zero between 80 % and 100 % of the fatigue life (Figure 4.31), suggesting that the bar at the support location (free end) had completely debonded and was no longer carrying load. This was accompanied by a very high slip at the free end as shown in Figure 4.28 that led to failure of the beam. For the high fatigue load range (Beam F-A-66-0), the strain values at the pocket location were higher than the values of the strain in the constant moment region. This was due to two factors. First the strain gauge location in the pocket was very close to the concrete face where a stress raiser was expected. Accordingly, the values of the strain in the pocket were increased by its proximity to the concrete face where the bar makes contact with the concrete. The other factor that caused the high strain values was cyclic creep of the steel bar. The maximum fatigue load (76 kN) was high enough to cause the bar in this section (to have a stress above the yield stress) to undergo cyclic creep also known as racheting that occurs in the presence of cyclic plastic strain and a high mean stress.

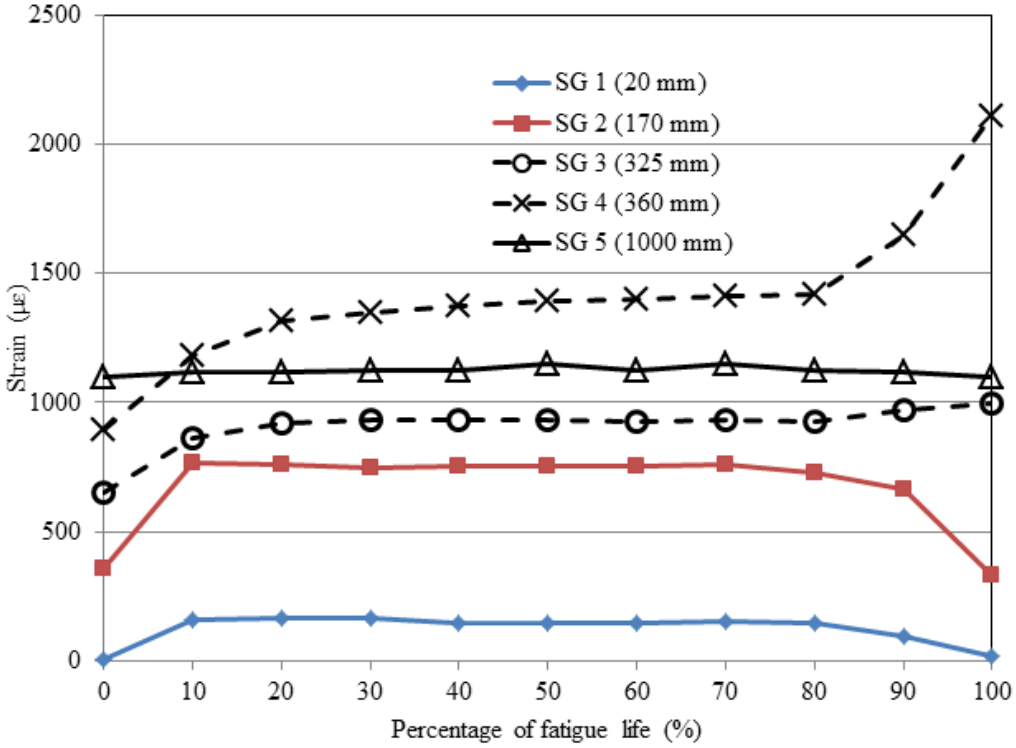


**Figure 4.31 Strain versus percentage of cycles of fatigue life for beam F-A-66-0.**

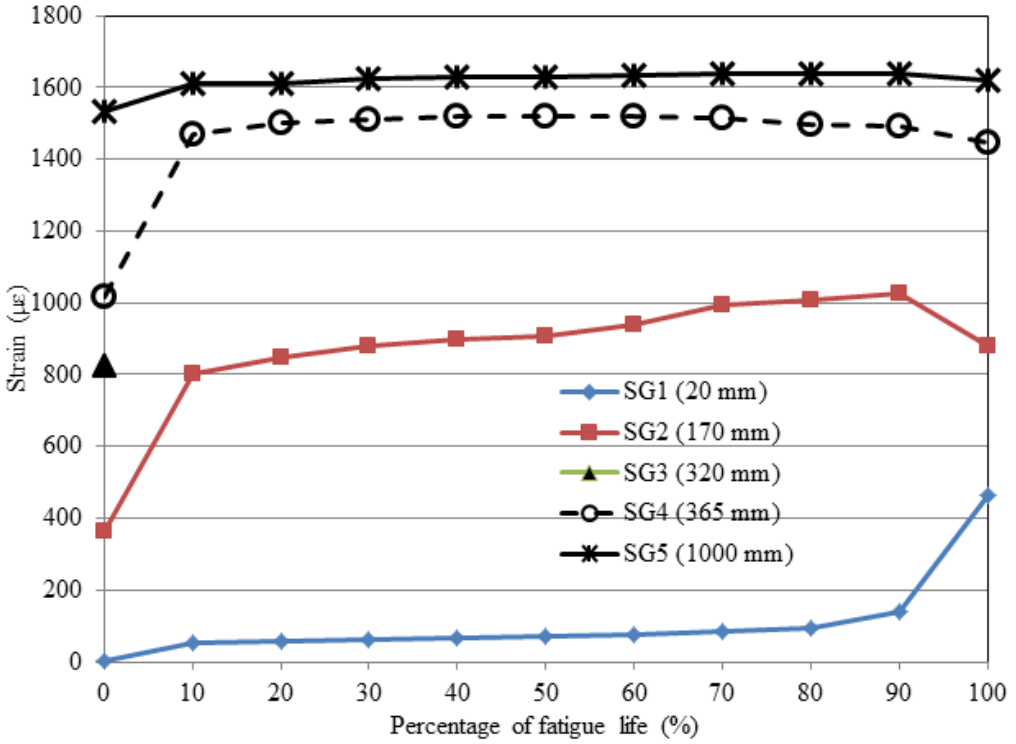


**Figure 4.32 Strain versus percentage of fatigue life for beam F-A-64-0.**

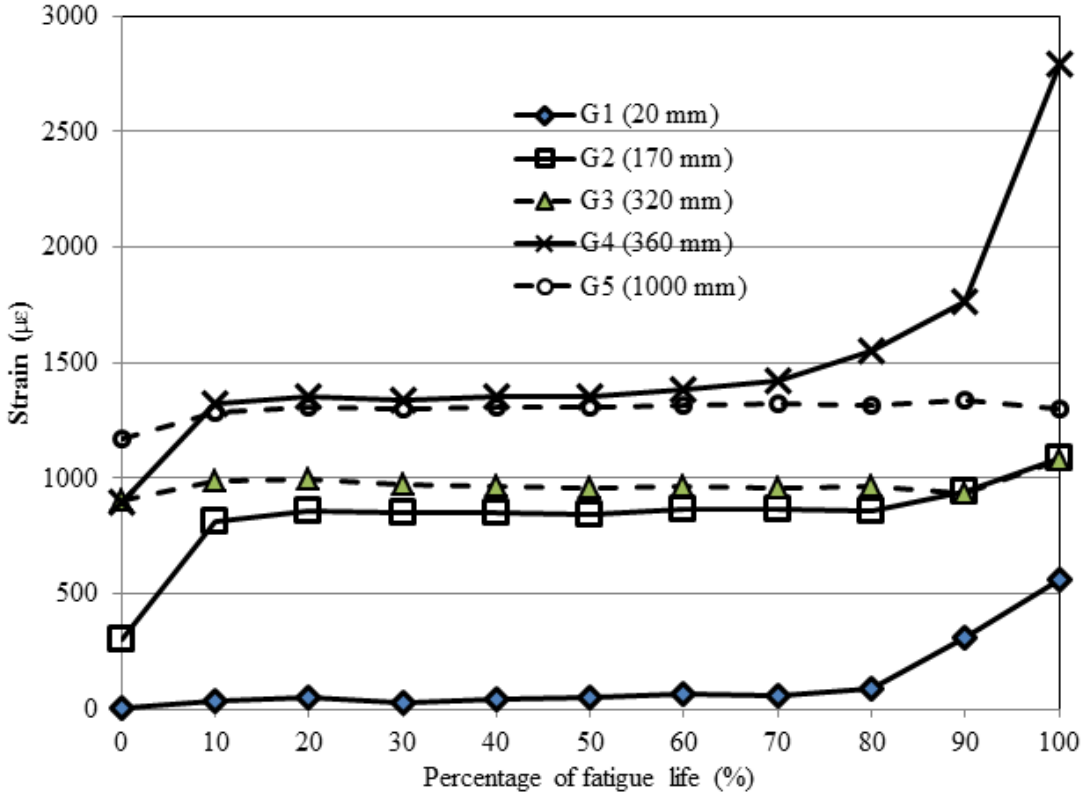


**Figure 4.33 Strain versus percentage of fatigue life behaviour for beam F-A-60-0.**

For Beam F-A-64-0 (Figure 4.32), the strain values in the bar close to the support (SG1) increased slightly (45 με) between 80% and 90% of the fatigue life. Then the strain at the location of SG 1 (20mm from the support) increased significantly (about 350 με) while the strain at SG2 location decreased by about 200 με. This can be explained as follows. The bearing force exerted by the bar on the concrete was pushing the bottom concrete away from the bar and causing it to spall. The concrete section between SG1 and SG2 was completely spalled (Figure 4.34). Compression from the support confined the concrete in that section and prevented it from spalling. The confinement from the support increased the stiffness of the bar to concrete connection which delayed the slip of the bar in this section. Once slip started, increased bearing forces on the concrete keys led to increased strain readings at the location of SG 1 which was close to the support. The vertical components of these bearing forces were resisted by the stirrups. At failure, the concrete at the stirrup location close to SG 2 was completely crushed as seen in Figure 4.35 leading to failure of the beam.

The strain values in Beam F-A-60-0 increased slightly between 80% and 90% of the fatigue life along the anchorage zone of the beam, followed by a large increase in strain at 100% of the fatigue life. The slip increased the bearing force from the bar lugs on the bottom concrete cover which spalled it off leaving the concrete keys intact. The support confined the concrete by preventing the bottom concrete from spalling at the support location and thus increased the stiffness of the connection between the bar and the concrete at this section. Figure 4.36 shows that the concrete keys were crushed close to the support where the stiffness was highest. The strain value in the bar in the pocket increased beyond the cyclic yield value that was reported by (Al-Hammoud, Soudki, & Topper, 2011). This suggested that the bar close to the pocket was undergoing cyclic creep leading to increased strain readings in the location of SG 3. The stirrup close to the pocket ruptured due to repeated loading causing the beam to fail ultimately by shear. After dissecting the beam, it was also found that the longitudinal bar (with no strain gauges installed) was ruptured. Thus Beam F-A-60-0 failed from a combination of flexure, shear and high slip of one bar from the support.

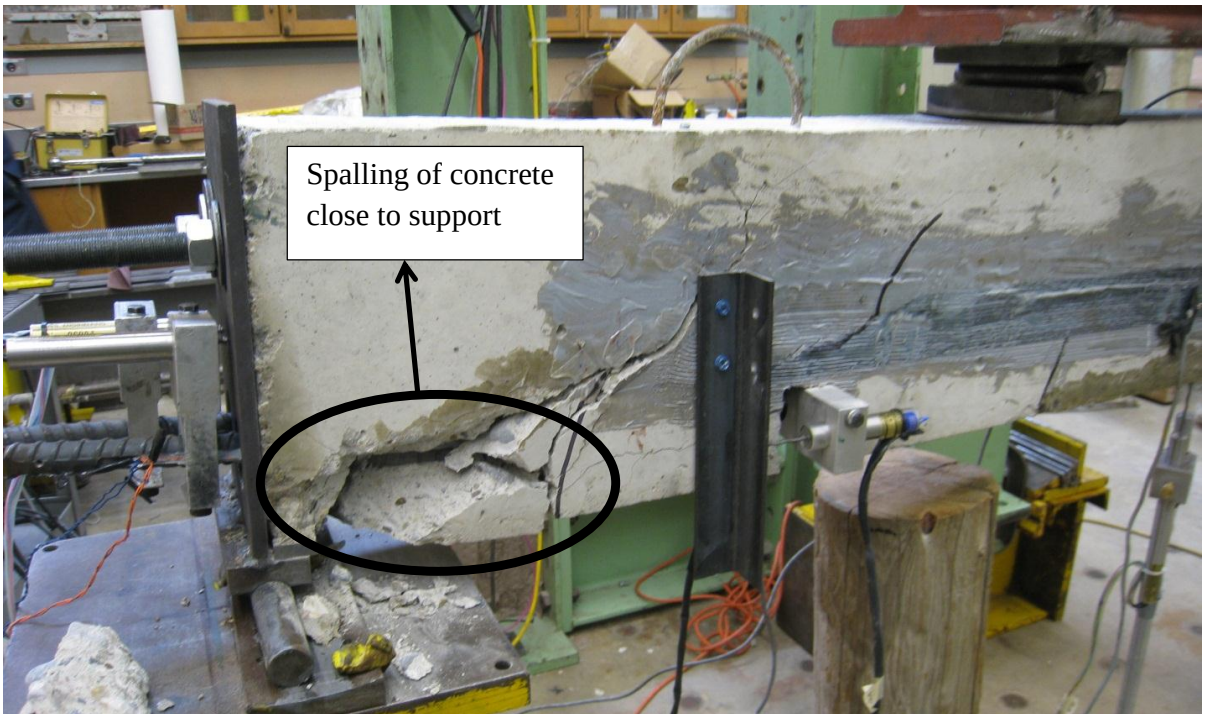


**Figure 4.34 Beam F-A-64-0 close to failure in the testing frame showin the concrete close to the support spalling.**

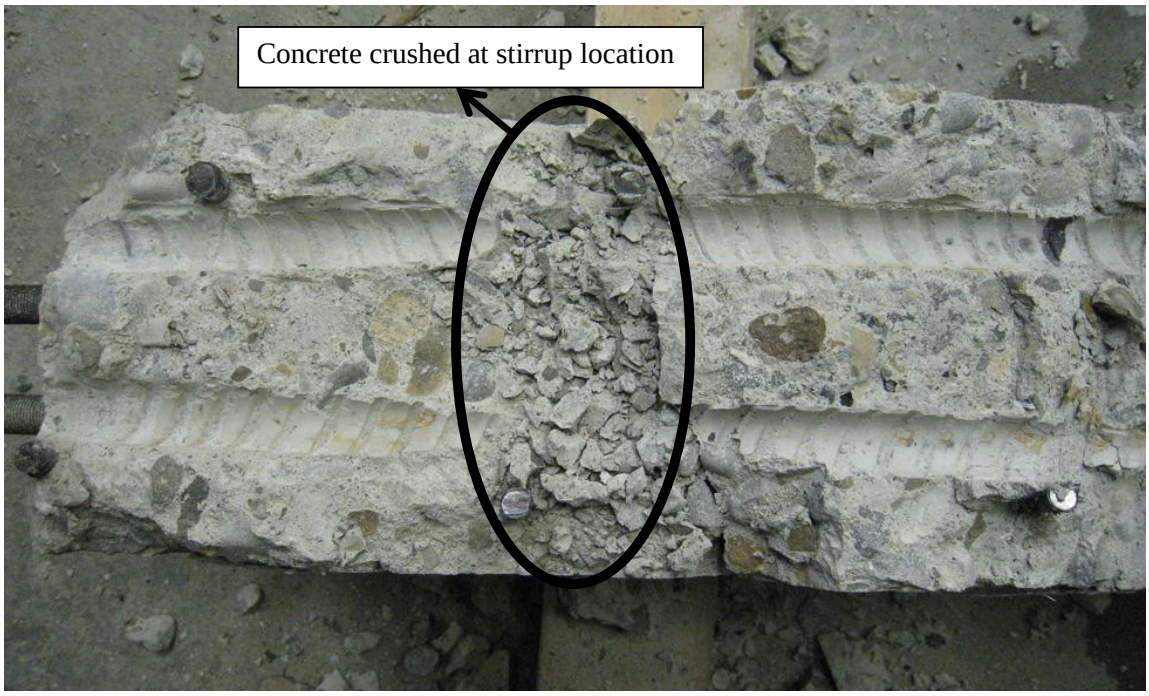


**Figure 4.35 Beam F-A-64-0 after failure and removing the reinforcing bars. The beam was turned upside-down.**

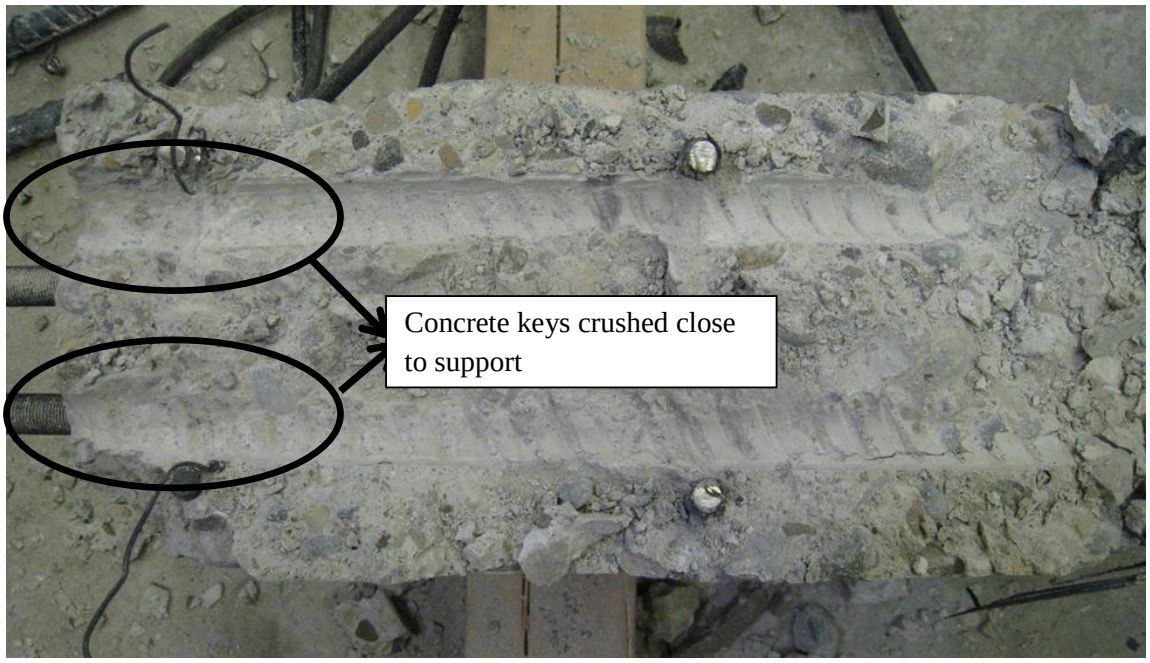


**Figure 4.36 Beam F-A-60-0 after failure and removing the reinforcing bars. The beam was turned upside-down.**

Figure 4.37 shows a strain profile for beam F-A-66-0 at different percentages of the fatigue life of the beam. The increase in strain value at the location of strain gauge 4 (SG 4) to above the calculated cracked section strain indicated that debonding had occurred between the pocket and the mid-section of the beam between cycle 1 and 10% of the fatigue life. The readings from SG1, 2 and 3 were also above the calculated cracked section strain at 10% of the fatigue life which indicated that partial debonding had occurred within the anchorage zone at this section. After slip between the steel and the concrete occurred in the anchorage zone, the vertical components of the bearing forces from the bar lugs on the concrete keys were resisted by the stirrups. From the graph (Figure 4.37) stirrup 1, the stirrup closest to the support, was responsible for the highest force transfer. This was deduced by calculating the bearing force resisted by the concrete keys close to each stirrup from the variation in strain readings in the steel bar. In general a large change in strain values, in the region close to the stirrup, suggested that there were high bearing forces in this region. The high bearing forces meant that the vertical components of these forces, which were resisted by the stirrups, were high. Accordingly, the high bearing force resulted in a high resisting force in the stirrups. The stirrups continued to resist the vertical component of the bearing force until the concrete at the stirrup location was crushed. This behaviour was similar to that of the static beams. The top concrete keys were crushed totally between the support and stirrup 1 but had little damage between the interior stirrups. This is clearly shown in Figure 4.38.

### 4.7.2 Stirrup Configuration B

The fatigue load ranges for the beams with stirrup configuration B were 97 kN for Beam F-B-97-0, 91 kN for Beam F-B-91-0, and 83 kN for Beam F-B-83-0, with respective fatigue lives of 7071 cycles, 3988 cycles and 44707 cycles. The cracking pattern for the beams with stirrup configuration B was similar to that seen in the static beams with the same stirrup configuration. As the load was cycled, two vertical cracks appeared at about 150 mm and 250 mm from the support and progressed across the bottom width of the beam. Diagonal cracks then combined with the vertical cracks. The vertical cracks introduced stress raisers in the bars at the location of the cracks. A horizontal splitting crack appeared along the length of the bar as load cycling continued.

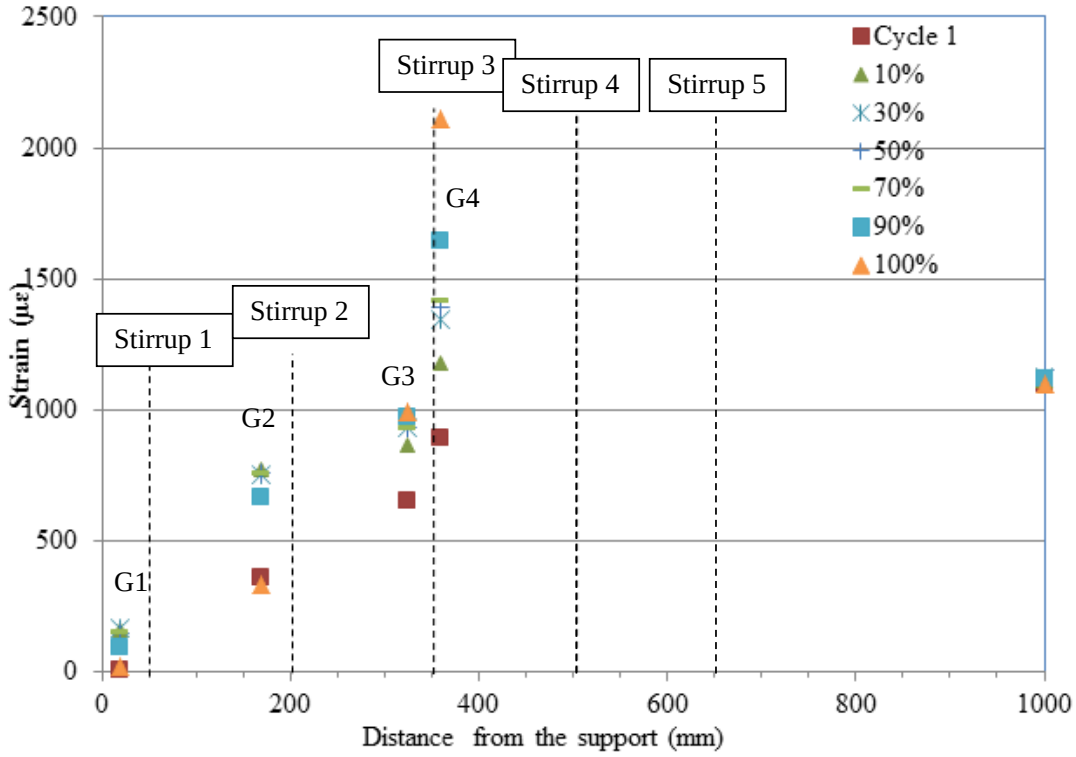


**Figure 4.37 Strain profile for beam F-A-66-0. The stirrups locations along the anchorage length of the beam are marked on the graph.**


**Figure 4.38 Beam F-A-66-0 after failure and reinforcing bars removed. The beam is turned upside-down.**

The fatigue failure of the beams with stirrup configuration B was more sudden in nature than the fatigue failures of beams with stirrup configuration A. After the concrete to steel adhesion was lost, shear forces were transferred by mechanical interlock between the concrete keys and the bar. The vertical components of the bearing force from the bar pushed the bottom and top concrete away. The presence of the stirrups prevented the bar from being pushed away from the top concrete and the vertical component of the bearing force was transferred to the stirrups in tension. Figure 4.39 shows the strain profile for beam F-B-97-0. Partial debonding started along the anchorage zone during the first cycle. This was deduced from the measured strain values along the anchorage length that were higher in value than the calculated strains at the strain gauge locations from a cracked section analysis. After partial debonding occurred and slip started, most of the vertical forces (that were the resultant vertical components of the bearing forces from the lugs onto the concrete keys) were resisted by stirrups 1, 2, 3 and 4 which were confirmed by the large changes in the strain values in between those stirrups. The other stirrups had much smaller changes in strain between them because slip was starting from the free end. As the beam was cycled the strains at the various locations along the beam were almost constant. At failure the strain change between the strain gauges close to the support dropped. This suggested that the force resisted by the stirrups in this region had decreased. This was due to the fact the concrete around the stirrups close to the support was crushed as seen in Figure 4.40 taken after dissecting the beam. The slip increased rapidly near failure (100% of the fatigue life) as shown in Figure 4.41. The slip increased after 80 % of the fatigue life and continued to increase until the bar was completely debonded and the concrete around the bar and the stirrups for about 130 mm (as measured after dissecting the beam) from the support was completely crushed. This was accompanied by an increase in the slip to about 12.5 mm. Since the bar was debonded along this section, the beam acted as an unreinforced concrete beam and the final failure was a flexural failure in the anchorage zone. Figure 4.42 shows the final failure for Beam F-B-97-0 where after debonding of the bar, the beam failed in flexure close to the support. After the bar debonded along the anchorage length and the concrete at the support crushed there was nothing transferring the load from the concrete section into the bar. The beam then behaved as an unreinforced member and failed in flexure at the location where the maximum flexural

capacity of an unreinforced beam was reached. This behaviour was similar at all load levels for the fatigue beams with stirrup configuration B.

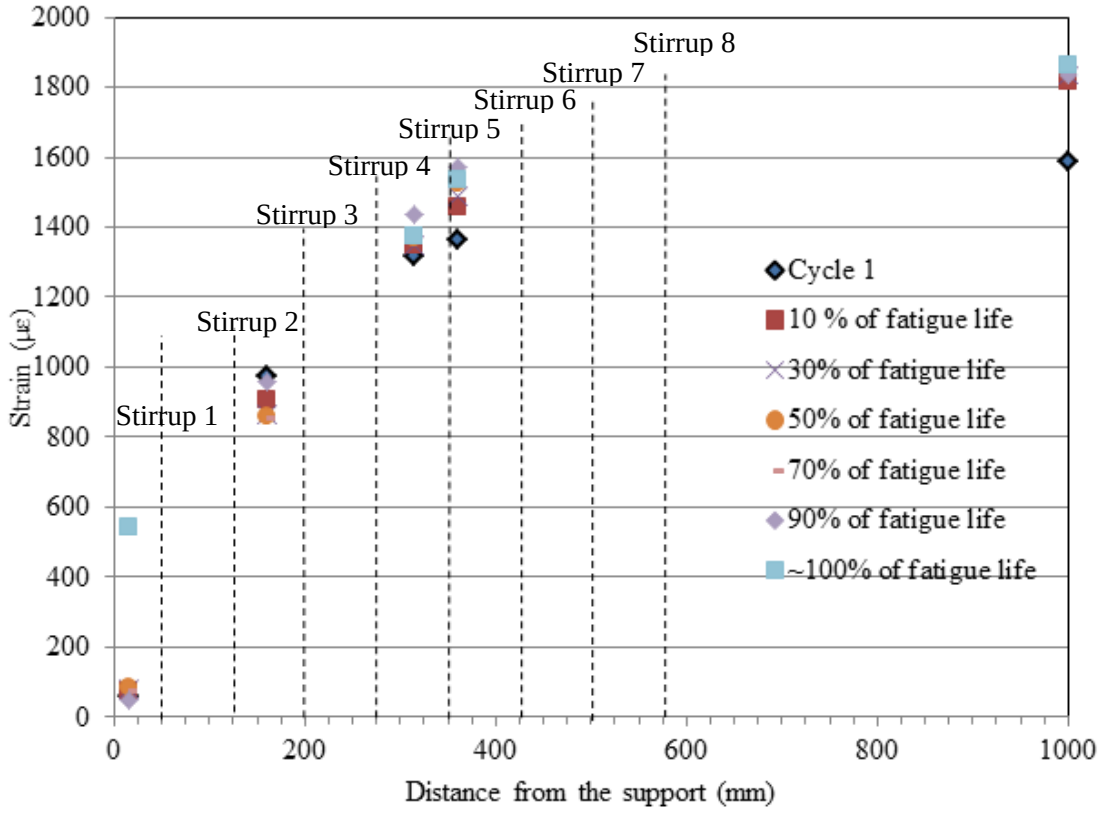


**Figure 4.39 Strain profile for beam F-B-97-0 along with the stirrup locations.**

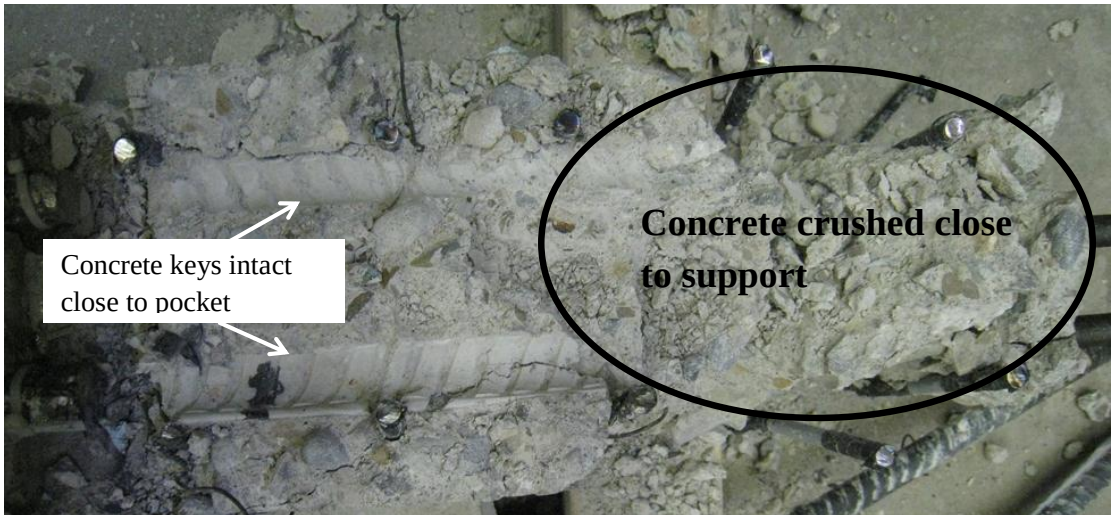


**Figure 4.40 Beam F-B-97-0 after failure and removing the reinforcing bars. The beam was turned upside-down.**

After failure the beams were inspected by removing the reinforcing bars and checking the concrete keys on top of the bars. The concrete keys were completely crushed close to the support and were undisturbed close to the pocket (Figure 4.40).

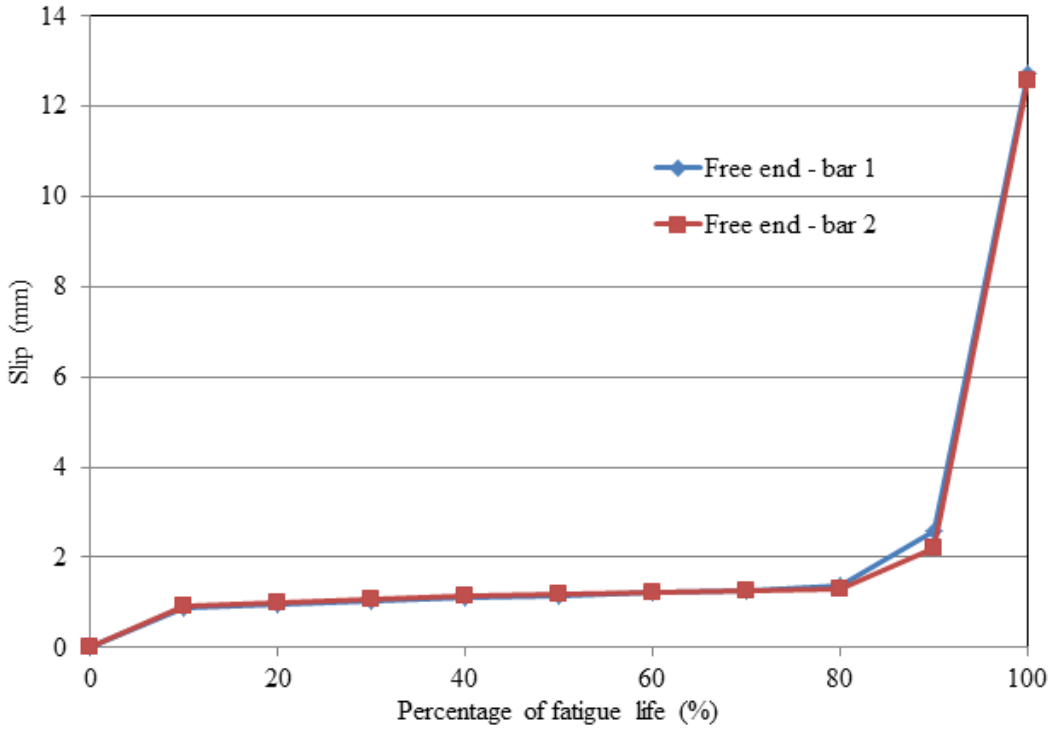


**Figure 4.41 Slip versus percentage of fatigue life behavior for beam F-B-97-0.**

**Figure 4.42 The anchorage zone for Beam F-B-97-0 after failure in the testing frame.**

### 4.7.3 Fatigue Life Discussion for Stirrup Configurations A and B

The fatigue failure mechanisms for beams with stirrup configurations A and B were different. For beams with stirrup configuration A (150 mm spacing between stirrups) the stirrups were able to resist the vertical components of the bearing force initiated from the bar lugs on the concrete keys due to bar slip. The spacing between the stirrups was great enough that it allowed the bar to bend in between the stirrups reducing the bearing force resisted by the concrete keys in these regions. This was consistent with the partially intact concrete keys in between the stirrup locations that were observed after dissecting the beam. The failure of the beam occurred once the concrete at the stirrup locations was crushed which reduced the resistance force carried by the stirrups and allowed the slip in the bar to increase leading to a bond failure of the beam. In the fatigue beams with stirrup configuration B (75 mm spacing between stirrups), the stirrups were close enough that the bar was not allowed to bend in between the stirrups. The stirrups maintained the interlock between the lugs of the reinforcing bars and the concrete keys along the anchorage zone even after debonding started to occur from the support. Failure occurred when the debonded length was long enough that the maximum flexural capacity of the beam section at the end of the debonded region was reached.

Figure 4.43 shows the fatigue life curve for all the beams tested with stirrup configurations A and B. The beams with stirrup configuration A behaved in a manner similar to that reported in the literature (Al-Hammoud, Soudki, & Topper, 2010; Rteil, Soudki, & Topper, 2011) in that the fatigue life of the beams varied linearly, on a semi-log scale, with the range of load applied with a shallow slope. Hence the range of load over which fatigue bond failures occurred was very small. The fatigue life for the beams with stirrup configuration B had a steeper slope and the range of load levels over which fatigue failure occurred was larger. This was attributed to the fact that the beams with stirrup configuration B resisted higher loads due to the increased number of stirrups that prevented the bar from bending in between the stirrups and increased the bearing force in the concrete to steel interface. The beams resisted load until the concrete close to the support was crushed and debonding of the bar occurred which caused the beam to fail in flexure at the end of the debonded section where the flexural capacity of a plain concrete member was reached. In conclusion, increasing the number of stirrups prevented the bar from bending in between the stirrups and

increased the concrete resistance to slip of the bar and increased the fatigue strength of the beam.

From Figure 4.43, it can be seen that reducing the spacing of the stirrups from 150mm to 75mm increased the fatigue capacity of the beam at short fatigue lives. This increase diminished with an increase in the number of cycles or long fatigue lives.

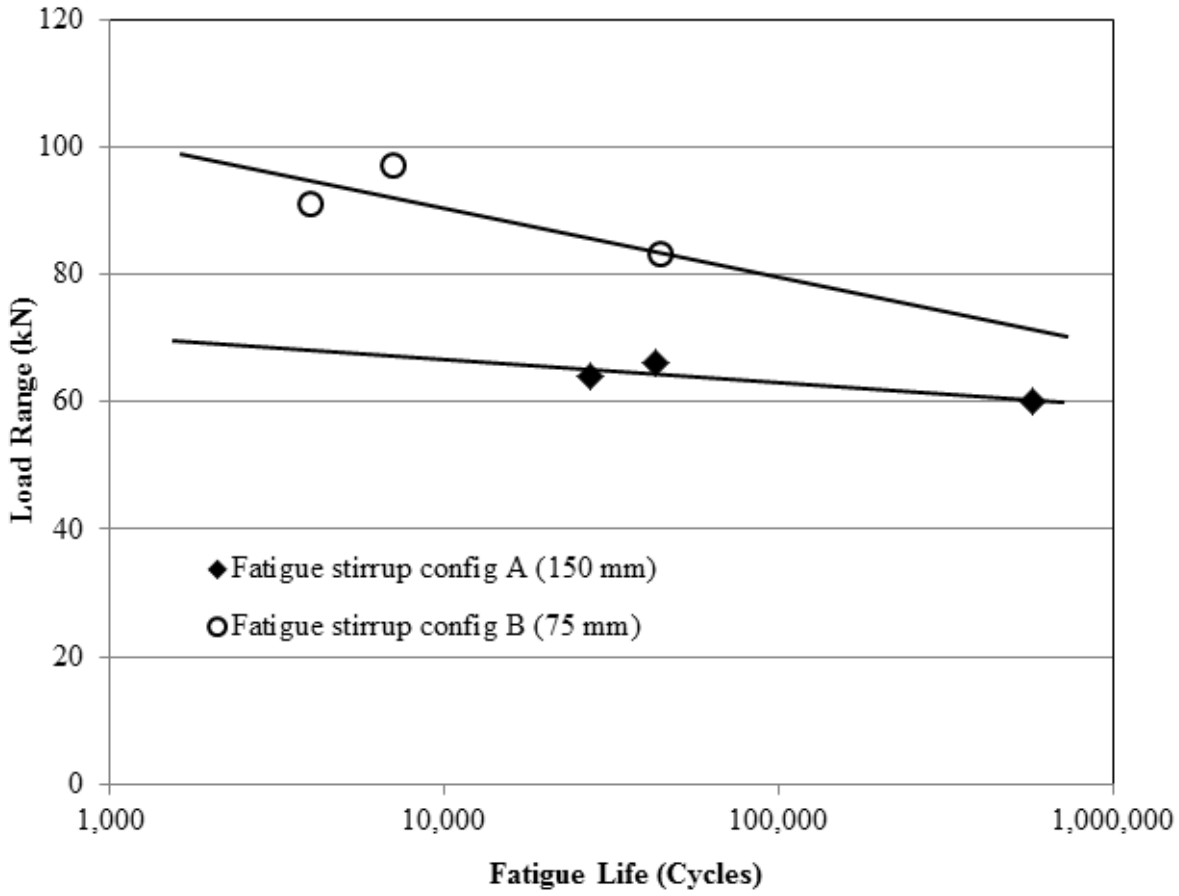


**Figure 4.43 Fatigue life curve for beams with stirrup configurations A and B.**

## 4.8 Concluding Remarks

Beams with two different stirrup configurations were tested under monotonic and repeated loading in this group. The following conclusions were drawn from this part of the study:

- Decreasing the stirrup spacing from 150 mm (stirrup configuration A) to 75 mm (stirrup configuration B) increased the monotonic bond capacity of the beams by about 30%.
- The static bond capacity of the beam with stirrup configuration A did not increase with an increase in anchorage length from 350 mm to 650 mm. Beam M-A-100-0-U (with a 350 mm anchorage length) failed at about the same load as beam M-A-100-0-2 (with a 650 mm anchorage length). For both cases failure initiated at the support. The confinement from the support increased the stiffness of the bar to concrete interface leading to higher forces in this section which resulted in the concrete keys close to the support being crushed as the bar slipped.
- The beams with stirrup configuration A tested under static loading failed in bond by concrete splitting. The concrete keys close to the support were crushed due to the confinement provided by the support. The spacing of the stirrups was great enough that the concrete keys in between the stirrups remained partially intact.
- The beams with stirrup configuration B tested under static loading failed by bond in a pull-out manner. The spacing between the stirrups was not enough to allow the bar to bend in between them. This led to the crushing of the concrete keys both at the stirrup locations and in between them.
- Corroding the beams to a mass loss of about 4.5% did not cause a reduction in the bond static capacity of the beams for either stirrup configuration.
- The beams with stirrup configuration A tested under repeated loading failed by bond fatigue.
- The fatigue life of the beams with stirrup configuration A varied linearly on a semi-log scale with the range of load applied with a shallow slope. The range of load over which fatigue bond failure occurred was very small.

- The beams with stirrup configuration B tested under repeated loading failed at higher load ranges than those beams with stirrup configuration A.
- The beams with stirrup configuration B tested under repeated loading failed by flexure at the end of a debonded region that started from the support.
- The fatigue life of the beams with stirrup configuration B varied linearly on a semi-log scale with the range of load applied with a steeper slope than the beams with stirrup configuration A.
- Doubling the number of stirrups in the anchorage zone increased the fatigue capacity of the beams at short fatigue lives. This increase diminished with increasing number of cycles.
- Further testing is required to confirm the effect of stirrups on the fatigue bond behaviour.

# Chapter 5
# Experimental Results_ Group 2 Beams

## 5.1 Introduction

This chapter presents and discusses the experimental results obtained for group 2 beams. The beams were divided into two sets according to their anchorage lengths (Set 1 – 200 mm anchorage length and Set 2 – 350 mm anchorage length). In Set 1, six beams were tested under monotonic loading and eighteen beams were tested under repeated loading. In Set 2, five beams were tested under monotonic loading and twelve beams were tested under repeated loading. The repeated loading of the beams had a fixed minimum load equal to 10 kN. The values of the maximum load were chosen to get a reasonable distribution of fatigue lives. The specimens tested in fatigue in each set were divided into four groups depending on the corrosion level and the repair condition. The four fatigue groups were:

- U-n: unrepaired and no corrosion.
- U-m: unrepaired and subjected to a mild corrosion level.
- R-m: Repaired by wrapping CFRP sheets after being subjected to a mild corrosion level.
- R-h: Repaired by wrapping CFRP sheets after being subjected to a high corrosion level

Test results are presented and discussed in the following sections.

## 5.2 Corrosion Results

The targeted theoretical mass losses were 5% and 15% according to Faraday's law. Figure 5.1 shows the actual corrosion level versus the induced current exposure time in days. For the beams corroded to a 5% theoretical mass loss, the actual mass loss varied between 4.0% and 9.66% with an average mass loss of 6.5%. This level was classified as a mild corrosion level (m). For the beams corroded to a 15% theoretical mass loss, the actual mass loss varied between 10.58% and 16.10%. This level was classified as a high corrosion level (h). The actual mass loss for the corroded beams is shown in Table 5.1 and Table 5.2 for the beams from set1 and set 2, respectively. The corrosion results from this study were consistent with previous studies with Faraday's law under-predicting the actual mass loss at low corrosion

levels and over predicting the actual mass loss at high corrosion level (Craig & Soudki, 2005; El Maadawy & Soudki, 2003; Rteil, 2007). The corrosion of the reinforcing bars was not uniform throughout the length of the bar, corrosion pits were produced (Figure 5.2). This is consistent with observations reported in the literature (Al-Hammoud, Soudki, & Topper, 2011; Absorra, Ashour, & Youseffi, 2011; Ou, Tsai, & Chen, 2012).

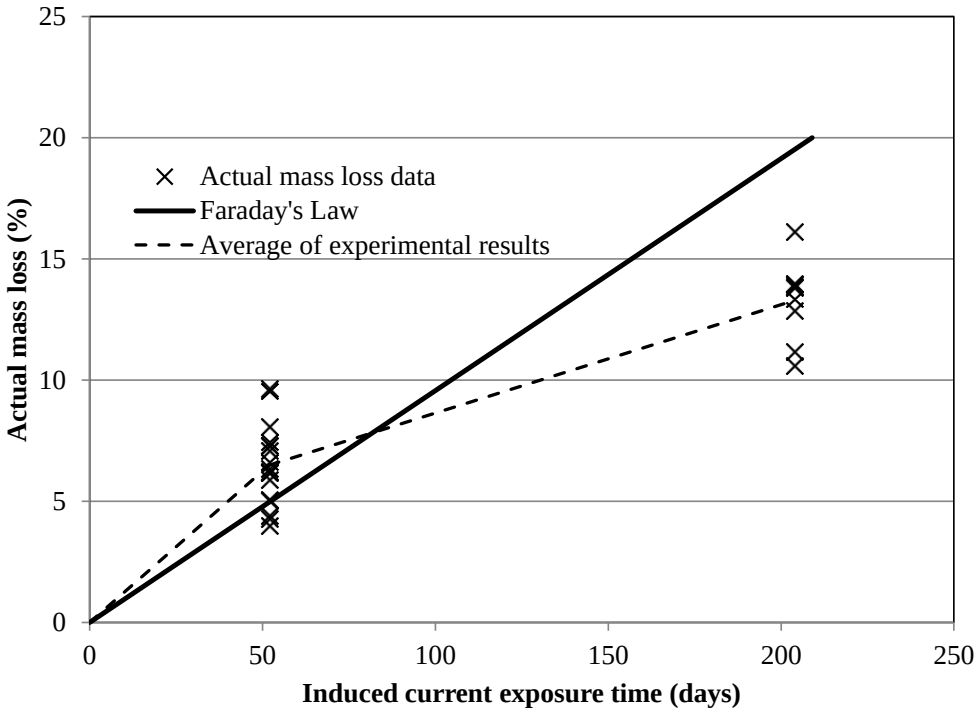


**Figure 5.1 Variation of the mass loss results versus the induced current exposure time in days.**

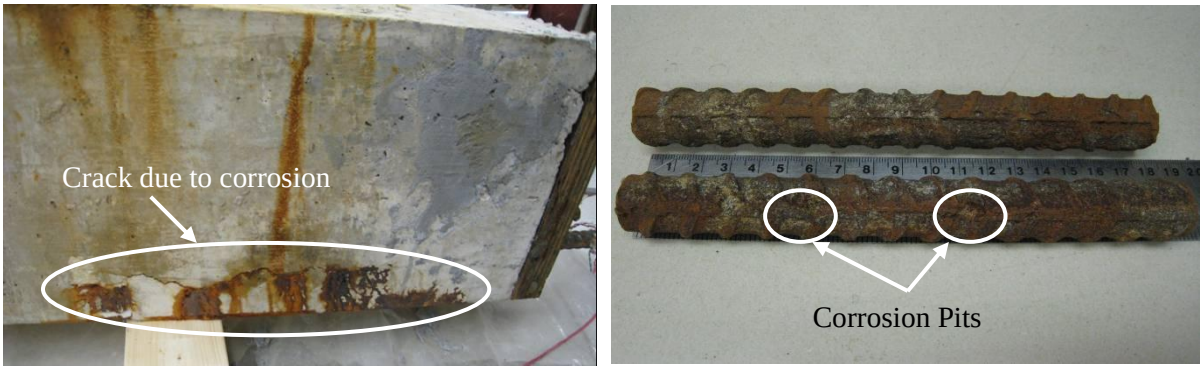


(a) (b)

**Figure 5.2: (a) cracks due to corrosion; (b) corroded bar extracted from beam F-200-R-h-88.**

The corrosion of the reinforcing steel bars in the beams caused cracks in the bottom and/or side faces. The cracks were parallel to the corroded length of the reinforcing steel bars (Figure 5.2). The crack widths for the corroded beams varied between 0.1 mm and 1.5 mm. Figure 5.3 shows a schematic drawing of the corrosion cracks for Beam M-200-R-h. The cracks were parallel to the reinforcing level from the sides and were about 0.5 mm in width. Fewer corrosion cracks were seen on the bottom of the beam and the crack widths were smaller varying between 0.1 to 0.3 mm. Figure 5.4 shows the corrosion cracks for the beams from set 1 (200 mm anchorage length) corroded to a high corrosion level (h) and tested under repeated loading (Set 1, Group R-h). Beam F-200-R-h-75 had the widest cracks from the right side close to the pocket varying between 0.8 to 0.9 mm. There were a few cracks on the bottom and left side with widths varying between 0.15 and 0.2 mm. Beam F-200-R-h-80 had wide crack widths on the three sides, 0.5 mm from the bottom, 0.6 to 0.8 mm from the left side and 0.9 to 1.0 mm from the right side. In Beam F-200-R-h-88 the corrosion cracks were wider near the right side reinforcement from the bottom and the side and varied between 1 and 1.5 mm in width. The corrosion cracks from the left side were about 0.5 mm in width. Beam F-200-R-h-96 had cracks parallel to both reinforcements in the beam. Two parallel cracks are clearly noticed on the bottom side of the beam that are about 0.6 mm in width closer to the right reinforcement and 0.8 mm in width closer to the left reinforcement. Similar parallel corrosion cracks were seen from both sides of the beam varying in width between 0.6 and 1.5 mm (Figure 5.4).

Figure 5.5 shows a schematic drawing of the corrosion cracks for Beam M-350-R-h from set 2 (350 mm anchorage length). Corrosion cracks were seen parallel to both reinforcements in the beam on the bottom and on the sides. The crack widths on the bottom were limited to widths between 0.1 and 0.2 mm. The cracks on the left side of the beam varied between 0.1 and 0.6 mm in width. The cracks were wider on the right side of the beam varying between 0.8 and 1 mm.

Figure 5.6 shows a schematic drawing of the corrosion cracks for the beams from set 2 (350 mm anchorage length) that were subjected to a mild corrosion level (Set 2, Group U-m). The corrosion cracks were drawn after the supports had been glued to the sides of the beams. This hid the cracks beyond the support point and hence the cracks were drawn only up to that point. In Beam F-350-U-m-70, corrosion cracks were parallel to both reinforcements in the

beam on the bottom and the sides. The cracks on the bottom were limited to a crack width between 0.1 and 0.3 mm. The cracks on the sides of the beam varied in width from 0.2 to 1 mm on the left side and 0.8 to 1 mm on the right side.

**Table 5.1: Actual mass loss for beams from Set 1 (200 mm anchorage length).**

| Group | Beam Notation | Corrosion Level | Theoretical mass loss (%) | Actual mass loss (%) |
|---|---|---|---|---|
| M | M-200-U-m | Mild | 5 | 4.0 |
| | M-200-R-m | Mild | 5 | 9.55 |
| | M-200-R-h | High | 15 | 13.86 |
| U-m | F-200-U-m-43 | Mild | 5 | 4.3 |
| | F-200-U-m-44 | | | 7.44 |
| | F-200-U-m-45 | | | 5.9 |
| | F-200-U-m-46 | | | 4.4 |
| | F-200-U-m-48 | | | 5.02 |
| R-m | F-200-R-m-72 | Mild | 5 | 6.18 |
| | F-200-R-m-80 | | | 6.36 |
| | F-200-R-m-90 | | | 6.18 |
| | F-200-R-m-96 | | | 7.28 |
| R-h | F-200-R-h-75 | High | 15 | 13.33 |
| | F-200-R-h-80 | | | 13.92 |
| | F-200-R-h-88 | | | 10.58 |
| | F-200-R-h-96 | | | 13.8 |

**Table 5.2: Actual mass loss for beams from Set 2 (350 mm anchorage length).**

| Group | Beam Notation | Corrosion Level | Theoretical mass loss (%) | Actual mass loss (%) |
|---|---|---|---|---|
| M | M-350-U-m | Mild | 5 | 7.09 |
| | M-350-R-m | Mild | 5 | 8.09 |
| | M-350-R-h | High | 15 | 13.98 |
| U-m | F-350-U-m-70 | Mild | 5 | 9.66 |
| | F-350-U-m-82 | | | 6.21 |
| R-m | F-350-R-m-126 | Mild | 5 | 5.06 |
| | F-350-R-m-135 | | | 7.3 |
| | F-350-R-m-140 | | | 6.62 |
| R-h | F-350-R-h-110 | High | 15 | 12.86 |
| | F-350-R-h-122 | | | 11.17 |
| | F-350-R-h-130 | | | 16.10 |

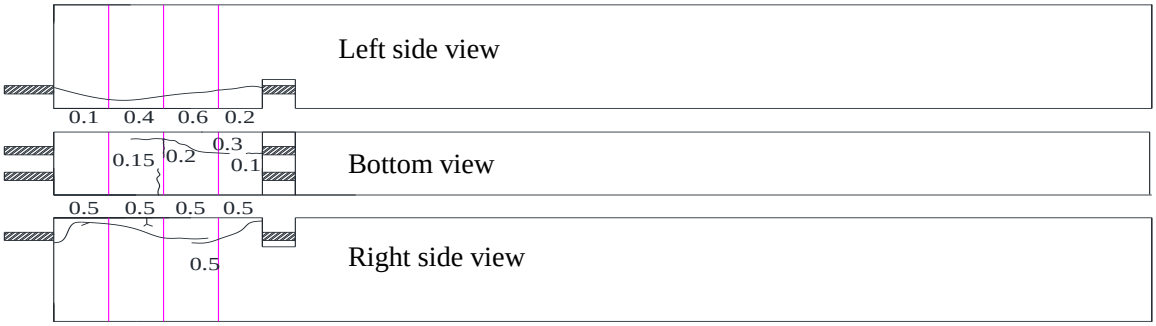


**Figure 5.3 Schematic drawing of the corrosion cracks for Beam M-200-R-h. The corrosion crack widths are measured in mm.**

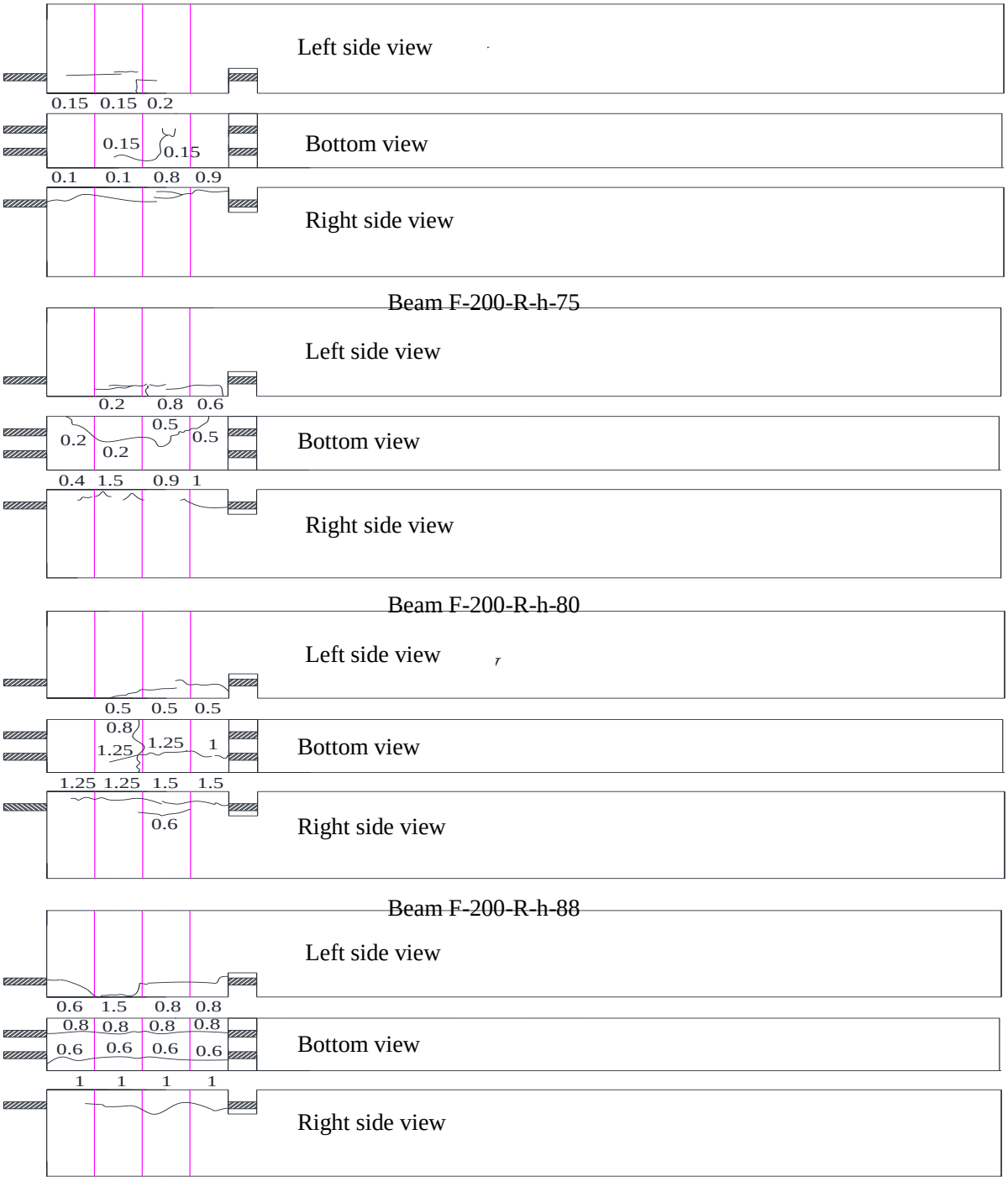


**Figure 5.4 Schematic drawing of the corrosion cracks for the beams from set 1 (200 mm anchorage length) corroded to a high corrosion level and tested for fatigue (Set 1 – Group R-h). The crack width measurements are given in mm.**

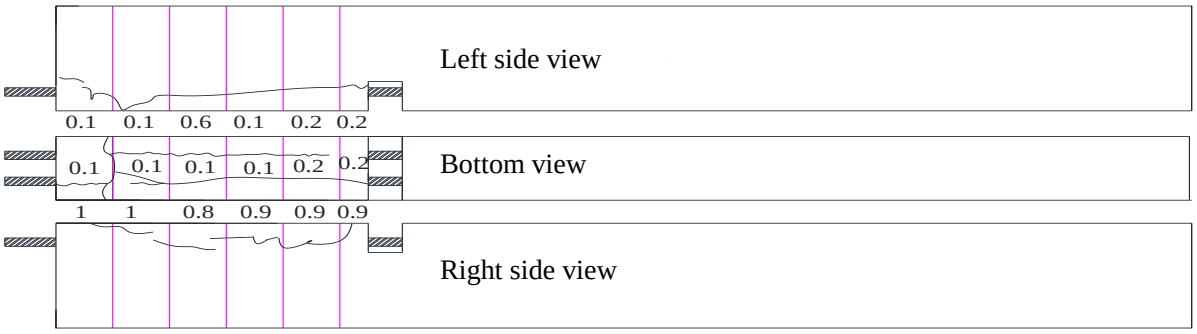


**Figure 5.5: Schematic drawing of the corrosion cracks for Beam M-350-R-h. The corrosion crack widths are measured in mm.**

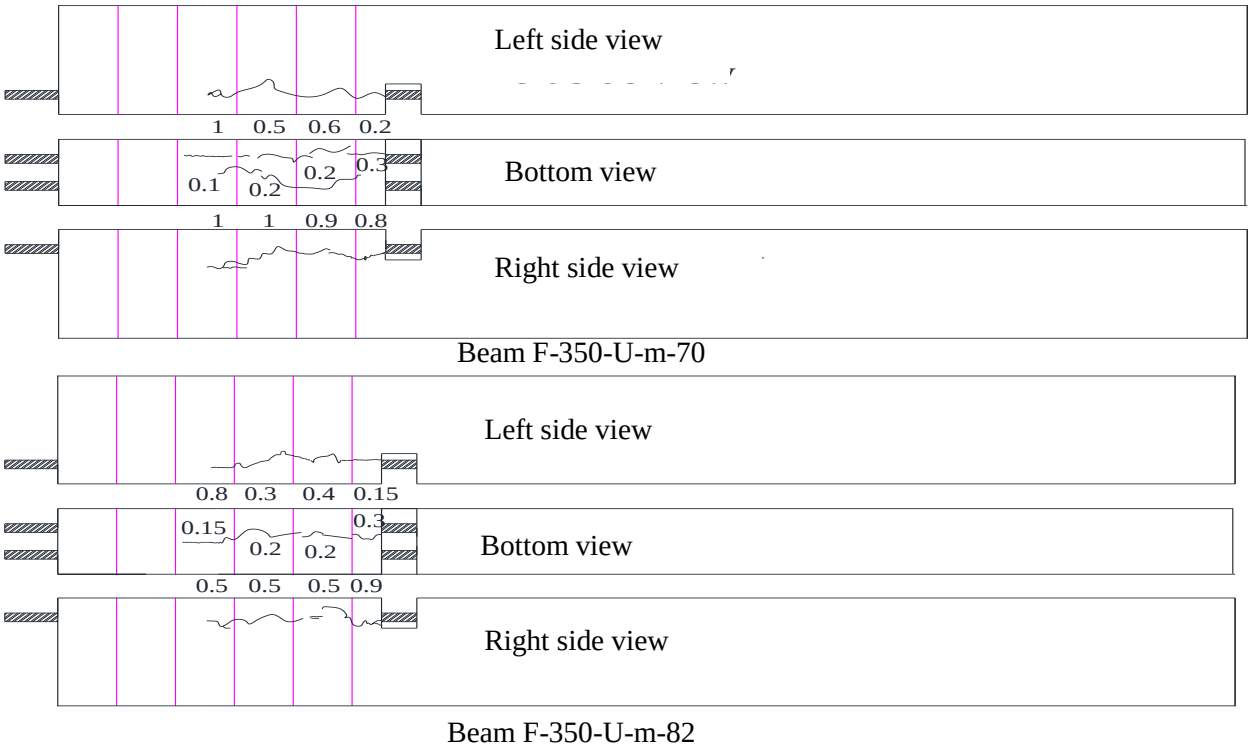


**Figure 5.6: Schematic drawing of the corrosion cracks for the beams from set 2 (350 mm anchorage length) corroded to a medium corrosion level and tested for fatigue (Set 2 – Group U-m). The crack width measurements are given in mm.**

Beam F-350-U-m-82 had corrosion cracks on both sides of the beam and the bottom of the beam. The crack widths on the bottom varied from 0.15 to 0.3 mm, while the crack widths on the sides varied between 0.15 and 0.9 mm (Figure 5.6).

Figure 5.7 shows a schematic drawing of the corrosion cracks for the beams from set 2 (350 mm anchorage length) that were corroded to a high corrosion level (Set 2, R-h). The

corrosion cracks were parallel to the reinforcement and varied in width along the corroded region (350 mm from the pocket). Beam F-350-R-h-110 had a corrosion crack width that varied between 0.2 and 1 mm on the left side, and between 0.3 and 0.4 mm on the right side and was 0.6 mm on the bottom. Beam F-350-R-h-122 had a smaller crack width of 0.1 mm on the bottom and crack widths that varied between 0.1 and 0.6 mm on both sides. The crack widths for Beam F-350-R-h-130 varied between 0.2 and 0.8 mm on the sides and were 1.25 mm wide on the bottom.

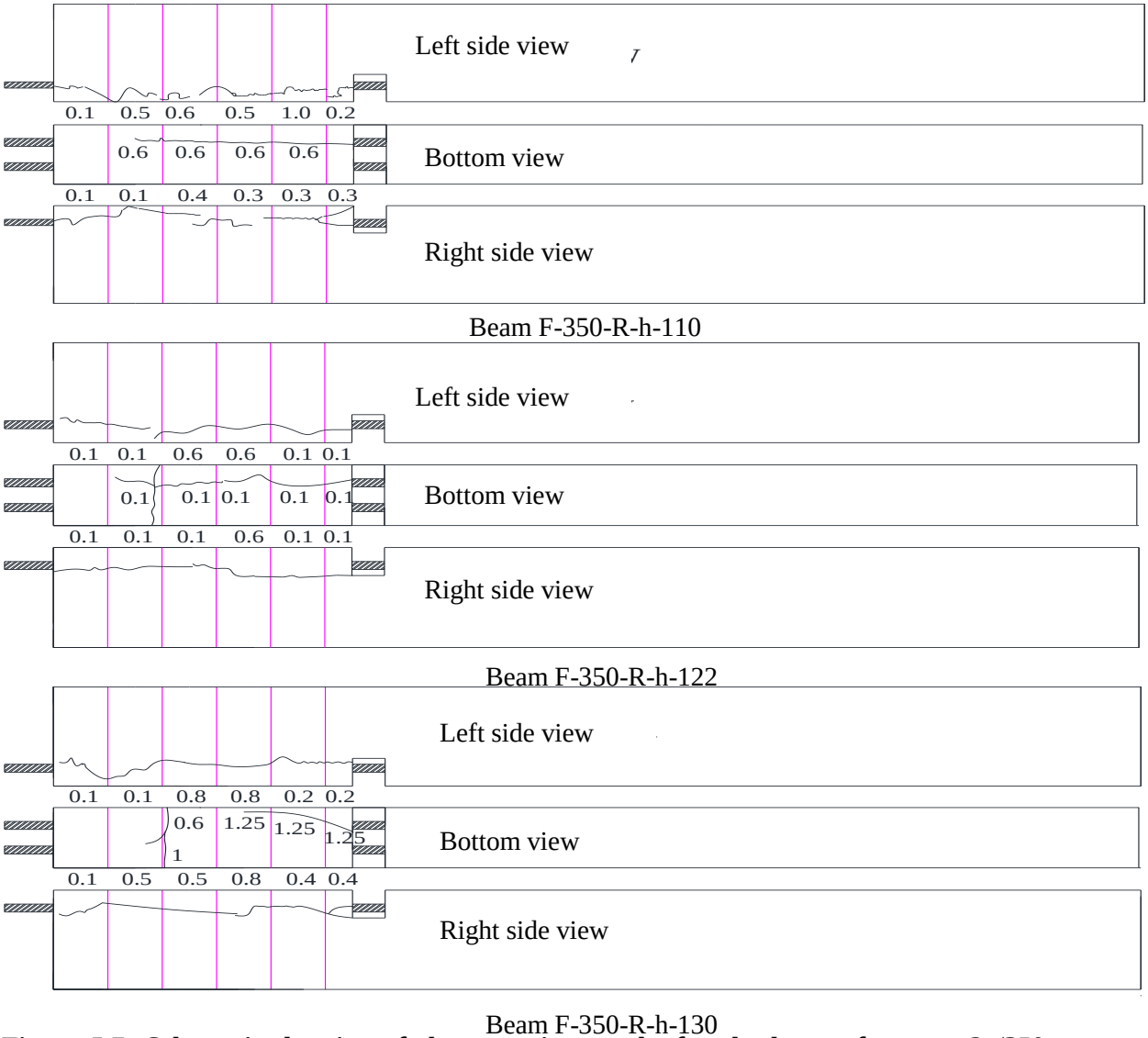


**Figure 5.7: Schematic drawing of the corrosion cracks for the beams from set 2 (350 mm anchorage length) corroded to a high corrosion level and tested for fatigue (Set 2 – Group R-h). The crack width measurements are given in mm.**

## 5.3 Static Test Results

Eleven beam-anchorage specimens were tested in this part of the study under monotonic loading. Six beams belonged to set 1, Group M (200 mm anchorage length) and five beams belonged to set 2, Group M (350 mm anchorage length). The aim of testing these beams was to determine the static capacity of the beams under different corrosion levels and/or repair conditions.

### 5.3.1 Set 1 Beams

#### 5.3.1.1 Overall behaviour and mode of failure

In set 1, Beams M-200-U-n-1 and M-200-U-n-2 were the control beams: not corroded and not repaired, but were repeated because they were from 2 different casts. Beams M-200-R-n, M-200-R-m and M-200-R-h were repaired with a U-wrapped CFRP sheet in the anchorage zone (200 mm length) and were subjected to different corrosion levels: no corrosion level (n), a mild corrosion level (m), and a high corrosion level (h) respectively. These beams were used to study the effect of repair with U-wrapped CFRP sheets on the beams with different corrosion levels. Finally beam M-200-U-m was corroded to a mild corrosion level and un-repaired. This beam was used to determine the effect of mild corrosion on the bond behaviour at the steel to concrete interface.

Four cracks were formed in the constant moment region of the beams, two cracks in the middle of the beam and the other two cracks under the point loads. The scarcity of cracks was attributed to the fact that the bar was unbonded over the central constant moment region.

A diagonal crack was observed while the beam was being tested that initiated close to the support point and propagated along the beam. As the load on the beam was increased a vertical crack propagated from this diagonal crack at the location of the middle stirrup in the anchorage zone and propagated across the bottom face of the beam. In addition, a longitudinal crack on the bottom of the beam that initiated at the loaded end of the anchorage zone (next to the pocket) was observed. This longitudinal crack propagated along the length of the anchorage zone parallel to the bar. The U-wrapped CFRP sheet in the repaired beams prevented the observation of any side cracks in the anchorage zone of the beam.

The beams all failed by bond (bar slipping). In the cases were the beams were repaired with U-wrapped CFRP sheets, the FRP ruptured after the bar slipped causing failure of the beam by bond. After failure, the bar in the bonded region was removed to inspect the failure which occurred at the bar-concrete interface. It was observed in the unrepaired beams that the concrete keys underneath the bars were intact (Figure 5.8). This suggested that the concrete below the bar was split off and pushed away offering little resistance to slip. The concrete above the bar was crushed close to the pocket, where a stirrup was located (Figure 5.9). The concrete keys along the rest of the anchorage zone were scraped but were still visible. The indentations of the concrete keys along the rest of the anchorage zone were measured and it was found that the indentations were smaller in height in the wrapped beams compared to the unwrapped beams. This suggested that the concrete above the bar, which was held to the bar by the stirrups, resisted slip and was crushed close to the stirrup but the bar bent in between stirrups decreasing the resistance provided by the concrete keys. In the case where CFRP sheets were used to repair the beams, the CFRP sheets confined the concrete and increased the resistance provided by the concrete keys which caused the concrete keys to be crushed along the entire anchorage length before the beam failed in bond at a higher load level.

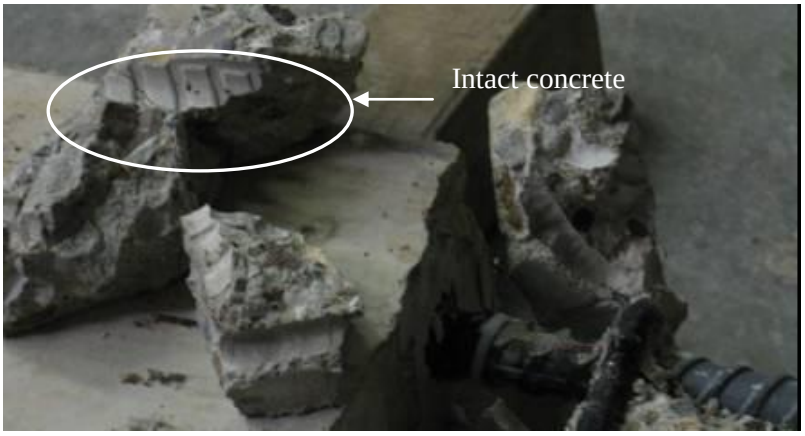


**Figure 5.8: intact concrete taken from the anchorage zone from below the steel bar.**

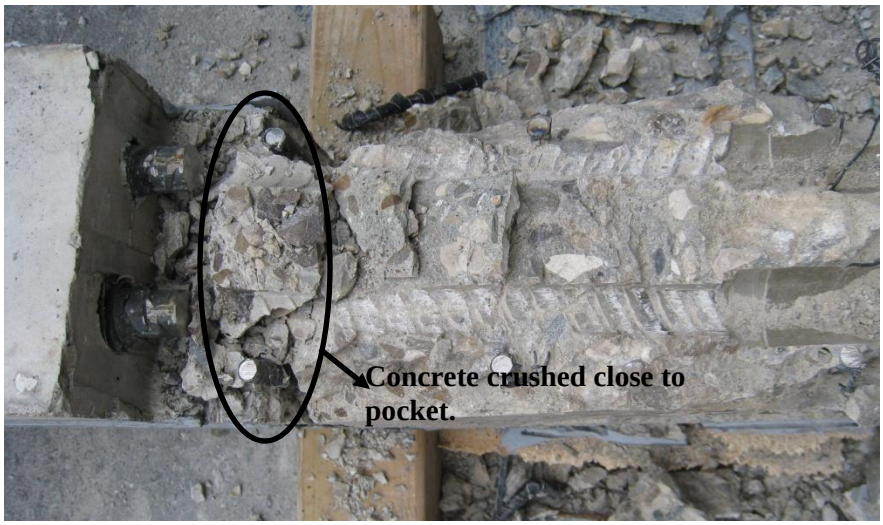


**Figure 5.9: Beam M-200-R-n after failure and removing the bar from the anchorage zone. The beam was turned upside-down.**

5.3.1.2 Load Deflection Behaviour

The load versus midspan deflection curves for the six beams from set 1 (200 mm anchorage length) tested monotonically to failure are shown in Figure 5.10. Beam M-200-U-n-1 cracked at a load of 13.5 kN and a mid-span deflection of 1.0 mm. The maximum load was 99.7 kN with a corresponding mid-span deflection of 6.79 mm. Then the load dropped to 91kN and maintained that level until a mid-span deflection of 8 mm was reached, beyond which a sudden load drop was observed with a complete bond failure. A similar behaviour was observed for Beam M-200-U-n-2 where the maximum load was 90.7 kN corresponding to a mid-span deflection of 6.57 mm. The corrosion of the internal steel reinforcement to a mild corrosion level (4% mass loss) caused a reduction in the maximum static capacity of the beam to a load of 73.7kN, i.e. a 23% decrease in comparison with the uncorroded beams. On the other hand, the use of the U-wrapped CFRP sheets in the anchorage zone of the uncorroded beam increased the beam's static capacity by 80% compared to the uncorroded, unstrengthened beam. The CFRP repaired beam reached 172.6 kN maximum load with a corresponding mid-span deflection of 11.26 mm. Repairing the beam that was corroded to a mild corrosion level, Beam M-200-R-m, increased the static capacity of the beam by 68% compared to the similar beam corroded to a mild corrosion level. Beam M-200-R-m reached a maximum load of 123.68 kN with a corresponding mid-span deflection of 8.85 mm. This was about 25 % above the maximum load reached by the control beams. Beam M-200-R-h

was corroded to a high corrosion level (13.86% actual mass loss) and then repaired with CFRP sheets before being tested. After the beam reached a load of 105 kN the LVDT measuring the displacement at mid-span stopped reading at 4.28 mm. The deflection reading were then calculated after this point using the data from the internal LVDT. The maximum load reached by this beam was 119.58 kN with a corresponding mid-span deflection of 6.6 mm. This load was above the maximum load reached by the control beams by about 26% and close to the load reached by the beam repaired and tested at a mild corrosion level (Beam M-200-R-m). Corroding the bars inside the beams decreased the bond at the steel-concrete interface; repairing the corroded beams with CFRP sheets confined the concrete around the interface. The capacity of the beams then depended on the capacity of the CFRP sheets since failure was by CFRP sheet rupture. Repairing the corroded beams with CFRP restored the strength of the beam and increased it by about 25% compared to the control (uncorroded and unrepaired) beams.

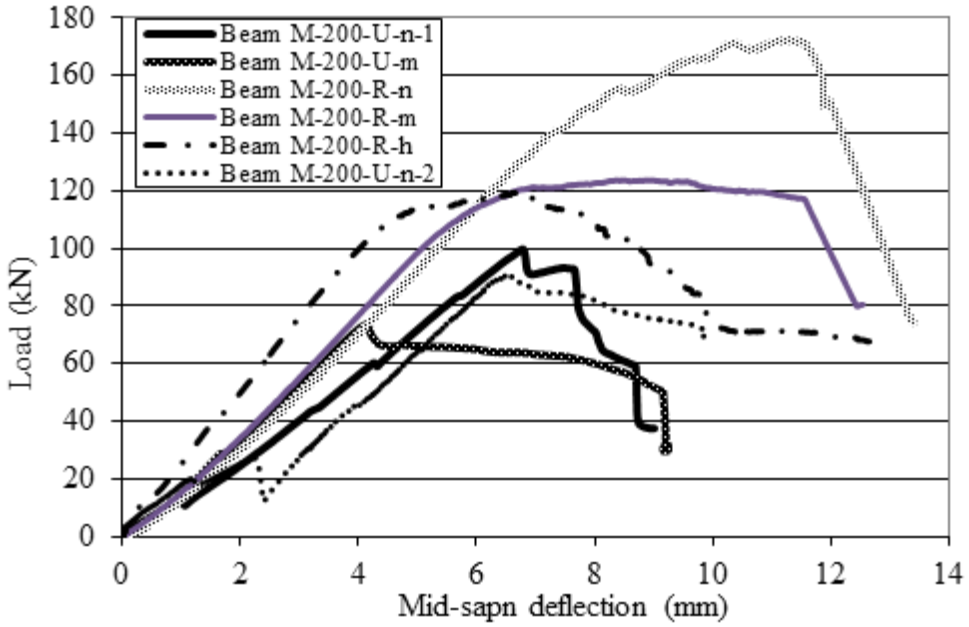


**Figure 5.10: Load versus midspan deflection for the beams from Set1-Group M.**

5.3.1.3 Strain Behaviour

Observations of the strain behaviour of the steel bar in the beam helped define the debonding stages of the bar and the failure location as explained in Section 4.4. All the monotonic beams in set 1 had similar load-strain behaviour where the strain increased linearly with

increasing load before cracking occurred. Debonding started from the pocket and moved towards the support. In some beams the strain values indicated that debonding started before the beam reached the maximum load (Figure 5.11). In other beams debonding was not evident until after the maximum load was reached (Figure 5.12). As shown in Figure 5.11 and Figure 5.12, the strain values increase with increasing load. Once cracking occurs the strain at the location of the crack would be equal to the value of the strain from the cracked section analysis. As the bar debonded, the value at the end of the debonded region from the pocket would be equal to the strain value at the beginning of the debonded region. As seen in Figure 5.11 and Figure 5.12, debonding started from the pocket and propagated towards the support. The strain behaviour for all the beams in set 1 of group 2 is shown in Appendix D.

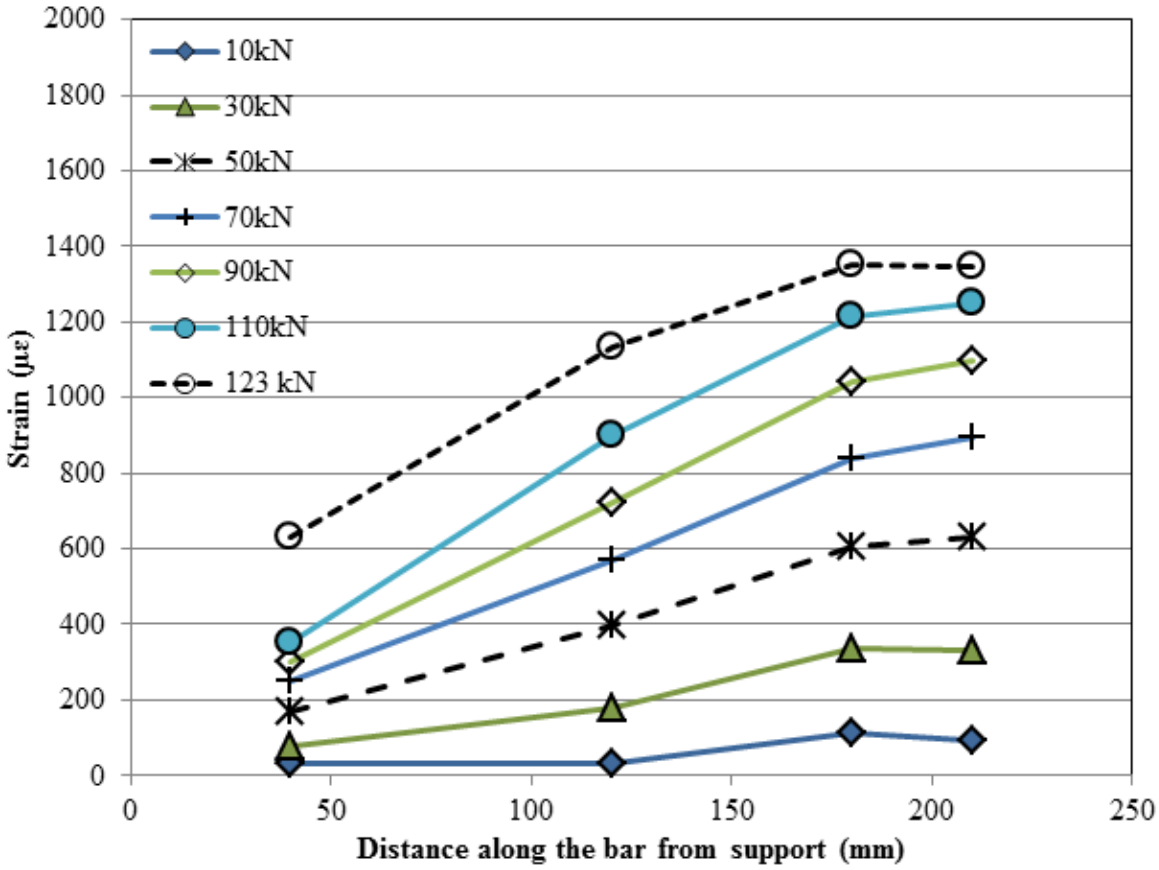


**Figure 5.11 Strain profile for Beam M-200-R-m.**

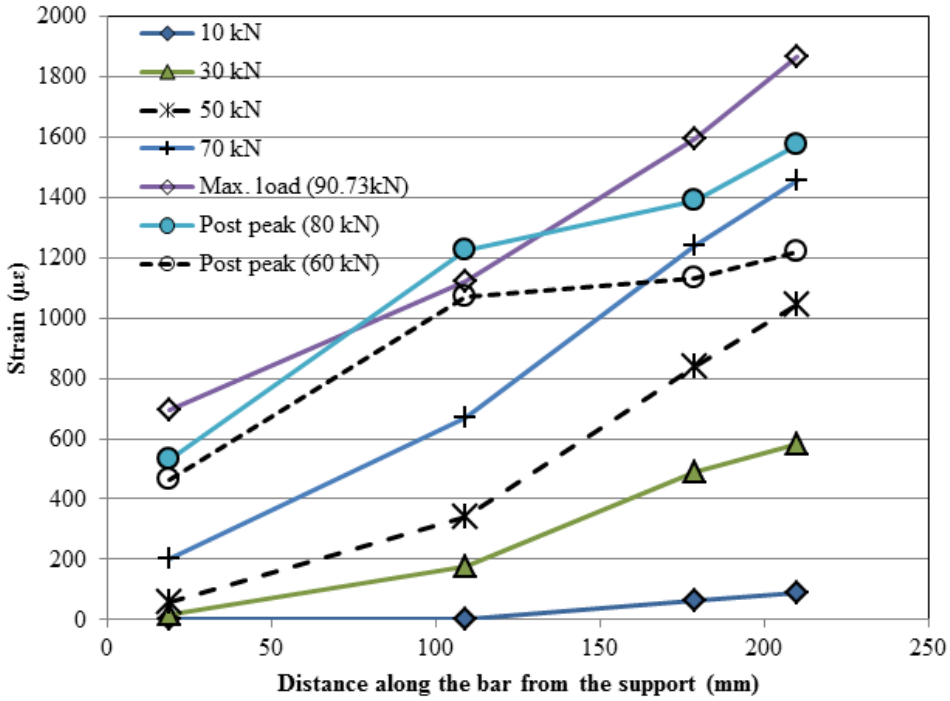


**Figure 5.12 Strain profile for bar 1 in Beam M-200-U-n-2.**

### 5.3.1.4 Steel slip behaviour

In the discussion in this section, "the loaded end" begins at the point close to the pocket where the anchorage zone starts. The free end refers to the end of the anchorage zone at the support location.

Figure 5.13 shows the load-slip behaviour of beam M-200-U-n-2. It can be seen that the slip increased with increasing load at a low rate until the maximum load was reached after which the slip increased at a higher rate. Up to the maximum load the slip increased more at the loaded end than at the free end. This was because the slip measured at the loaded end included the axial deformation of the bar due to the applied load (FIB, 2000). As the slip increased with decreasing load the bar moved as a rigid body causing the changes in slip values from the loaded end and the free end to be equal. Initially the longitudinal cracking in the concrete started at the loaded end causing a decrease in the bond between the steel and concrete. Since the concrete at the free end was still uncracked, the slip was small. At the maximum load longitudinal cracking propagated along the anchorage zone causing the bar to slip at an increasing rate until the complete failure of the beam occurred. The slip reached at maximum load was about 0.1 mm after which the slip increased with decreasing load. Once

the slip was 0.5 mm the slip increased at a higher rate with decreasing load until total failure of the beam (Figure 5.13).

The repaired beams behaved slightly differently. The confinement from the CFRP maintained the load and prevented a drop in the load until the slip was 1.5 mm after which the CFRP ruptured causing the load to drop at an increasing rate with increasing slip (Figure 5.14). CFRP confinement enhanced the ductility of bond failure and increased the overall toughness of the repaired beam.

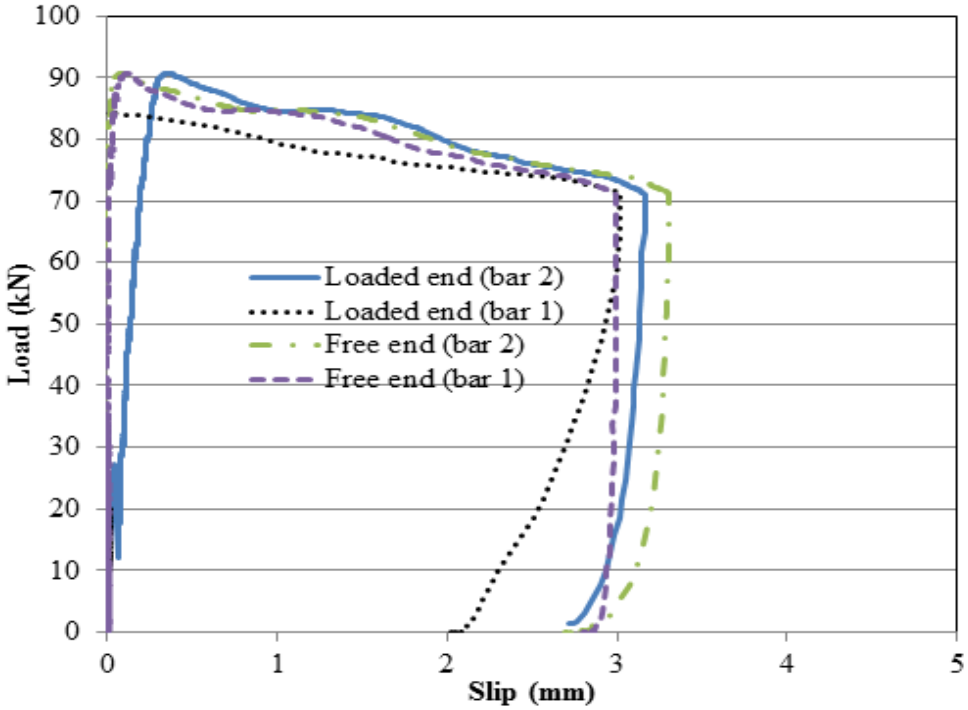


**Figure 5.13: Load Slip behaviour for Beam M-200-U-n-2.**

The free end slip for both bars in the corroded beam Beam M-200-U-m was the same. There was almost no slip until a load of about 40 kN. The slip then increased with increasing load until it reached 0.03 mm at the maximum load. Beyond maximum load the slip increased slowly with decreasing load until the slip was about 0.5 mm after which the slip increased at a faster rate with decreasing load (Figure 5.15).

Repairing the corroded beam caused the load capacity to increase with increasing slip until the slip was 1.5 mm at maximum load for Beam M-200-R-m (Figure 5.16). The slip then increased rapidly with a small decrease in load (clearly demonstrating an enhancement in

ductility of failure) until the FRP debonded from one side causing the load to drop at a higher rate with increasing slip (Figure 5.17).

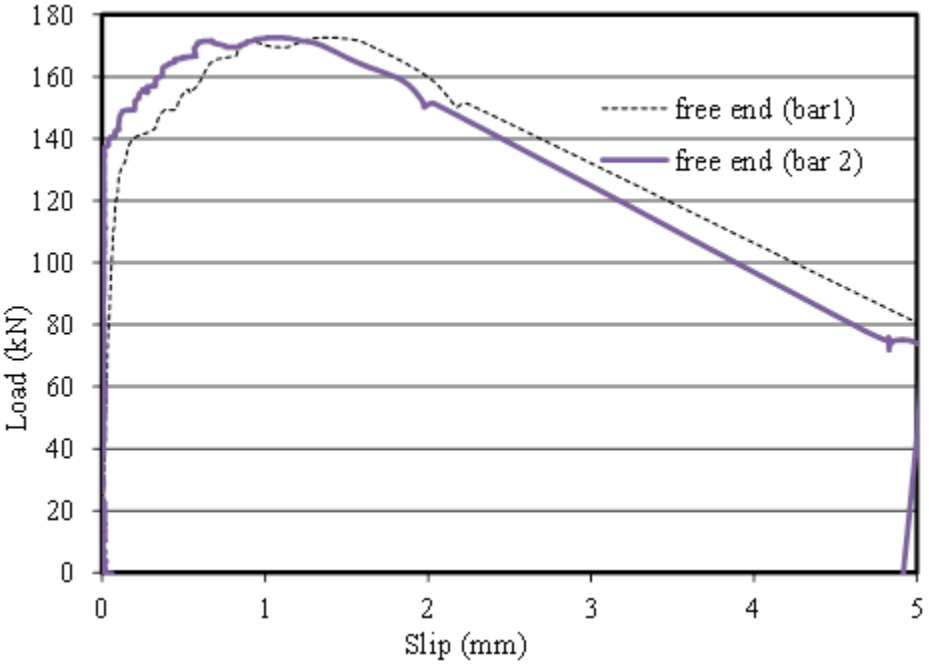


**Figure 5.14 Load versus slip behaviour for Beam M-200-R-n.**

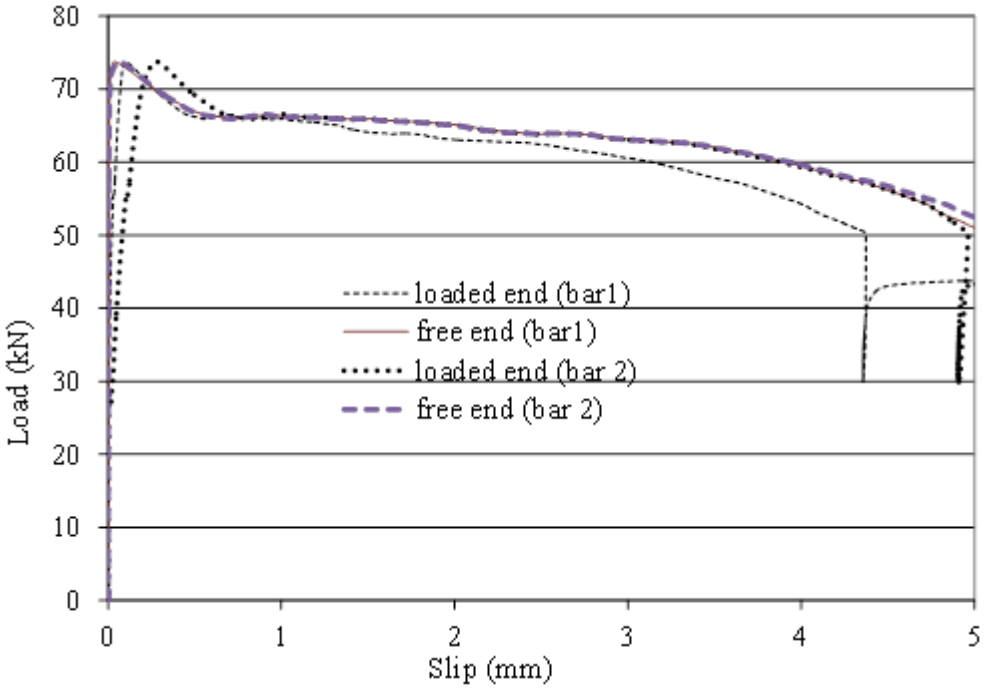


**Figure 5.15 Load versus slip behaviour for Beam M-200-U-m.**

Beam M-200-R-h, the beam that was corroded to a high corrosion level and then repaired with U-wrapped CFRP sheets, reached a maximum load at a 1.5 mm slip. The CFRP sheet then ruptured causing the load to drop with increasing slip.

Figure 5.18 shows a schematic drawing of the geometry of the M-20 deformed bar used to reinforce the beams for this study. The 1.5 mm slip that caused complete failure of the repaired beams was enough to destroy half of the concrete key at each lug. For the unrepaired uncorroded beams the maximum load was reached when the slip was 0.1 mm which was enough to cause a slight crushing of the concrete keys close to the lugs and a drop in the load. Once slip reached 0.5 mm, the amount of crushed concrete was enough to cause an increased slip rate with decreasing load and this led to failure of the beam. The concrete was not confined except at the stirrup locations allowing for the bar to slip and separate from the concrete keys in between the stirrups, leaving the concrete keys intact or partially scraped in most cases. Figure 5.19 shows the concrete keys on top of the reinforcing bar after failure for Beam M-200-U-n-2. The concrete keys are crushed at the loaded end stirrup location and are intact along the rest of the bonded length. For the corroded unrepaired beam, the rust products caused enough damage to the concrete keys that the maximum load was reached when only 0.03 mm slip had occurred (Figure 5.20). Similarly, once the slip reached 0.5 mm, enough concrete was crushed that the bar continued to slip at an increasing rate. The 0.5 mm slip in both cases was enough to cause crushing of the concrete close to the stirrups at the loaded end and complete slip of the bar. The repaired beams with the confinement from the CFRP attained a higher slip (1.5 mm) before the rupturing or debonding of the CFRP sheet. Then there was complete slip of the bars. In the CFRP repaired beams, the concrete keys were crushed along the entire bonded length (Figure 5.21).

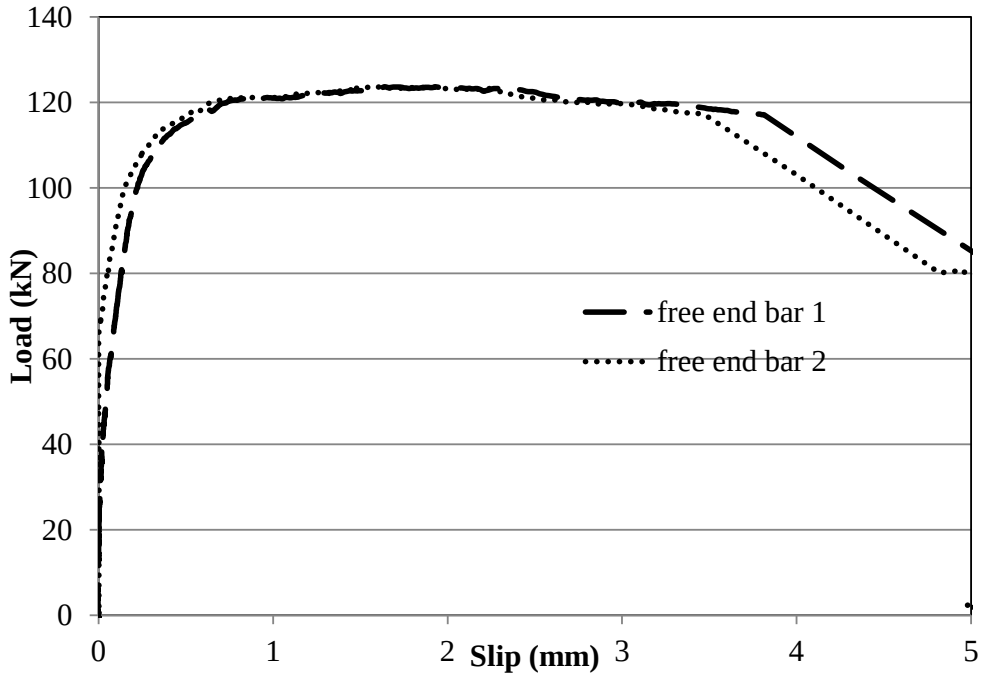


**Figure 5.16 Load versus slip for Beam M-200-R-m.**

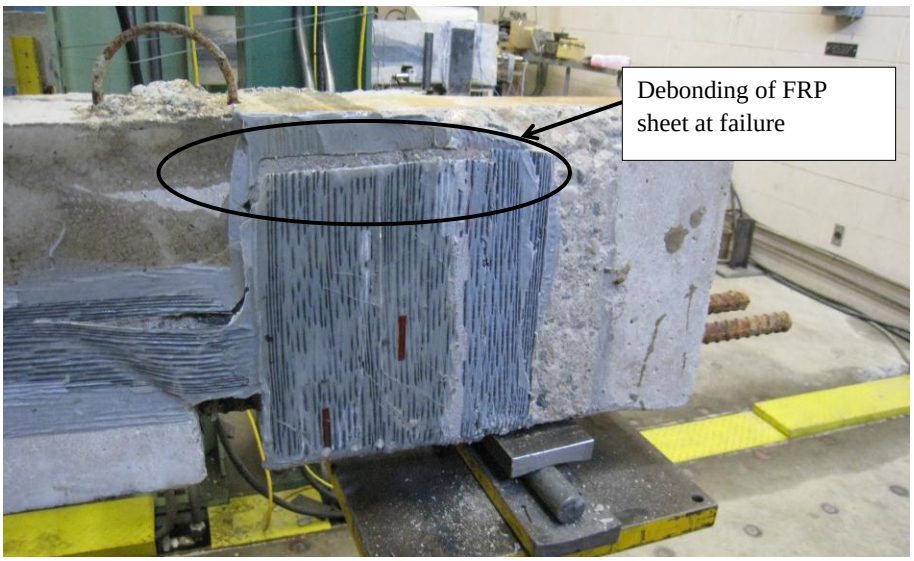


**Figure 5.17 Beam M-200-R-m after failure.**

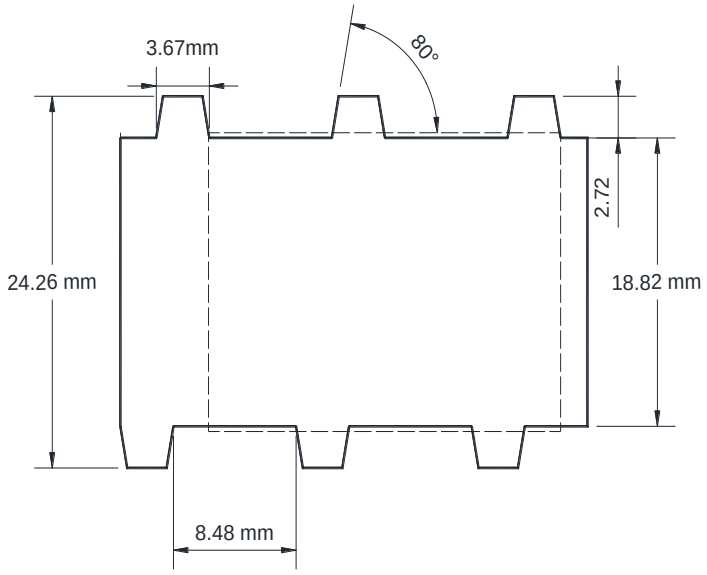


**Figure 5.18 Schematic drawing showing bar dimensions for M-20 bars used to reinforce the beams in the current study. All dimensions are in mm.**

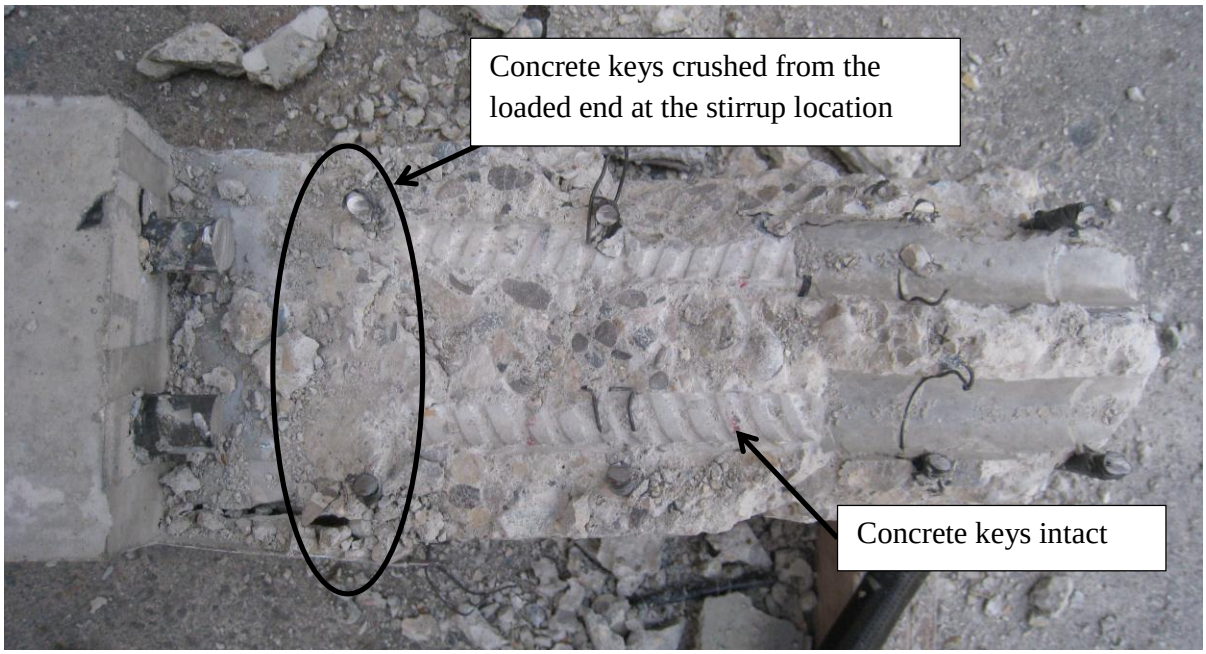


**Figure 5.19 Beam M-200-U-n-2 after failure and removing the reinforcing bars to examine the concrete keys. The beam was turned upside down.**

**Figure 5.20 Beam M-200-U-m after failure and removing the reinforcing bars to examine the concrete keys. The beam was turned upside down.**

**Figure 5.21 Beam M-200-R-n after failure and removing the reinforcing bars to the concrete keys. The beam was turned upside down.**

#### 5.3.1.5 Bond Stress

Three strain gauges were mounted on the bars in each beam along the bonded length and one in the pocket. Some beams had the three strain gauges mounted in both bars, and others had the strain gauges mounted on only one bar, but all the bars in all the beams had strain gauges mounted in the pocket. The average bond stress was calculated as the applied force in the bar between two strain gauges divided by the bar surface area between the two strain gauges as given in **Equation 5-1**.

$$u = \frac{A_b(\Delta f_s)}{\pi d_b l} = \frac{(\Delta f_s) d_b}{4l}$$ **Equation 5-1**

where, $u$ is the average bond strength in MPa,

$A_b$ is the cross-sectional area of the steel bar in mm$^2$,

$\Delta f_s$ is the change in steel stress in the bar along the length $l$ in MPa,

$d_b$ is the bar diameter in mm,

$l$ is the length of the bar between two gauges in mm.

The change in steel stress along the bar length was calculated from the change in strain along a length $l$ measured by the strain gauges installed in the anchorage zone of the bar and in the pocket multiplied by the modulus of elasticity (200,000MPa) ($\Delta f_s = E.\Delta\varepsilon$).

Figure 5.22 shows the average bond stress versus applied load behaviour for one bar in beam M-200-U-n-2. The average bond stresses reported were for regions in between the strain gauges mounted in the bar. G1, G2, G3 and G4 refer to strain gauges 1, 2, 3, and 4 located along the length of the bar as shown in Figure 5.23. From Figure 5.22 G1-2 refers to the average bond stress calculated for the bar region between strain gauges 1 and 2, similarly G2-3 and G3-4 refer to average bond stresses calculated between strain gauges 2 and 3, and 3 and 4 respectively. G1-FE refers to the average bond stress calculated between strain gauge 1 and the free end (FE). As seen in Figure 5.23, stirrups are found between G1 and G2 as well as G3 and G4, suggesting that the bond stress calculated between these strain gauges included the effect of the stirrups. No stirrups were located between G2 and G3 or between G1 and FE. From Figure 5.22 it can be seen that up to 10 kN the bond stress for G1-2 and G1-FE was zero suggesting that the bar from the support to G2 was taking almost no bond force. Thus the length of the bar between G2 and the pocket was enough to resist the force in the bar up to 10kN load. As the load increased from 10 kN to 30kN the bond force was being taken almost uniformly along the length of the bar from G1 to the pocket (Figure 5.12). The length of the bar between the support (FE) and G1 was taking little force and the bond stress (G1-FE) was nearly zero up to 30 kN load (Figure 5.22). As the applied load increased beyond 30 kN the bond stress was distributed along the entire anchorage length of the bar

(200 mm) up to about 60 kN applied load. As the load increased above 60 kN, the average bond stress between G3-4 (close to the pocket) remained constant at about 7.6MPa with increasing load until the load applied reached about 80 kN (Figure 5.22). This coincided with an increase in slip from 0.01 mm at 60 kN load to 0.03 mm at 80 kN from the free end (Figure 5.24). The bond stress then increased to about 9 MPa at maximum load after which it decreased with decreasing load, this increase in bond stress is associated to the effect of the stirrup that was confining the bar at this location. The average bond stress between G2-3 dropped from a maximum of 8.2 MPa at 60 kN to an average bond stress of 6.8 MPa at 80 kN. The bond stress then remained constant at 6.8 MPa with increasing load and increasing slip from 0.03 mm at 80 kN to 0.12mm at maximum load after which the bond stress decreased with decreasing load. The average bond stress in G1-2 continued to increase from 3.8 MPa at 60 kN until 5.5 MPa at 75 kN after which it remained constant until just before peak load where it dropped slightly then started to increase with decreasing load. The bond stress between G1-FE increased from 2.1 MPa at 60 kN to 17.8 MPa at peak load after which it dropped with decreasing load.

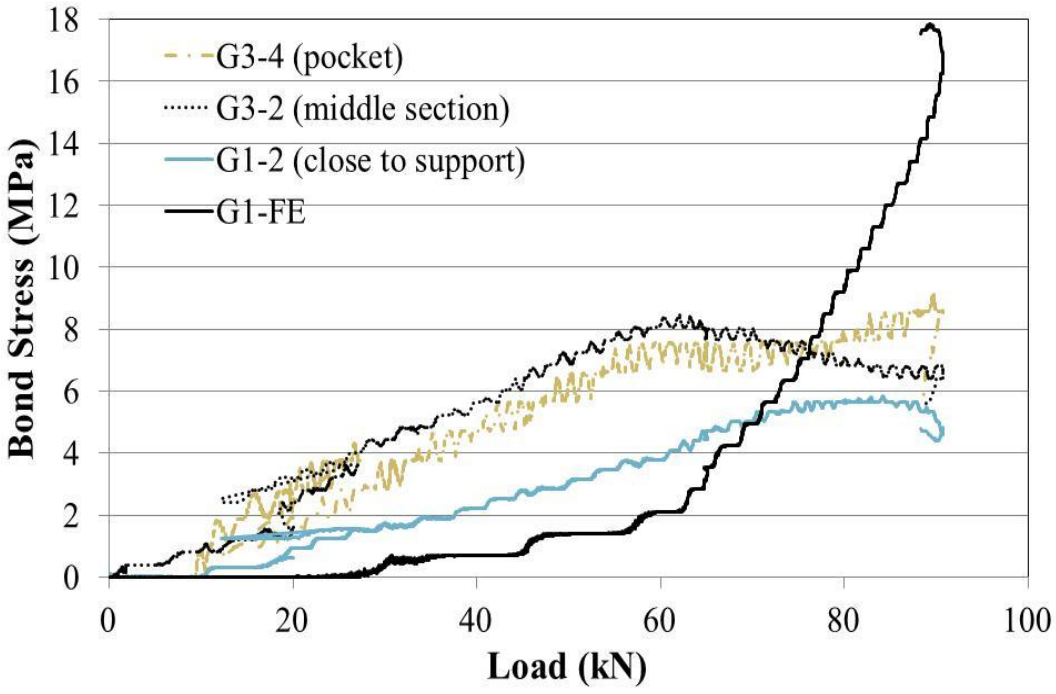


**Figure 5.22 Bond Stress versus load for Beam M-200-U-n-2.**

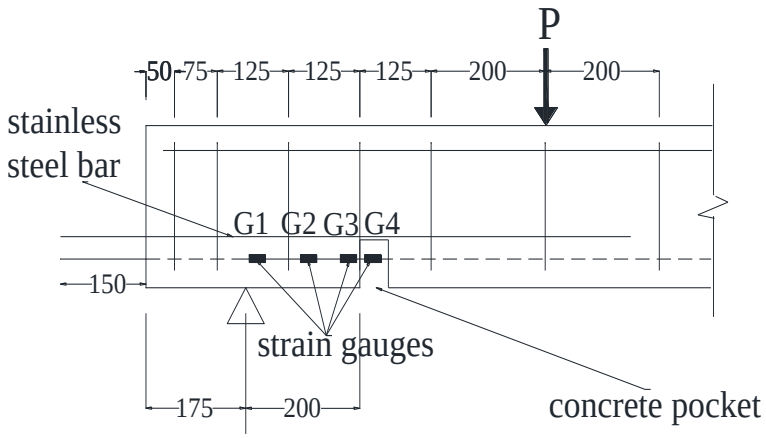


**Figure 5.23 A section of Set1 beams along with the locations of the strain gauges along the length of the bar.**

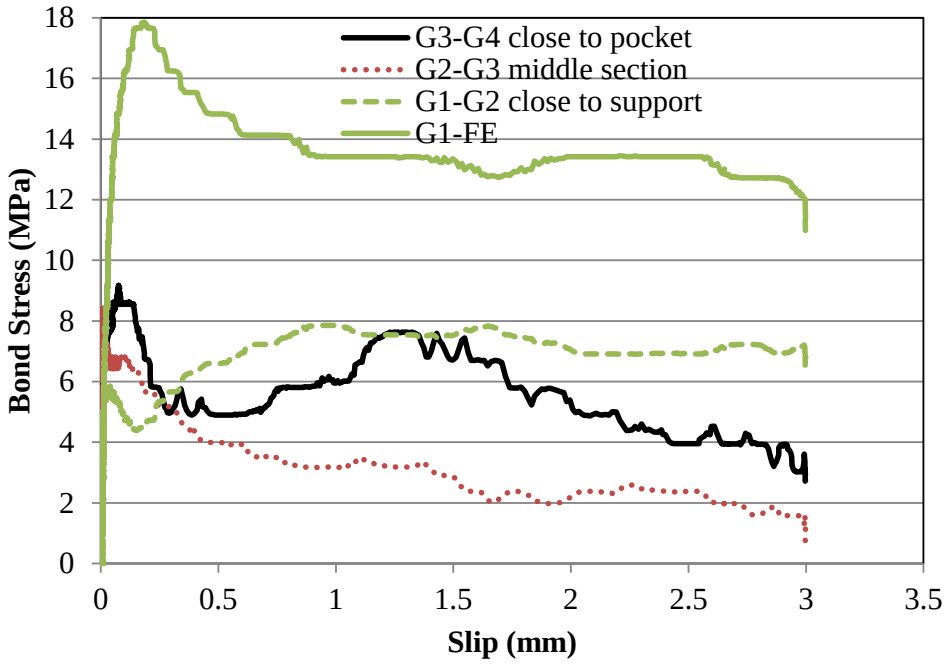


**Figure 5.24 Average bond stress along the length of the bar versus slip for Beam M-200-U-n-2.**

In summary, the tensile force in the bar at midspan was resisted by the bond force along the anchorage length. As slip reached 0.01 mm at 60 kN load, the bond stress close to the pocket decreased between G2-3 and remained constant between G3-4 with increasing load. The bonded area close to the support resisted the increase in tensile force in the bar causing the bond stress to increase at an increasing rate. The concrete keys close to the pocket then

crushed at the stirrup location reducing the bond stresses at these locations causing failure of the beam.

Gluing the supports to the sides of the beam was supposed to reduce the confinement effect of the supports to the concrete-steel interface. The high bond stress values near the support indicated that the supports still confined the concrete near the concrete-steel interface. It was noticed that in the cases where the concrete cracked from the side along the length of the bar, the steel plate used to transfer the load to the beam prevented the longitudinal crack from opening past the edge of the plate in that location causing confinement of the concrete. Another crack then propagated from the bottom of the beam reducing the bond stress close to the support and allowing slip leading to failure of the beam (Figure 5.25).

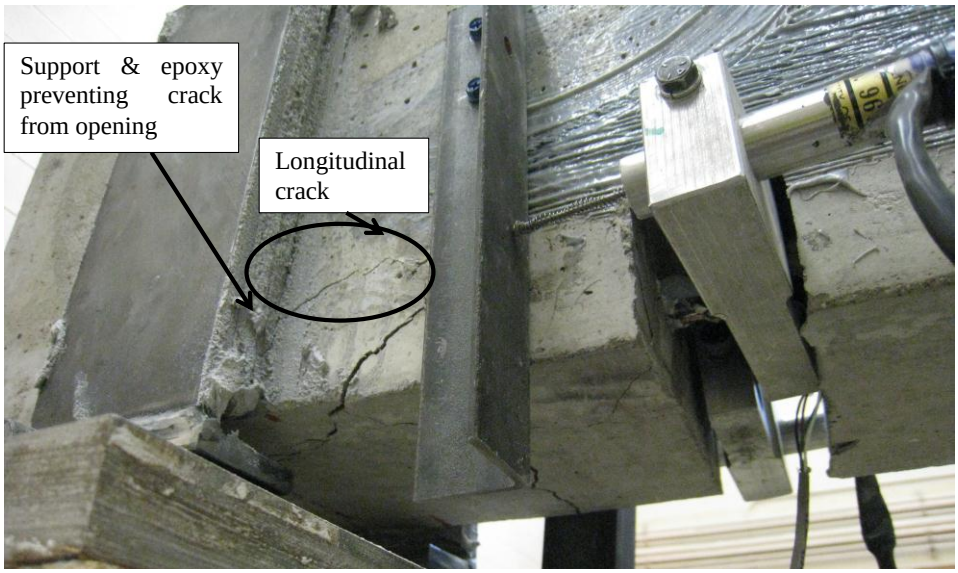


**Figure 5.25 Beam M-200-U-n-2 after failure**

Beam M-200-R-n was first tested with the same support plate width of 100 mm as the rest of the group. While testing the beam, the supports failed at a load of 137 kN without failure of the beam. Wider support plates of 200 mm width were then glued to the sides of the beam and used as supports. The wider support plates increased the confinement effect from the plates. This was clear from the increased bond stress resisted by the bar close to the support (Figure 5.26). Figure 5.26 shows the bond stress versus load behaviour in the final test to failure for Beam M-200-R-n. The bond stress was almost uniform along the bonded length, between the support (FE) and G3 (approximately 197 mm), until the bond stress in the region

G2-3 reached 8.7 MPa, after which the region G2-3 remained at a constant bond stress with increasing load. The bond stress between G1-2 and G1-FE continued to increase with increasing load until the bond stress value was 17 MPa. The load then dropped and the beam failed.

In summary, the maximum bond stress reached was between 8 and 9 MPa for the areas that were not confined by the supports. After the maximum bond stress of 8 or 9 MPa was reached, the bond stress either stayed constant or dropped in these regions, and the bond close to the support resisted the extra force in the bar due to the increase in applied load. The confinement from the support allowed this region to take up the extra bond force until a maximum bond stress ranging between 17 and 18 MPa was reached in this region causing failure of the beam. This observation was similar for the control repaired and un-repaired beams.

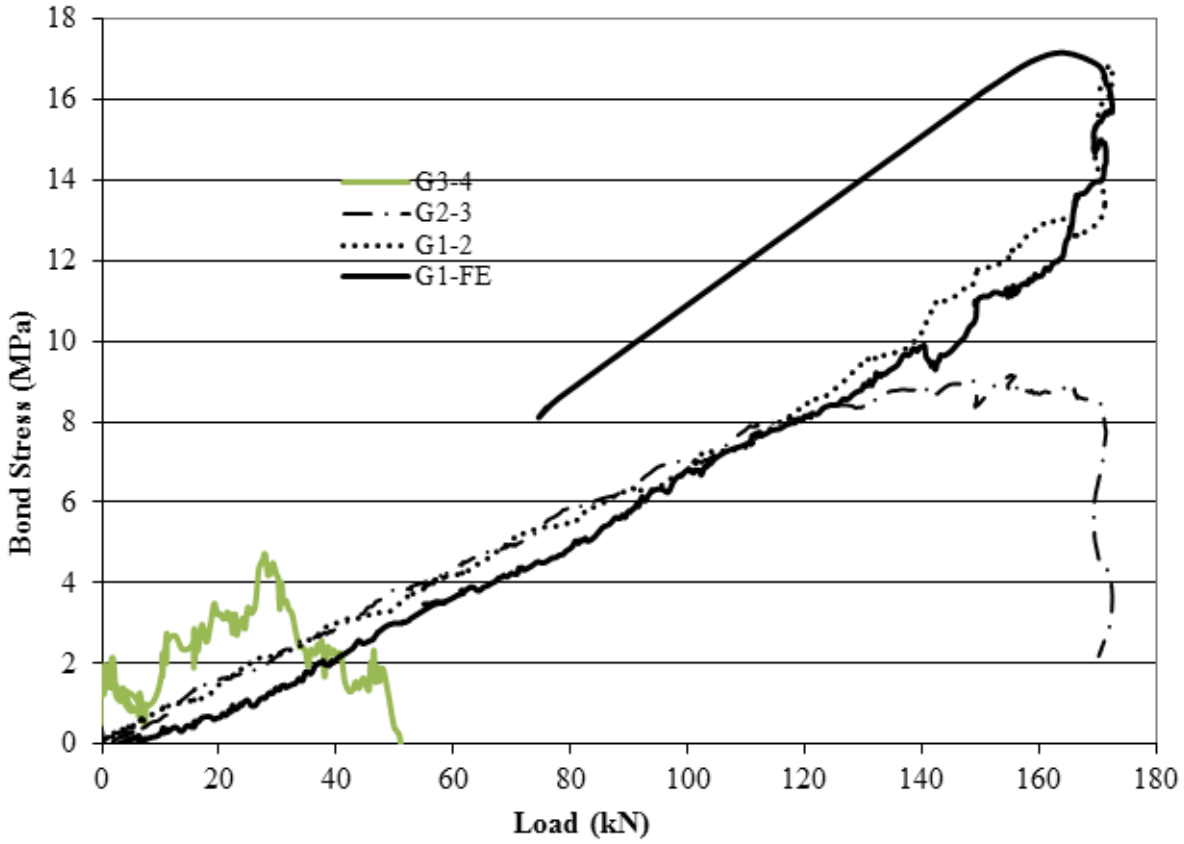


**Figure 5.26 Bond stress versus applied load behaviour for Beam M-200-R-n.**

The maximum bond stress in the corroded beams along the bonded regions away from the support was lower. This was attributed to the fact that corroded beams had longitudinal cracks that initiated during the corrosion process as explained in Section 5.2 hence reducing the bond stress at the concrete-steel interface. The maximum bond stresses observed varied between 5.5 and 7 MPa. However, the trend was similar in that after the bond stress in the areas away from the support reached their maximum stress, the region close to the support resisted the extra tensile force in the bar due to increasing load and hence had a higher bond stress. Once the bond stress in the region close to the support reached 16 MPa, the beam was not able to resist a further increase in load, and the load dropped with decreasing bond stress (Figure 5.27).

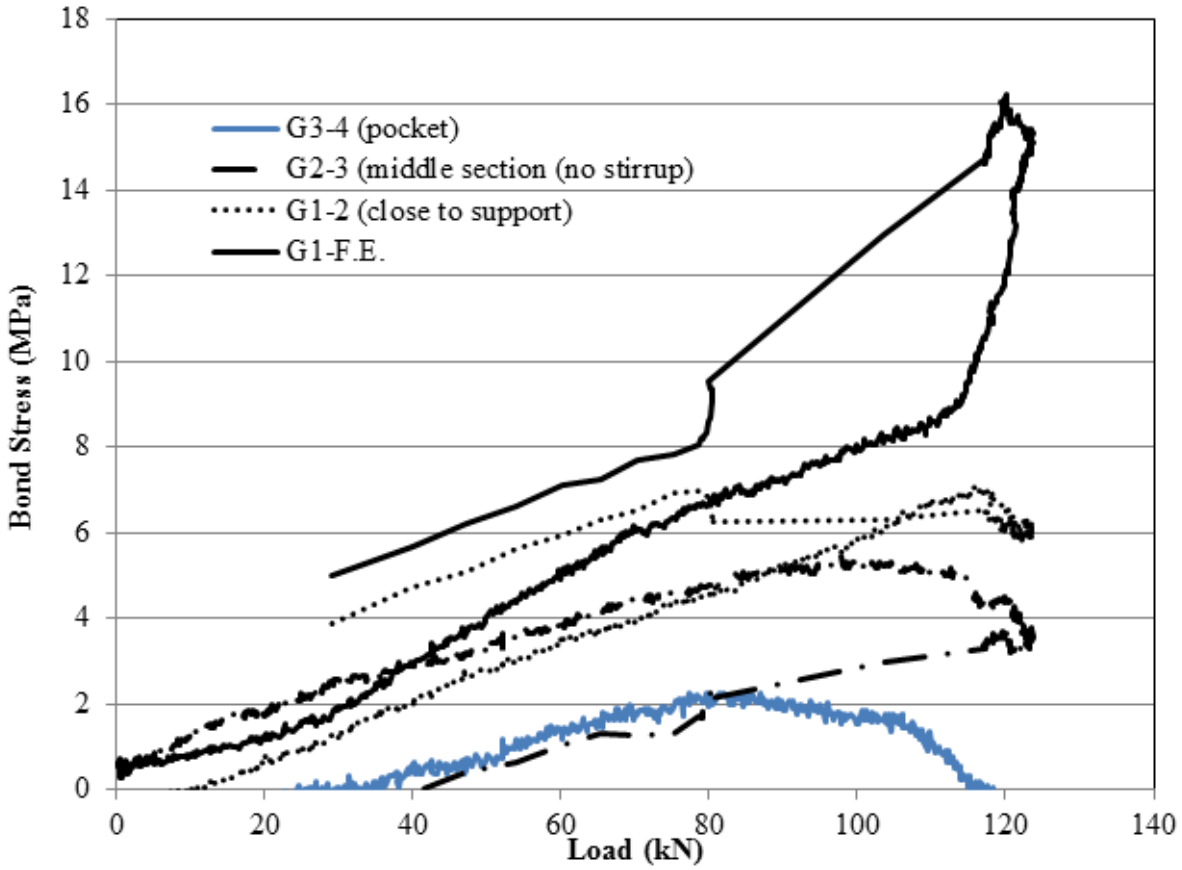


**Figure 5.27 Bond stress versus load for Beam M-200-R-m.**

### 5.3.2 Set 2 Beams

#### 5.3.2.1 Overall behaviour and mode of failure

In set 2, Beams M-350-U-n was not corroded and not repaired. Beams M-350-R-n, M-350-R-m and M-350-R-h were repaired with a U-wrapped CFRP sheet in the anchorage zone (350 mm length) but were subjected to different corrosion levels: no corrosion level (n), a mild corrosion level (m), and a high corrosion level (h) respectively. These beams were used to study the effect of repair with U-wrapped CFRP sheets on the beams with different corrosion levels. Finally beam M-350-U-m was corroded to a mild corrosion level and un-repaired. This beam helped determine the effect of mild corrosion on the bond behaviour at the steel to concrete interface.

Few flexural cracks were formed in the constant moment region of the beams. The scarcity of cracks was attributed to the fact that the bar was unbonded over the central constant moment region.

The unrepaired beams all failed by bond (bar slipping). A longitudinal crack appeared from the pocket and propagated towards the support during loading (Figure 5.28 (a)). The steel plate acting as a support stopped the propagation of the longitudinal crack toward the support point by confining the concrete and resisting the widening of the crack. The longitudinal crack continued to widen within the bonded length and additional cracks opened on the bottom of the beam (Figure 5.28 (b)). The cracks continued to open until the bar slip was large and the beam failed by bond failure. After failure, the bar in the bonded region was removed to inspect the failure which occurred at the bar-concrete interface. It was observed that the concrete keys underneath the bars were intact in the unrepaired beams. This suggested that the concrete below the bar was split off and pushed away offering little resistance to slip. The concrete above the bar was crushed close to the pocket (Figure 5.29). The concrete keys along the rest of the anchorage zone were scraped but were still visible. This suggested that the concrete above the bar, which was held to the bar by the stirrups, resisted slip and was crushed close to the stirrup but the bar bent in between stirrups decreasing the resistance provided by the concrete keys.

The beams that were repaired with U-CFRP sheets, all failed in flexure when the steel yielded followed by concrete crushing in the constant moment region (Figure 5.30). The CFRP sheets confined the concrete and increased the resistance provided by the concrete keys allowing the strains in the bar to increase above the yield strain. In conclusion, repairing the beams of 350 mm bonded length with CFRP sheets changed the failure mode from bond failure to flexural failure.

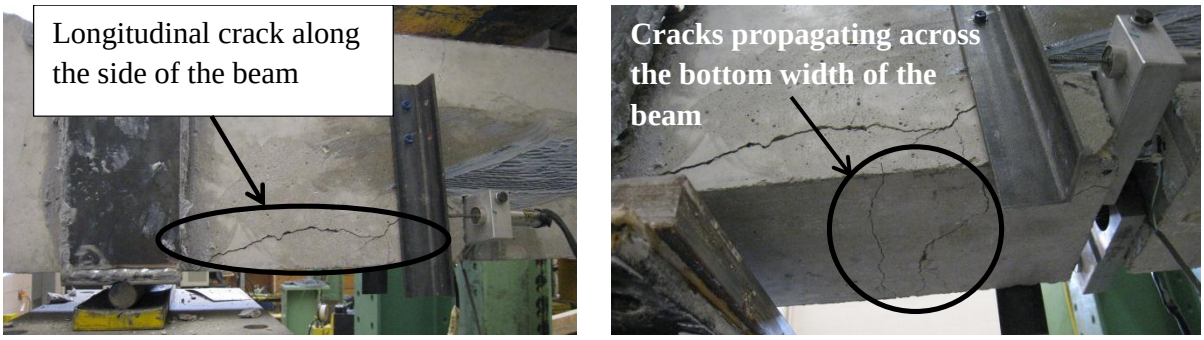


**(a)** **(b)**

**Figure 5.28 Cracks in the bonded length of Bream M-350-U-n along (a) side of the beam and (b) bottom of the beam.**

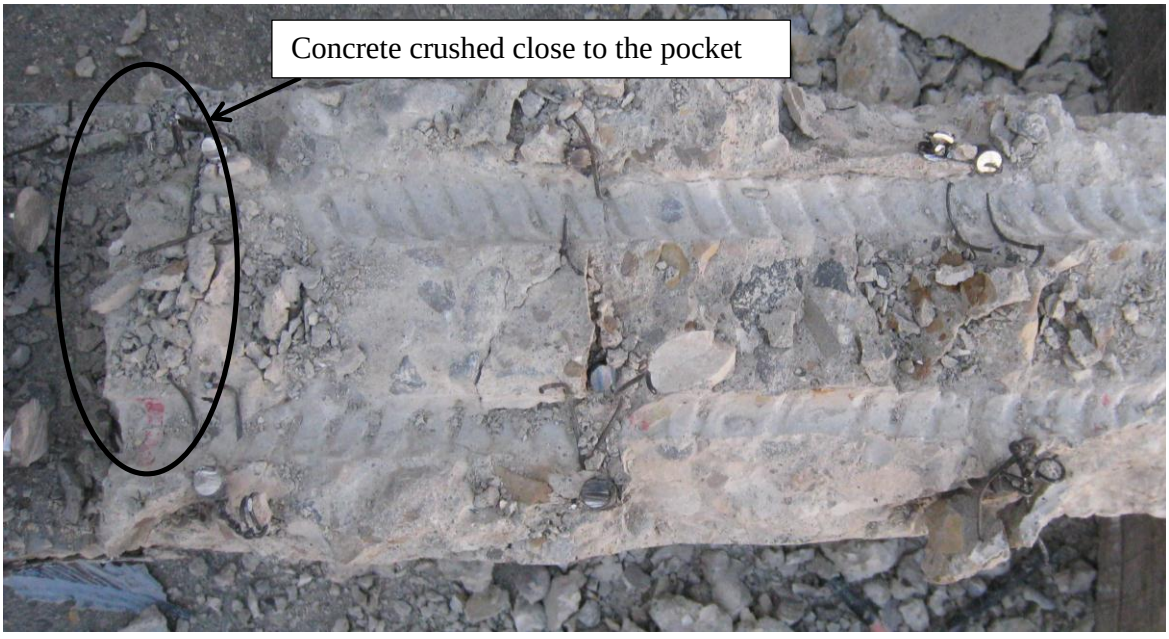


**Figure 5.29 Beam M-350-U-n turned upsode down showing concrete crushed close to the pocket on top of the bar.**

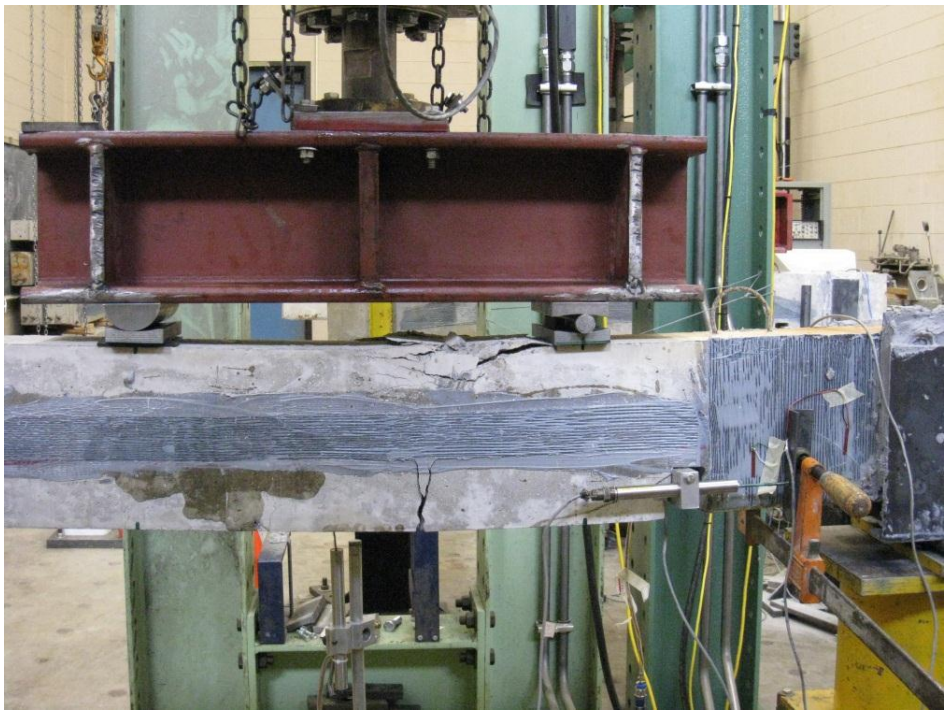

**Figure 5.30 Flexural failure of Beam M-350-R-m.**

#### 5.3.2.2 Load Deflection Behaviour

The load versus mid-span deflection curves for the five beams from set 2 (350 mm anchorage length) tested monotonically to failure are shown in Figure 5.31. Beam M-350-U-n and Beam M-350-R-n had similar initial load versus deflection behaviours. Beam M-350-U-n reached a maximum load of 151 kN with a corresponding mid-span deflection of 8.6 mm beyond which a sudden load drop was observed. Beam M-350-R-n reached a maximum load of 178.3 kN with a corresponding mid-span deflection of 12.9 mm. Repairing an uncorroded beam with a U-CFRP sheet increased the maximum capacity of the beam by 18% and changed the mode of failure from bond failure to flexural failure. This led to a more ductile behaviour post peak. A similar initial load versus deflection behaviour was observed for Beam M-350-U-m and Beam M-350-R-m. Beam M-350-U-m reached a maximum load of 118.1 kN with a corresponding mid-span deflection of 5.9 mm beyond which a sudden load drop was observed. Beam M-350-R-m reached a maximum load of 184.5 kN with a corresponding mid-span deflection of 17.5 mm. Repairing a beam that was corroded to a mild corrosion level with a U-wrapped CFRP sheet increased the maximum capacity of the

beam by 56% and changed the mode of failure from bond failure to flexural failure. This led to more ductile post peak behaviour.

Comparing the un-repaired corroded beam to the un-repaired uncorroded beam, it was noted that corroding the beam to a mild corrosion level reduced its maximum static capacity by 22%. This was similar to what was reported for the 200 mm bonded length. Beam M-350-R-h was corroded to a high corrosion level (13.98% actual mass loss) and then repaired with CFRP sheets before being tested. After the beam reached a load of 89 kN the LVDT measuring the displacement at mid-span stopped reading at 3.8 mm. The midspan deflection was then calculated from the internal LVDT and was drawn with respect to the load applied. The maximum load reached by this beam was 174.7 kN which was similar to the load reached by all the repaired beams in this group. Corroding the bars inside the beams decreased the bond at the steel-concrete interface; repairing the corroded beams with CFRP sheets confined the concrete around the interface and changed the mode of failure from bond failure to flexural failure. The capacity of the beams then depended on the flexural capacity of the beam. Repairing the corroded beams with CFRP not only restored the strength of the beam but increased it by about 18% compared to the control (uncorroded and unrepaired) beams.

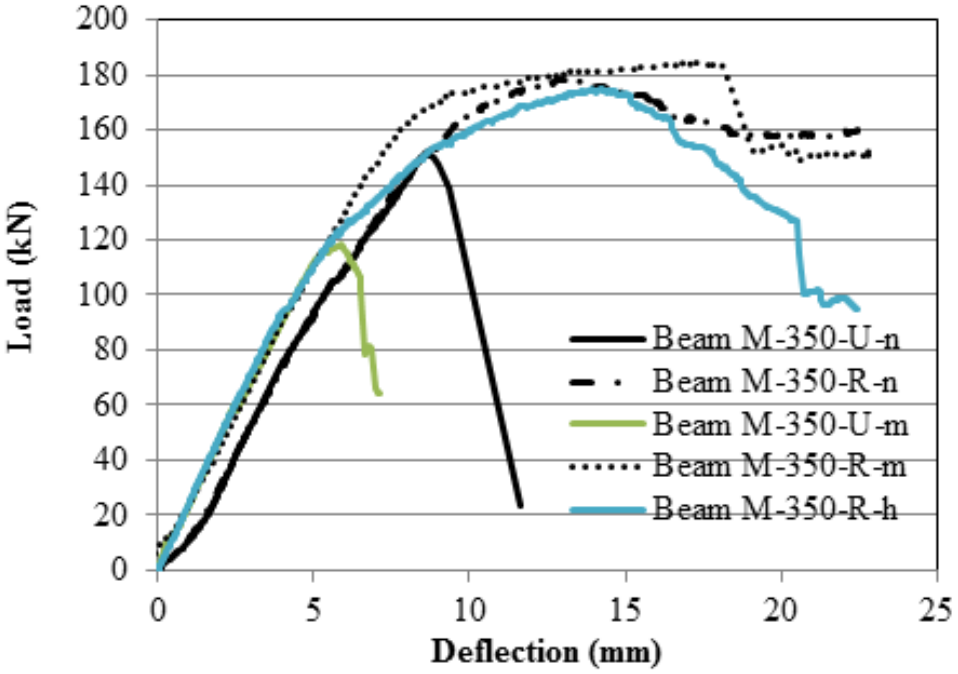


**Figure 5.31 Load versus mid-span deflection for the beams from Set 2 - Group M.**

### 5.3.2.3 Strain Behaviour

Observations of the strain behaviour of the steel bar in the beam helped define the debonding stages of the bar and the failure location as explained in Section 4.4. All the monotonic unrepaired beams in set 2 had similar load-strain behaviour where the strain increased linearly with increasing load. Debonding started from the pocket and moved towards the support. Debonding was not evident until after the maximum load was reached (Figure 5.32 and Figure 5.33 ).

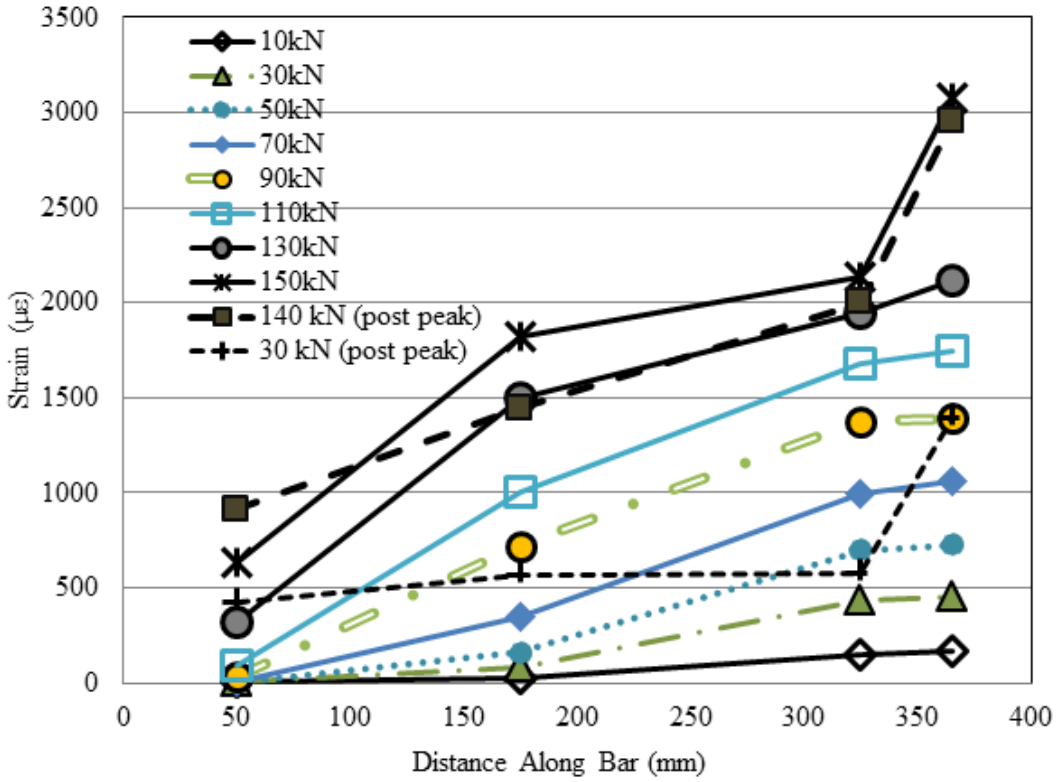


**Figure 5.32 Strain profile for Beam M-350-U-n.**

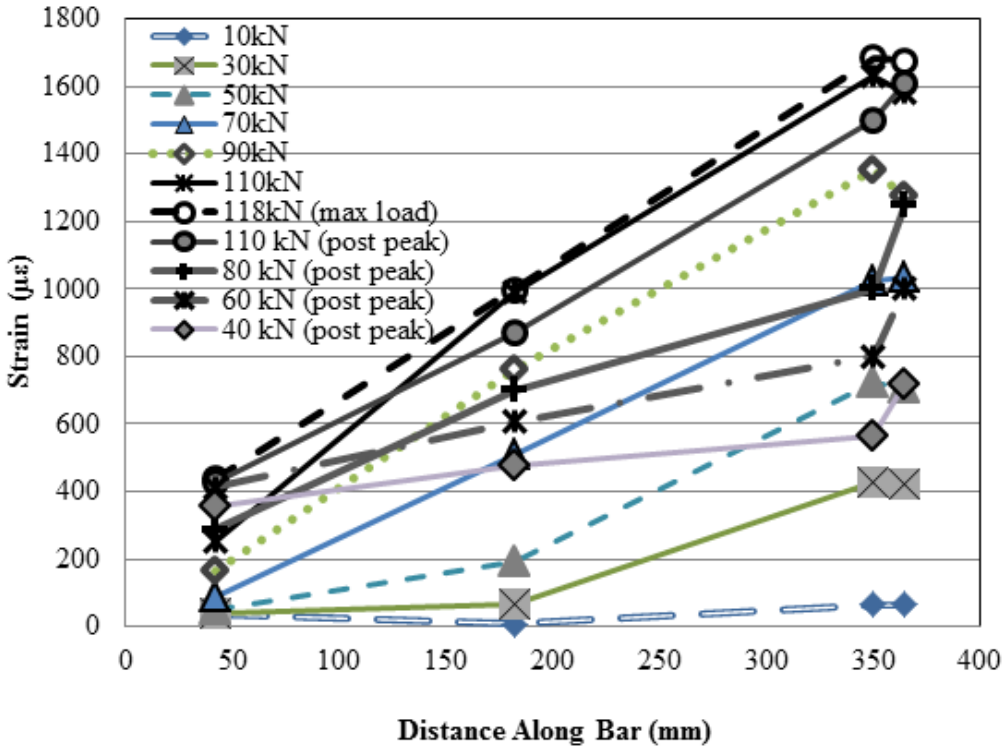


**Figure 5.33 Strain Profile for Beam M-350-U-m.**

The repaired beams all failed in flexure. Beam M-350-R-n reached a strain of 21681 με in the pocket at the peak load which was above the yield strain of 2000 με (Figure 5.34). The yielding only happened close to the pocket. No debonding was clear from the strain data. Beam M-350-R-m reached a strain of 15637 με in the pocket at the peak load (Figure 5.35). Similarly to Beam M-350-R-n the yielding only happened close to the pocket area. Beam M-350-R-h reached a strain of 24146 με at peak load in the pocket (Figure 5.36). The strains from the middle of the bonded length up to the pocket were all above yield strain. Debonding was seen in this beam and as discussed later the slip was greater than the other repaired beams of the same group. Although the final failure of the beam was by concrete crushing, part of the CFRP sheet close to the pocket ruptured due to increased slip (Figure 5.37).

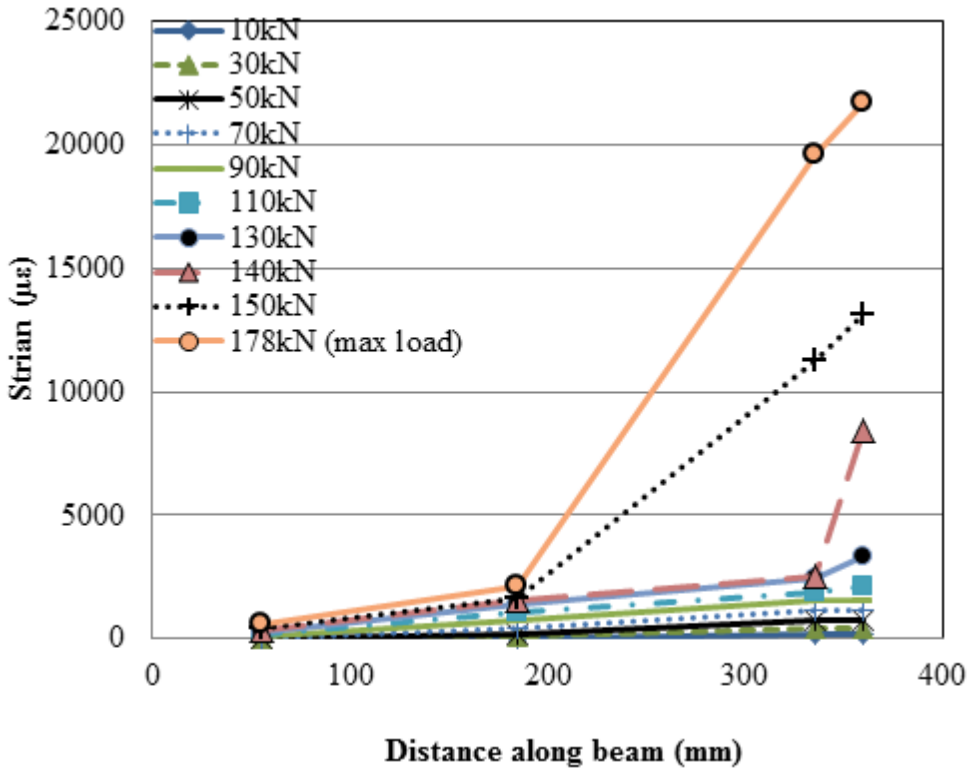


**Figure 5.34 Strain profile for Beam M-350-R-n.**

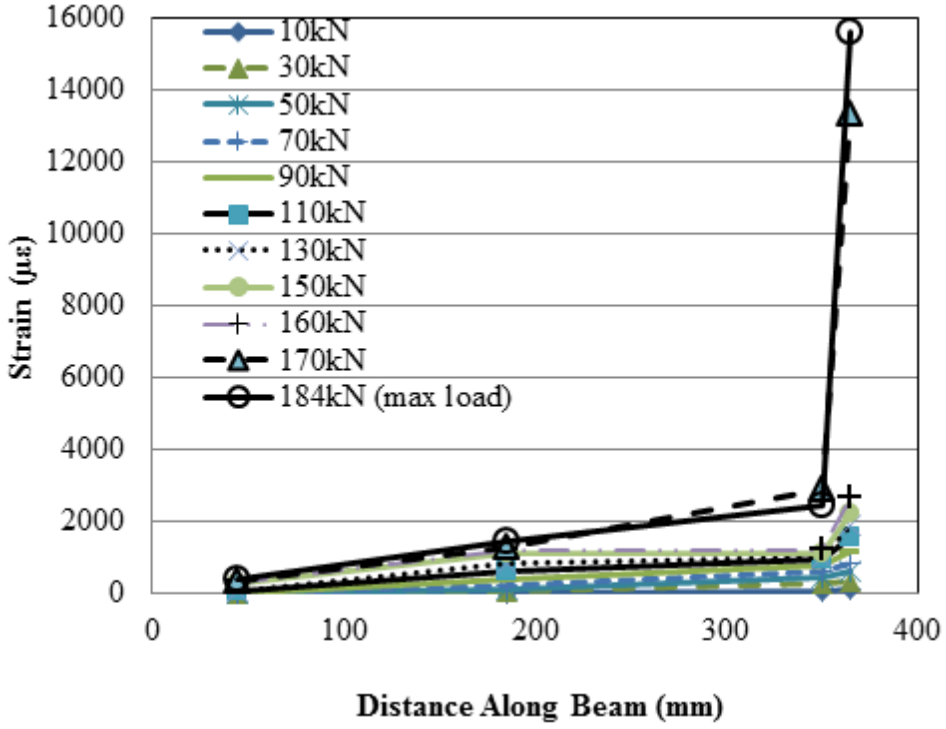


**Figure 5.35 Strain profile for Beam M-350-R-m.**

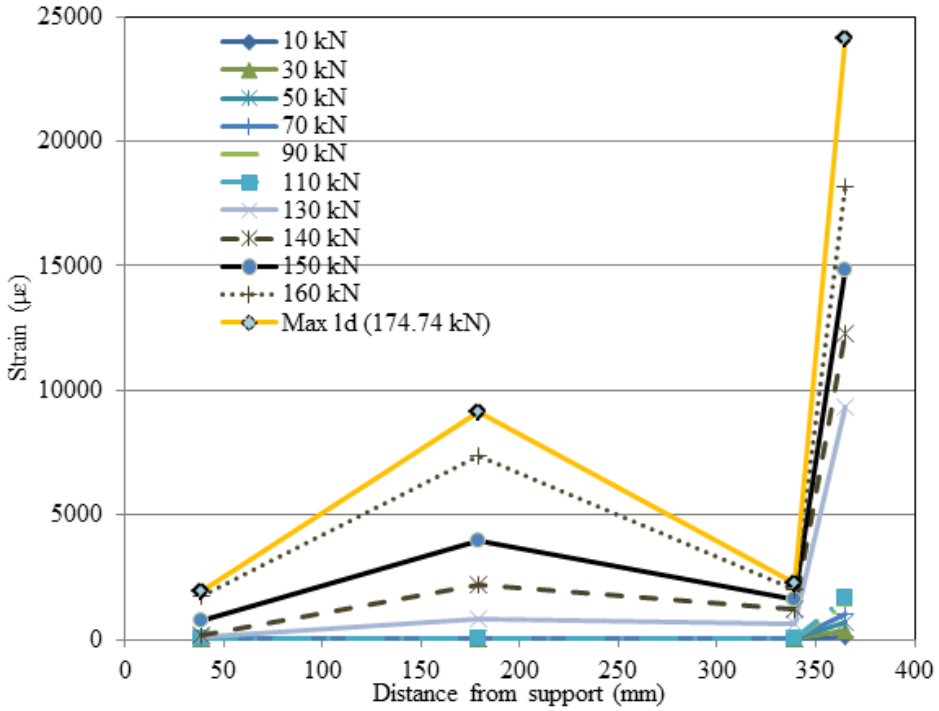


**Figure 5.36 Strain profile for Beam M-350-R-h.**


(a) (b)

**Figure 5.37 Final failure of Beam M-350-R-h by crushing of concrete. Part of the FRP ruptured close to the pocket.**

### 5.3.2.4 Steel slip behaviour

Figure 5.38 shows the load-slip behaviour of beam M-350-U-n. It can be seen that the slip increased with increasing load at a low rate until the maximum load was reached after which the slip increased at a higher rate. The free end slip reached at the maximum load was

0.07mm. The slip then increased with decreasing load. The support failed when the free end slip reached by bar 2 was 1.04 mm and the test was stopped.

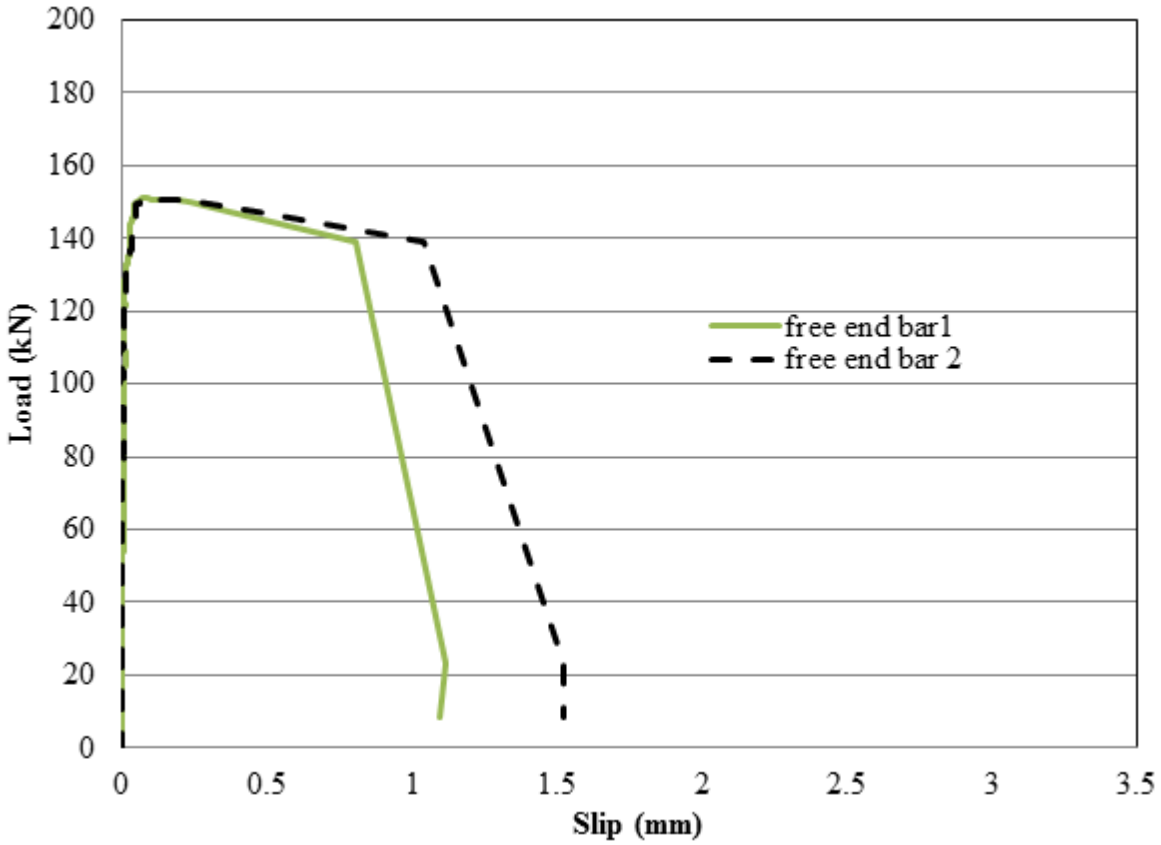


**Figure 5.38 Load versus slip behaviour for Beam M-350-U-n.**

Figure 5.39 shows the load-slip of Beam M-350-U-m. The slip increased with increasing load at a low rate until the maximum load was reached after which the slip increased at a higher rate. The free end slip reached at the maximum load was 0.27 mm. The top concrete at the support location was crushed when the free end slip reached 0.9 mm causing a sudden drop in the load. The slip then continued to increase with decreasing load until the supports completely failed and the test was stopped.

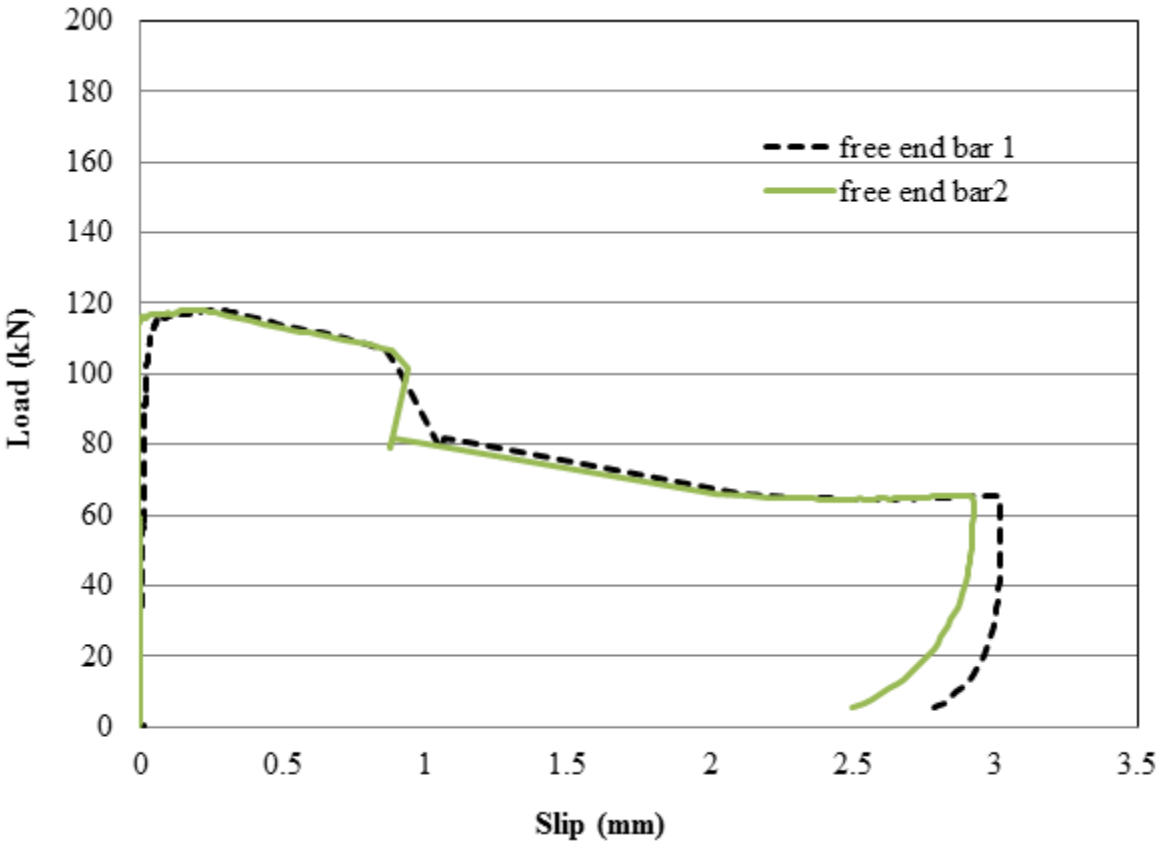


**Figure 5.39 Load versus slip behaviour for Beam M-350-U-m.**

The repaired beams behaved differently. The slip reached at maximum load was 0.17 mm for Beam M-350-R-n (Figure 5.40) and 0.7 mm for Beam M-350-R-m (Figure 5.41) which was not large enough to cause the beams to fail by bond. Beam M-350-R-h reached a slip of 1.23 mm at maximum load which was higher than that of the other repaired beams (Figure 5.42). This was due to the higher corrosion level and wider corrosion cracks that were reported for this beam. Although the final failure of this beam was by concrete crushing, the slip was high enough to cause part of the CFRP sheet to rupture close to the pocket (Figure 5.37). The slip continued to increase with decreasing load.

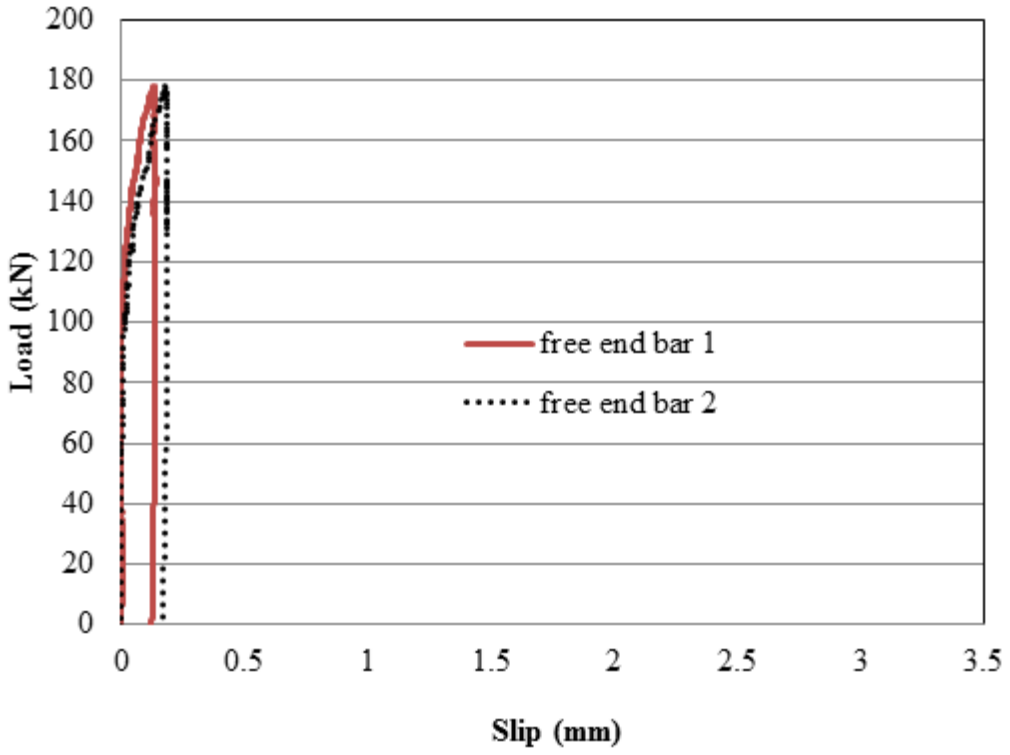


**Figure 5.40 Load versus slip behaviour for Beam M-350-R-n.**

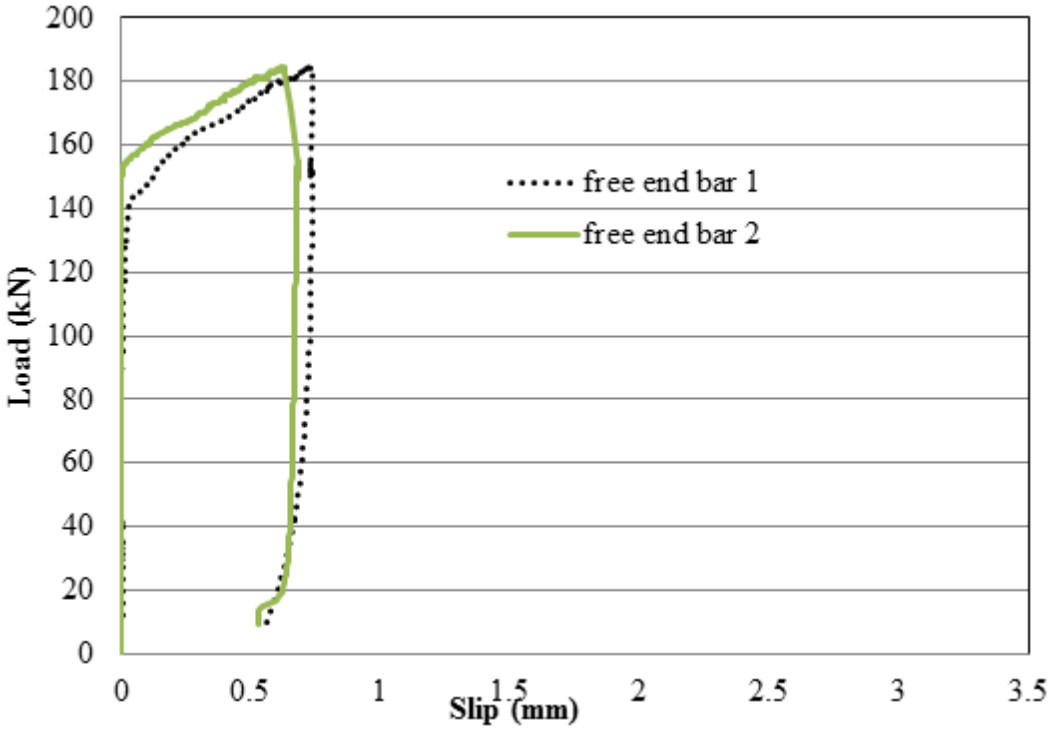


**Figure 5.41 Load versus slip behaviour for Beam M-350-R-m.**

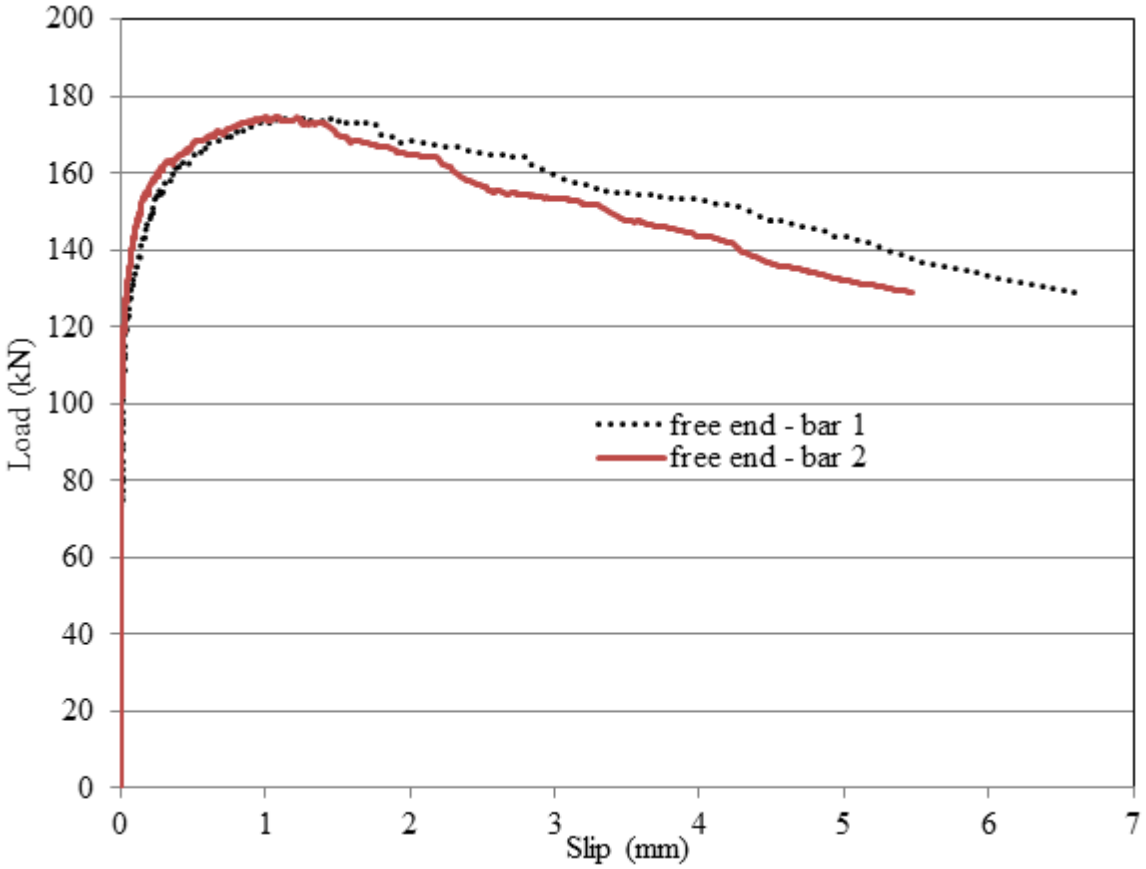


**Figure 5.42 Load versus slip behaviour for Beam M-350-R-h.**

### 5.3.2.5 Bond Stress

The average bond stress was calculated from the readings of three strain gauges mounted inside the bar in a manner similar to that discussed in Section 5.3.1.5.

The bond behaviour of the beams in this set was similar to that discussed in Section 5.3.1.5. The bond stress was redistributed along the bonded length with increasing load. Once the maximum bond stress was reached along the bonded length, the region close to the support continued to resist an increased bond stress with increasing load. As the bond stress of the area close to the support reached its capacity of 18 MPa the load dropped indicating failure of the beam by bond (Figure 5.43).

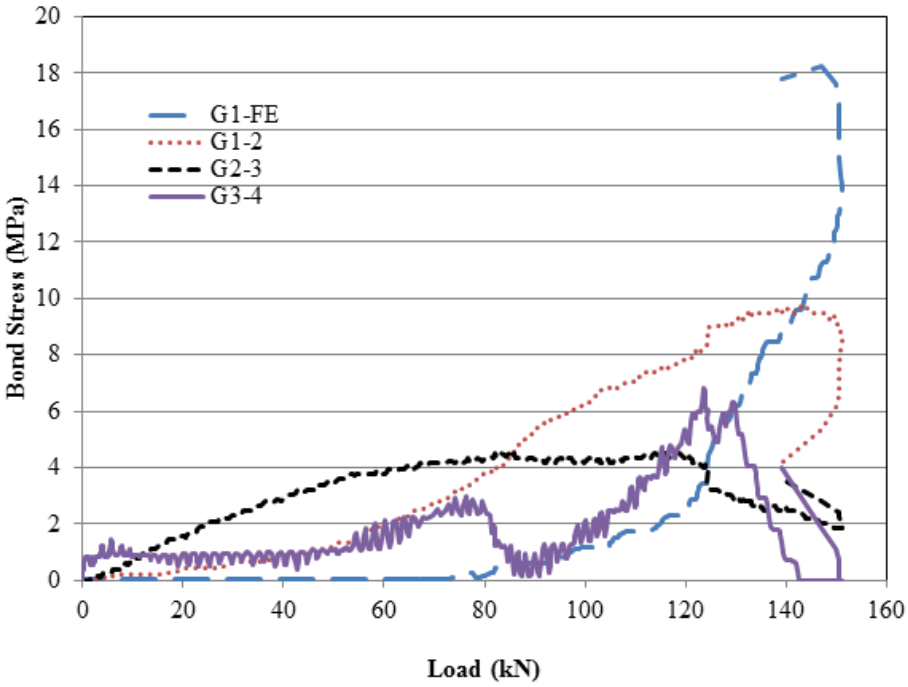


**Figure 5.43 Bond stress versus load behaviour for Beam M-350-U-n.**

## 5.4 Fatigue Beam Results

All of the beams tested under repeated loading were first loaded up to the maximum load manually. The load was then decreased to the mean load, after which the beam was cycled at a frequency of 1Hz. The minimum load was fixed for all the beams at 10kN and the maximum load was varied in order to achieve a wide range of fatigue lives. The fatigue behaviour for the beams from set 1 and set 2 was different.

### 5.4.1 Set 1 Beams – Fatigue Behaviour

#### 5.4.1.1 Overall behaviour and mode of failure

While the beams were being manually loaded up to the maximum load a flexural crack in the middle of the constant moment region was initiated. Another two cracks under the point loads were initiated after the beam had run for a few cycles.

As the number of cycles increased, a longitudinal crack initiated and propagated at the loaded end of the anchorage zone towards the support. This crack continued to increase in length and width until final failure of the beam by bond. These cracks were not visible in the beams repaired with CFRP sheets. The FRP sheets confined the concrete increasing the bond

strength. The beams corroded and repaired with CFRP sheets failed either in flexure by bar rupture or in bond with CFRP rupturing in the bonded region. Table 5.3 gives a summary of the fatigue life of the beams tested in Set 1 as well as the corresponding failure modes.

**Table 5.3 Fatigue lives for Beams from Set 1.**

| Group | Beam Notation | Corrosion mass loss (%) | Load | | Fatigue Life (Cycles) | Failure Mode |
|---|---|---|---|---|---|---|
| | | | Maximum (kN) | Range (kN) | | |
| U-n | F-200-U-n-40[§] | No Corrosion (0%) | 50 | 40 | 1,000,000[**] | No failure |
| | F-200-U-n-48[1] | | 58 | 48 | 1,000,000[2] | No failure |
| | F-200-U-n-55[1] | | 65 | 55 | 1,000,000[2] | No failure |
| | F-200-U-n-57.5[††] | | 67.5 | 57.5 | 1,000,000[2] | No failure |
| | F-200-U-n-60 | | 70 | 60 | 120,756 | Bond |
| | F-200-U-n-61.5[3] | | 71.5 | 61.5 | 1,000,000[2] | No failure |
| | F-200-U-n-63[1] | | 73 | 63 | 1,000,000[2] | No failure |
| | F-200-U-n-63[3] | | 73 | 63 | 1,000,000[2] | No failure |
| | F-200-U-n-66 | | 76 | 66 | 365,153 | Bond |
| | F-200-U-n-68[3] | | 78 | 68 | 123,485 | Bond |
| | F-200-U-n-70-1[1] | | 80 | 70 | 4,022 | Bond |
| | F-200-U-n-70-2 | | 80 | 70 | 6,524 | Bond |
| U-m | F-200-U-m-40[‡‡] | 5.9 | 50 | 40 | 1,000,000[2] | No failure |
| | F-200-U-m-41.5[4] | 5.9 | 51.5 | 41.5 | 1,000,000[2] | No failure |
| | F-200-U-m-42.5[4] | 5.9 | 52.5 | 42.5 | 1,000,000[2] | No failure |
| | F-200-U-m-43-1[4] | 5.9 | 53 | 43 | 1,000,000[2] | No failure |
| | F-200-U-m-43 | 4.3 | 53 | 43 | 31,662 | Bond |
| | F-200-U-m-44-1[4] | 5.9 | 54 | 44 | 1,000,000[2] | No failure |
| | F-200-U-m-44 | 7.44 | 54 | 44 | 254,700 | Bond |
| | F-200-U-m-45[4] | 5.9 | 55 | 45 | 343,586 | Bond |
| | F-200-U-m-46 | 4.4 | 56 | 46 | 2,518 | Bond |
| | F-200-U-m-46-1[§§] | 5.02 | 56 | 46 | 1,000,000[2] | No failure |
| | F-200-U-m-48[5] | 5.02 | 58 | 48 | 181,780 | Bond |
| R-m | F-200-R-m-72 | 6.18 | 82 | 72 | 301,163 | Flexure |
| | F-200-R-m-80 | 6.36 | 90 | 80 | 714,313 | Flexure |
| | F-200-R-m-90 | 6.18 | 100 | 90 | 63,961 | Bond |
| | F-200-R-m-96 | 7.28 | 106 | 96 | 19,723 | Bond |
| R-h | F-200-R-h-75 | 13.33 | 85 | 75 | 523,369 | Bond |
| | F-200-R-h-80 | 13.92 | 90 | 80 | 634 | Bond |
| | F-200-R-h-88 | 10.58 | 98 | 88 | 70,553 | Bond |
| | F-200-R-h-96 | 13.80 | 106 | 96 | 4,093 | Bond |

[§] One beam tested at maximum loads of 50, 58, 65, 73 and 80 kN.
[**] These beams reached a run-out, 1,000,000 cycles, without failure.
[††] One beam tested at maximum loads of 67.5, 71.5, 73 and 78 kN.
[‡‡] One beam tested at maximum loads of 50, 51.5, 52.5, 53, 54, and 55 kN.
[§§] One beam tested at maximum loads of 56 and 58 kN.

5.4.1.1.1 Uncorroded Beams

Five uncorroded beams were tested under repeated loading. The minimum load was fixed for all the beams at 10kN. The results of Rteil (2007) were initially used as a guide in choosing the maximum loads applied to the beams. The first beam was tested at a load range of 40kN. This beam reached 1 million cycles with no failure (one million cycles was considered as a run-out for the beams and defined as the one million cycle endurance limit). This beam was then retested at load ranges of 48kN, 55kN, and 63kN. At all these levels the beam reached one million cycles without failure. The beam was then tested at a load range of 70kN which resulted in a failure at 4,022 cycles. This beam was named F-U-n-70-1. Another beam (F-U-n-70-2) was tested at a load range of 80kN to confirm that the run-outs the previous beam was exposed to didn't cause any noticeable damage. Beam F-U-n-70-2 experienced a bond failure at 6,524 cycles. The next beam was tested at a load range of 66 kN (Beam F-200-U-n-66). This beam failed in bond at a fatigue life of 365,153 cycles. Two beams were then tested from this set but were from a different cast. Beam F-200-U-n-60 tested under a cyclic load range of 60 kN failed in bond at a fatigue life of 120,756 cycles. The next beam was then tested at load ranges of 57.5kN, 61.5kN and 63kN. At all these levels the beam reached one million cycles with no failure. The beam was then tested at a load range of 68kN which resulted in a bond failure at 123,485 cycles (Beam F-200-U-n-68).

After failure of the beams, the failure surface was inspected. It was observed that the bottom concrete of the beam cracked into pieces (Figure 5.44 (a)). When these pieces were removed the concrete was found to be intact. The bars were then cut and removed from the beam to inspect the upper concrete to which the bar was held by the stirrups. It was found that the upper concrete between the lugs was partially crushed (Figure 5.44 (b)).

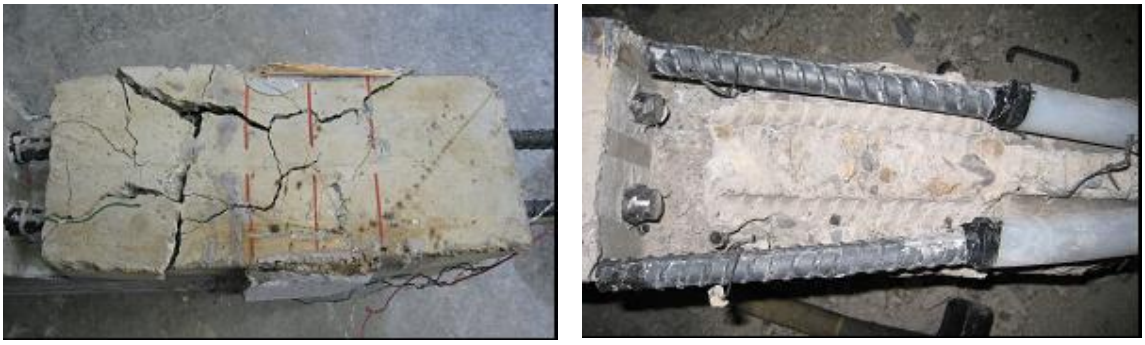

**(a)** **(b)**

**Figure 5.44 (a) the cracks after failure in the bonded region of beam F-200-U-n-70-1. (b) intact concrete above the bar in Beam F-200-U-n-70-2. The beam was turned upside-down.**

5.4.1.1.2 Corroded un-repaired beams

Using the results of the fatigue tests of the uncorroded beams as a guide; the first corroded beam Beam F-200-U-m-46 was tested at 76% of its static capacity which corresponds to a cyclic load range of 46 kN. This beam failed in bond at a fatigue life of 2,518 cycles. Then Beam F-200-U-m-43 was tested under a cyclic load range of 43kN. The beam failed in bond after 31,662 cycles. To achieve a higher fatigue life, the next beam was tested at a lower load range. The beam was tested at load ranges of 40kN, 41.5kN, 42.5kN, 43kN and 44kN. At all these load ranges the beam reached one million cycles without failure. The beam was then tested at a cyclic load range of 45kN (Beam F-200-U-m-45) and failed in bond at a fatigue life of 343,586 cycles. An additional two beams were cast to verify the results from this set. Beam F-200-U-m-44 was tested at a cyclic load range of 44kN and failed in bond after 254,700 cycles. The next beam was then tested at a cyclic load range of 46kN with no failure after one million cycles. This beam was then retested at a load range of 48kN (Beam F-200-U-m-48) and failed in bond after 181,780 cycles.

After examining the contact surface at failure, it was noted that the concrete in between the lugs was partially crushed and filled with the rust product from the corrosion process (Figure 5.45). The corrosion cracks, due to the formation of rust, reduced the confinement from the

concrete at the concrete-steel interface and increased the rate of slip in the bar under repeated loading.


**Figure 5.45: (a) upper concrete above bar and (b) lower concrete below the bar in beam F-200-U-m-43.**

5.4.1.1.3 Repaired Corroded Beams

Four beams were corroded to a mild corrosion level and another four beams to a high corrosion level and repaired with CFRP sheets in the bonded region. The four beams from Group R-m (Beams corroded to a mild corrosion level and repaired with CFRP sheets) had two different modes of failure. Two beams from this set failed in flexure by bar rupture and the other two beams failed in bond after the CFRP confining sheet ruptured.

As explained in Section 3.9.1, corrosion was expected to damage the bond between the strain gauge and the steel bar, hence installing encapsulated strain gauges or FOS in gundrilled holes was used as an alternate solution. Beams in Group R-m had gundrilled reinforcing bars. Beam F-200-R-m-72 and Beam F-200-R-m-80 tested at cyclic load ranges of 72kN and 80kN respectively both failed in flexure by bar rupture. The load range was increased in an attempt to reach bond failure before flexural failure occurred. A strain life approach with the help of the data from Al-Hammoud, Soudki & Topper (2011) was used to get the flexural curve encompassing the different load ranges within this group. For the mild corrosion level the maximum fatigue notch factor reported by Al-Hammoud, Soudki & Topper (2011) was 1.93. Considering a reduced area of the bars due to gundrilled holes as

well as the actual mass loss reported in this study, the strain life approach analysis led to the fatigue predicted lives shown as a dashed curve in Figure 5.46.

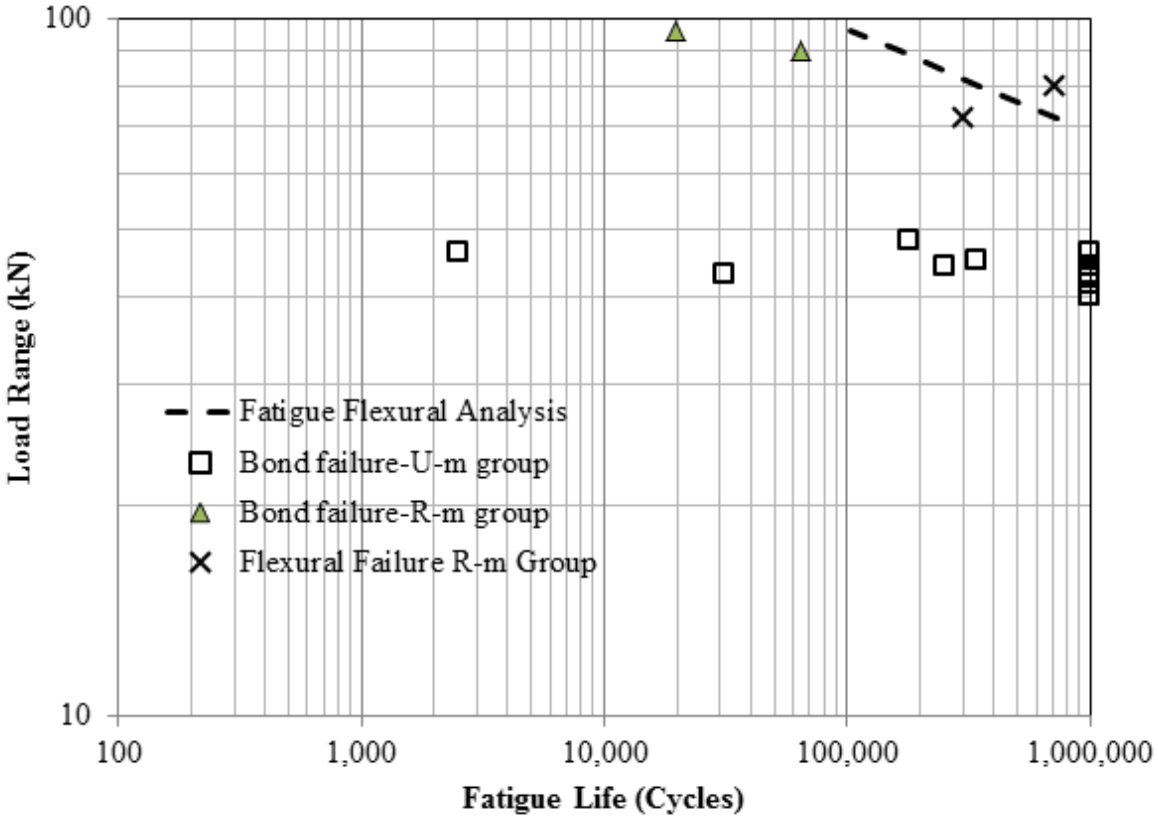


**Figure 5.46 Load range versus fatigue life for Beams Corroded to a mild corrosion level from set 1 along with flexural analysis.**

Beam F-200-R-m-72 failed pre-maturely at the end of the gundrilled hole that had a conical shape (Figure 5.47). The abrupt change in section at the end of the gundrilled hole caused a stress-raiser in the bar at this location. This caused Beam F-200-R-m-72 to fail in flexure by rupturing the bar at the end of the gundrilled hole after 301,163 cycles (Figure 5.48).

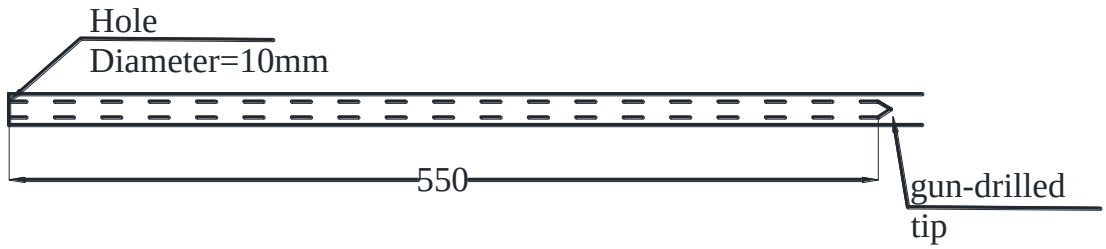


**Figure 5.47 Gundrilled holes in the reinforcements for the beams with 200mm anchorage length.**

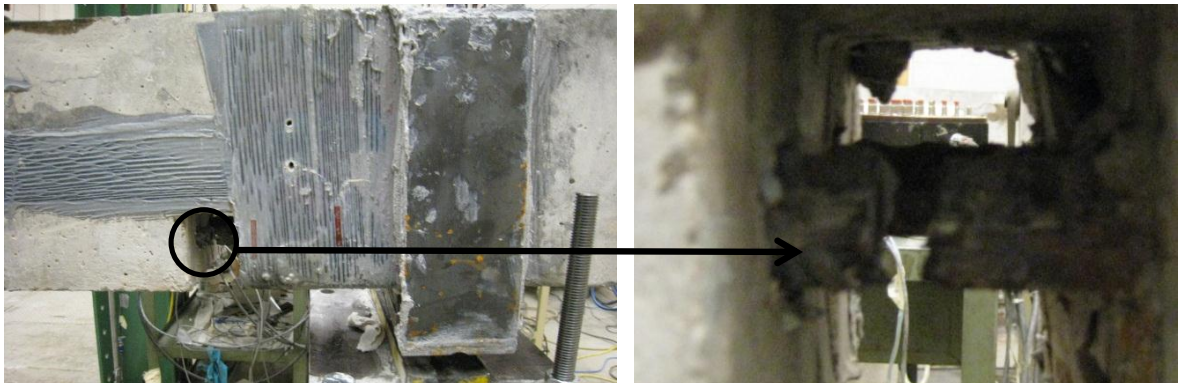

**Figure 5.48 Beam F-200-R-m-72 failed by bar rupture in the pocket.**

From Figure 5.46 it was noted that fatigue flexural failure was not an issue for the corroded unrepaired beams as bond failure occurred at load ranges well below the endurance limit of the beam. Repairing the beams with CFRP sheets in the bonded region increased the fatigue bond strength of the beam to a level close to the flexural behaviour of the beam. It was not possible to achieve higher bond fatigue lives than 100,000 cycles since flexural failure occurred before bond failure for this beam section.

The beams in group R-h, that were corroded to a high corrosion level and then repaired with CFRP sheets, all failed in bond fatigue after the FRP sheet ruptured in the area close to the pocket (Figure 5.49). In this group, Beam F-200-R-h had gundrilled holes in its reinforcing bars. The rest of the beams in this group had a 6mm by 5mm groove in the reinforcing bars for strain gauges installation purposes.


**Figure 5.49 FRP rupture close to the pocket in Beam F-200-R-h-80.**

After failure, the beams were examined in the failure region. The concrete keys below and above the bar were crushed (Figure 5.50). The CFRP sheets confined the concrete at the steel-concrete interface which increased the fatigue bond strength of the beams. This caused the concrete keys to crush along the entire length of the anchorage zone causing slip of the bars in a pull-out manner and CFRP rupture.

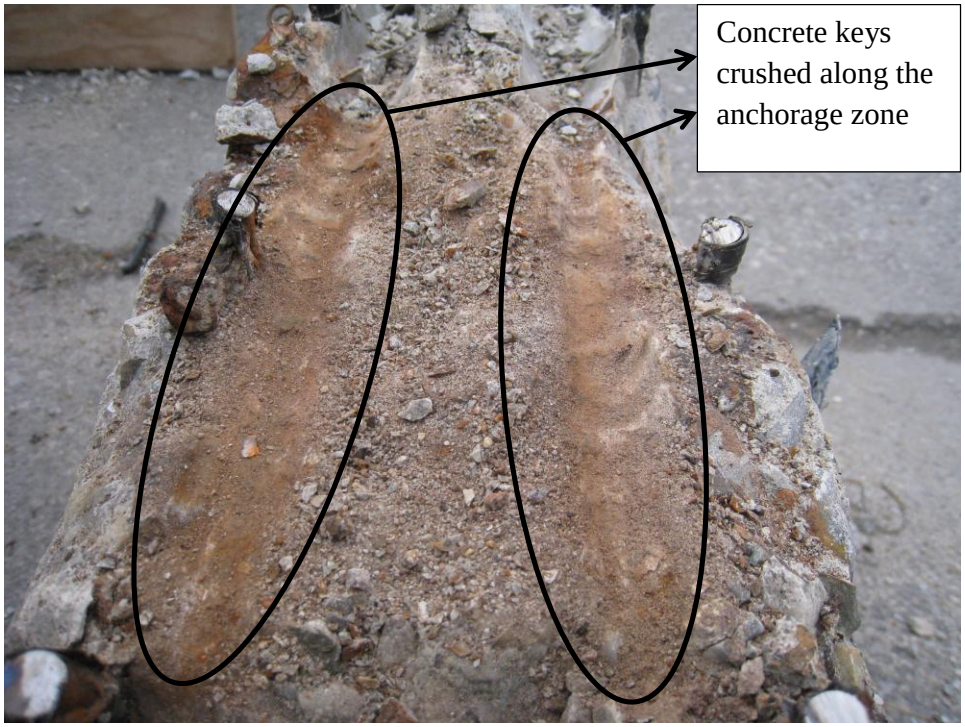


**Figure 5.50 Concrete Keys crushed along the anchorage zone for Beam F-200-R-h-80. The beam was upside down and the reinforcing bars removed.**

5.4.1.2 Fatigue Strength- Set1

The fatigue life of the tested beams was plotted with respect to the load range applied (Figure 5.51). It can be seen that the fatigue life of the beams varied linearly on a logarithmic scale with the range of applied load with a very shallow slope. Hence the range of load over which fatigue failure occurred was small. Corroding the beams to a mild corrosion level decreased the fatigue strength by about 34%. This decrease did not vary significantly with fatigue life. Corrosion leads to the formation of rust products that are greater in volume than the metal corroded. These rust products formed a weak layer between the concrete and the steel and decreased the overlap of bar lug and concrete. This caused a reduction in the fatigue bond strength of the beam. Repairing the corroded beams with U-wrapped CFRP sheets in the anchorage zone increased the fatigue bond strength on average by 83% compared to the corroded unrepaired beams. This increase was 23% above the fatigue bond strength of the uncorroded unrepaired beams. Not much difference in bond strength was noticed between the

beams that were repaired after being subjected to a mild corrosion level or a high corrosion level. The governing factor for the repaired beams was the rupture of the CFRP sheets.

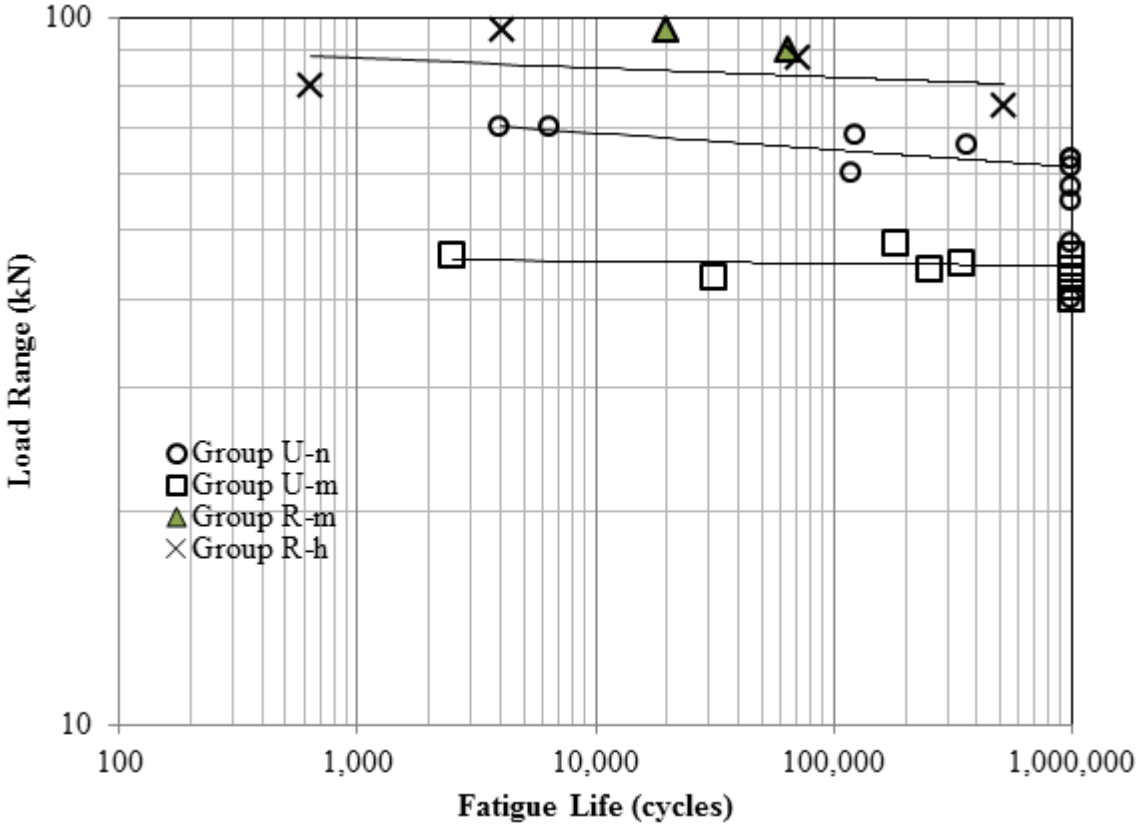


**Figure 5.51: Variation in load range with life for Set 1 beams failing in fatigue of bond.**

5.4.1.3 Steel Slip Behaviour – Set 1

The slip was measured as the relative movement between the steel bar and the concrete. The steel slip was measured using LVDT's that were mounted on the steel bar at the free end (end of beam) and the loaded end (in the pocket). The measured slip at the loaded and the free ends for bars 1 and 2 was almost the same. In the control uncorroded beams there was not much increase in slip with cycles until failure occurred. The slip remained almost constant as the number of cycles increased until close to failure when the slip increased suddenly (Figure 5.52). On the other hand, the corroded beams showed an increase in slip earlier in the fatigue life (Figure 5.53). The slip in Beams F-200-U-m-43, F-200-U-m-44, and F-200-U-m-48 increased with cycles until reaching a slip of about 1mm at 90% of the fatigue life after

which the slip increased rapidly until 100% of the fatigue life to reach a value between 6.3 mm and 8.6 mm. Beam F-200-U-m-46 reached a slip of 3.33 mm at 90% of the fatigue life before it increased rapidly to 10.6 mm at 100% of the fatigue life. This was not the case in Beam F-200-U-m-45 that showed almost no increase in slip until almost 100% of the fatigue life where the slip increased rapidly to 8.3 mm. This beam had reached several run-outs at one million cycles at the following load ranges 40kN, 41.5 kN, 42.5 kN, 43 kN, and 44 kN before it failed at 343,586 cycles when tested at a load range of 45 kN. Every time the beam was retested the LVDT measurement for slip was reset to zero. An accumulated slip of 0.1 mm from the free end resulted from the several run-outs of this beam.

The repaired beams showed an increase in slip early in the fatigue life. This was due to the fact that at the beginning the CFRP was unstressed and did not give much constraint. As slip occurred, the CFRP stress increased and provided the constraining force that decreased the slip rate. For the two beams failing in bond in Group R-m (repaired with CFRP sheets after being exposed to a mild corrosion level) the slip increased with life and reached about 3mm of slip at 90% of the fatigue life before it increased rapidly until 100% of the fatigue life. Beam F-200-R-m-90 reached a 2.06 mm slip at 10% of the fatigue life, then the slip increased at a slower rate until it reached a value of 2.9 mm at 80% of the fatigue life (Figure 5.54). This slip continued to increase to a value of 3.77mm at 90% of the fatigue life after which it increased rapidly to 10 mm at 100% of the fatigue life. Beam F-200-R-m-96 reached a 2.4 mm slip at 60% of the fatigue life. The slip remained constant between 60% and 80% of the fatigue life after which it increased slowly to 2.67mm at 90%. The slip then increased rapidly to reach 9.4 mm at 100% of the fatigue life (Figure 5.55).

All the beams in Group R-h (the beams corroded to high corrosion level and then repaired with CFRP sheets) showed about 1mm of slip at 10% of the fatigue life followed by a linear increase in slip with life to a slip between 2 and 4 mm at 90% of the fatigue life. At 100% of the fatigue life the slip was between 10 mm and 15 mm when the CFRP ruptured causing failure of the beams (Figure 5.56).

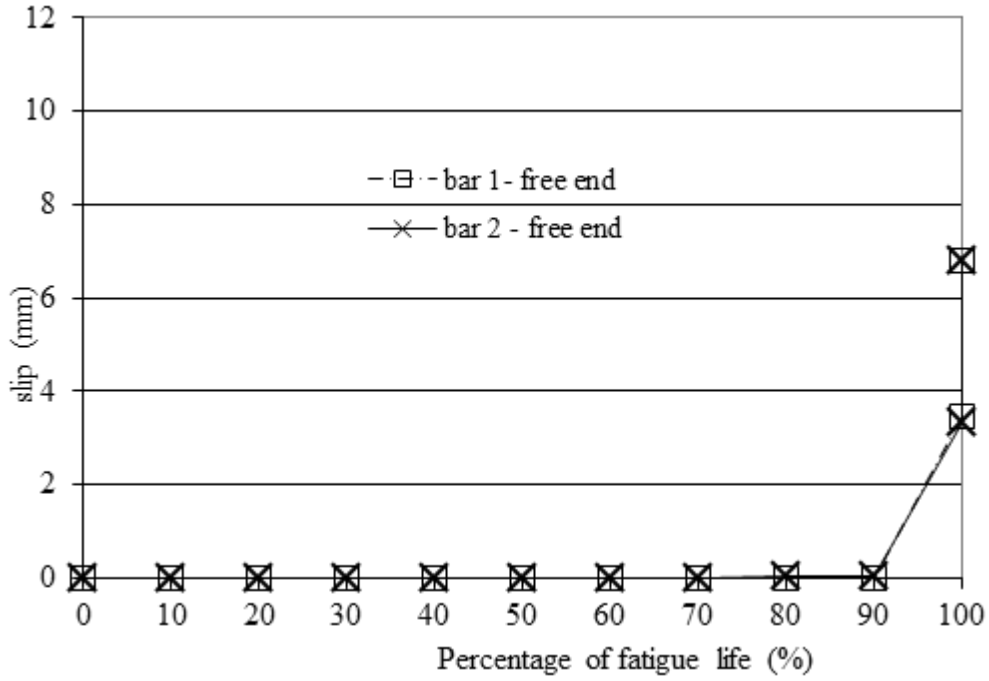


**Figure 5.52 Slip versus percentage of fatigue life behaviour for Beam F-200-U-n-70-1.**

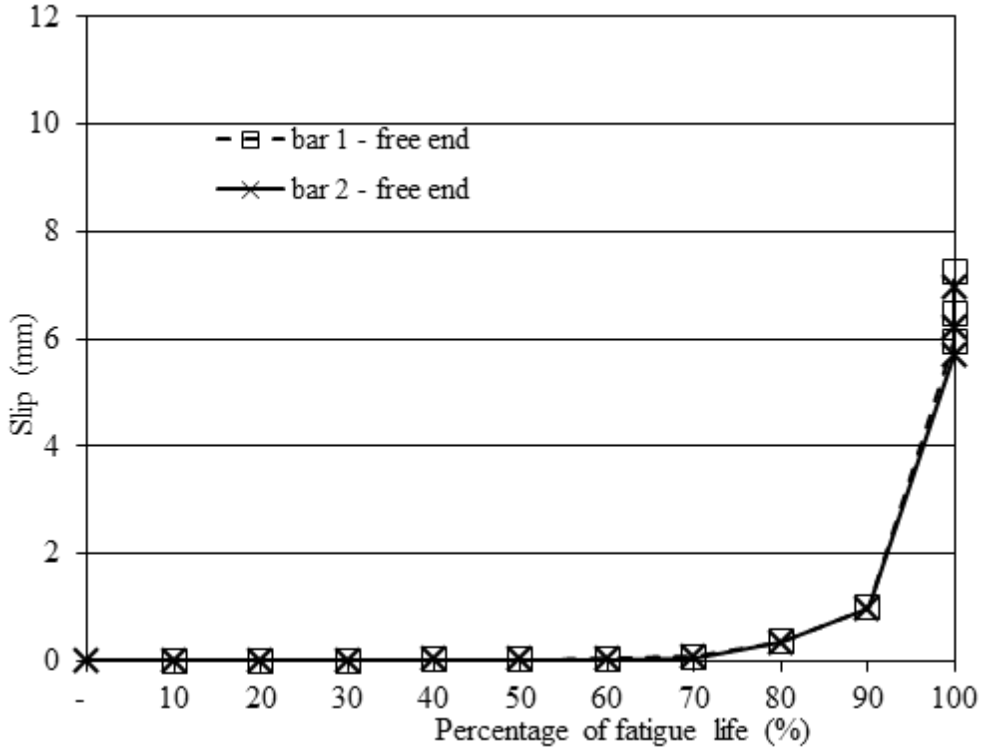


**Figure 5.53 Slip versus percentage of fatigue life for Beam F-200-U-m-43.**

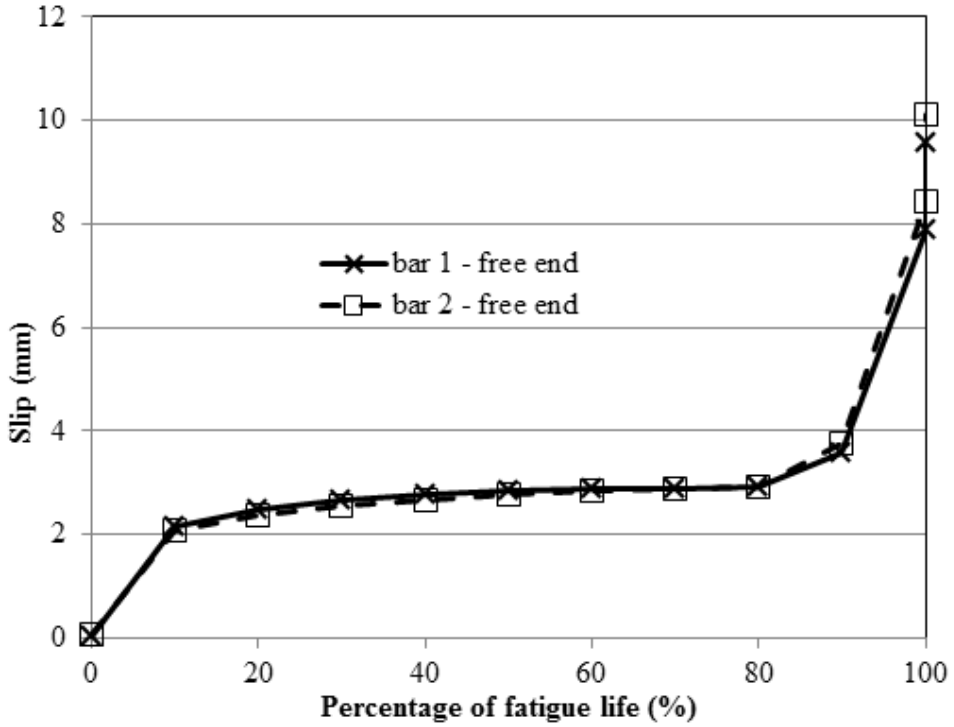


**Figure 5.54 Slip versus percentage of fatigue life behaviour for Beam F-200-R-m-90.**

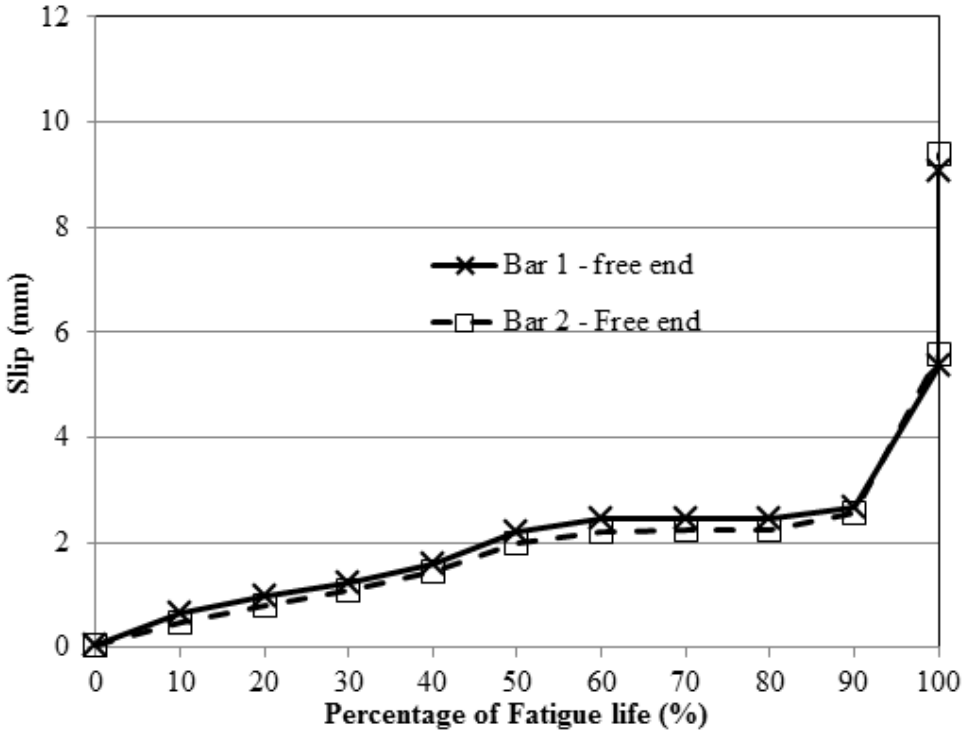


**Figure 5.55 Slip versus percentage of fatigue life behaviour for Beam F-200-R-m-96.**

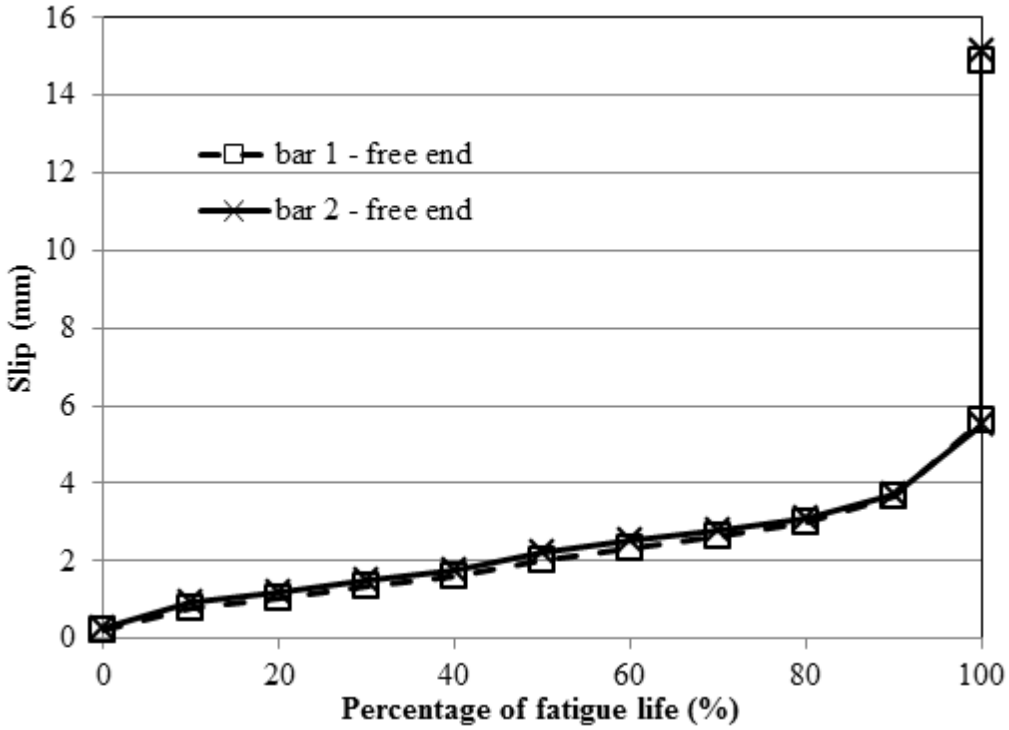


**Figure 5.56 Slip versus percentage of fatigue life behaviour for Beam F-200-R-h-80.**

In conclusion, the uncorroded unrepaired beams showed almost no increase in slip until near failure when the slip increased suddenly. The corroded beams showed an earlier increase in slip reaching about 1mm slip at 90% of the fatigue life. Similarly to the uncorroded beams, from 90% of the fatigue life to failure there was a great increase in slip. The corrosion products of the rebars induced rust products that were larger in volume than the steel itself. This induced tensile stresses in the concrete causing it to crack. Due to corrosion cracks the bar slipped early in the fatigue life at lower load ranges than the control beams. The repaired beams showed a slip of about 1 mm in the first 10% of the fatigue life. At 90% of the fatigue life the slip was between 3mm and 4mm before it increased to a slip value between 10 mm and 15 mm at 100 % of the fatigue life. The CFRP sheets confined the concrete at the concrete-steel interface allowing for higher slips to occur at 90% of the fatigue life compared to the unrepaired beams. As the slip of the bars increased the bottom concrete was pushed away from the bar creating tensile forces on the CFRP sheets. The beam

continued to carry load until the tensile forces in the CFRP sheets exceeded their ultimate strength causing rupturing of the sheets and failure of the beam in bond.

#### **5.4.1.4** Strain Variation for the fatigue beams – Set 1

The readings from the strain gauges mounted on the steel bar were plotted versus their locations on the bar for various percentages of the fatigue life of a beam. Figure 5.57 shows the strain variation along the length of the steel bar for Beam F-200-U-n-70-2 starting from the support (0 mm). The strain increased linearly with distance from the support. The last data point in each plot is the strain in the bar mounted at the pocket. The strain values increased with an increase in the number of cycles. As local cracks appeared, the local strains showed a sudden increase. At 100% of the fatigue life, a horizontal crack ran between the locations of strain gauges 2 and 3 as part of the concrete debonded along the bar between these two points (dashed line in Figure 5.57). There was a reduction in the strain reading at point 3 that can probably be attributed to a reduction in the bar force as the central cracks opened, the neutral axis moved up, and the distance between the centroid of the concrete force and the steel bar increased. This behaviour was similar for the other beams from this group (Group U-n) where debonding started from the pocket and progressed towards the support. The steel plates confined the concrete at the support location causing the closest strain gauge to report higher strains with an increase in the number of cycles. Figure 5.58 shows the strain profile for Beam F-200-U-n-60 where debonding from the pocket towards the support location similar to what was reported above was observed at 100% of the fatigue life.

Three beams from the first cast belonged to group U-m (corroded and unrepaired beams) and had electrical strain gauges installed in the grooved bars. Unfortunately the strain gauges in the bar grooves for these corroded beams did not function properly and hence no readings were obtained from them. It was believed that the exposure of the strain gauges to the induced current needed for the corrosion process damaged the strain gauges. The rest of the corroded beams from this study had either encapsulated strain gauges installed in the grooved bars or the gundrilled bars, or FBG sensors installed in the gundrilled bars.

During loading, the bars inside the reinforced concrete beams experienced tensile stresses that caused the bar to strain. The strain in the bar caused a strain in the gauge of the FBG sensor. The straining of the gauge caused a change in the center wavelength of the sensor (Tennyson, Mufti, Rizkalla, Tadros, & Benmokrane, 2001). The wavelength reading was transmitted through an optical transmission cable to the FBG interrogator (sm130) that determined the change in wavelength. This change in wavelength was then recorded in a custom software (ENLIGHT) and transformed to strain values (Zhou & Ou, 2004).

The strains along the length of the bar were plotted for different percentages of the fatigue life. Figure 5.59 shows the strain results from the FBG sensors while Figure 5.60 shows the strain results from the encapsulated strain gauges for the corroded unrepaired beam F-200-U-m-44. The strains from both the FBG sensors and the encapsulated strain gauges were combined with the strain reading from an electrical resistance strain gauge that was placed on the bar in the pocket region (~210mm from the support) before testing. The strain values initially showed an approximately linear behaviour along the length of the bar which suggested a uniform shear stress along the length of the bar in the anchorage zone. The strain values increased as slip started to occur (Table 5.4). From Table 5.4, the increase in slip from 0 to about 0.8 mm from the first cycle to 20% of the fatigue life explains the increase seen in the strain readings (Figure 5.59 and Figure 5.60) (Al-Hammoud, Soudki, & Topper, CDCC).

At 100% of the fatigue life, the support at the side of the bar containing the FBG sensors debonded reducing its confinement effect, thus reducing the strain reading close to the support. Debonding for both bars started from the pocket and progressed towards the support. This was clear from the uniform strain readings between gauge 3 and gauge 4 at 100% of the fatigue life (Figure 5.59 and Figure 5.60).

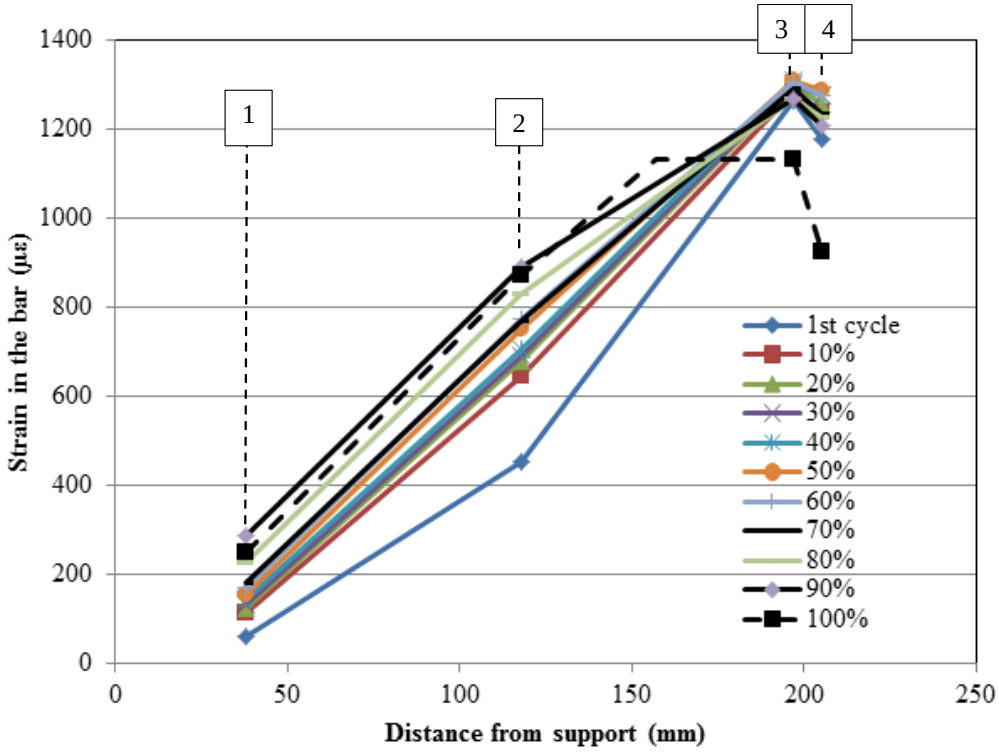


**Figure 5.57 Strain Profile at different percentages of the fatigue life for Beam F-200-U-n-70-2.**

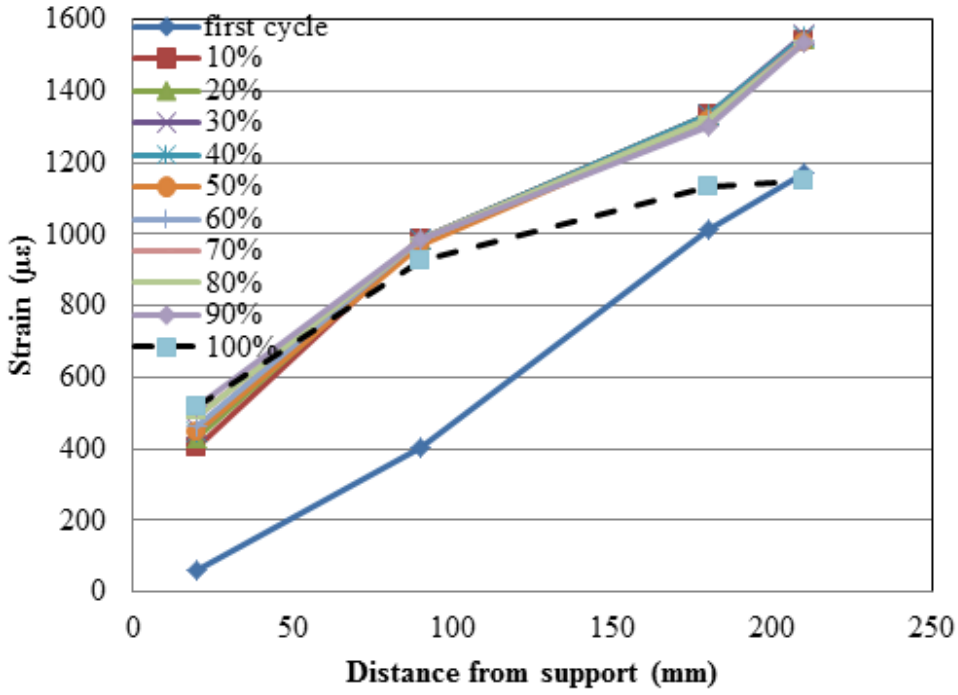


**Figure 5.58 Strain profile at different percentages of the fatigue life for Beam F-200-U-n-60.**

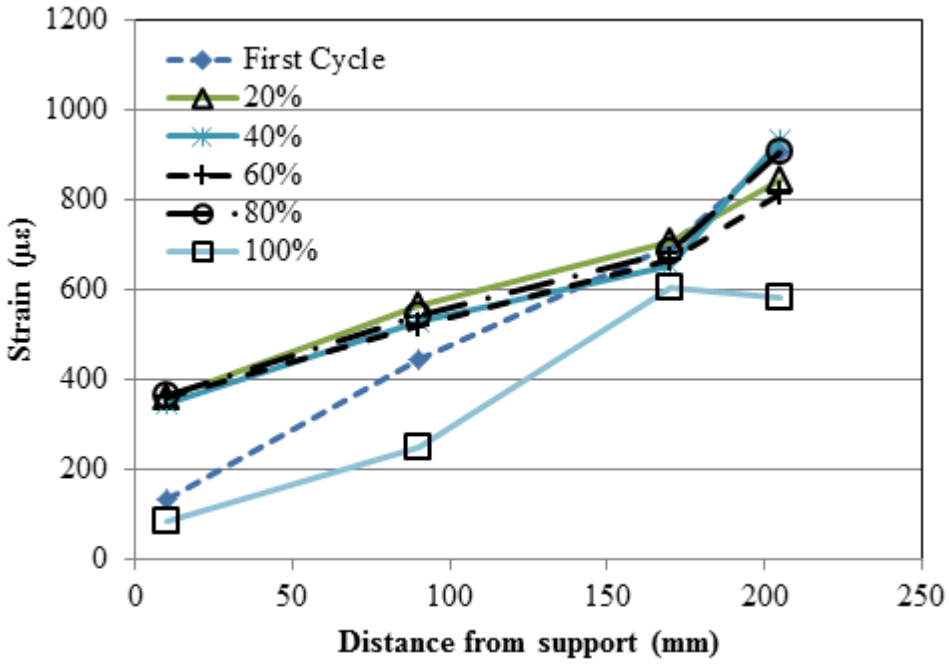


**Figure 5.59 Strain Readings from FBG sensors along the length of the beam for Beam F-200-U-m-44.**

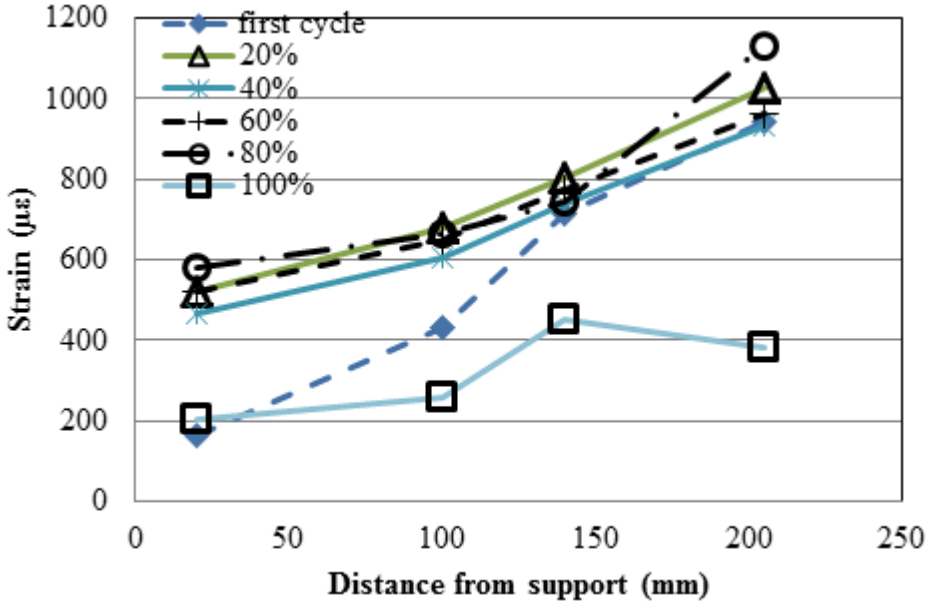


**Figure 5.60 Strain Readings from encapsulated strain gauges along the length of the beam from Beam F-200-U-m-44.**

**Table 5.4 Recorded slip for the different percentages of the fatigue life of the unrepaired beam (F-200-U-m-44).**

| Fatigue life (%) / Bar | cycle 1 | 10 | 20 | 30 | 40 | 50 | 60 | 70 | 80 | 90 | 100 |
|---|---|---|---|---|---|---|---|---|---|---|---|
| Slip in bar with FBG sensors (mm) | 0.017 | 0.58 | 0.86 | 1.13 | 1.28 | 1.38 | 1.48 | 1.63 | 1.77 | 1.78 | 8.1 |
| Slip in bar with encapsulated strain gauges (mm) | 0.022 | 0.50 | 0.74 | 0.97 | 1.11 | 1.18 | 1.28 | 1.43 | 1.54 | 1.54 | 8.6 |

After the FBG sensors were installed inside the bars of the repaired beams, a change in the beam design took place. This led to 2 sensors being placed in the unbonded region of the beam and hence the recordings from those sensors were not helpful for this study. Thus for the repaired beams with an anchorage length of 200 mm, one sensor reading was reported in the anchorage zone of the bar. For the repaired beams with a 350 mm anchorage length, the readings from 2 sensors in the anchorage zone of the bar were reported. As for the encapsulated strain gauges, they were placed in the bars after the design change took place and hence there are 3 gauge readings reported for both anchorage lengths (200 mm and 350 mm) along the length of the bar.

In the repaired beams corroded to mild corrosion level, the strain increased with the number of cycles until the final cycle (100% of the fatigue life) where the strain values have dropped. During the last cycle, the CFRP ruptured before reaching the maximum load causing an increased slip in the bar, a drop in load and failure of the beam (Figure 5.61). It was not clear from the strain profile for the repaired beams where the debonding initiated from (pocket or support) unlike the unrepaired beams where it was clear that debonding initiated from the pocket. This was attributed to the fact that the bar when slipping pushed the bottom concrete cover away. This induced tensile stresses on the CFRP sheets confining the concrete and hence added to the compression on the concrete cover. The bar-concrete

interface then continued to resist the force until the strains in the CFRP sheets were high enough to cause rupture. After the CFRP ruptured the compression force in the concrete was released allowing for an increased slip in the bar and failure of the beam. As with the monotonic beams the steel plate support added to the confinement from the CFRP sheets causing the strain values close to the support to increase thus increasing the bond stress in this region (Figure 5.62).

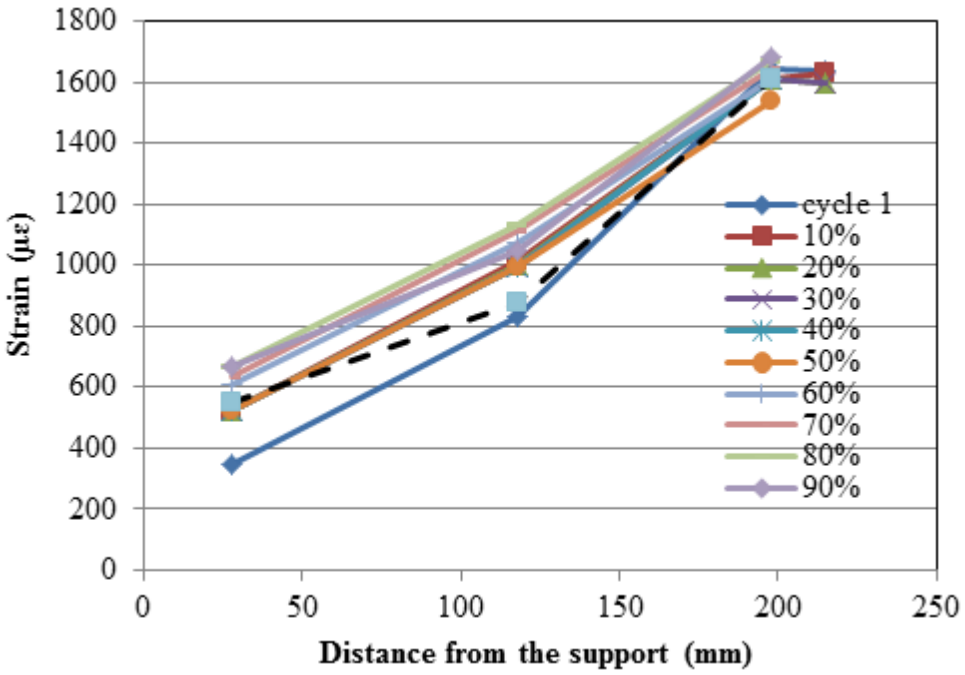


**Figure 5.61 Strain profile for Beam F-200-R-m-90.**

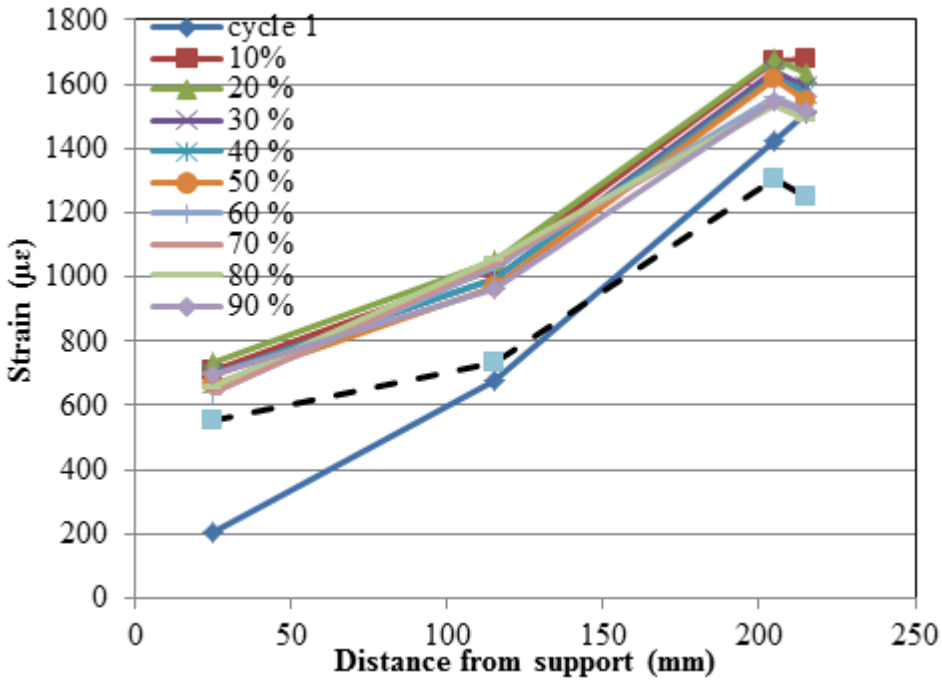


**Figure 5.62 Strain profile for Beam F-200-R-m-96.**

Strain gauges were installed on the CFRP wrapping sheets one at each side of the beam. Figure 5.63 shows the CFRP strains with the percentage of the fatigue life for Beam F-200-R-m-90. As the slip in bar 1 increased at a high rate from cycle 1 to 10% of the fatigue life (Figure 5.54), it caused an increase in the tensile strain in the CFRP sheet from 117με to 2214 με between cycle 1 and 10% of the fatigue life. The strain in the CFRP sheet then remained almost constant until 90% of the fatigue life where it increased to 2660 με and 3048 με by 100 % of the fatigue life after which it dropped due to rupturing of the sheet (Figure 5.63). This coincided with an increase in slip of bar 1 from 80% of the fatigue life to 100% of the fatigue life (Figure 5.54). The strain gauges gave a good indication of the behaviour of the CFRP sheets during testing. The strain gauge on the CFRP sheets from the beam side of bar 1 was installed only 42 mm from the pocket. The strain gauge on the CFRP sheet from the beam side of bar 2 was installed approximately at the middle of the bonded length and hence did not show much variation with life since the CFRP rupture occurred close to the pocket.

Figure 5.64 shows the strains on the CFRP sheets versus percentage of fatigue life for Beam F-200-R-m-96. Both strain gauges were installed at a similar distance from the pocket at about the steel reinforcement level. Similarly with increase in slip the CFRP tensile strains increased until at 100% of the fatigue life were the CFRP strains increased at a higher rate due to the higher increase in slip rate.

For the beams that were corroded to a high corrosion level and then repaired with CFRP sheets, the strain values in the steel bar increased with the number of cycles. At 100% of the fatigue life debonding was noticed from the pocket to the middle of the bonded length (as explained earlier equal values of strain indicate zero shear stress in this region and hence uniform movement) (Figure 5.65). Once slip started, tensile strains were introduced in the CFRP sheets. This strain increased with number of cycles until close to failure (at 100% of the fatigue life) when it increased rapidly before it dropped suddenly indicating FRP rupture and failure of the beam (Figure 5.66).

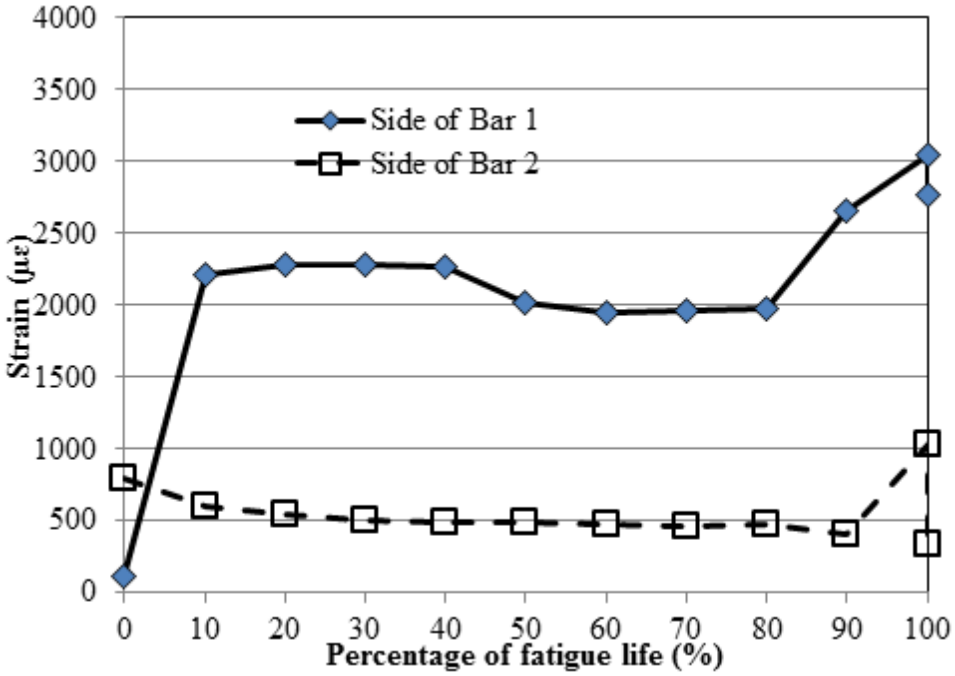


**Figure 5.63 Strains on the FRP wrapping sheet versus percentage of fatigue life for Beam F-200-R-m-90.**

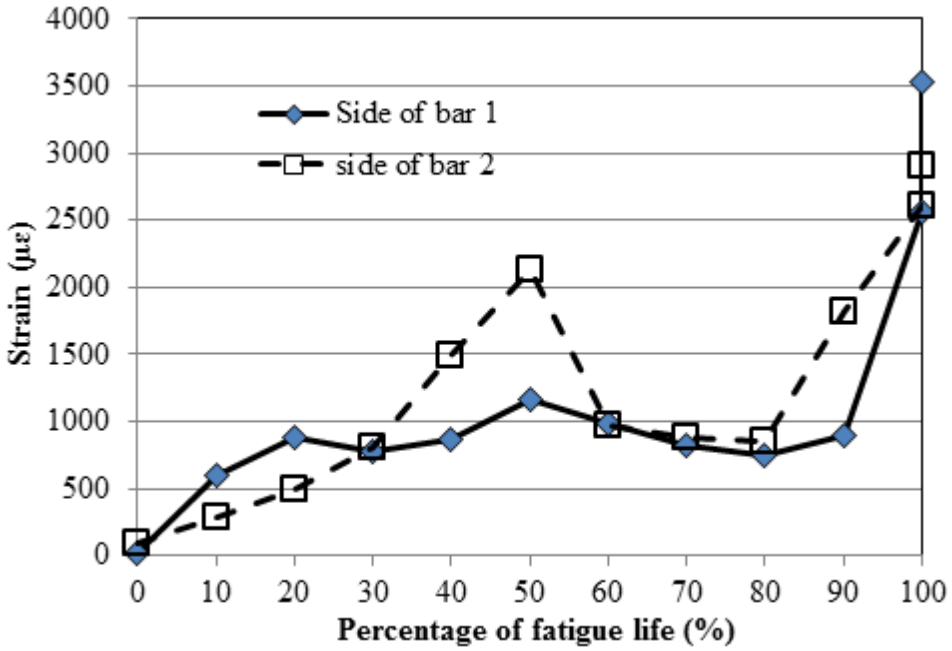


**Figure 5.64 Strains on the FRP wrapping sheet versus percentage of fatigue life for Beam F-200-R-m-96.**

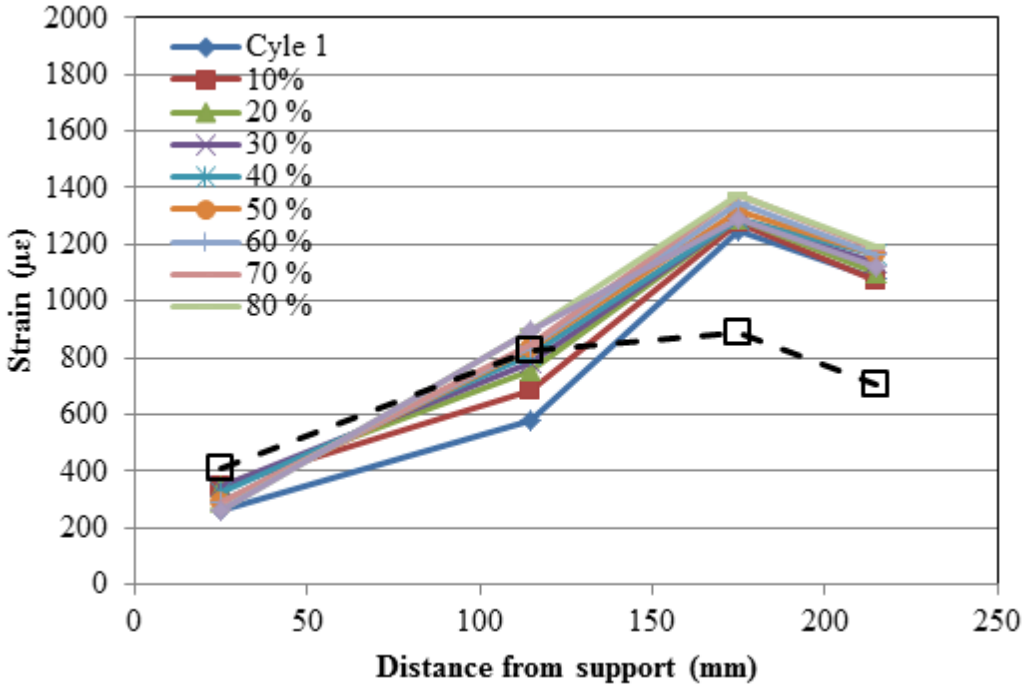


**Figure 5.65 Strain profile of the bar with percentage of fatigue life for Beam F-200-R-h-80.**

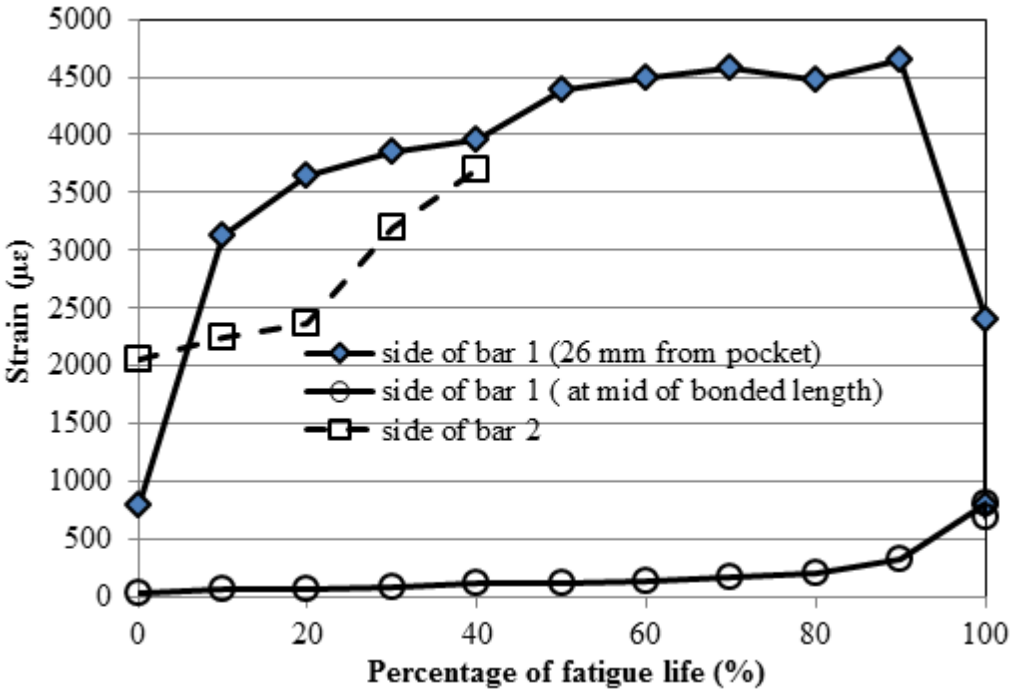


**Figure 5.66 Strains on the FRP wrapping sheet versus percentage of fatigue life for Beam F-200-R-h-80.**

### 5.4.2 Set 2 Beams – Fatigue Behaviour

#### 5.4.2.1 Overall behaviour and mode of failure

Two flexural cracks in the middle of the constant moment region were initiated while the beams were being manually loaded up to the maximum load. Another crack under the point load was initiated after the beam had run for few cycles.

As the number of cycles increased, a longitudinal crack initiated and propagated from the edge of the support towards the middle of the anchorage zone. This crack continued as a diagonal crack from the middle of the anchorage zone to the point load. These cracks were not visible in the beams repaired with CFRP sheets. The CFRP sheets confined the concrete increasing the shear and bond strengths. Three different failure modes were observed: flexure by bar rupture, flexure by concrete crushing in the constant moment region and bond. Table

5.5 gives a summary of the fatigue lives of the beams tested in Set 2 as well as the corresponding failure modes.

In the unrepaired beams whether corroded or not, the longitudinal/diagonal crack widened with an increase in the number of cycles causing the concrete to crush around the bar between the middle of the anchorage zone and the edge of the support. This led to failure of the beams by a combination of bond and shear failure. This was evident from the high slip as well as a shear crack opening at failure (Figure 5.67). In one case the shear was severe that it ruptured the stirrup (Figure 5.68) after a high slip occurred.

The repaired beams all failed by flexure. The flexural failure was either by bar rupture (Figure 5.69) or concrete crushing (Figure 5.70). The beams that failed in flexure were not helpful for the purpose of this study and are not discussed further.

**Table 5.5 Fatigue lives for beams from Set 2.**

| Group | Beam Notation | Corrosion mass loss (%) | Load | | Fatigue Life (Cycles) | Failure Mode |
|---|---|---|---|---|---|---|
| | | | Maximum (kN) | Range (kN) | | |
| U-n | F-350-U-n-70 | No Corrosion (0%) | 80 | 70 | 450,028 | Flexure |
| | F-350-U-n-74 | | 84 | 74 | 13,659 | Bond |
| | F-350-U-n-80 | | 90 | 80 | 43,330 | Bond |
| | F-350-U-n-90 | | 100 | 90 | 2,833 | Bond |
| U-m | F-350-U-m-70 | 9.66 | 80 | 70 | 910,711 | Flexure |
| | F-350-U-m-82 | 6.21 | 92 | 82 | 225,948 | Bond |
| R-m | F-350-R-m-126 | 5.06 | 136 | 126 | 20,428 | Flexure |
| | F-350-R-m-135 | 7.3 | 145 | 135 | 7,152 | Flexure |
| | F-350-R-m-140 | 6.62 | 150 | 140 | 4,059 | Flexure |
| R-h | F-350-R-h-110 | 12.86 | 120 | 110 | 110,944 | Flexure |
| | F-350-R-h-122 | 11.17 | 132 | 122 | 11,830 | Flexure |
| | F-350-R-h-130 | 16.1 | 140 | 130 | 14,728 | Flexure |

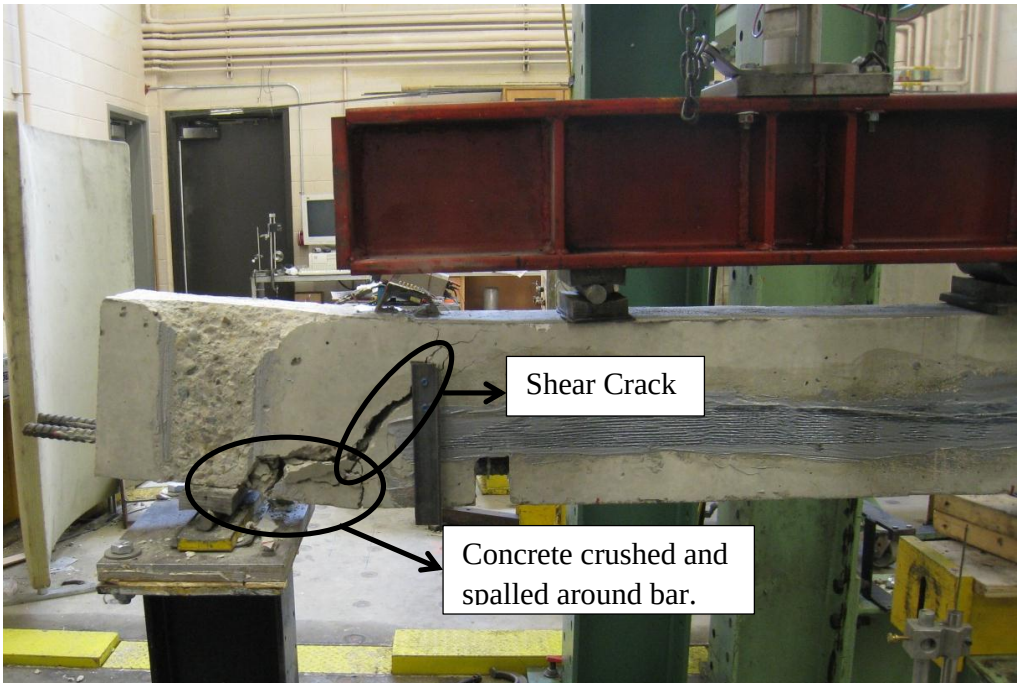


**Figure 5.67 Failure mode for Beam F-350-U-n-74.**

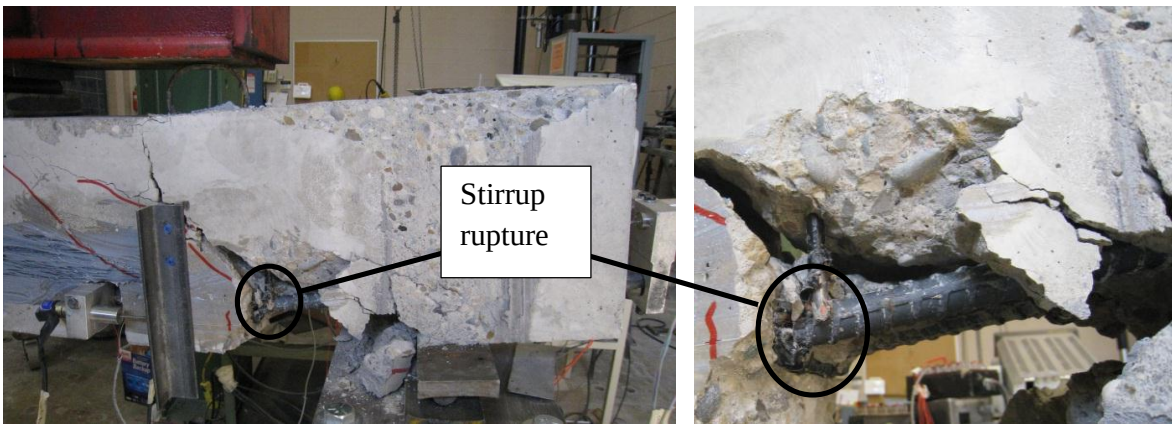


**Figure 5.68 Stirrup rupture in Beam F-350-U-n-80.**

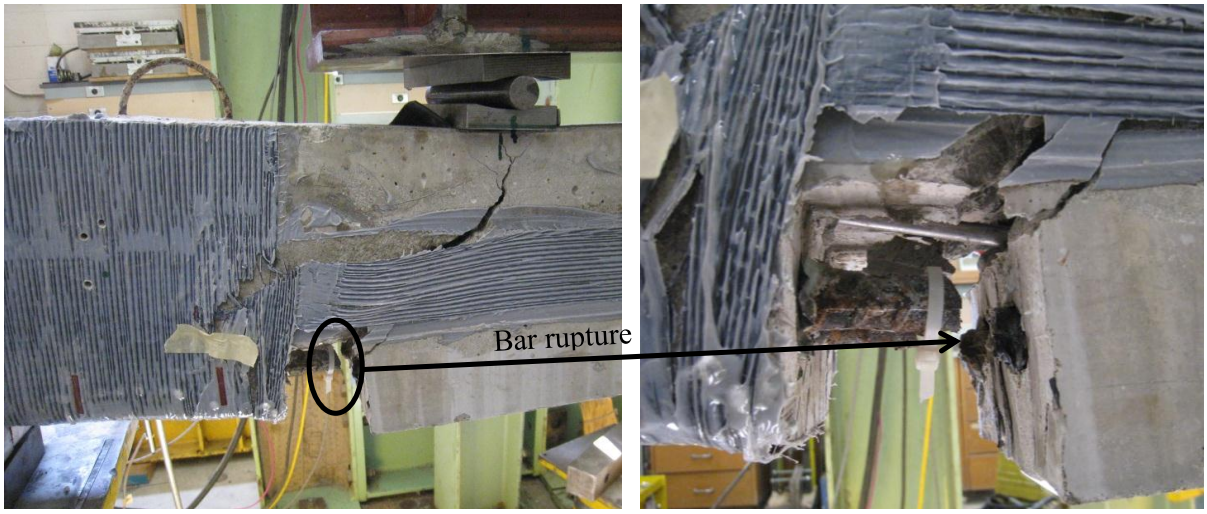


**Figure 5.69 Bar rutpture in Beam F-350-R-m-126.**

**Figure 5.70 Failure of Beam F-350-R-m-140 by concrete crushing.**

All the unrepaired beams had similar modes of failure. A flexural crack started at the middle of the anchorage zone and propagated into a diagonal shear crack as the test progressed. The crack caused the strain in the bar at the crack location to increase rapidly (Figure 5.71). This increase in the bar strain was due to the tensile forces transferred from the concrete to the bar as the diagonal crack propagated. In other words as the diagonal crack propagated, a thrust force was developed in the concrete section along the crack (Figure 5.72). The horizontal component of the concrete compression thrust force was resisted by the tensile reinforcement at the edge of the crack causing the strains at this location to increase (Figure 5.72). The increase in the bar strain at the location of gauge 2 (G2) (Figure 5.73)

corresponded to high forces in the bar and a large slip (Figure 5.74) and crushing of the concrete around the bar between the edge of the support and the middle of the anchorage zone (where the strain was highest) (Figure 5.67). The strain profile and the slip for the unrepaired beams that failed in bond are shown in Appendix E and Appendix F respectively.

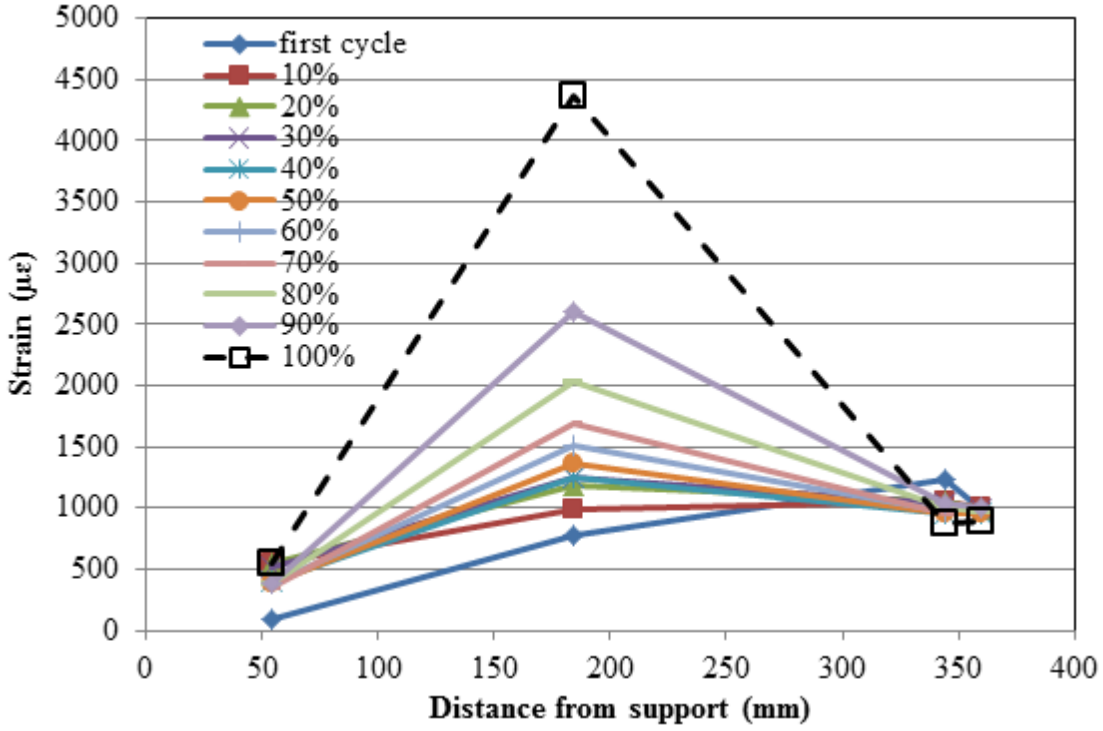


**Figure 5.71 Strain Profile for Beam F-350-U-n-74.**

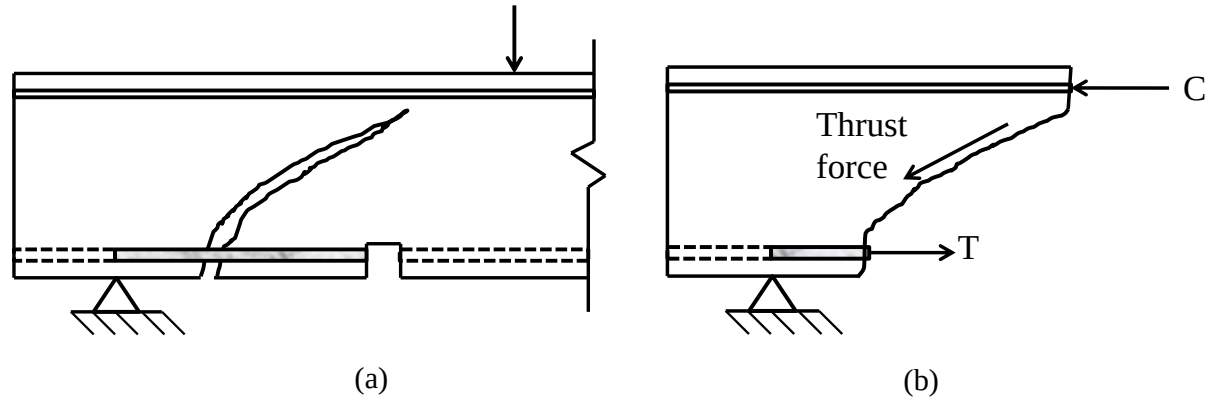


**Figure 5.72 (a) Schematic drawing of beam with diagonal crack, (b) a section of the beam at the crack.**

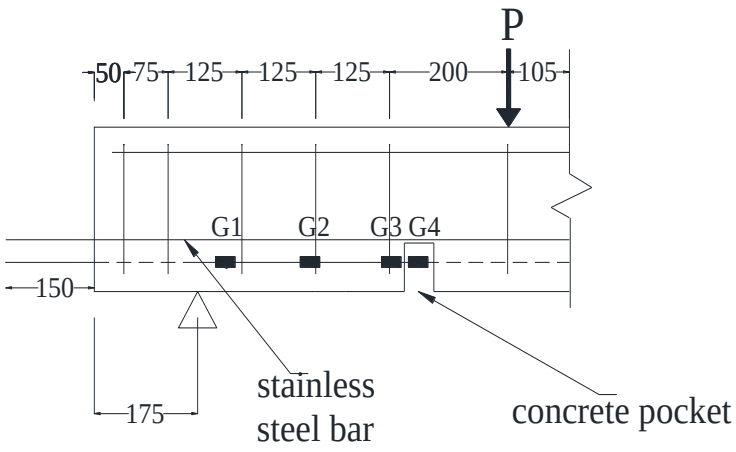


**Figure 5.73 Schematic drawing showing the location of the strain gauges in the beams with 350 mm anchorage length.**

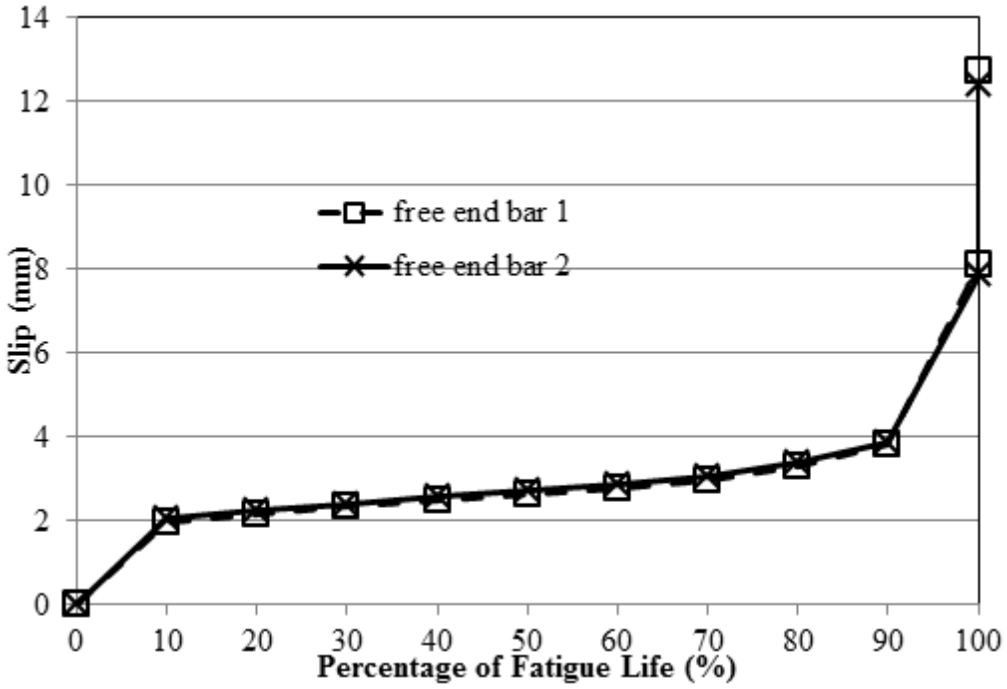


**Figure 5.74 Slip versus percentage of fatigue life for Beam F-350-U-n-74.**

#### 5.4.2.2 Fatigue Strength- Set2

Figure 5.75 shows the fatigue life of the tested beams versus the applied load range. It can be seen that the fatigue life of the beams varied linearly on logarithmic scales with the range of applied load with a very shallow slope. Hence the range of load over which fatigue failure occurred was small. Corroding the beams to a mild corrosion level did not affect the fatigue bond strength for the single beam that failed in bond.

## 5.5 The effect of bonded length

Group 2 beams discussed in this chapter consisted of two sets where the only difference was the anchorage length. Set 1 beams had a 200 mm anchorage length, while set 2 beams had a 350 mm anchorage length. A comparison of the experimental results from the two sets was discussed to clarify the effect of changing the anchorage length from 200 mm to 350 mm on the static and fatigue bond behaviour.

### 5.5.1 Monotonic Behaviour

The failure mode for the unrepaired beams was by bond for both sets (200 mm and 350 mm anchorage length) where the bar slipped causing the load to drop and the beam to fail. The increase in the maximum static capacity for the unrepaired beams with 350 mm anchorage length in comparison to beams with 200 mm anchorage length was about 60% which is a ratio of 1.6 (Table 3.2 and Table 3.3). This is slightly less than the ratio of the change in anchorage length from 350 mm to 200 mm which is 1.75 due to the non-uniform nature of bond forces.

The repaired beams of set 1 all failed by bond where the bar slipped followed by CFRP rupture. In set 2 beams the load was high enough that the steel yielded causing the final failure of the repaired beams by flexure due to concrete crushing in the constant moment region. The change in failure mode did not allow for a comparison to calculate the increase in bond strength due to the increase in anchorage length.

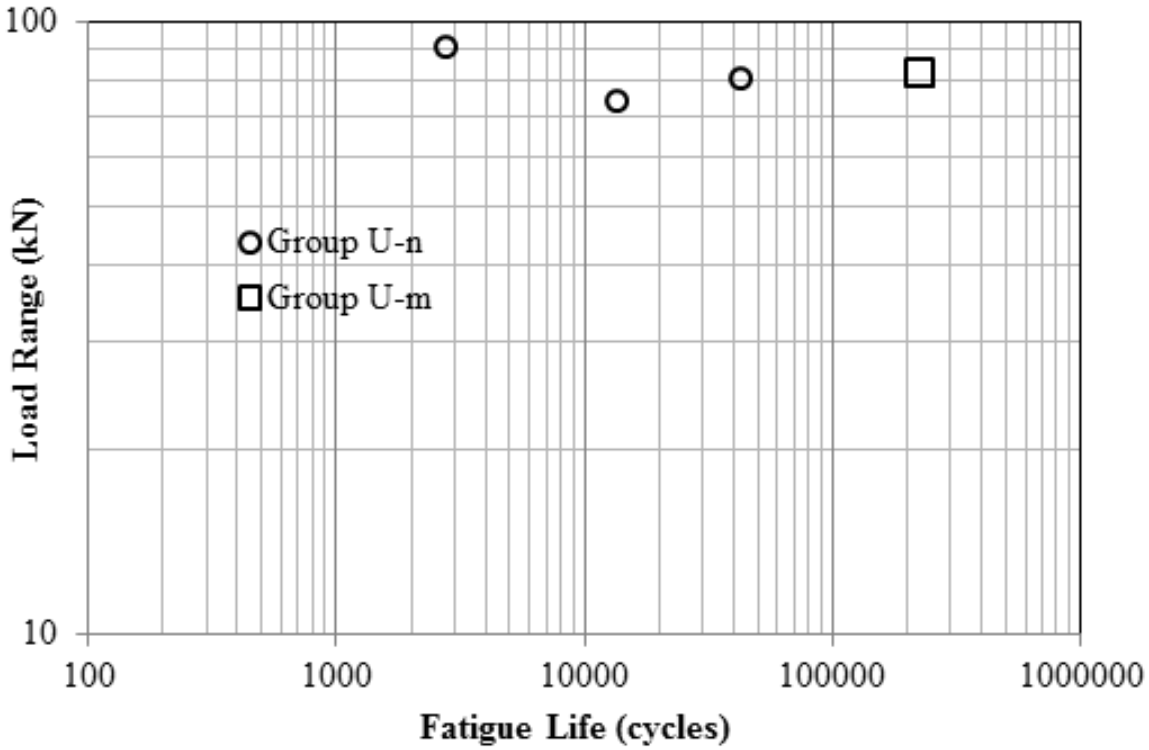


**Figure 5.75 Fatigue life with respect to load range applied for Beams from Group 2- Set 2 failing in bond.**

### 5.5.2 Fatigue Behaviour

Figure 5.76 shows a comparison between the beams from set 1 and set 2 of the same group that failed in bond. Increasing the bonded length from 200 mm to 350 mm caused an increase in the fatigue strength of about 12.5% for the control uncorroded beams. This increase (1.13 ratio) was well below the 1.75 ratio due to the change in the bonded length from 350 mm to 200 mm. It was also well below the increase observed for the static beams (a ratio of 1.6). For the beam corroded to a mild corrosion level the increase in fatigue strength with the change in bonded length from 200 mm to 350 mm was 77.7%. This is close to the 1.75 ratio of increase expected due to the change in bonded length; however there was only one corroded beam from set 2 that failed in bond and hence not enough to come to a firm conclusion.

The increase in the bonded length from 200 mm to 350 mm also caused a change in the failure pattern. In the 200 mm bonded length beams failure started from the pocket and propagated towards the support. In the 350 mm bonded length beams failure initiated at the middle of the anchorage zone where a shear crack was formed inducing higher bar strains. As the beam was cycled the shear crack would widen until there is no interlock forces from the concrete aggregates. This leads to a value force that was transferred through the concrete into the reinforcing bars at the edge of the shear crack, causing the forces in the bar at this location to increase. Failure then occurred from the middle of the anchorage zone (at the edge of the shear crack) towards the support.

The repaired beams from set 2 had higher load ranges which caused them to be above the flexural endurance limit for this beam design. Thus, all the repaired beams of set 2 failed by flexural fatigue and no comparison was made between the different anchorage length for the repaired beams.

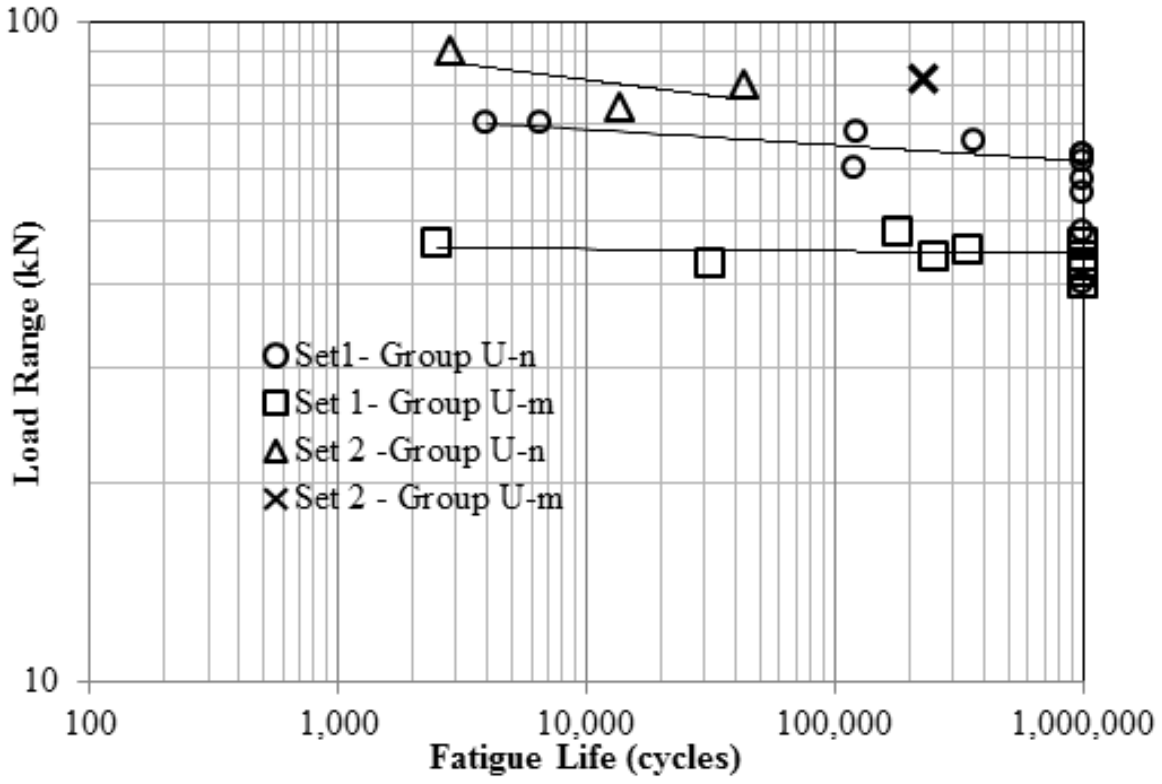


**Figure 5.76 Fatigue with respect to load range applied for Beams from group 2, Set 1 and Set 2.**

## 5.6 Concluding Remarks

Group 2 consisted of 2 sets of beams with 2 different anchorage lengths: Set 1 (200 mm anchorage length) and Set 2 (350 mm anchorage lengths). The general conclusions are presented first followed by the concluding remarks from each set.

### 5.6.1 General Conclusions

- Gluing the steel plates as supports to the sides did not prevent their confinement effect. The steel plates prevented the concrete cracks from propagating towards the support. This caused the concrete-steel interface close to the support to be confined and hence resisted higher bond stresses in this region.
- Faraday's law was used to estimate the corrosion mass loss of the bars in the beams. Faraday's law over-estimated the time needed to achieve a 5% mass loss, and under-estimated the time needed to achieve a 15% mass loss even though the time to which the beams were exposed to an induced current was increased by 30% to that required by Faraday's law (for the beams corroded to 15% mass loss).
- Corrosion of the reinforcing bars was not uniform throughout the length of the bar, corrosion pits were produced.
- The cracks in the concrete due to corrosion of the embedded steel bars were parallel to the corroded length of the reinforcing steel bars.
- Increasing the bonded length from 200 mm to 350 mm caused an increase in the static capacity by about 60%.
- Increasing the bonded length from 200 mm to 350 mm caused an increase in the fatigue strength of 12.5% for the control uncorroded beams.
- Increasing the bonded length from 200 mm to 350 mm caused a change in the failure pattern under repeated loading. In the 200 mm bonded length beams failure started from the pocket and propagated towards the support. In the 350 mm bonded length beams failure initiated at the middle of the anchorage zone where a shear crack was formed

inducing higher bar strains. Failure then propagated from the middle of the anchorage zone towards the support.

### 5.6.2 Set 1 beams

- The static beams from group 2 – set 1 all failed by bond (bar slipping). In the cases were the beams were confined with CFRP sheets, the CFRP ruptured after the bar slipped causing failure of the beam by bond.
- Corroding the beams to a mild corrosion level reduced their maximum static capacity by 23% and their fatigue strength by about 34%.
- Strengthening the uncorroded beam with a transverse U-shaped CFRP sheet in the anchorage zone increased the static capacity and the fatigue strength of the beam by about 80% compared to the uncorroded, unstrengthened beam.
- Repairing the corroded beams with CFRP sheets restored the strength of the beam and increased its static capacity by about 25 % and its fatigue strength by about 23% compared to the control (uncorroded and unrepaired) beam.
- The static bond capacity of the corroded beams repaired with CFRP sheets depended on the capacity of the CFRP sheets, irrespective of the corrosion level, since failure was by CFRP sheet rupture.
- Examining the concrete around the bar after failure, it was noticed that in the unrepaired beams, the concrete above the bar, which was held to the bar by the stirrups, resisted slipping and was crushed while the concrete below the bar was split off and pushed away offering little resistance to slip. In the CFRP repaired beams, the concrete keys above and below the bar were crushed along the entire length.
- The fatigue life of the beams varied linearly on logarithmic scales with the range of load applied with a very shallow slope.
- Repairing the beams with CFRP sheets increased their fatigue bond strength above the fatigue flexural endurance limit of the beam. This prevented the achievement of a wider

range of fatigue life at this load level without achieving flexural failure instead of bond. This was described by the mapping of the flexure and bond failure presented for this set.

### 5.6.3 Set 2 beams

- Three different modes of failure were observed in this set: flexure by bar rupture, flexure by concrete crushing in the constant moment region after the steel bar yielded, and bond.
- The repaired beams from this set all failed by flexure.
- Corroding the beams to a mild corrosion level reduced their maximum static capacity by 22% and did not affect the fatigue bond strength for the single beam that failed in bond.
- Strengthening the uncorroded beam with a transverse U-shaped CFRP sheet in the anchorage zone increased the static capacity by about 18% compared to the uncorroded, unstrengthened beam. It also changed the mode of failure from bond to flexure leading to a more ductile post-peak behaviour.
- Repairing the corroded beams with CFRP sheets restored the strength of the beam and increased its static capacity by about 18 % compared to the control (uncorroded and unrepaired) beam.

# Chapter 6
# Reliability of Fatigue Life

Considerable scatter was shown in the fatigue life results within a small variation in load range for the control and corroded beams. A reliability or probabilistic approach would be the best criterion to determine the mean and design fatigue life for a specified load range. In this chapter, the probability distribution function for the fatigue life of the different groups (Set1 – Group U-n, Set1-Group U-m, Set1 – Group R-h and Set2-Group U-n) was determined. The parameters of the statistical distribution were calculated using the S-N relationship. After the probability density function (pdf) for the groups was determined, the pdf and reliability plots were graphed. The mean fatigue life and the design fatigue life were then tabulated for the different stress ratios.

## 6.1 Estimation of the pdf parameters using the S-N relationship

Fatigue life was best fitted as a lognormal or a Weibull probability density function (Yang, 1996; Singh, Singh, & Kaushik, 2005; Singh, Mohammadi, Goel, & Kaushik, 2007; Castillo, Canteli, & Ripoll, 2008; Singh & Ambedkar, 2008; Singh, Singh, & Bajaj, 2012). Several researchers have established a relationship between the parameters of the S-N (stress – number of cycles) curve and the Weibull parameters. This relationship was established for flexural fatigue strength of plain concrete (Oh B. , 1986), and steel fibre reinforced concrete (Singh, Mohammadi, Goel, & Kaushik, 2007). Therefore it was decided to use the Weibull pdf in the reliability analysis of the fatigue bond behaviour in this study.

The pdf for a Weibull distribution is given by the following function:

$$f(x) = \frac{\alpha}{\beta^{\alpha}}(x_i - \mu_x)^{(\alpha-1)} e^{-(\frac{x_i-\mu_x}{\beta})^{\alpha}} \qquad \textbf{Equation 6-1}$$

Where,

$f(x)$ is the probability density function

$x_i$ is the random variable, in this case the fatigue life

$\mu_x$ is the location parameter

$\beta$ is the scale parameter

$\alpha$ is the shape parameter

The S-N relationship for beams subjected to repeated loading could be represented as (Oh B. , 1986; Wirsching & Yao, 1970):

$$N(S)^m = C$$ **Equation 6-2**

Where N is the fatigue life, S is the normalized stress, and m and C are empirical constants.

In this study the stresses were normalized by taking the maximum nominal stress and dividing it by the maximum stress from the static beam tests. The nominal stresses were calculated from cracked section analysis based on the maximum applied load and taking into account the cross-sectional mass loss due to corrosion if any for each beam. Hence **Equation 6-2** can be re-written as:

$$N\left(\frac{f_{\max}}{f_{static}}\right)^m = C$$ **Equation 6-3**

Taking the logarithm for both sides, **Equation 6-3** can be written as:

$$\log_{10}(N) = \log_{10} C - m\log_{10}\left(\frac{f_{\max}}{f_{static}}\right)$$ **Equation 6-4**

This equation resembles a linear equation:

$$Y = ax + b$$ **Equation 6-5**

Where, $Y = \log_{10}(N)$; $X = \log_{10}\left(\frac{f_{\max}}{f_{static}}\right)$; $a = -m$ and $b = \log_{10} C$

The best fit equation for the fatigue data for the different groups was determined using linear regression as follows:

Set 1- Group U-n: $Y = -26.924X + 2.1978; R^2 = 0.6013$ **Equation 6-6**

Set 1- Group U-m: $Y = -11.422X + 3.9771; R^2 = 0.0393$ **Equation 6-7**

Set 1- Group R-h: $Y = -21.234X + 2.55887; R^2 = 0.9916$ **Equation 6-8**

Set 2- Group U-n: $Y = -10.636X + 1.7357; R^2 = 0.451$ **Equation 6-9**

Accordingly, the S-N relation for each group can be written as:

Set 1- Group U-n: $N\left(\frac{f_{\max}}{f_{static}}\right)^{26.924} = 157.7$ **Equation 6-10**

Set 1- Group U-m: $N\left(\frac{f_{\max}}{f_{static}}\right)^{11.422} = 9486$ **Equation 6-11**

Set 1- Group R-h: $N\left(\frac{f_{\max}}{f_{static}}\right)^{21.334} = 362$ **Equation 6-12**

Set 2- Group U-n: $N\left(\frac{f_{\max}}{f_{static}}\right)^{10.636} = 54.4$ **Equation 6-13**

The parameters of the Weibull distribution function can then be determined as follows (Oh B. , 1986; Wirsching & Yao, 1970; Singh, Mohammadi, Goel, & Kaushik, 2007):

$$\alpha^2 = \frac{\pi^2}{6s^2}$$ **Equation 6-14**

$$\ln(\beta) = \frac{0.5772}{\alpha} + \ln\left[C\left(\frac{f_{\max}}{f_{static}}\right)^{-m}\right]$$ **Equation 6-15**

Where, $s$ is the standard error estimated for $\log_{10}(N)$ and was derived using the following equation for each group:

$$s = \sqrt{\frac{1}{\nu}\sum_{i=1}^{n}\left(\hat{y}_i - y_i\right)^2}$$ **Equation 6-16**

Where "$\nu$ is the degree of freedom which is equal to n, the sample size, minus the number of unknowns estimated by the regression procedure" (Ayyub & McCuen, 2002). In the case provided in this study, $\nu = n - 2$.

$\hat{y}_i = \log_{10}(N)$ is calculated from either **Equation 6-6**, **Equation 6-7**, **Equation 6-8** or **Equation 6-9**.

Solving **Equation 6-14** and **Equation 6-15** for $\alpha$ and $\beta$ in the Weibull distribution function, we found that $\alpha$, the shape parameter, is independent of the stress ratio, while $\beta$, the scale parameter, varies with the variation of the stress ratio. The results are shown in Table 6.1 for the different stress ratios presented in this study for two of the groups. In both cases the scale parameter ($\beta$) increased with decreasing load or stress ratio, while the shape parameter ($\alpha$) remained constant for each group and was above unity, which indicated that the hazard rate would increase with increasing life. This complies with the expected fatigue behaviour of engineering materials.

**Table 6.1: Weibull parameters values for each group with the different stress ratios**

| Group Name | Standard error of estimate | Shape parameter, α | Stress Ratio, $S=\frac{f_{max}}{f_{static}}$ | Scale Parameter, $\beta$ |
|---|---|---|---|---|
| Set 1 – Group U-n | 0.658 | 1.95 | 0.705 | 2,608,191 |
| | | | 0.731 | 968,001 |
| | | | 0.749 | 509,870 |
| | | | 0.762 | 318,356 |
| | | | 0.793 | 109,423 |
| | | | 0.815 | 52,328 |
| | | | 0.837 | 25,521 |
| Set 1 – Group U-m | 0.893 | 1.44 | 0.714 | 661,809 |
| | | | 0.72 | 555,902 |
| | | | 0.725 | 468,169 |
| | | | 0.736 | 606,346 |
| | | | 0.747 | 395,287 |
| | | | 0.758 | 334,576 |
| | | | 0.764 | 308,091 |
| | | | 0.769 | 283,870 |
| | | | 0.797 | 190,129 |

Using the data from Table 6.1 and **Equation 6-14** and **Equation 6-15**, the scale parameters ($\beta$) for selective stress ratio ($S=\frac{f_{max}}{f_{static}}$) were calculated and are presented in Table 6.2.

**Table 6.2: Weibull parameters for selective stress ratios.**

| Group Name | Standard error of estimate | Shape parameter, α | Stress Ratio, $S=\frac{f_{max}}{f_{static}}$ | Scale Parameter, $\beta$ |
|---|---|---|---|---|
| Set 1 – Group U-n | 0.658 | 1.95 | 0.70 | 3,140,552 |
| | | | 0.75 | 490,090 |
| | | | 0.80 | 86,225 |
| | | | 0.85 | 16,856 |
| Set 1 – Group U-m | 0.893 | 1.44 | 0.70 | 833,582 |
| | | | 0.75 | 379,060 |
| | | | 0.80 | 181,369 |
| | | | 0.85 | 90,748 |
| Set 1 – Group R-h | 0.137 | 9.35 | 0.65 | 3,614,920 |
| | | | 0.70 | 749,358 |
| | | | 0.75 | 173,161 |
| | | | 0.80 | 43,983 |
| | | | 0.85 | 12,140 |
| Set 2- Group U-n | 0.623 | 2.06 | 0.50 | 114,611 |
| | | | 0.55 | 41,589 |
| | | | 0.60 | 16,484 |
| | | | 0.65 | 7,036 |

The probability density function for each group was then drawn with the different stress ratios varying between 0.7, 0.75, 0.80, and 0.85 for Set 1 beams and 0.5, 0.55, 0.60 and 0.65 for Set 2 beams (Figure 6.1, Figure 6.2, Figure 6.3 and Figure 6.4). From these curves, the probability of the beam to exceed a fatigue life of one million cycles for a given stress ratio could be determined by calculating the area under the respective curve between the one million cycle and the top end of the curve. The reliability function was then drawn with respect to the fatigue life for Set 1- Group U-n (Figure 6.5), Set 1- Group U-m (Figure 6.6), Set 1 – Group R-h (Figure 6.7) and Set 2- Group U-n (Figure 6.8). The reliability function predicts the probability of the beam surviving a specified fatigue life with a given stress ratio.

For example there is a 27% probability that a beam from Group U-m tested at a stress ratio of 0.7 would survive one million cycles (Figure 6.6). Also there is a 70% probability that a beam from group U-n would survive 10,000 cycles at a stress ratio of 0.85 (Figure 6.5).

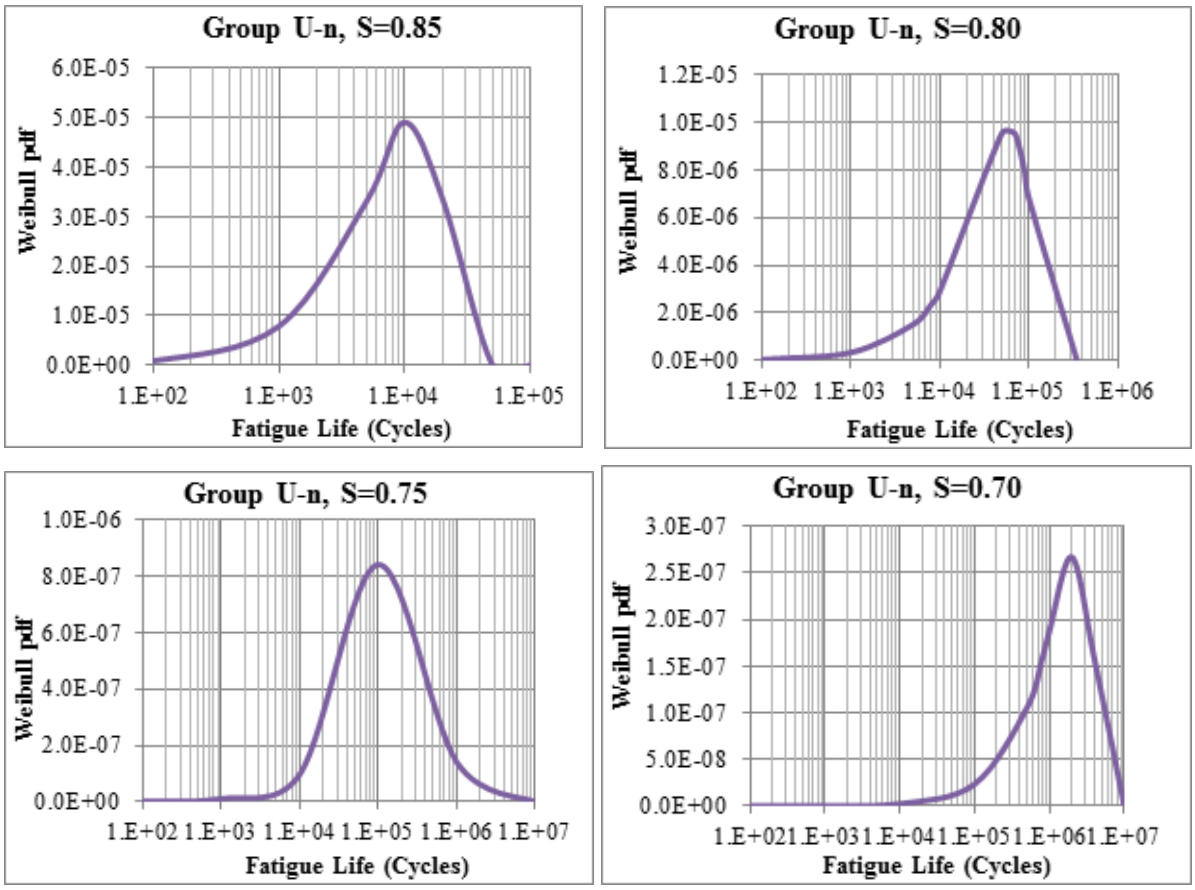


**Figure 6.1 The Weibull pdf for Set 1 - Group U-n for the different stress ratios.**

0.

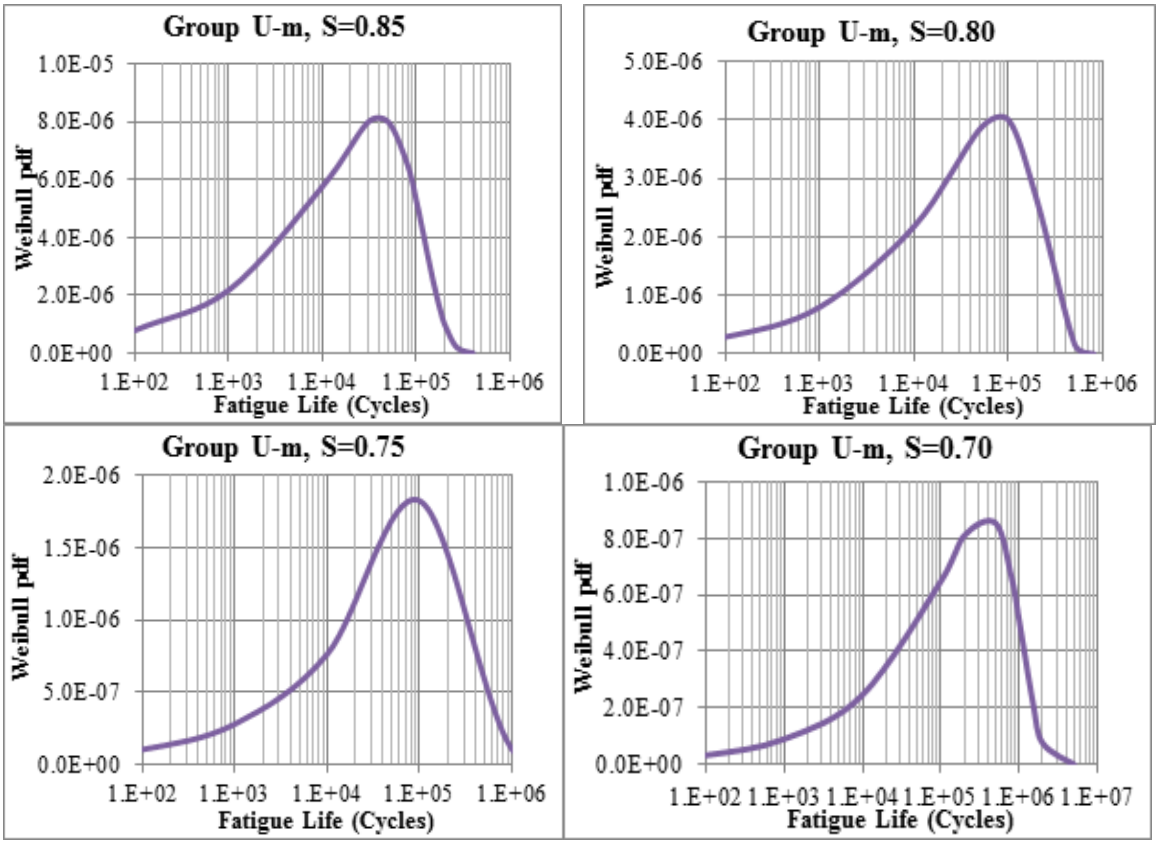


**Figure 6.2 The Weibull pdf for Set 1 - Group U-m for the different stress ratios.**

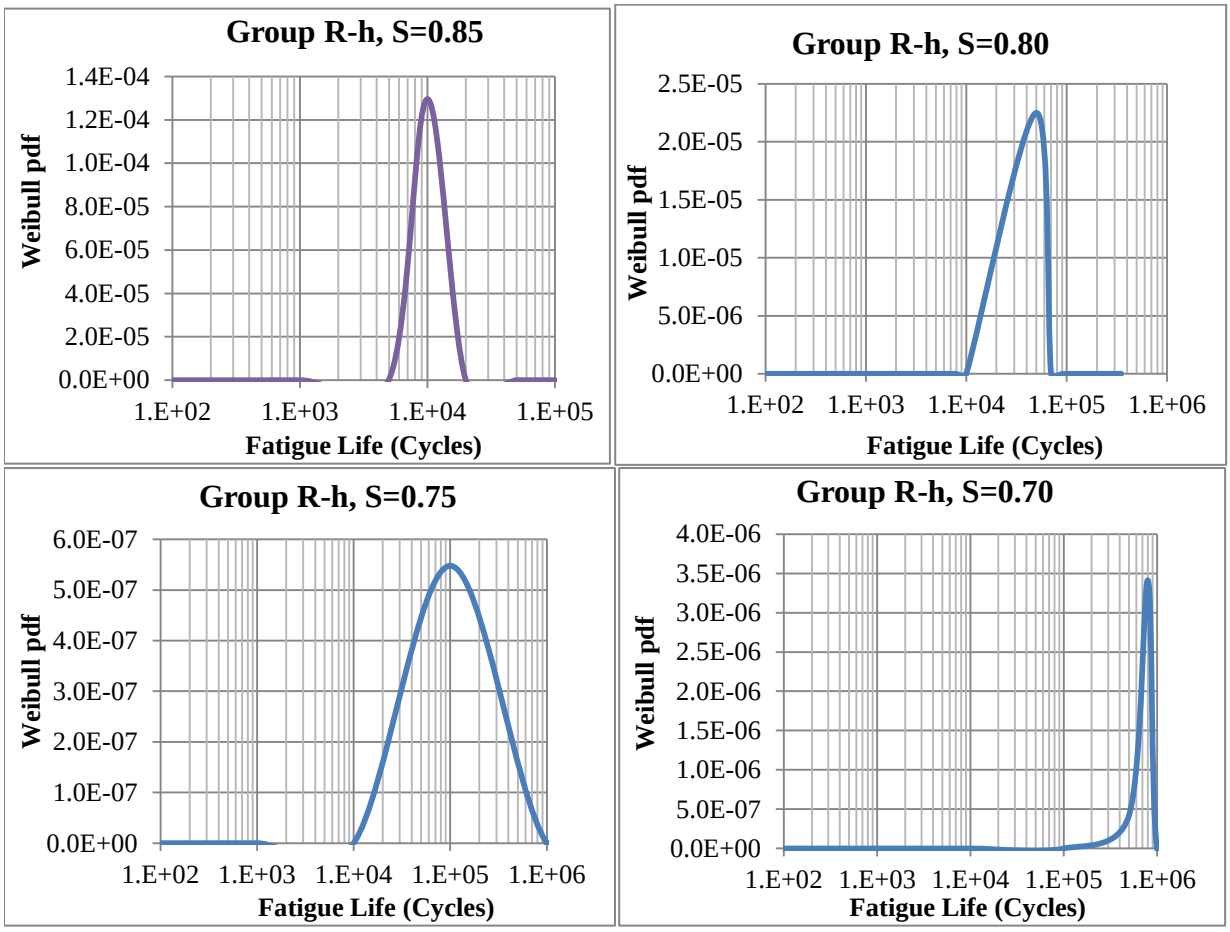


**Figure 6.3 The Weibull pdf for Set 1- Group R-h for the different stress ratios.**

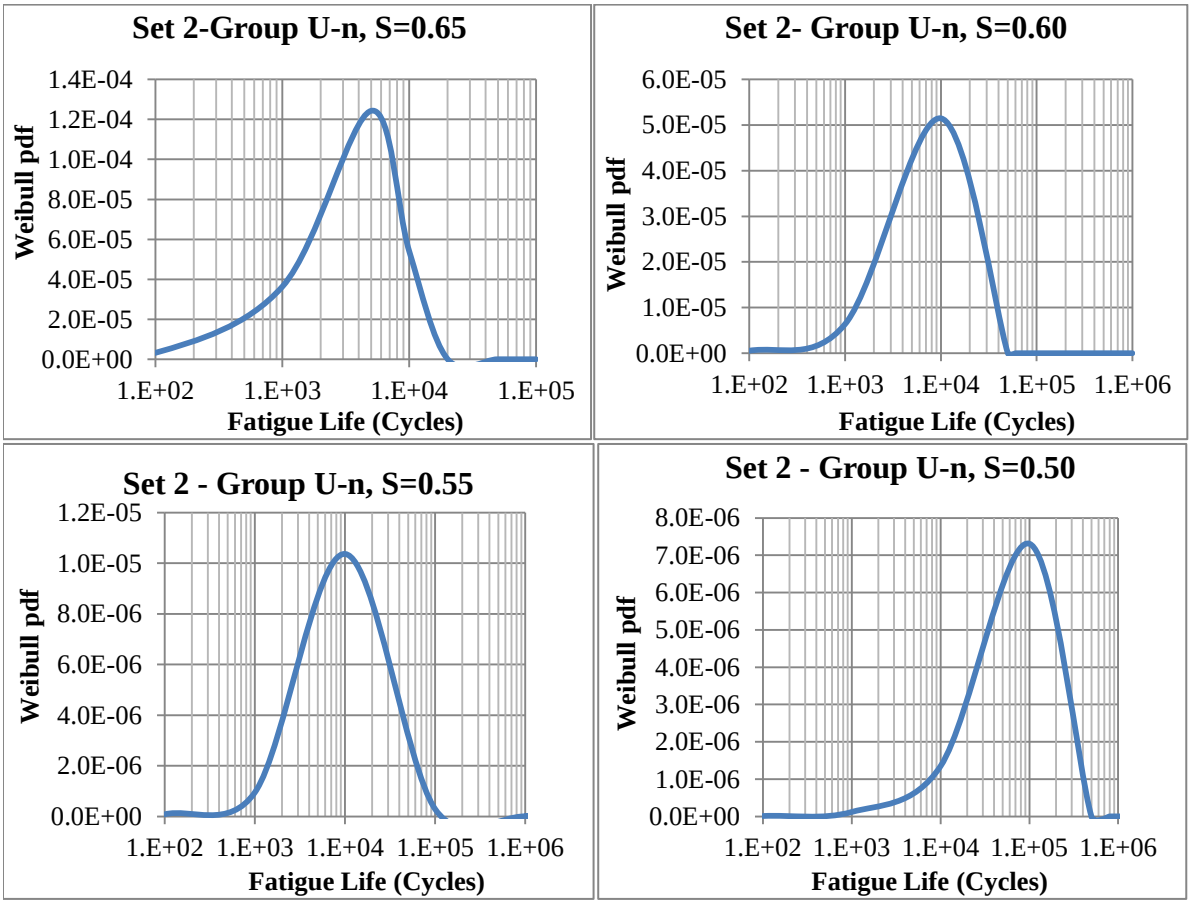


**Figure 6.4 The Weibull pdf for Set 2 - Group U-n for the different stress ratios.**

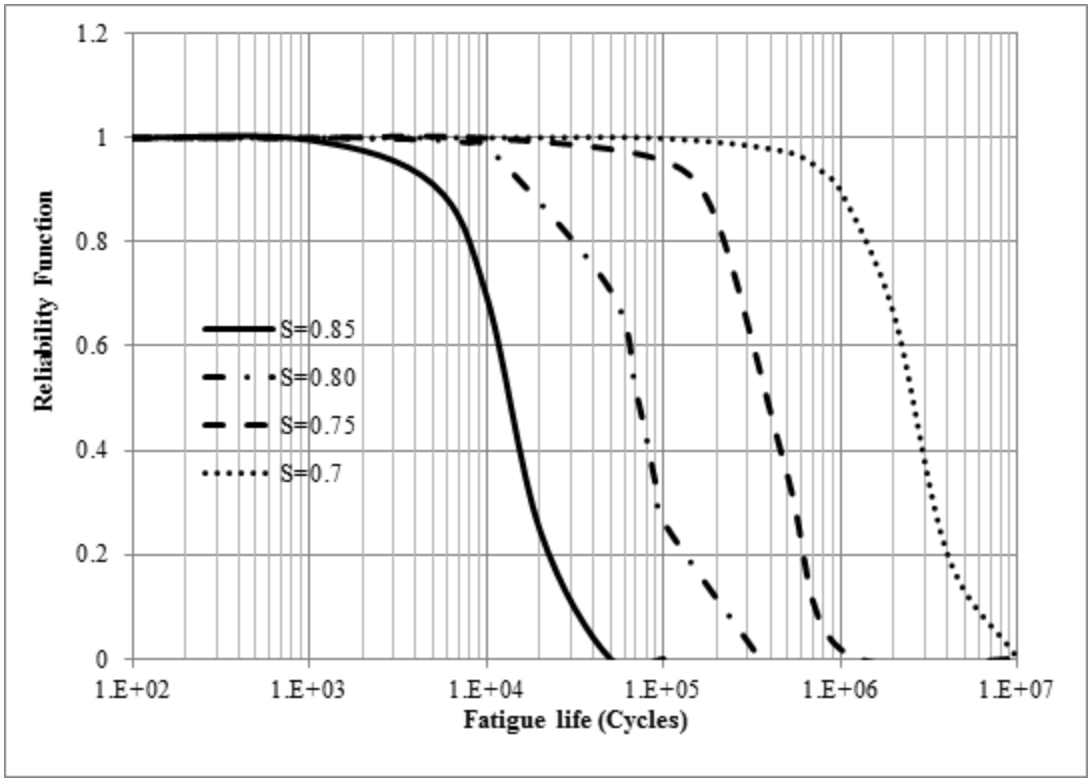


**Figure 6.5 Reliability function for Set 1 - Group U-n for the different stress ratios.**

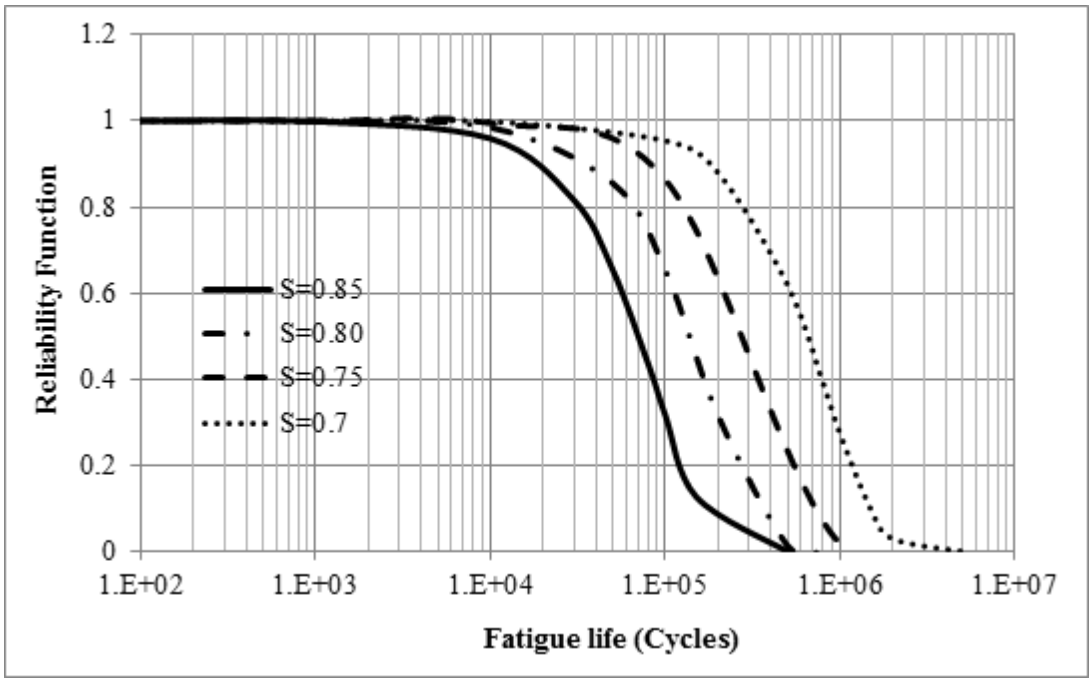


**Figure 6.6 Reliability function for Set 1- Group U-m for the different stress ratios.**

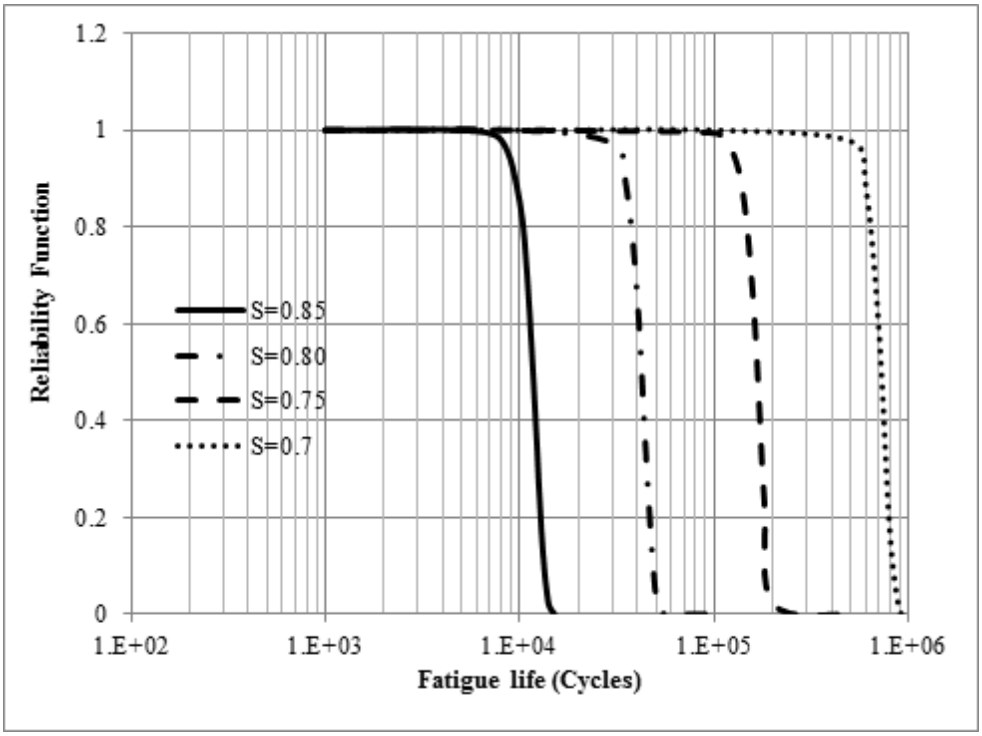


**Figure 6.7 Reliability function for Set 1 - Group R-h for the different stress ratios.**

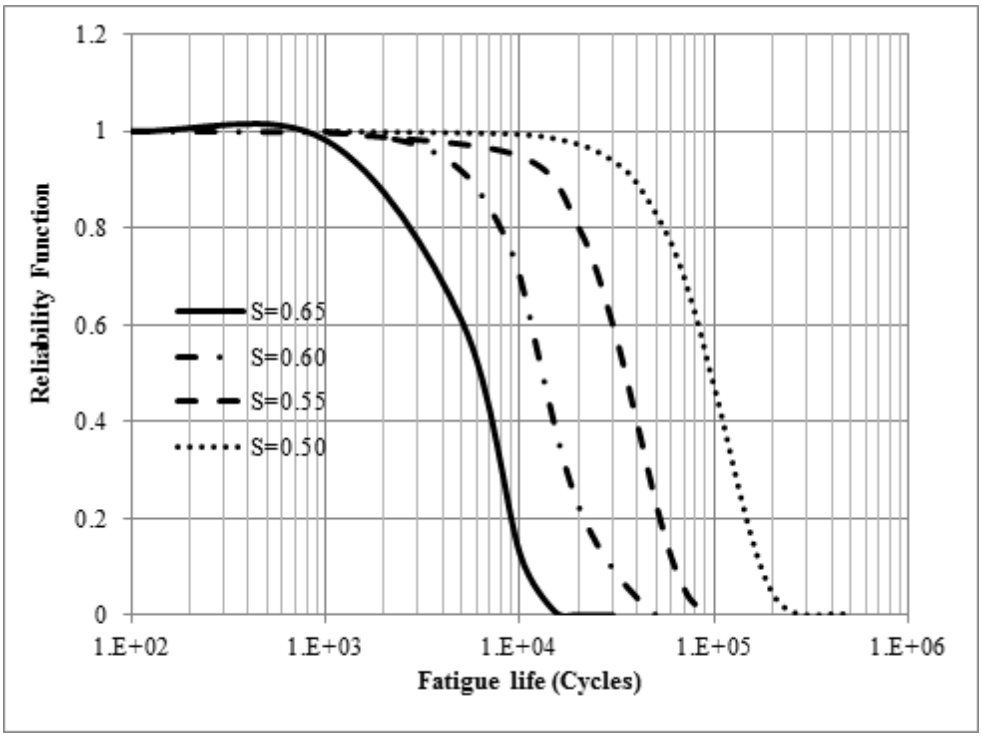


**Figure 6.8 Reliability function for Set 2 - Group U-n for the different stress ratios.**

## 6.2 Estimation of the Mean and Design Fatigue Lives

As discussed by (Oh B. , 1986; Singh, Mohammadi, Goel, & Kaushik, 2007), the mean fatigue life for a given stress ratio could be calculated as follows:

$$E[N] = C\left(\frac{f_{\max}}{f_{static}}\right)^{-m} \exp\left[\frac{0.5772}{\alpha}\right]\Gamma\left(1+\frac{1}{\alpha}\right) \qquad \textbf{Equation 6-17}$$

Where $\Gamma(\ )$ is the gamma function and $E[N]$ is the mean fatigue life. The design fatigue life $N_d$ is then determined depending on the acceptable probability of failure, $p_f$. Several probabilities of failure were considered and the results for the corresponding design fatigue lives are shown in Table 6.3 for Set 1- Group U-n , Table 6.4 for Set 1- Group U-m, Table 6.5 for Set 1 – Group R-h and Table 6.6 for Set 2 – Group U-n. The design fatigue life was calculated using **Equation 6-18**.

$$N_D = \beta\left[\ln\left(\frac{1}{1-p_f}\right)\right]^{\frac{1}{\alpha}} \qquad \textbf{Equation 6-18}$$

The mean fatigue life for Set 1 - Group U-n varied from 2,784,280 cycles at a stress ratio of 0.70 to 14,944 cycles at a stress ratio of 0.85. As the stress ratio increased, the mean fatigue life decreased, which is expected in the fatigue behaviour of engineering materials. The mean fatigue life for Set 1 - Group U-m varied from 755,724 cycles at a stress ratio of 0.70 to 82,272 cycles at a stress ratio of 0.85. There was not much variation in the fatigue life with the variation of the stress ratio. This was due to the fact that there was a very shallow slope between the load range and the fatigue lives of the beams tested from this group.

From Table 6.3 , it can be stated that with 95% probability, the beams from Set 1- Group U-n would survive a fatigue life of 1,000,000 cycles at a stress ratio of 0.69. The same was not true for Group U-m (Table 6.4). For group U-m, a stress ratio of 0.57 would allow the beams to reach a fatigue life of greater than 1,000,000 cycles with 95% probability.

**Table 6.3 Mean and Design Fatigue Lives for different probabilities of failure for beams from Set 1 - Group U-n.**

| Stress Ratio | | 0.60 | 0.70 | 0.75 | 0.80 | 0.85 |
|---|---|---|---|---|---|---|
| Mean Life E[N] | | 176,680,351 | 2,784,280 | 434,493 | 76,443 | 14,944 |
| Design fatigue lives $N_D$ | | | | | | |
| $P_f$ | 0.01 | 18,834,695 | 296,813 | 46,318 | 8,149 | 1,593 |
| | 0.05 | 43,448,420 | 684,697 | 106,849 | 18,799 | 3,675 |
| | 0.10 | 62,847,868 | 990,410 | 154,556 | 27,192 | 5,316 |
| | 0.15 | 78,490,435 | 1,236,919 | 193,024 | 33,960 | 6,639 |

**Table 6.4 Mean and Design Fatigue Lives for different probabilities of failure for beams from Set 1 - Group U-m.**

| Stress Ratio | | 0.60 | 0.70 | 0.75 | 0.80 | 0.85 |
|---|---|---|---|---|---|---|
| Mean Life E[N] | | 4,395,715 | 755,724 | 343,656 | 164,429 | 82,272 |
| Design fatigue lives $N_D$ | | | | | | |
| $P_f$ | 0.01 | 198,719 | 34,164 | 15,536 | 7,433 | 3,719 |
| | 0.05 | 616,344 | 105,964 | 48,186 | 23,055 | 11,536 |
| | 0.10 | 1,016,058 | 174,684 | 79,435 | 38,007 | 19,017 |
| | 0.15 | 1,372,875 | 236,029 | 107,331 | 51,355 | 25,695 |

**Table 6.5 Mean and Design Fatigue Lives for different probabilities of failure for beams from Set 1- Group R-h.**

| **Stress Ratio** | | **0.65** | **0.70** | **0.75** | **0.80** | **0.85** |
|---|---|---|---|---|---|---|
| **Mean Life E[N]** | | **3,429,132** | **710,845** | **164,261** | **41,723** | **11,516** |
| | | **Design fatigue lives $N_D$** | | | | |
| **$P_f$** | **0.01** | **2,210,183** | **458,162** | **105,872** | **26,891** | **7,422** |
| | **0.05** | **2,631,099** | **545,416** | **126,034** | **32,013** | **8,836** |
| | **0.10** | **2,841,661** | **589,064** | **136,121** | **34,575** | **9,543** |
| | **0.15** | **2,976,483** | **617,012** | **142,579** | **36,215** | **9,996** |

**Table 6.6 Mean and Design Fatigue Lives for different probabilities of failure for beams from Set 2 - Group U-n.**

| **Stress Ratio** | | **0.50** | **0.55** | **0.60** | **0.65** |
|---|---|---|---|---|---|
| **Mean Life E[N]** | | **27,360** | **11,107** | **4,877** | **2,287** |
| | | **Design fatigue lives $N_D$** | | | |
| **$P_f$** | **0.01** | **12,286** | **4,458** | **1,767** | **754** |
| | **0.05** | **27,105** | **9,835** | **3,898** | **1,664** |
| | **0.10** | **38,441** | **13,949** | **5,529** | **2,360** |
| | **0.15** | **47,443** | **17,216** | **6,823** | **2,913** |

Figure 6.9, Figure 6.10, Figure 6.11and Figure 6.12 show a comparison between the experimental test data and the predicted data with 95% and 99% reliability for the different groups of beams. The reliability lines gave a good prediction of the fatigue lives for the different groups.

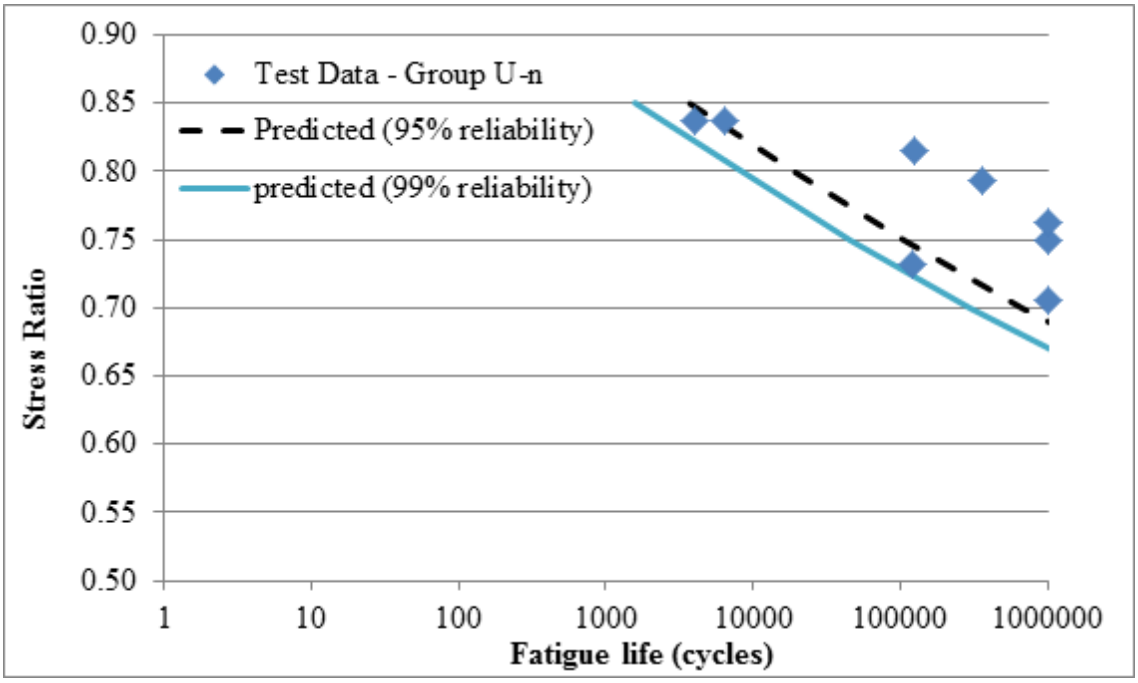


**Figure 6.9 Stress ratio versus fatigue life for the test data and predicted data from Set 1 - Group U-n.**

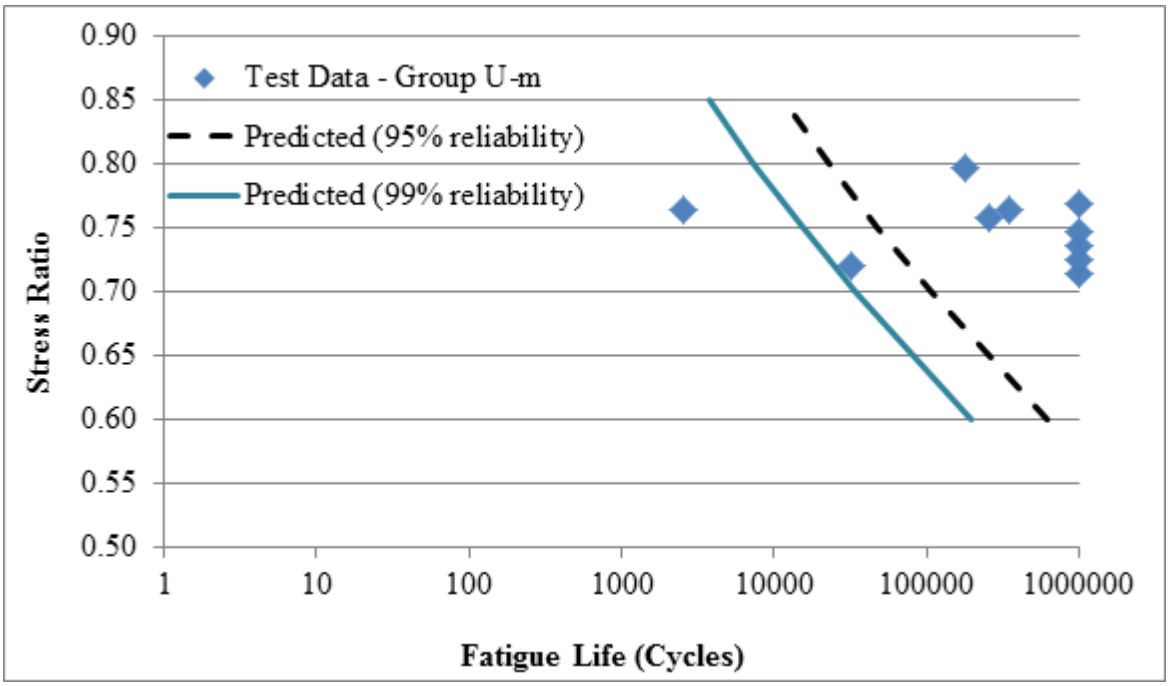


**Figure 6.10 Stress ratio versus fatigue life for the test data and predicted data from Set 1 - Group U-m.**

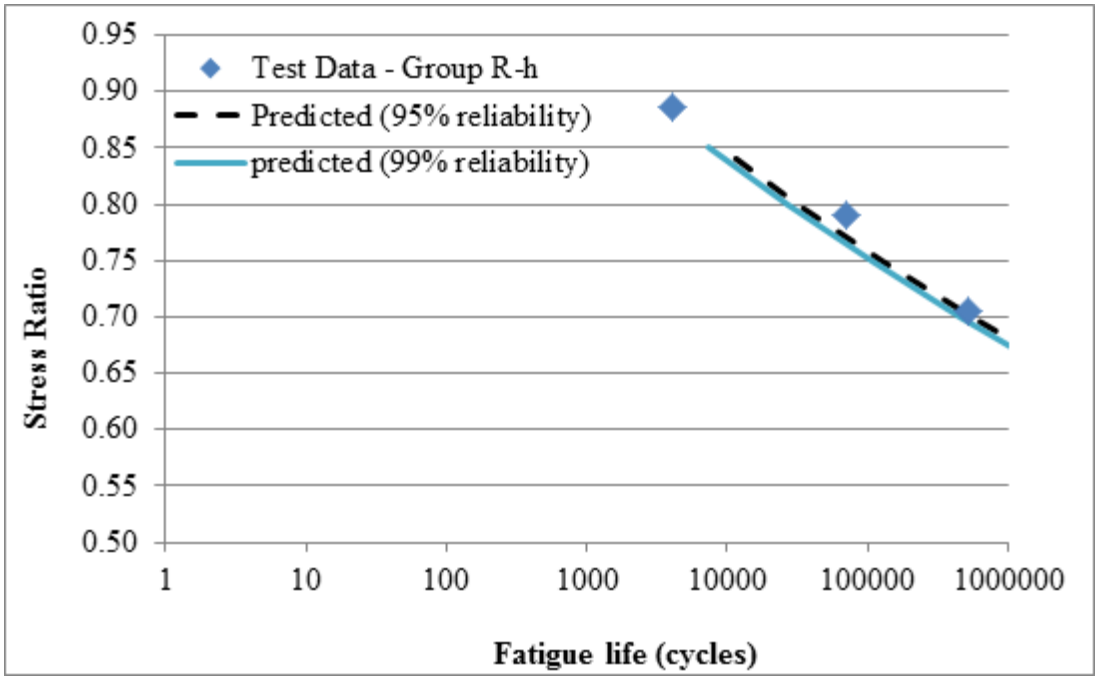


**Figure 6.11 Stress ratio versus fatigue life for the test data and predicted data from Set 1 - Group R-h.**

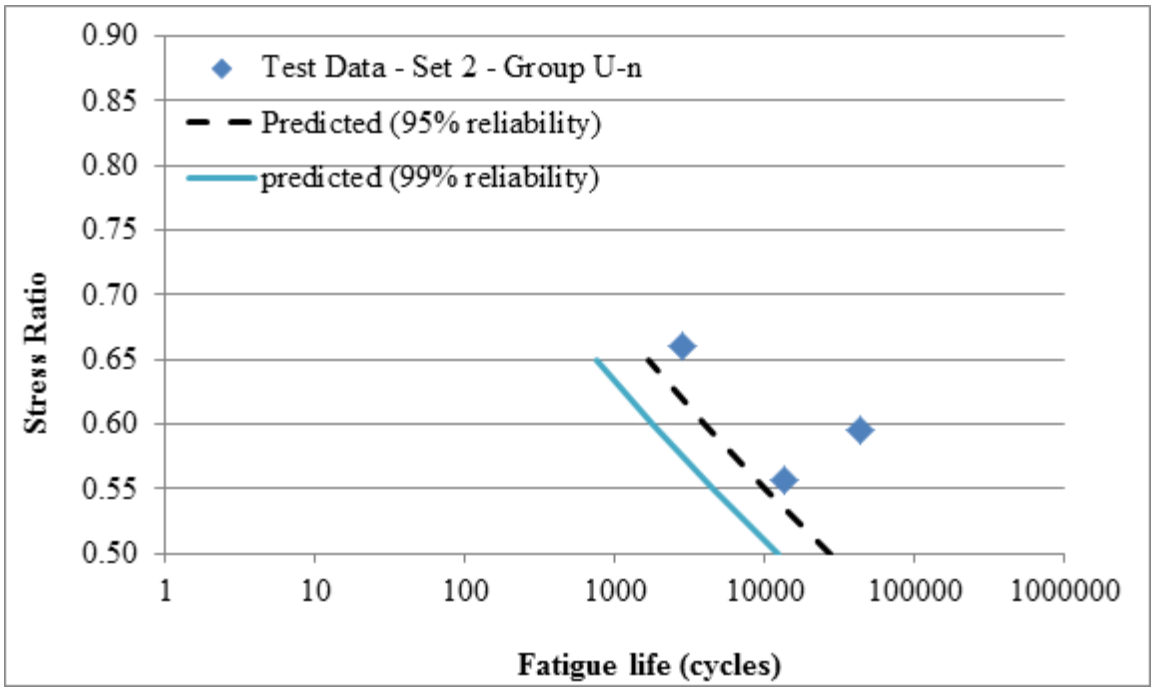


**Figure 6.12 Stress ratio versus fatigue life for the test data and predicted data from Set 2 - Group U-n.**

## 6.3 Conclusion

The Weibull parameters for the fatigue life were obtained from the relationship between the stress ratio and the fatigue life. The stress ratio for each beam was calculated by taking the maximum nominal applied stress divided by the maximum static stress. It was found that the shape parameter for the Weibull function was independent of the stress ratio and was constant for each group of beams. The scale parameter varied with the change in the stress ratio and was increasing with decreasing stress ratio. This complies with what was reported in the literature.

After the Weibull parameters were determined, the mean fatigue life was determined for each group as well as the design fatigue lives corresponding to the different probabilities of failure. It was found that for Group U-n beams (beams with 200 mm anchorage length uncorroded and unrepaired) to reach a fatigue life of greater than one million cycles with 95% probability, the stress ratio should be less than or equal to 0.69. For Group U-m (the beams corroded to a mild corrosion level), the fatigue life would be greater than one million cycles for a stress ratio less than or equal to 0.57 with 95 % probability.

# Chapter 7
# Conclusions and Recommendations for Future Work

Test results of fifty-seven beams were analyzed and discussed in this thesis to evaluate the effect of confinement, corrosion, repair and anchorage length on the bond behaviour of beams under monotonic and repeated loadings. The beams were divided into two groups. Group 1 beams were designed to study the effect of confinement from the supports and the stirrups on the bond behaviour. Group 2 beams were designed to study the effect of anchorage length, corrosion and repair on the bond behaviour. The most important conclusions are summarized in this chapter.

## 7.1 Summary of Conclusions

From this study, it was found that the resistance to bond stresses (forces) between the steel and concrete was mechanical and provided mainly by the concrete keys. The bond stresses increased with the number of the concrete keys engaged. The following factors were found to increase the resistance provide by the concrete keys:

- Confinement by the supports: The support confined the concrete around the bar increasing the stiffness of the bar to concrete interface in the region close to the support thus engaging all the concrete keys in this region.
- Confinement by the stirrups: As the bar slipped, the stirrup prevented the bar from moving away from the top concrete, hence engaging the concrete keys in the location of the stirrup and increasing the bond stress.
    - In beams with a 150 mm stirrup spacing, the bar was held in place at the stirrup location but bent in between the stirrups. This reduced the contact of the concrete keys with the bar in between the stirrups and the amount of force transferred from the concrete to the steel. Reducing the stirrup spacing from 150 mm to 75 mm was enough to prevent the bar from bending in between the stirrups. This caused all the concrete keys to be crushed when the bar slipped leading to an increase in

the force transferred from the concrete to the steel and increased the bond strength and the eventual failure of the beam by bond in a pull-out mode.

- Confinement due to wrapping with CFRP sheets: Wrapping the beams with CFRP sheets caused both bottom and top concrete keys to take part in transferring the force from the concrete to the steel. Initially when there was no slip, the CFRP sheet was not stressed. As the bar slipped, it pushed the top and bottom concrete away from the bar. A tensile force in the CFRP resisted this splitting force and prevented the bottom concrete from spalling by confining the concrete around the bar. This resulted in the concrete keys at both the top and bottom of the bar to be crushed and led to an increase in the bond stress of the wrapped beams. The bond strength of the beams repaired with CFRP sheet was governed by the strength of the CFRP sheets for all anchorage lengths and corrosion levels. In the case of the 350 mm anchorage length beams that were repaired with CFRP sheets, the increase in bond strength was great enough that the beam failed in flexure.
- Change of anchorage length: The change of anchorage length might or might not change the capacity of the beam depending on how the failure was initiated:
    - The change in anchorage length from 350 mm to 650 mm in the group 1 beams did not cause a change in the capacity of the beams. In both cases, failure initiated from the support. The confinement from the support increased the stiffness of the bar to concrete interface in this section which resulted in the concrete keys close to the support being crushed as the bar slipped. Since the failure mode involved only the region near the support, the change in anchorage length had no effect on the bond strength in this case.
    - The change in anchorage length from 200 mm to 350 mm in the group 2 beams increased the static capacity by a factor of 1.6. Since failure in these beams progressed from the pocket towards the support, increasing the anchorage length increased the number of concrete keys resisting slip thus increasing the capacity of the beam.

- Increasing the anchorage length from 200 mm to 350 mm increased the fatigue strength for the control uncorroded beams by a ratio of 1.13. This was not as high as observed in the static beams. This smaller increase was attributed in part to a change in failure mode. In the beams with a 200 mm anchorage length, debonding of the bar started from the loaded end and progressed towards the supports until final failure of the beam. In the beams with a 350 mm anchorage length, a flexural crack initiated at the middle of the anchorage zone and propagated into a diagonal crack. The diagonal crack widened with the cycling of the beam. This caused an increased tensile force in the bar at the location of the crack leading to a failure of the beam by bond that progressed from the location of the crack to the support. Thus the increase in anchorage length did not have much effect in this case.

Other general conclusions from this study included the effect of corrosion, wrapping with CFRP sheets and repeated loading on the bond behaviour of the beams.

- Corrosion produced rust products around the bar that were greater in volume than the steel bar itself. This caused increased stresses in the concrete leading to cracking of the concrete along the anchorage length of the bar. Corrosion was not uniform throughout the length of the bar, corrosion pits were produced. The effect of corrosion on the bond strength can be summarized as follows:
  - In group 1 beams (beams with stirrup spacing A (150 mm) and stirrup spacing B (75 mm)) the failure initiated from the support and no effect of corrosion on the static capacity of the beams was observed.
  - In group 2 beams (beams with 200 mm and 350 mm anchorage lengths) bond failure started from the loaded end and progressed towards the support. Corrosion initiated longitudinal concrete cracks along the anchorage length that reduced the bond static capacity of the beams by about 23% compared to the control (uncorroded and unrepaired) beams.
  - The beams from group 2-set 1 (200 mm anchorage length), that were corroded to a mild corrosion level and not repaired failed in fatigue bond with debonding

starting from the loaded end and progressing towards the support. A 23% reduction in the fatigue bond strength was observed compared to the control beams.

  - In group 2 – set 2 beams (350 mm anchorage length), corrosion had no effect on the fatigue bond strength for the single beam that failed in bond. In this case cycling the beam caused the longitudinal crack starting at the middle of the anchorage zone to widen and progress to the support.

- Repairing the beams with CFRP sheets increased the bond strength of both corroded and uncorroded beams. Wrapping the beams with FRP sheets increased their fatigue strengths to a level above the fatigue flexural strength at long fatigue lives so that bond failures were observed only at short fatigue lives and higher loads.

- The fatigue life for the beams varied linearly on a logarithmic scale with the applied load range with a shallow slope. The beams with stirrup spacing B (75 mm) had a steeper slope than the other beams. Decreasing the spacing of the stirrups from 150 mm to 75 mm in the anchorage zone increased the fatigue capacity of the beams at short fatigue lives. This increase diminished with increasing fatigue life.

A probabilistic approach was used to determine the probability density function for the fatigue life of the beams with a 200 mm anchorage length, Group U-n (uncorroded and unrepaired) and Group U-m (corroded to a mild corrosion level and unrepaired). The aim was to allow the design engineers to estimate the design fatigue life for a similar beam with 95% probability for a given nominal stress ratio. The nominal stress ratio was calculated by dividing the maximum nominal stress applied under repeated loading by the failure stress of the respective static beam test. The nominal stresses were calculated from a cracked section analysis based on the maximum load applied and taking into account the cross-sectional mass loss due to corrosion if any for each beam. It was found that:

- The Weibull probability density function (pdf) best fits the data for Groups U-n and U-m beams. The shape parameter for the Weibull pdf was independent of the stress ratio

and was constant for each group of beams. The scale parameter varied with the change in stress ratio increasing with a decreasing stress ratio.

- The beams from Group U-n have a design fatigue life greater than one million cycles at a stress ratio less than or equal to 0.69 with a 95% probability.
- The beams from Group U-m have a design fatigue life greater than one million cycles at a stress ratio less than or equal to 0.57 with a 95% probability.

## 7.2 Recommendations for Future Studies

The current study has contributed to the understanding of several factors that influence the bond behaviour of steel to concrete in concrete beams. These factors included the effect of active and passive confinement, corrosion, anchorage length and the type of loading. However, additional topics require further examination in future studies:

- Tests on longer beams similar to the ones used in practice are required to determine whether the results from the current study can be extrapolated to the sizes of the beams used in the field.
- An increase in the number of beams tested under repeated loading to at least three beams at each fatigue load level will improve the accuracy of the values of the parameters for the reliability analysis of the fatigue life.
- Testing beams with several different anchorage lengths will allow a determination of whether the bond strength varies linearly with the change in anchorage length.
- Experiments with different bar diameters and different concrete covers under static and repeated loading.
- Experiments with different beam configurations and support conditions that would eliminate the effect of confinement from the support.

# Appendix A

# Beam Design

## Beam Design M20

### Material Properties

| | | | |
|---|---|---|---|
| **Concrete:** | $f'_c$ = | **40** | MPa |
| | $\phi_c$ = | **1** | |
| | $\alpha_1$ = | 0.79 | |
| | $\beta_1$ = | 0.87 | |
| **Tension Steel:** | $d_b$ = | **19.5** | mm |
| | $A_s$ = | **300** | $mm^2$ |
| | number of bars = | **2** | |
| | $f_y$ = | **400** | MPa |
| | E = | **200,000** | MPa |
| | $\phi_s$ = | **1** | |
| **Shear Steel:** | $d_b$ = | **8** | mm |
| | $A_v$ = | 100.5 | $mm^2$ |
| | $f_y$ = | **340** | MPa |
| | $\phi_s$ = | **1** | |

### Beam Properties

| | | | |
|---|---|---|---|
| **Cross-Section** | h = | **254** | mm |
| | b = | **152** | mm |
| | clear cover = | **35** | mm |
| | d = | 209.25 | mm |
| **Length** | beam span = | **1800** | mm |
| | ct moment length = | **600** | mm |
| | moment arm = | 600 | mm |
| | stirrup spacing = | **125** | mm |
| | $l_d$ = | **350** | mm |
| neutral axis | c = | **187.6262** | mm |

**Bond Capacity**

| | | | |
|---|---|---|---|
| $k_1$ = | **1.0** | | |
| $k_2$ = | **1.0** | | |
| $k_3$ = | **1.0** | | |
| $k_4$ = | **1.0** | | (0.8 in ACI 318-02/CSA A23.3-94, 1.0 in ACI 408-03 document) |
| $c_1$= | 44.8 | mm | |
| $c_2$= | 88.3 | mm | |
| $d_{cs}$ = | 44.8 | mm | |
| $k_{tr}$ = | 13.02 | | |
| $d_{cs}+K_{tr}$ = | 57.77 | | |
| $2.5*d_b$ = | 48.75 | | |
| $l_d$ required= | 377.7 | mm | |
| $l_d$ provided/required = | 92.67 | % | |
| $M_f$ = | **28.4** | kN.m | |
| $P_b$ = | **94.6** | kN | |
| Check Pb<Pf | **OK** | | |

**Check capacity**

**Flexural**

| | | | |
|---|---|---|---|
| Minimum Steel | $A_{smin}$ = | 122.1 | $mm^2$ |
| | $A_s>A_{smin}$? | OK | |
| Factored Moment Capacity | | | |
| | c = | 187.6 | mm |
| | c/d = | 0.90 | |
| | $(c/d)_{bal}$ = | 0.6 | |
| | c/d < $(c/d)_{bal}$? | N.G. | 140.9% |
| | $M_r$ = | 30.63 | kNm |
| | $P_f$ = | **102.11** | kN |

**Shear**

| | | | |
|---|---|---|---|
| Min Spacing | $s_{min}$ = | 593 | mm |
| | a/d = | 2.87 | |
| Factored Shear Capacity | | | |
| | $V_c$ = | 40.23 | kN |
| | $V_s$ = | 57.22 | kN |
| | $V_r$ = | 97.45 | kN |
| | $V_{rmax}$ = | 201.16 | kN |
| | $V_r<V_{rmax}$? | OK | |
| | $P_f$ = | **194.90** | kN |

# Appendix B

## Calculation of the Induced Corrosion Level

The time to achieve the theoretical mass loss was calculated based on Faraday's Law. First we calculate the amount of electric current required to achieve the current density specified, then we calculate the number of days required to reach the desired mass loss.

- The current density required was set at $i = 150$ $\mu A/cm^2$
- The bar diameter is 20 mm.
- Each beam has 2 bars
- Surface area of steel bars to be corroded $A_s = \pi dL \times 2$, where L = 200 mm or 350 mm for beams with 200 mm or 350 mm anchorage length
- The bar surface area, $A_s$, for group 1 (200 mm anchorage length) and group 2 (350 mm anchorage length) is 251 $cm^2$ and 440 $cm^2$, respectively.

Accordingly the required current would be: $I = i*A_s$ = 38 mA for group 2 – set 1 beams and 66 mA for group 2- set 2 beams.

The time to achieve the desired mass loss is calculated using Faraday's Law

$$m = \frac{Ita}{ZF}$$

where,
m is the mass loss (g)
I is the corrosion current (A)
t is the corrosion time (s)
a is the atomic weight (56 g for iron)
Z is the valence of the corroding metal (2 for iron)
F is Faraday's constant (96,500 A.s)

Accordingly, the time (days) required to achieve the following desired mass losses was as follows:

$$t = \frac{mZF}{Ia(3600*24)}$$

| M% | t (days) |
|---|---|
| 5 | 52 |
| 15 | 157 |

# Appendix C

# Experimental Mass Loss Calculation

Experimental mass loss was performed on all specimens after testing in order to validate theoretical values derived by Faraday's Law. The procedure used for conducting the mass loss experiment is based on the ASTM standard G1-03 (2011).

The apparatus used consists of:

- Chemical fume hood
- 1 litre beaker
- Acid resistant basin
- Tongs
- Bristle (nonmetallic) brush
- Stirrer
- Dryer
- Scale
- Proper disposal of acid solution
- Safety eyewear (eye goggles)
- Gloves

**Figure B. 1 Chemical fume hood**

The chemical reagents include:

- Distilled water
- Concentrate hydrochloric acid (HCL)
- Hexamethylenetetramine (chemical buffer)

Procedure:

<u>Corroded Bar:</u>

1. Cut the steel bar to a representative corroded length (length of the bar exposed to corrosion).
2. Clean mechanically the specimen by scrubbing the bar with a bristle brush to remove concrete off the surface.

3. Measure the length and the weight of the steel bar after it is cut.
4. Place the steel specimens in an acid resistant basin.
5. In a 1 litre beaker mix 500ml of distilled water with 500 ml of HCL acid. Distilled water should be placed in the beaker before HCL acid is added.
6. Stir the solution for one minute.
7. Add 3.5 g of hexamethylenetetramine to the solution and stir it until the buffer dissolves.
8. Pour the solution with cautious into the acid resistant basins.
9. Repeat steps from 5 till 8 until all the steel bars are fully submerged into the solution.
10. Allow the steel bars to soak for a minimum of 10 minutes in the solution until no reaction between steel bars and solution is detected .Heavily corroded bars may require longer times of contact.
11. Carefully remove the steel bars from the basin with tongs and clean them with water using the bristle brush.
12. After cleaning the bars allow them to dry, an electrical dryer can be used to assure that all the water is removed.
13. Measure and record the weight of the steel specimens after the cleaning cycle is finished.
14. Properly dispose the hydrochloric waste solution.
15. Clean the apparatus and repeat the whole procedure until the weight of the steel bars become constant.
16. Depending on the amount of corrosion, up to five cleaning cycles may be required to reach a constant weight.

Control Bar:

The control bar should be free from any corrosion. The cleaning procedure followed should be the same as for the corroded bar (refer to the steps mentioned above).Less cleaning cycles can be valid. By weighting the control specimen prior and after cleaning, the extent of metal loss resulting from cleaning can be utilized to correct the corrosion mass loss.

Mass Loss Calculation:

The density of the control bar is calculated after cleaning it by measuring its mass and volume. Then to calculate the mass loss of the corroded bar from each cleaning cycle, the following procedure is used:

Mass Loss (%) = $(m_f - m_i)/m_c$

Where,

$m_f$ = the mass of the corroded bar after each cleaning cycle.

$m_i$ = the mass of the corroded bar before cleaning started.

$m_c$ = the mass of the control bar of an equivalent length. It is calculated by multiplying the density of the control bar by the length of the corroded bar to be measured.

The mass loss is then graphed as a function of the number of cleaning cycles as shown in Figure B. 2. Two lines will be formed AB and BC. Line BC corresponds to corrosion of the metal after removal of the corrosion product. Hence, point B will be the approximate mass loss due to corrosion (ASTM G1-03, 2003).

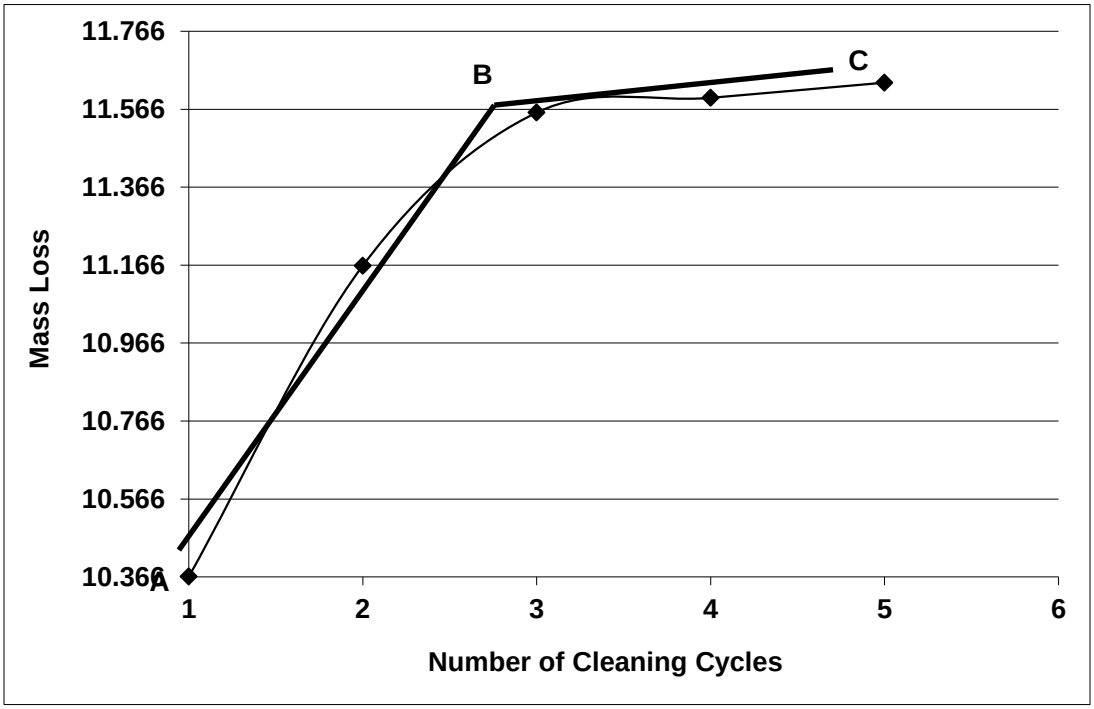


**Figure B. 2 Mass loss of corroded bar resulting from repetitive cleaning cycles.**

# Appendix D

## Strain behaviour for Beams from Group 2- Set 1

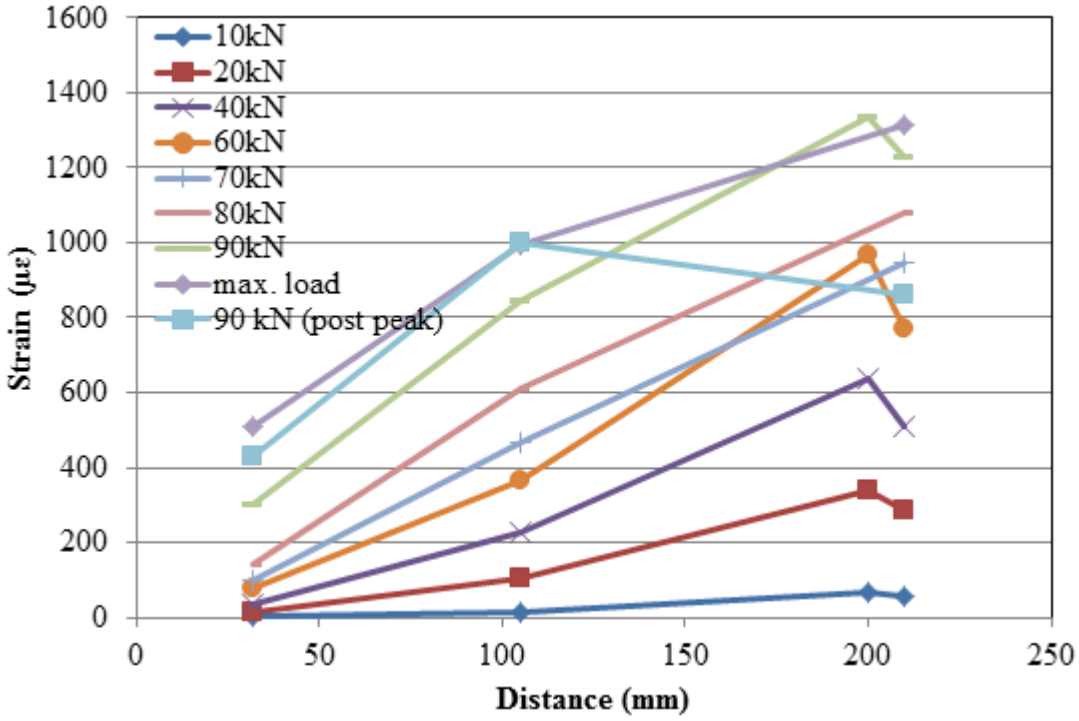


**Figure C. 1 Strain profile of the bar in Beam M-200-U-n-1.**

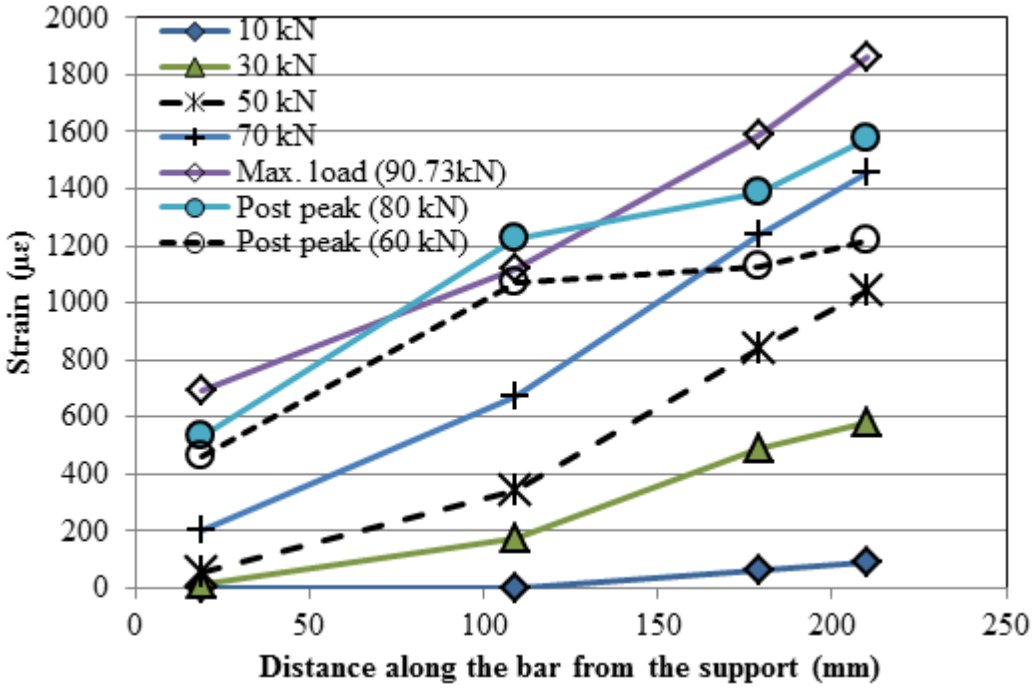


**Figure C. 2 Strain profile for bar 1 in Beam M-200-U-n-2.**

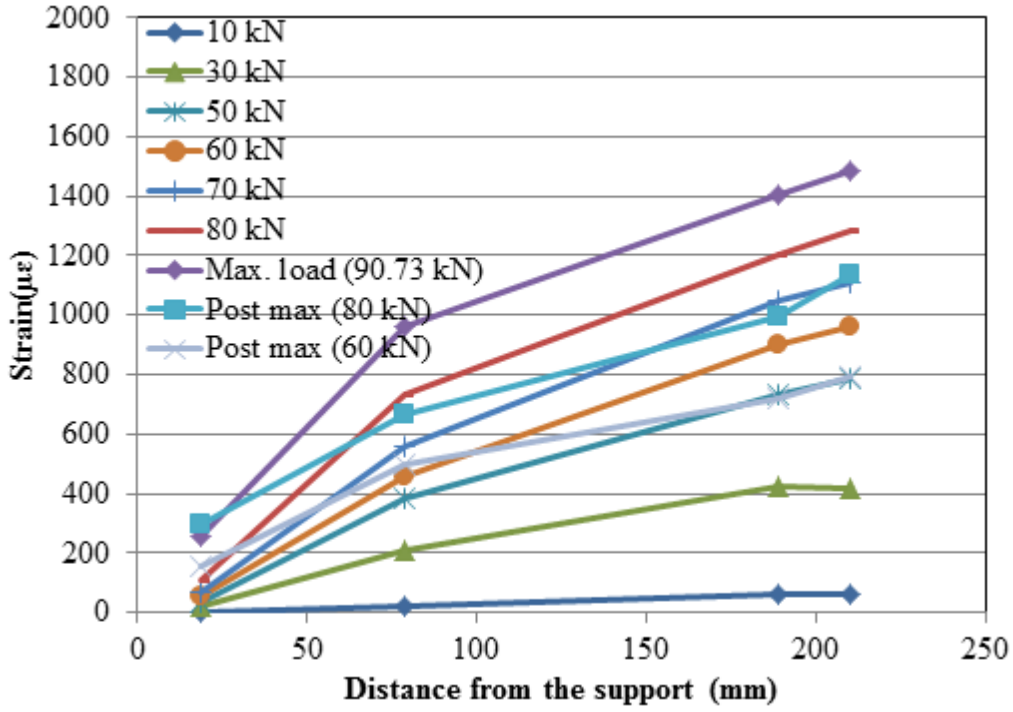


**Figure C. 3 Strain profile for bar 2 in Beam M-200-U-n-2.**

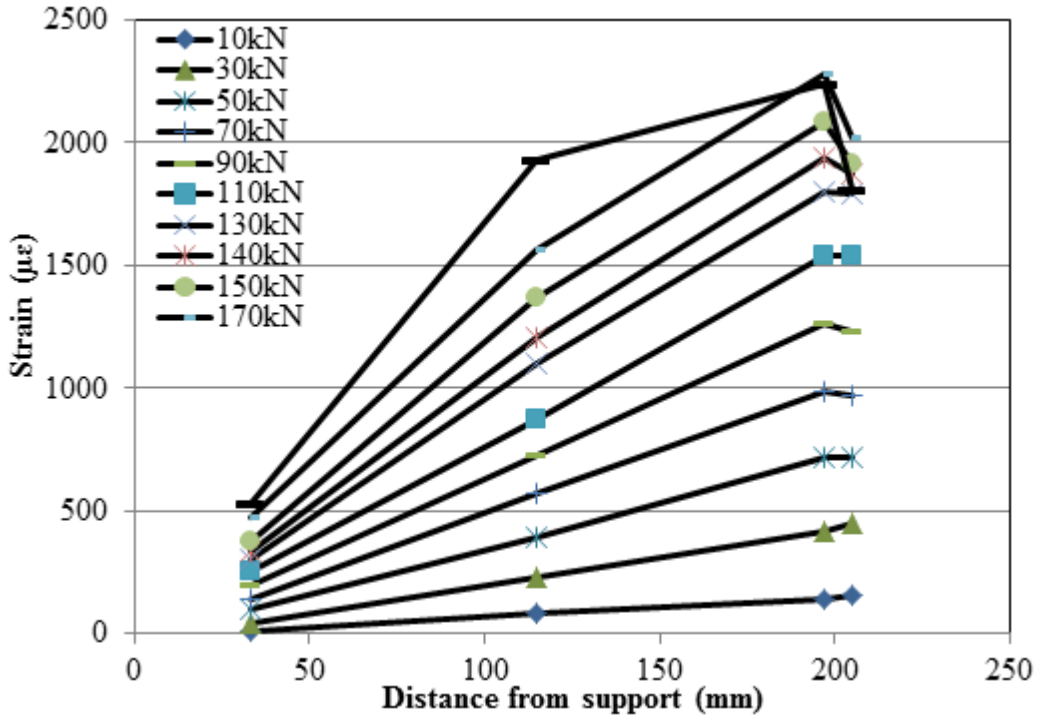


**Figure C. 4 Strain profile for the bar in Beam M-200-R-n.**

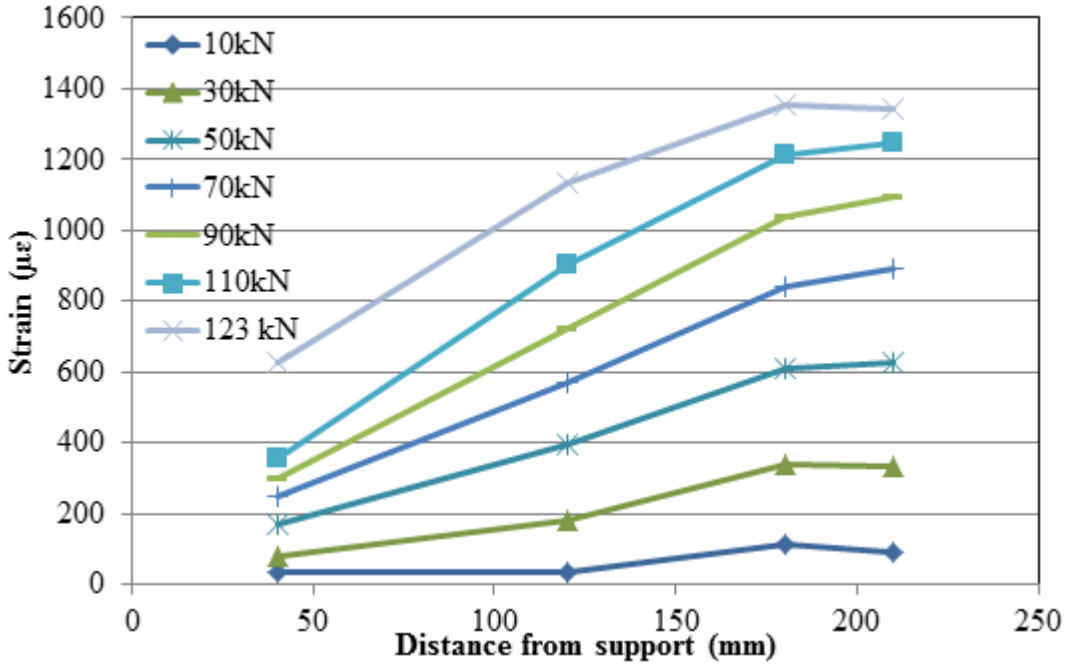


**Figure C. 5 Strain profile for bar in Beam M-200-R-m.**

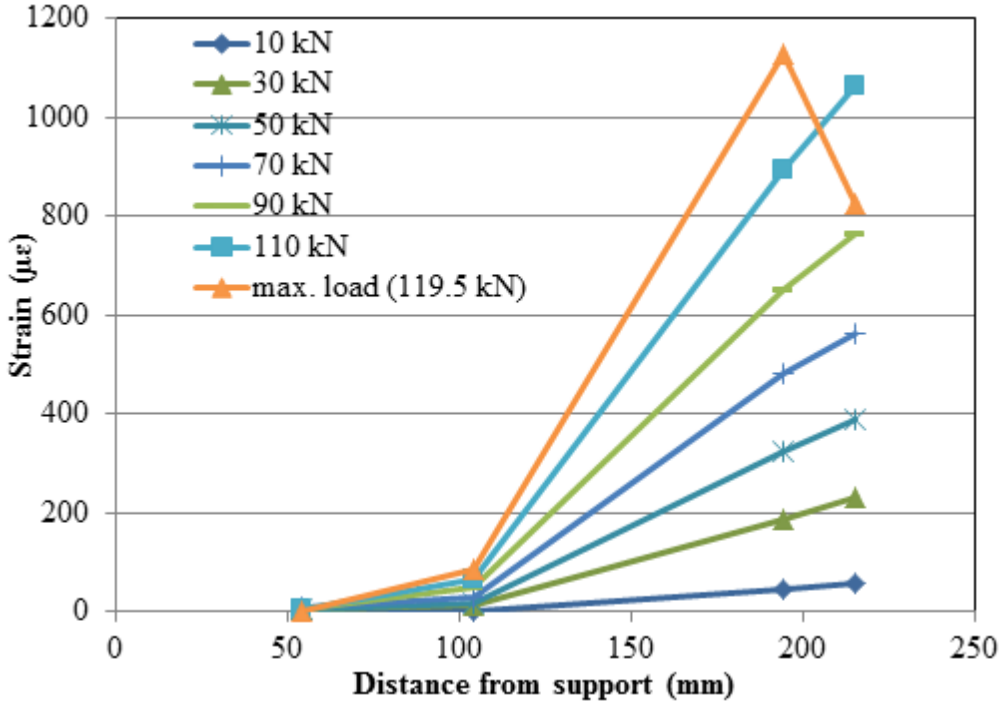


**Figure C. 6 Strain profile for bar in Beam M-200-R-h.**

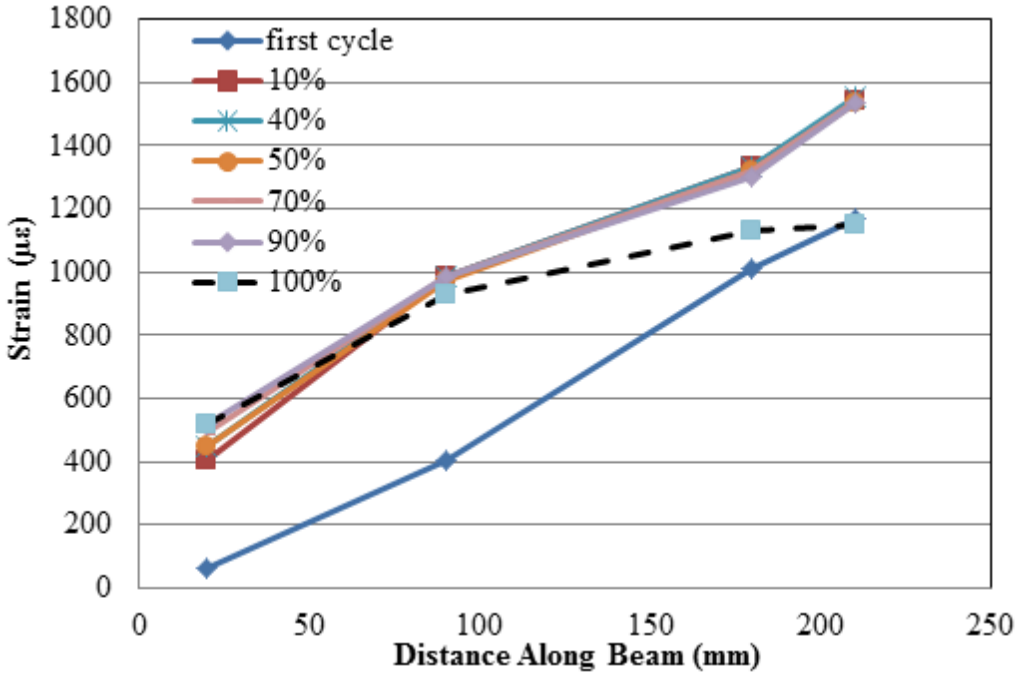


**Figure C. 7 Strain profile for bar in Beam F-200-U-n-60 with respect to percentage of fatigue life.**

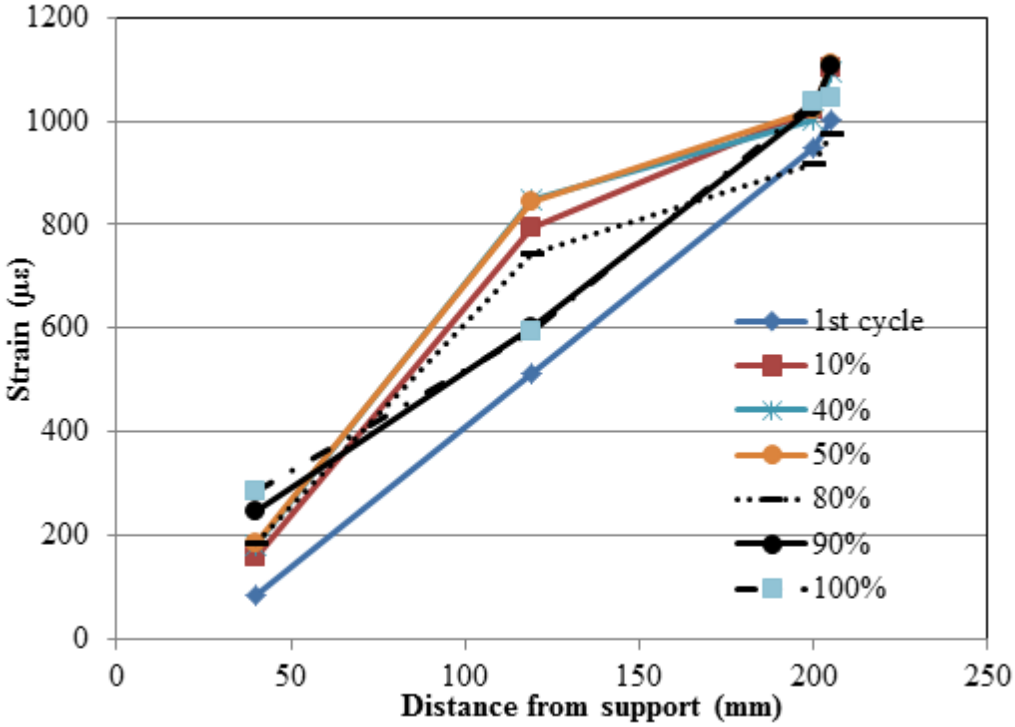


**Figure C. 8 Strain profile for bar in Beam F-200-U-n-66 with respect to % of fatigue life.**

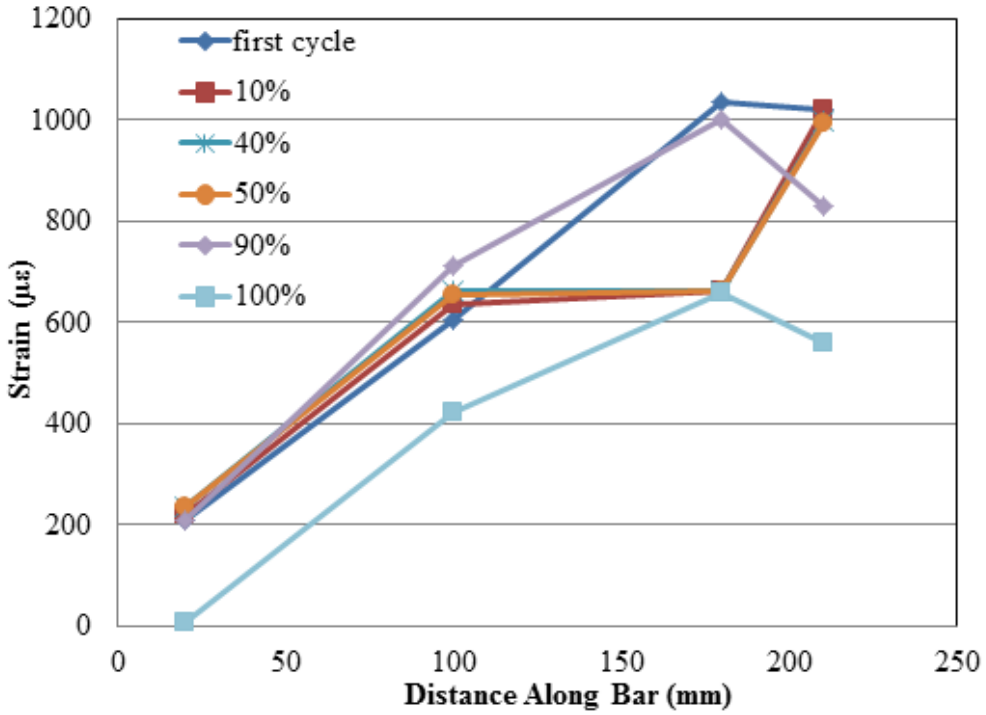


**Figure C. 9 Strain profile for bar in Beam F-200-U-n-68 with respect to % of fatigue life.**

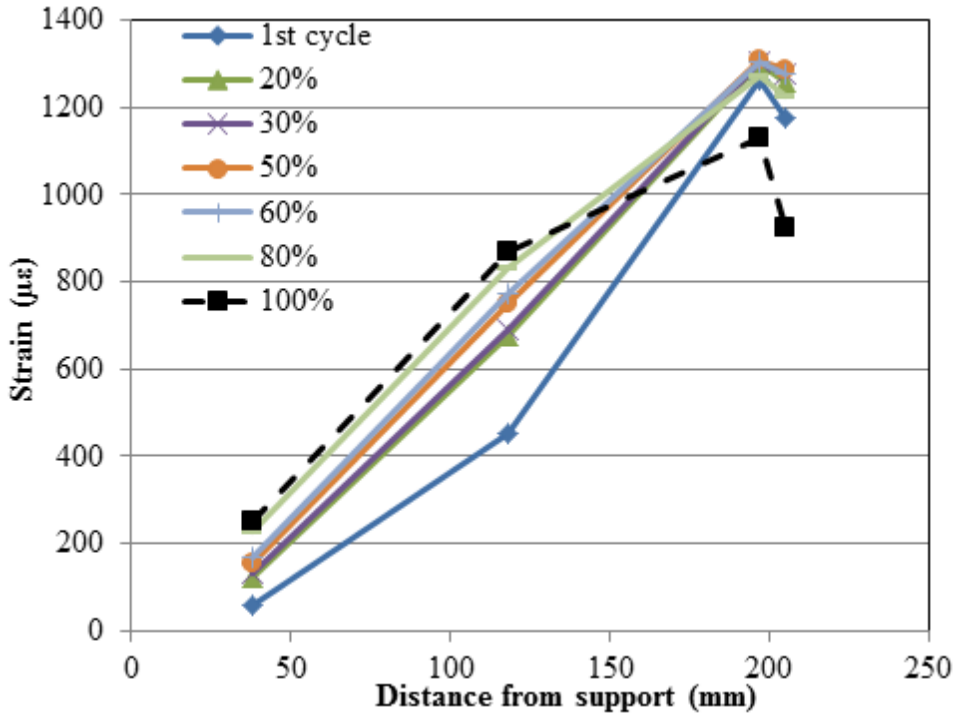


**Figure C. 10 Strain profile for bar in Beam F-200-U-n-70-2 with respect to % of fatigue life.**

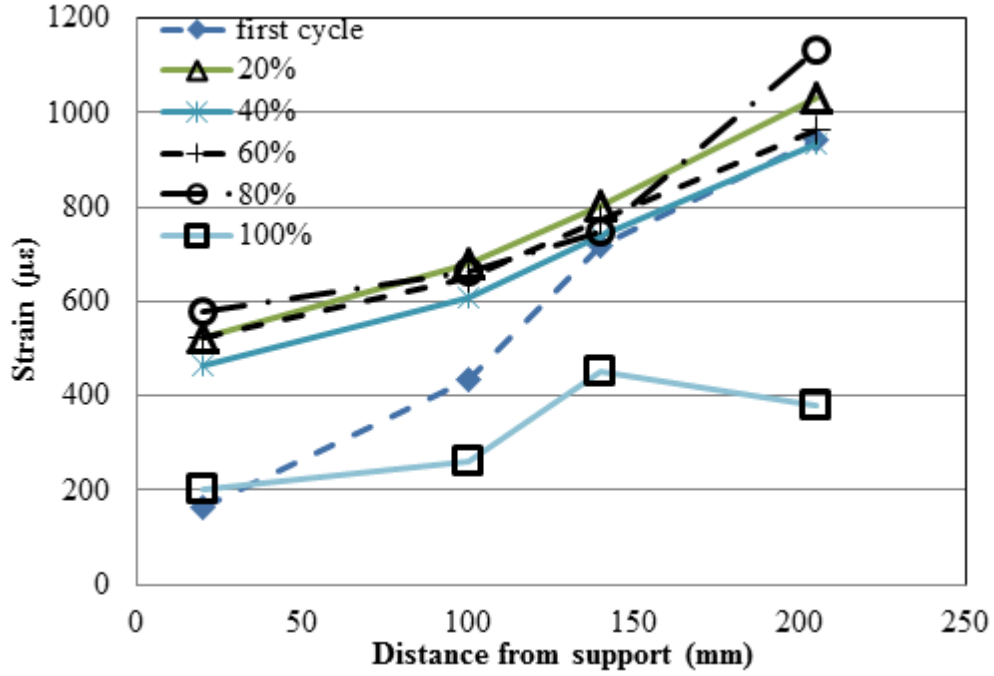


**Figure C. 11 Strain profile for bar 1 with encapsulated strain gauges in Beam F-200-U-m-44.**

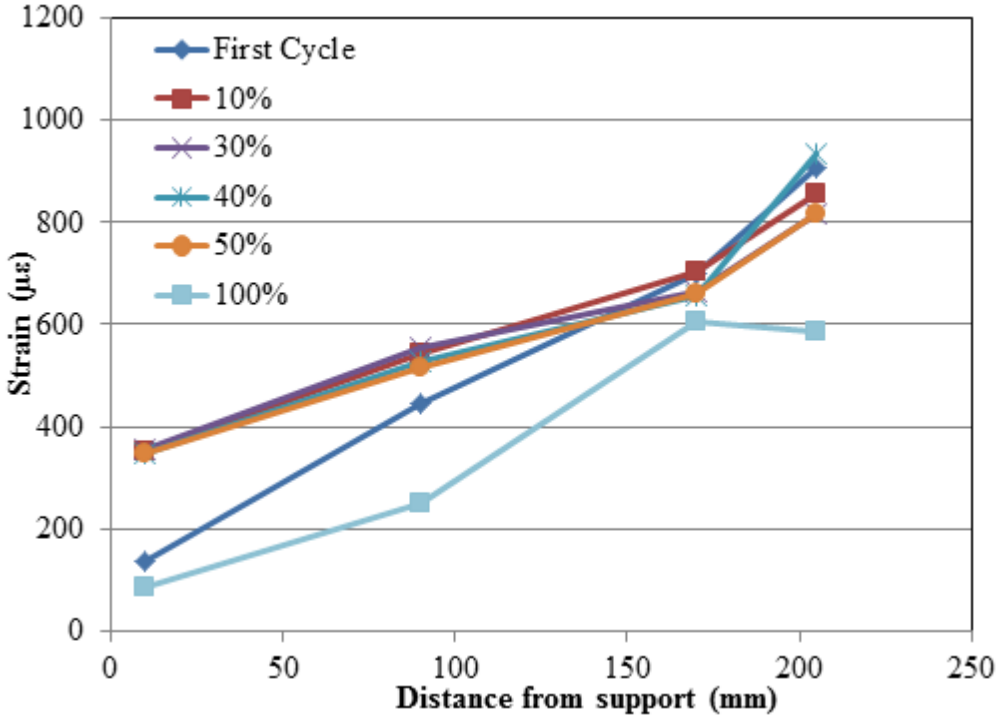


**Figure C. 12 Strain profile for bar with FOS in Beam F-200-U-m-44 with respect to % of fatigue life.**

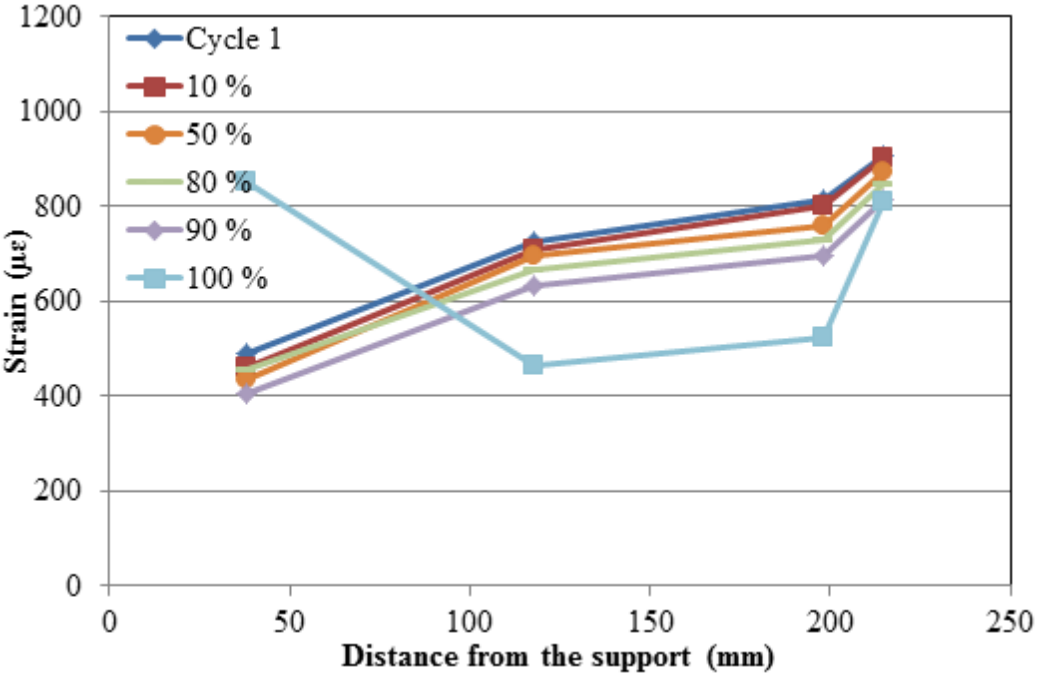


**Figure C. 13 Strain profile for bar in Beam F-200-U-m-48 with respect to % of fatigue life.**

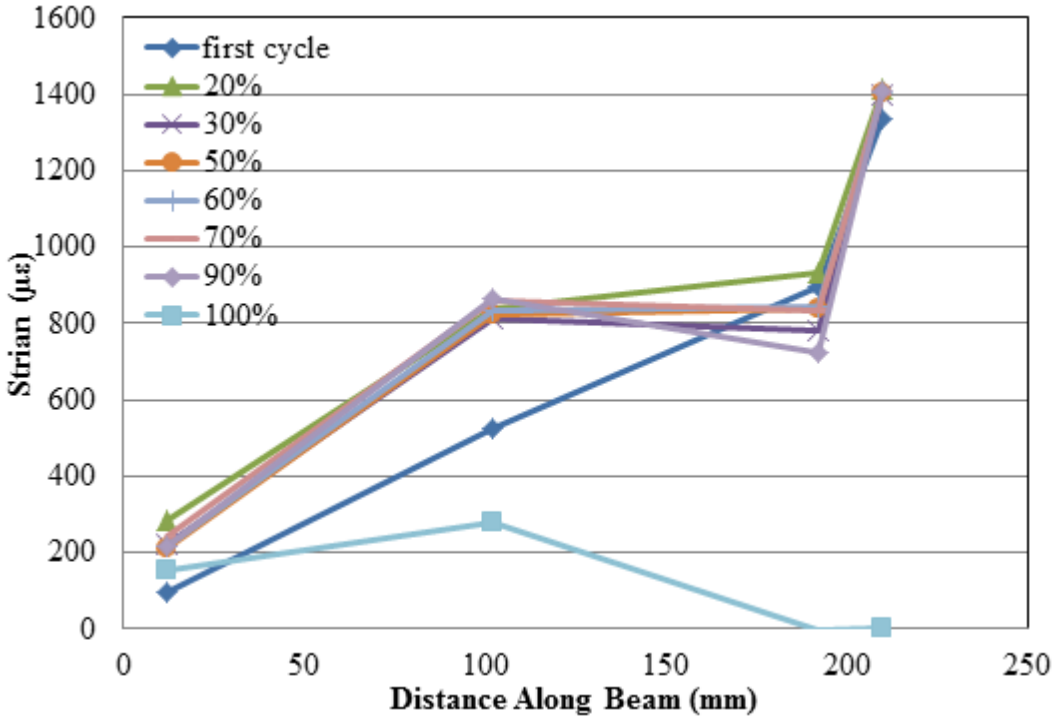


**Figure C. 14 Strain profile for bar in Beam F-200-R-m-72 with respect to % of fatigue life.**

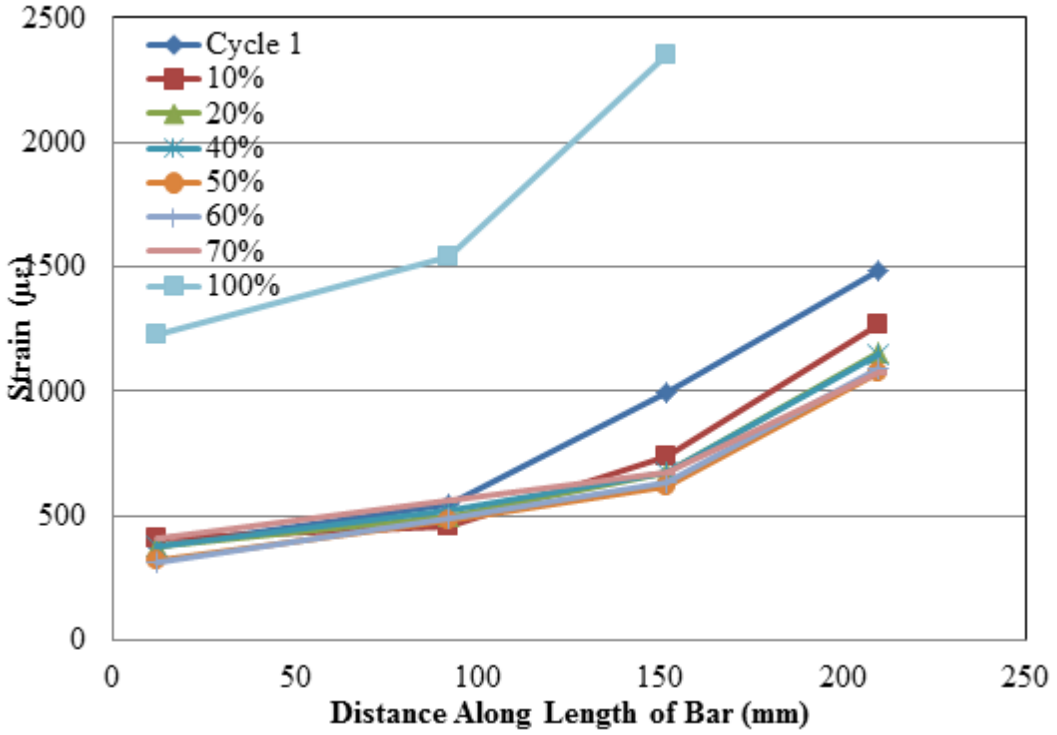


**Figure C. 15 Strain profile for bar in Beam F-200-R-m-80 with respect to % of fatigue life.**

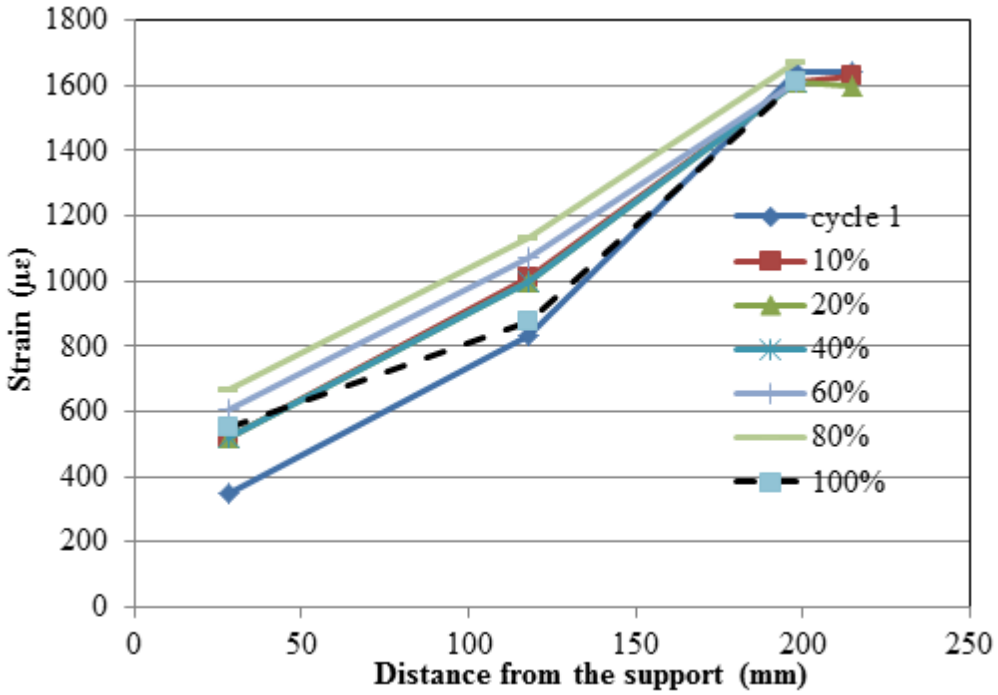


**Figure C. 16 Strain profile for bar in Beam F-200-R-m-90 with respect to % of fatigue life.**

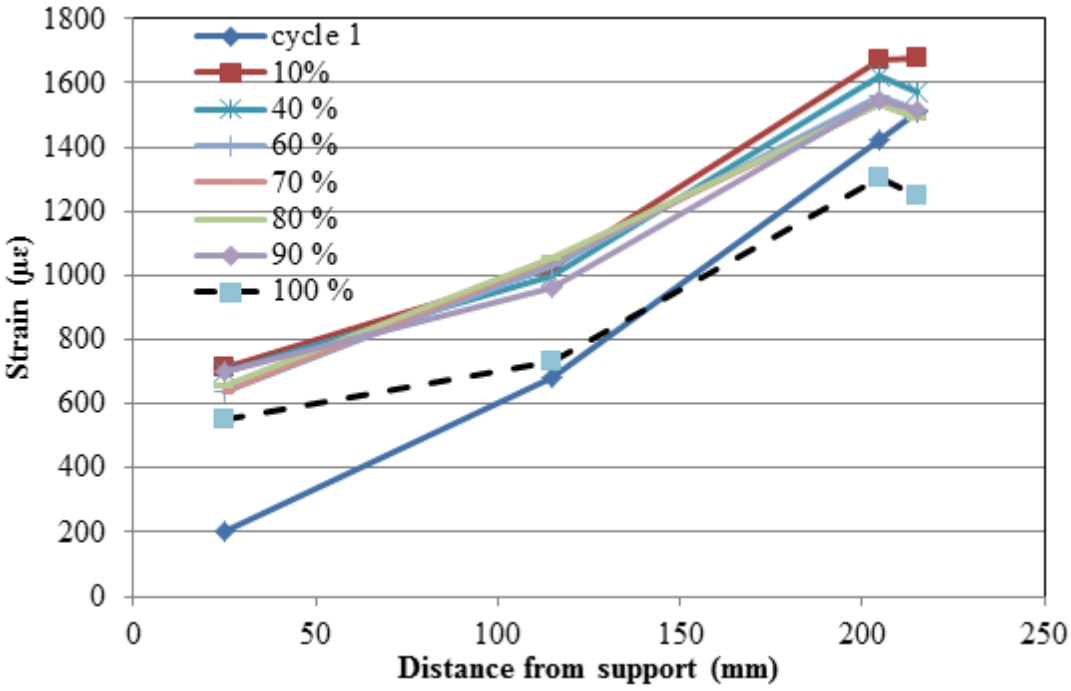


**Figure C. 17 Strain profile for bar in Beam F-200-R-m-96 with respect to % of fatigue life.**

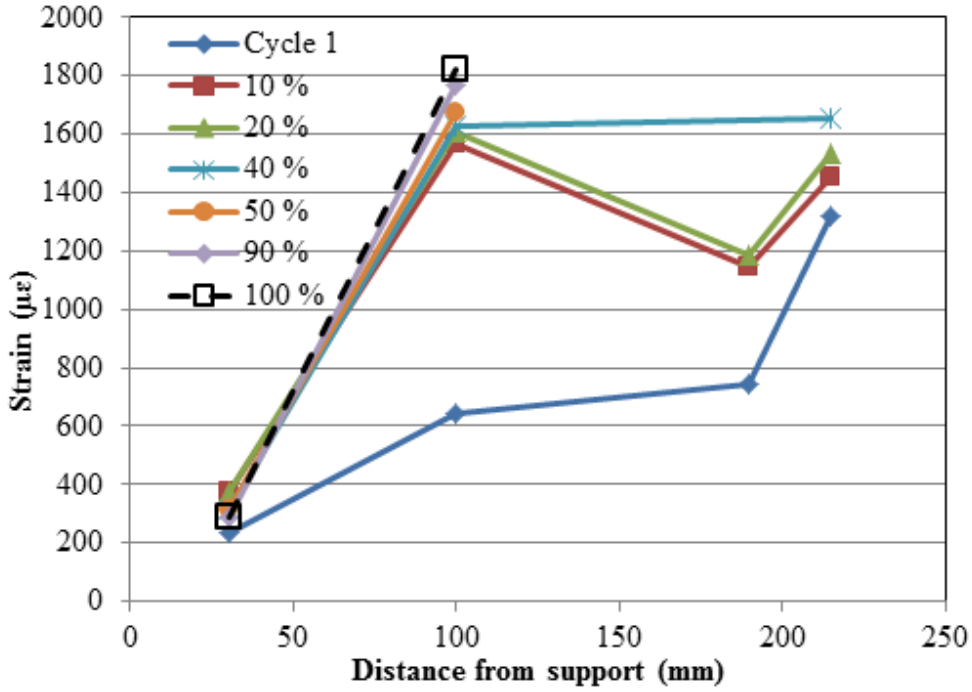


**Figure C. 18 Strain profile for bar in Beam F-200-R-h-75 with respect to % of fatigue life.**

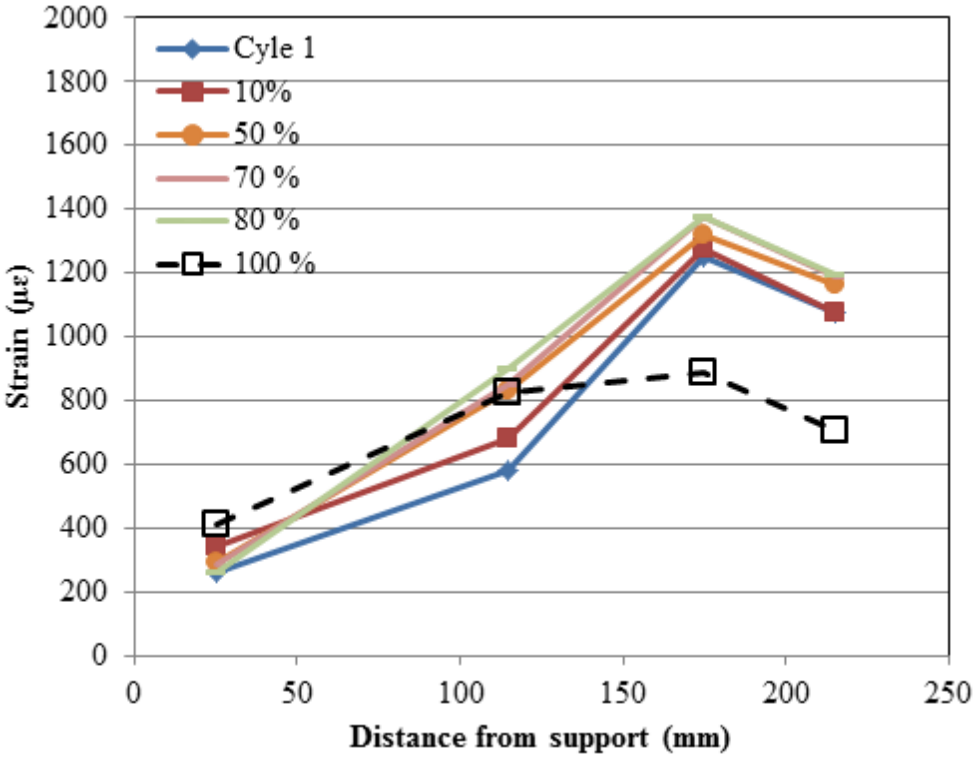


**Figure C. 19 Strain profile for bar in Beam F-200-R-h-80 with respect to % of fatigue life.**

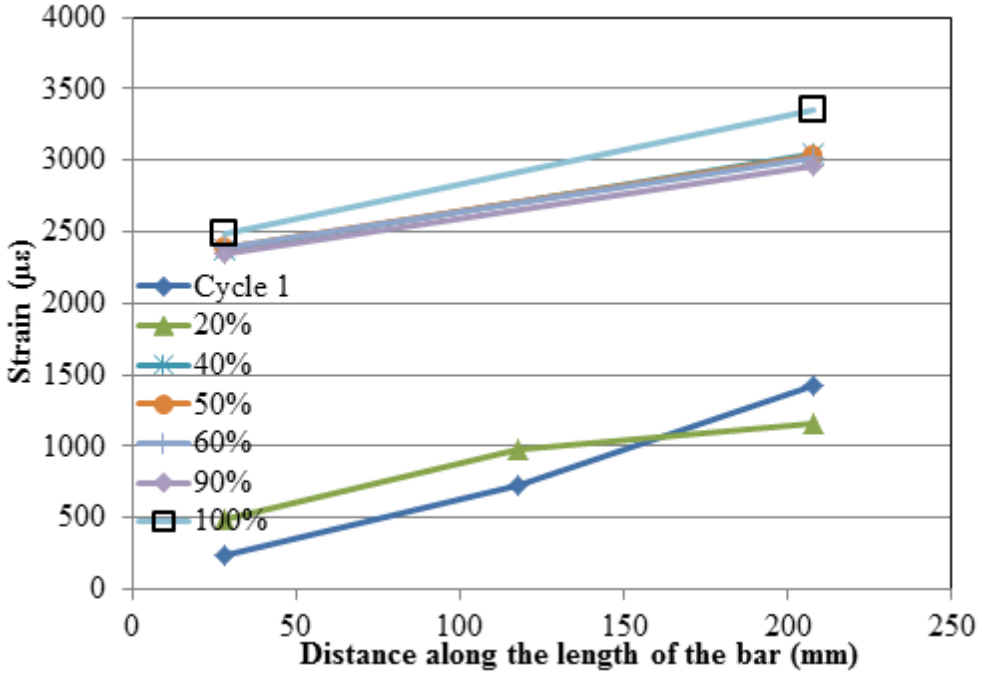


**Figure C. 20 Strain profile for bar in Beam F-200-R-h-88 with respect to % of fatigue life.**

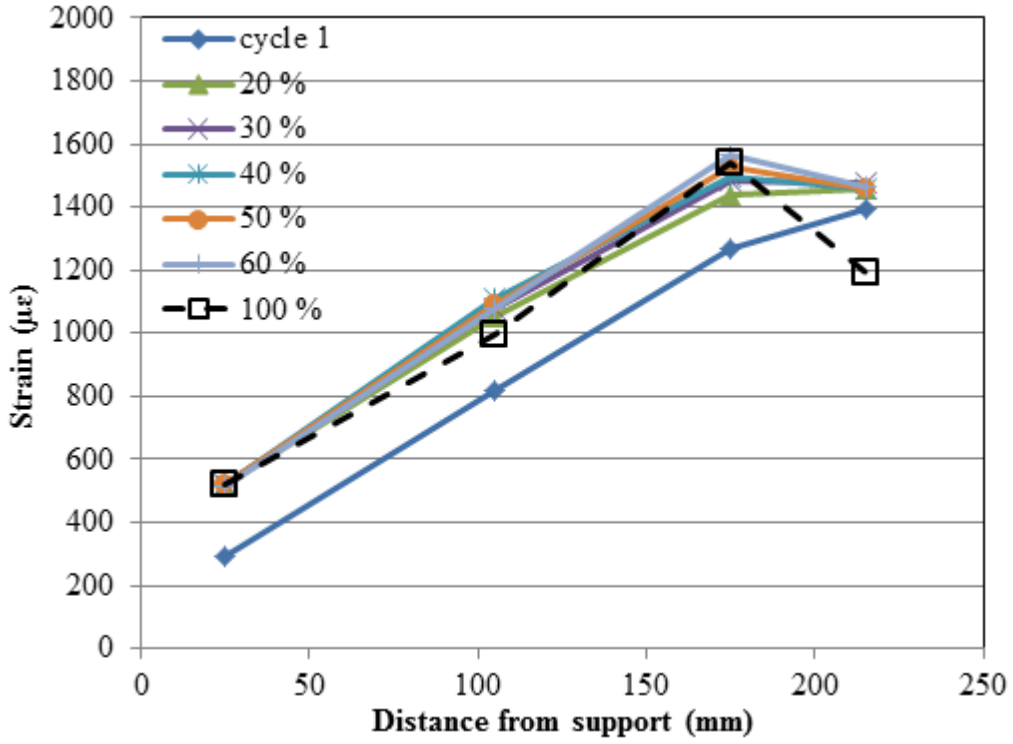


**Figure C. 21 Strain profile for bar in Beam F-200-R-h-96 with respect to % of fatigue life.**

# Appendix E

## Strain Profile for Group 2- Set 2 unrepaired beams that failed in bond

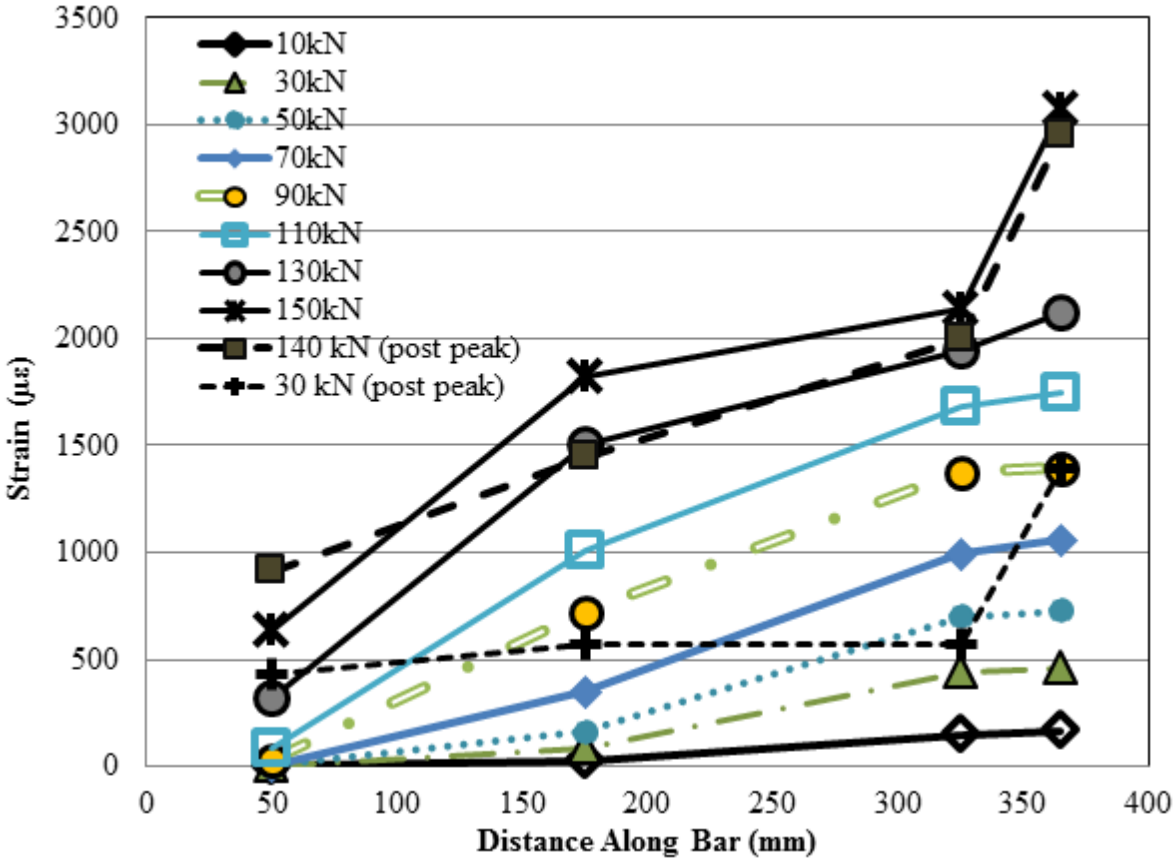


**Figure D. 1 Strain profile for bar in Beam M-350-U-n.**

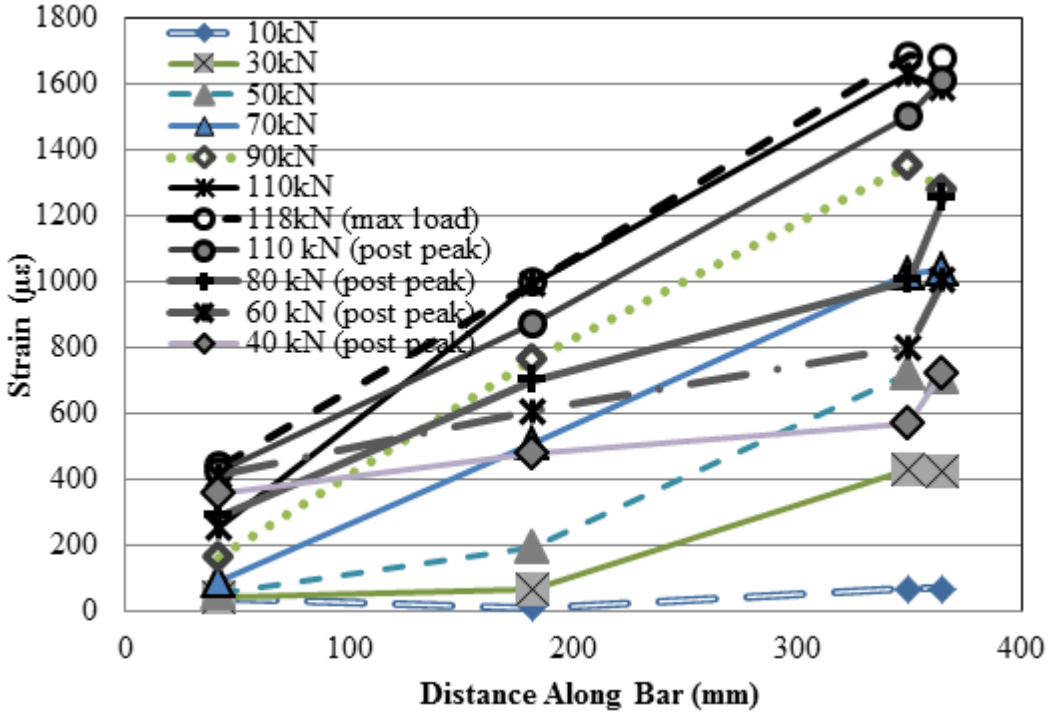


**Figure D. 2 Strain profile for bar in Beam M-350-U-m.**

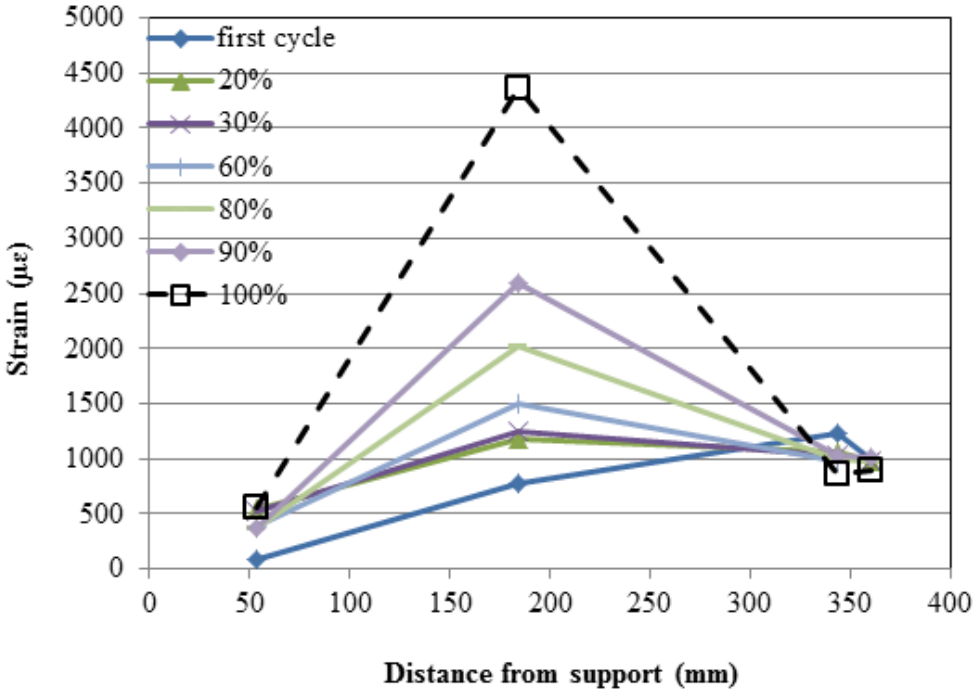


**Figure D. 3 Strain profile for bar in Beam F-350-U-n-74 with respect to % of fatigue life.**

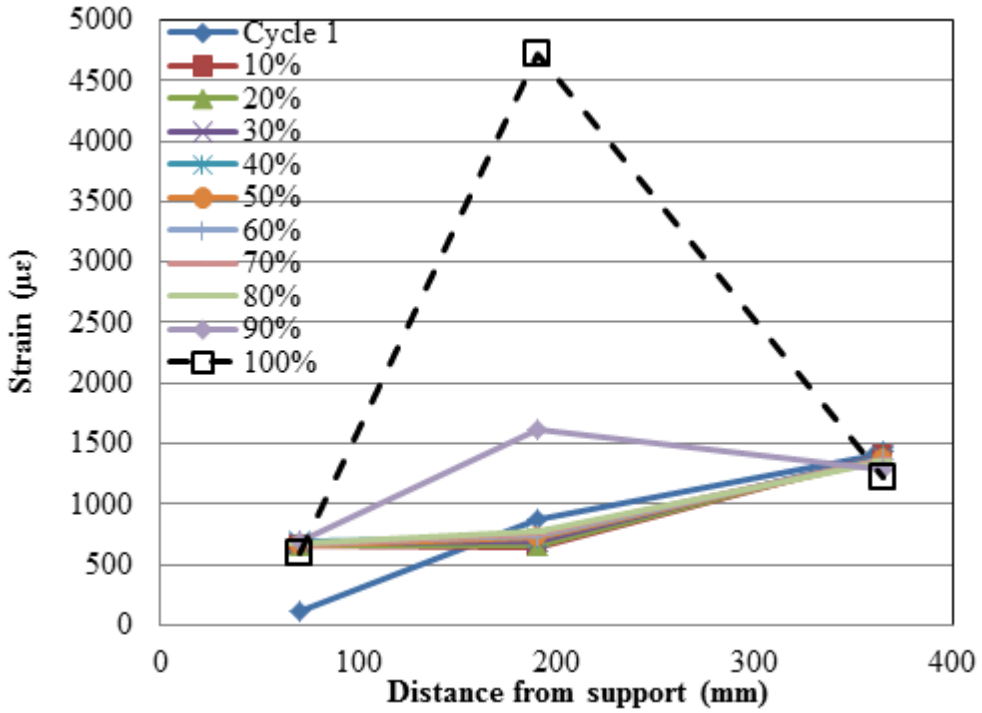


**Figure D. 4 Strain profile for bar in Beam F-350-U-n-80 with respect to % of fatigue life.**

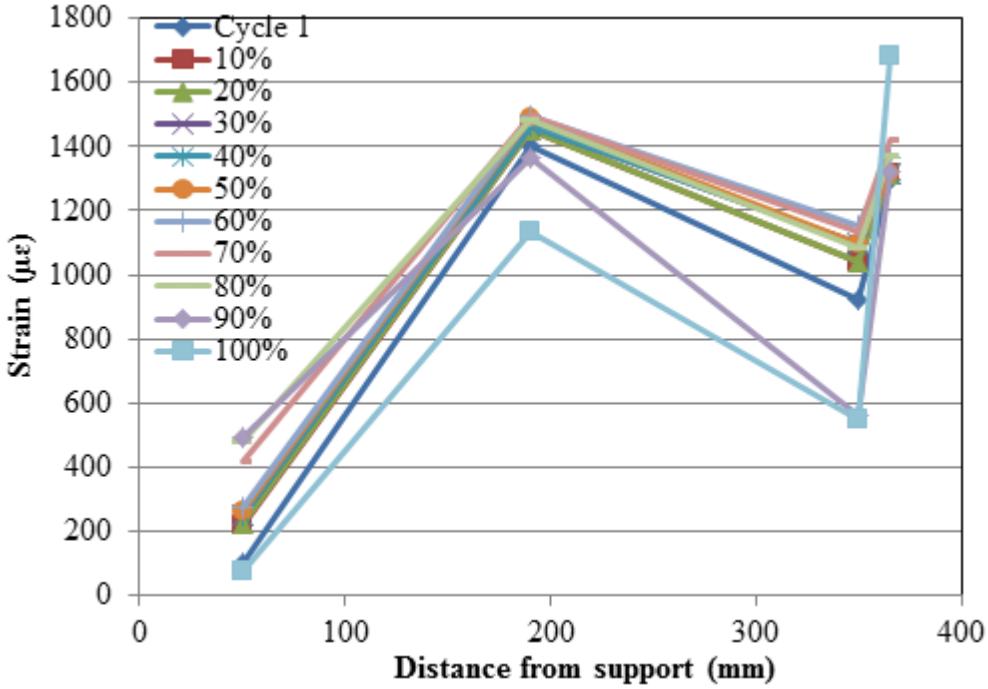


**Figure D. 5 Strain profile for bar in Beam F-350-U-n-90 with respect to % of fatigue life.**

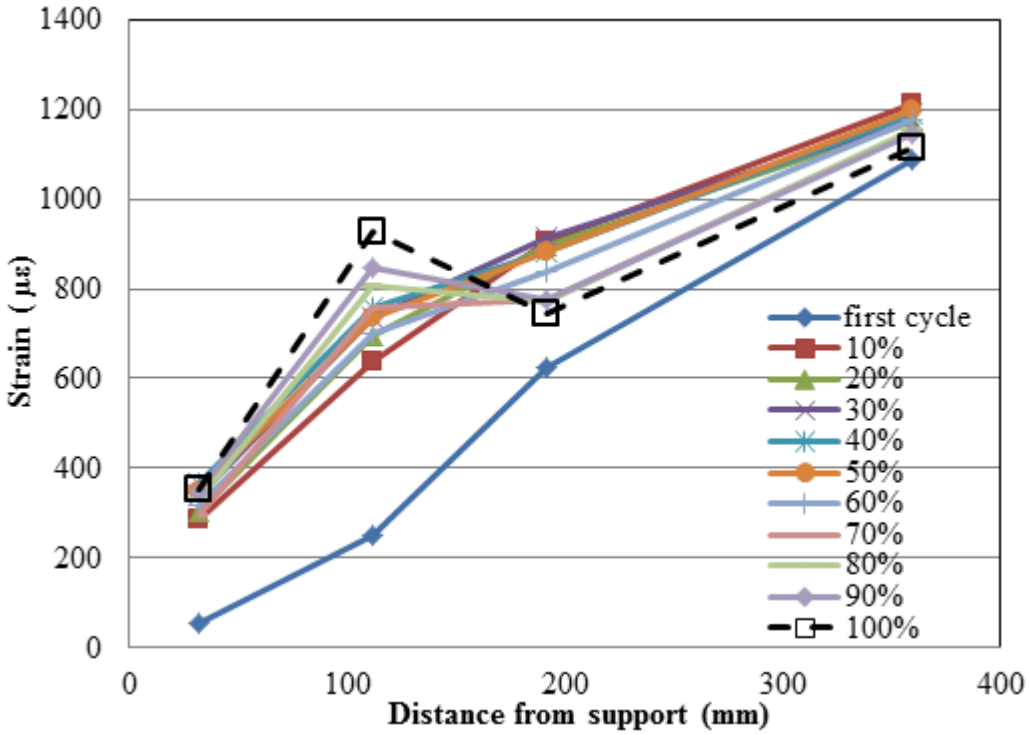


**Figure D. 6 Strain profile for bar in Beam F-350-U-m-82 with respect to % of fatigue life.**

# Appendix F

# Fatigue Slip Behaviour for Group 2 – Set 2 unrepaired beams that failed in bond

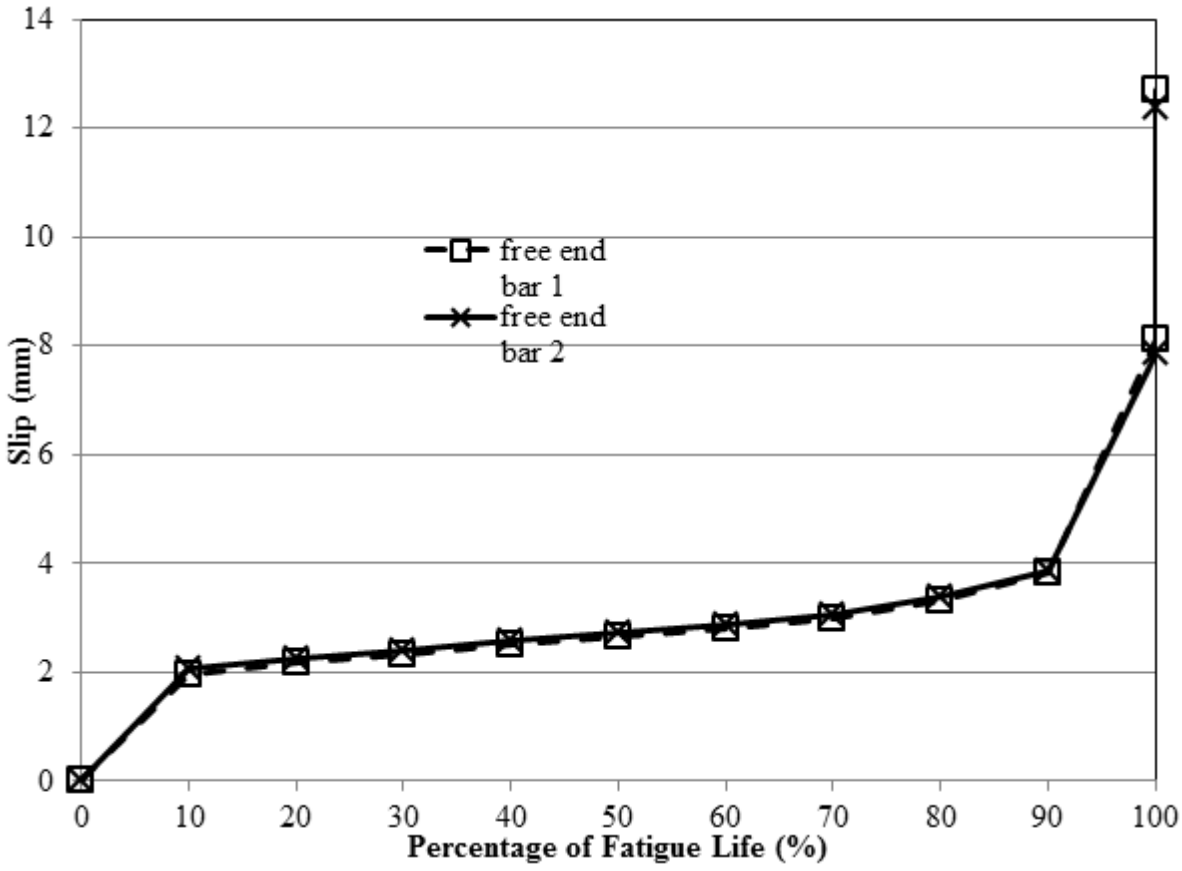


**Figure E. 1 Slip behaviour with respect to % of fatigue life for Beam F-350-U-n-74.**

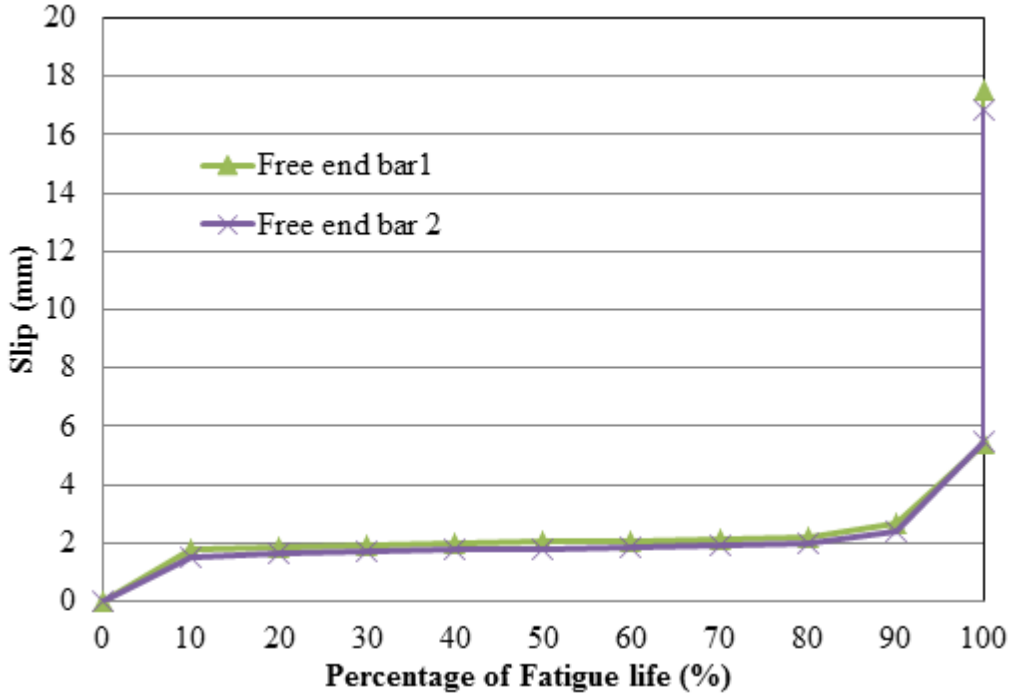


**Figure E. 2 Slip behaviour with respect to % of fatigue life for Beam F-350-U-n-80.**

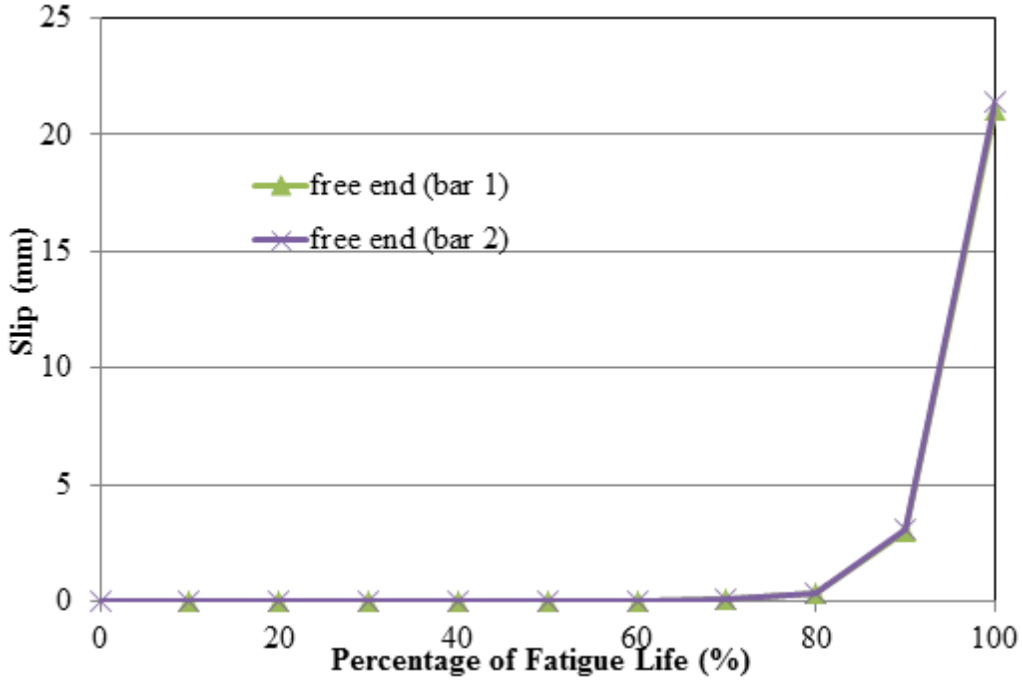


**Figure E. 3 Slip behaviour with respect to % of fatigue life for Beam F-350-U-n-90.**

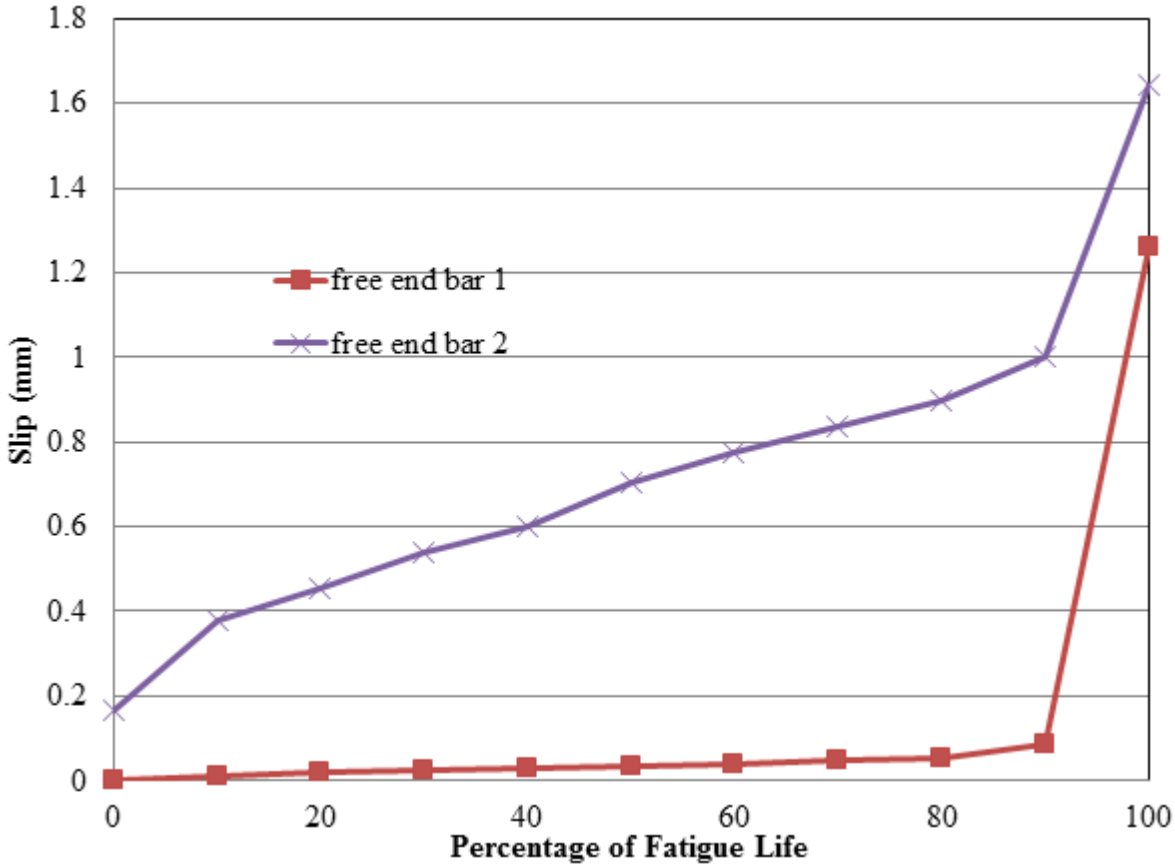


**Figure E. 4 Slip behaviour with respect to % of fatigue life for Beam F-350-U-m-82.**

# Bibliography


Absorra, L., Ashour, A., & Youseffi, M. (2011). Corrosion of Steel Reinforcement in Concrete of Different Compressive Strengths. *Construction and Building Materials, 25*, 3915 - 3925.

ACI Committee 215. (1974). *Considerations for Design of Concrete Structures Subjected to Fatigue Loading (ACI 215 R-74, revised 1992, reapproved 1997).* Farmington Hills: American Concrete Institute.

ACI Committee 222. (2001). *Protection of Metals in Concrete Against Corrosion (ACI 222-01).* Farmington Hills: American Concrete Institute.

ACI Committee 408. (1992). *State-of-the-Art Report on Bond Under Cyclic Loads (ACI 408.2 R-92, reapproved 2005).* Farmington Hills, MI: American Concrete Institute.

ACI Committee 408. (2003). *Bond and Development of Straight Reinforcing Bars in Tension (ACI 408R-03).* Farmington Hills, MI: American Concrete Institute.

ACI Committee 440. (2007). *Report on Fibre-Reinforced Polymer (FRP) Reinforcement fpr Concrete Structures (ACI 440R-07).* Farmington Hills, MI: American Concrete Institute.

ACI Committee 440.2. (2002). *Guide for the design and construction of externally bonded FRP systems for strengthening concrete structures (ACI 440.2 R - 08).* Farmington Hills, MI: American Concrete Institute.

Al-Hammoud, R., Soudki, K., & Topper, T. (2010, March). Bond Analysis of Corroded Reinforced Concrete Beams Under Monotonic and Fatigue Loads. *Cement and Concrete Composites, 32*(3), 194 - 203.

Al-Hammoud, R., Soudki, K., & Topper, T. (2011). Fatigue Flexural Behavior of Corroded Reinforced Concrete Beams Repaired with CFRP Sheets. *Journal of Composites for Construction, 15*(1), 42-51.

Al-Hammoud, R., Soudki, K., & Topper, T. (2011). Structural Health Monitoring of Corroded Steel Reinforcement in FRP Repaired Beams Using Multiplexed Fibre Bragg Grating Sensors. *The Fourth International Conference on Durability and Sustainability of Fiber Reinforced Polymer (FRP) Composites for Construction and Rehabilitation.* Sherbrook: University of Sherbrook.

Almusallam, A., Al-Gahtani, A., Aziz, A., & Rasheeduzzafar. (1996). Effect of reinforcement corrosion on bond strength. *Construction and Building Materials, 10*(2), 123 - 129.

Al-Sulaimani, G., Kaleemullah, M., & Basunbul, I. (1990, March - April). Influence of corrosion and cracking on bond behaviour and strength of reinforced concrete members. *ACI Structural Journal, 87*(2), 220 231.

ASTM Standard G1-03 (2011). (2011). Standard Practice for Preparing, Cleaning, and Evaluating Corrosion Test Specimens. West Conshohocken, PA, USA. Retrieved from www.astm.org: www.astm.org

Auyeung, Y., Chung, L., & Balaguru, P. (2000, March). Bond behaviour of corroded reinforced bars. *ACI Materials Journal, 97*(2), 214 - 220.

Ayyub, B., & McCuen, R. (2002). *Probability, Statistics, and Reliability for Engineers and Scientists.* Florida: Chapman & Hall/CRC Press LLC.

Badawi, M. (2003). *Flexural response of uniform and shear-span corroded RC beams repaired with CFRP laminates.* Waterloo: University of Waterloo.

Badawi, M., & Soudki, K. (2005). Control of Corrosion-Induced Damage in Reinforced Concrete Beams Using Carbon Fibre-Reinforced Polymer Laminates. *Journal of Composites for Construction, 9*(2), 195-201.

Balazs, G. (1991, Nov - Dec). Fatigue of bond. *ACI Materials Journal, 88*(6), 620 - 629.

Balazs, G. (1998). Bond under repeated loading. *Proceedings: Bond and Development of Reinforcement - A Tribute to Peter Gergely* (pp. 125 - 143). Leon, R. Ed.: ACI SP-180.

Balazs, G., & Koch, R. (1992, October). Influence of load history on bond behaviour. *Proceedings: Bond in concrete - from research to practice*, 7.1 - 7.10.

Bamonte, P., & Gambarova, P. (2007). High-Bond Nars in NSC and HPC: Study on Size Effect and on the Local Bond Stress-Slip Law. *Journal of Structural Engineering, 133*, 225 - 234.

Bentur, A., Diamond, S., & Berke, N. (1997). *Steel Corrosion in Concrete: Fundamentals and Civil Engineering Practice.* London: E & FN Spoon.

Bresler, B., & Bertero, V. (1968, June). Behaviour of reinforced concrete under repeated loading. *ASCE Journal of Structural Division, 94*(6), 1567 - 1589.

Brettmann, B., Darwin, D., & Donahey, R. (1986, Jan - Feb). Bond of reinforcement to superplasticized concrete. *ACI Journal, Proceedings, 83*(1), 98 - 107.

Broomfield, J. P. (1997). *Corrosion of Steel in Concrete: Understanding, Investigation and Repair.* London: E & FN Spon.

Cabrera, J., & Ghodoussi, P. (1992, October). The effect of reinforcement corrosion on the strength of the steel/concrete bond. *Proceedings: Bond in Concrete - From Research to Practice*, 10.11 - 10.24.

Castillo, E., Canteli, A., & Ripoll, M. (2008). A general model for fatigue damage due to any stress history. *International Journal of Fatigue, 30*, 150 - 164.

Clark, L., & Saifullah, M. (1993). Effect of corrosion on reinforcement bond strength. *Proceedings of the Fifth International Conference on Structural Faults and Repair* (pp. 113 - 119). UK: University of Edinburgh.

Craig, B., & Soudki, K. (2005). Post-repair performace of corroded bond critical RC beams repaired with CFRP. *Proceedings: FRP Reinforcement for Concrete Structures (FRPRCS-7), 7th International Symposium* (pp. 563 - 578). Shield, C. et al. Eds., ACI SP-230.

CSA-A23.2. (2009). *Methods of Test and Standard Practices for Concrete.* Rexdale: CSA-A23.2.

Debaiky, A., Green, M., & Hope, B. (2000). Efficiency of FRP wraps on corrosion damaged concrete cylinders. *Third International Conference on Advanced Composite Materials in Bridges and Structures* (pp. 679 - 686). Toronto, Canada: ACMBS.

El Maadawi, T., & Soudki, K. (2005, April). Carbon-fibre-reinforced polymer repair to extend service life of corroded reinforced concrete beams. *ASCE Journal of Composites for Construction, 9*(2), 187 - 194.

El Maadawy, T., & Soudki, K. (2003). Effectiveness of Impressed Current Technique to Simulate Corrosion of Steel Reinforcement in Concrete. *ASCE Journal of Materials in Civil Engineering*, 41-47.

Fang, C., Lundgren, K., Chen, L., & Zhu, C. (2004). Corrosion influence on bond in reinforced concrete. *Cement and Concrete Research, 34*, 2159 - 2167.

FIB. (2000). *Bond of Reinforcement in Concrete, State-of-Art Report.* Switzerland: International Federation for Structural Concrete.

Giuriani, E., Plizzari, G., & Schumm, C. (1991). Role of Stirrups and Residual Tensile Strength of Cracked Concrete on Bond. *Journal of Structural Engineering, 117*, 1 - 18.

Guizani, L., & Chaallal, O. (2011). An Experimental Study on Bond-Slip in Moderately Confined Concrete Subjected to Monotonic and Cyclic Loading Using an Experimental Plan. *Cnadian Journal in Civil Engineering, 38*, 272 - 282.

Hamad, B., & Rteil, A. (2006, August). Comparison of roles of FRP sheets, stirrups, and steel fibers in confining bond critical regions. *ASCE Journal of Composites for Construction, 10*(4), 330 - 336.

Hamad, B., Hage Ali, A., & Harajli, M. (2005, February). Effect of fiber-reinforced-polymer confinement on bond strength of reinforcement in beam anchorage specimens. *ASCE Journal of Composites for Construction, 9*(1), 44 - 51.

Hamad, B., Rteil, A., & Soudki, K. (2004, February). Bond strength of tension lap splices in high-strength concrete beams strengthened with GFRP wraps. *ASCE Journal of Composites for Construction, 8*(1), 14 - 21.

Hamad, B., Rteil, A., Selwan, B., & Soudki, K. (2004, May). Behavior of bond critical regions wrapped with FRP sheets in normal and high strength concrete. *ASCE Journal of Composites for Construction, 8*(3), 248 - 257.

Hamad, B., Rteil, A., Soudki, K., & Harajli, M. (2004, November). Experimental and analytical evaluation of the bond strength of reinforcement in FRP wrapped HSC beams. *ACI Structural Journal, 101*(6), 747 - 754.

Hanjari, K., Coronelli, D., & Lundgren, K. (2011, December). Bond capacity of severely corroded bars with corroded stirrups. *Magazine of Concrete Research, 63*(12), 953 - 968.

Harajli, M., Hamad, B., & Rteil, A. (2004, September). Effect of confinement on bond strength between steel bars and concrete. *ACI Structural Journal, 101*(5), 595 - 603.

Jeanty, P., Mitchell, D., & Mirza, M. (1988, May - June). Investigation of 'top bar' effects in beams. *ACI Structural Journal, 85*(3), 251 - 257.

Kawamura, A., Maruyama, K., Yoshida, S., & Masuda, T. (1995). Residual capacity of concrete beams damaged by salt attack. *Proceedings: Concrete Under Severe Conditions - Environment and Loading* (pp. 1448 - 1457). London, UK: Sakai, K. et al., Eds, E. Spon.

Khoe, C., Sen, R., & Bhethanabotla, V. (2012, June). Oxygen Permeability of FRP-Concrete Repair Systems. *Journal of Composites for Construction, 16*(3), 277-285.

Koch, R., & Balazs, G. (1992, October). Influence of preloading on bond strength and related slip. *Proceedings: bond in concrete - from research to practice*, 7.1 - 7.21.

Kono, S., Inazumi, M., & Kaku, T. (1998). Evaluation of confining effects of CFRP sheets on reinforced concrete members. *Proceedings: Second International Conference on Composites in Infrastructure. I*, pp. 343 - 355. Tucson, AZ, USA: Saadatmanesh, H. and Ehsani, M., Eds.

Lundgren, K., Kettil, P., Hanjari, K., Schlune, H., & San Roman, A. (2012, February). Analytical model for the bond-slip behaviour of corroded ribbed reinforcement. *Structure and Infrastructure Engineering, 8*(2), 157-169.

Mangant, P., & Elgarf, M. (1999). Bond characteristics of corroded reinforcement in concrete beams. *Materials and Structures, 32*, 89 - 97.

Masoud, S., Soudki, K., & Topper, T. (2005, Oct.). Postrepair fatigue performance of FRP-repaired corroded RC beams: experimental and analytical investigation. *ASCE Journal of Composites for Construction, 9*(5), 441 - 449.

Mor, A., Gerwick, B., & Hester, W. (1992, March - April). Fatigue of High Strength Reinforced Concrete. *ACI Materials Journal, 89*(2), 197 - 207.

Oh, B. (1986, February). Fatigue analysis of plain concrete in flexure. *ASCE Journal of Structural Engineering, 112*(2), 273 - 288.

Oh, B., & Kim, S. (2007, March). Advanced crack width analysis of reinforced concrete beams under repeated loads. *ASCE Journal of Structural Engineering, 133*(3), 411 - 420.

Okada, K., Kobayashi, K., & Miyagawa, T. (1988, March). Influence of longitudinal cracking due to reinforcement corrosion on characteristics of reinforced concrete members. *ACI Structural Journal, 85*(2), 411 - 420.

Ou, Y.-C., Tsai, L.-L., & Chen, H.-H. (2012, April). Cyclic Performance of large-scale corroded reinforced concrete beams. *Earthquake Engineering and Structural Dynamics, 41*(4), 593 - 604.

Papakonstantinou, C., Balaguru, P., & Auyeung, Y. (2011, May). Influence of FRP Confinement on Bond Behaviour of Corroded Steel Reinforcement. *Cement and Concrete Composites, 33*(5), 611 - 621.

Perry, E., & Jundi, N. (1969, May). Pullout bond stress distribution under static and dynamic repeated loadings. *ACI Journal, Proceedings, 66*(5), 377 - 380.

Plizzari, G., Lundgren, K., & Balazs, G. (2002). Bond and splitting in fibre reinforced concrete under repeated loading. *Proceedings: Bond in concrete - from research to standards*, (pp. 221 - 229). budapest, hungary.

Rehm, G., & Elingehausen, R. (1979, Feb). Bond of ribbed bars under high cycle repeated loads. *ACI Journal, Proceedings, 76*, 297 - 309.

Rodriguez, J., Ortega, L., & Casal, J. (1994). Corrosion of reinforcement bars and service life of reinforced concrete structures: corrosion and bond. *Proceedings: Concrete Across Borders, 2*, 315 - 326.

Rodriguez, J., Ortega, L., & Casal, J. (1997, June). Load carrying capacity of concrete structures with corroded reinforcement. *Construction and Building Materials, 11*(4), 239 - 248.

Rteil, A. (2007). *Fatigue Bond Behaviour of Corroded Reinforcement and CFRP Confined Concrete.* Waterloo, Ontario: University of Waterloo.

Rteil, A., Soudki, K., & Topper, T. (2007). Confinement effect of CFRP sheets on the bond between concrete and steel subjected to repeated loading. *8th Interantional Symposium on FRP Reinforcement for Concrete Structures* (p. on CD ROM). Patras, Greece: FRPRCS-8.

Rteil, A., Soudki, K., & Topper, T. (2007). Effect of CFRP sheets on the corroded steel-concrete bond subjected to repeated loading. *3rd Interantional Conference on Durability & Field Applications of FRP Composites for Construction* (pp. 287 - 294). Quebec, QC: CDCC 2007.

Rteil, A., Soudki, K., & Topper, T. (2007, April). Preliminary experimental investigation of the fatigue bond behaviour of CFRP confined RC beams. *Construction and Building Materials, 21*(4), 746 - 755.

Rteil, A., Soudki, K., & Topper, T. (2011). Mechanics of Bond Under Repeated Loading. *Construction and Building of Materials, 25*, 2822 - 2827.

Singh, S., & Ambedkar, B. (2008). Flexural fatigue strength prediction of steel fibre reinforced concrete beams. *Electronic Journal of Structural Engineering*, 46 - 54.

Singh, S., Mohammadi, Y., Goel, S., & Kaushik, S. (2007). Prediction of mean and design fatigue lives of steel fibrous concrete beams in flexure. *Advances in Structural Engineering, 10*(1), 25 36.

Singh, S., Singh, A., & Bajaj, V. (2012). Flexural fatigue strength of hybrid fibrous concrete beams. *Proceedings of the Institution of Civil Engineers. 165*, pp. 99 - 110. ICE Construction Materials.

Singh, S., Singh, B., & Kaushik, S. (2005, March). Probability of fatigue failure of steel fibrous concrete. *Magazine of Concrete Research, 57*(2), 65 - 72.

Soudki, K., & Sherwood, T. (2000). Behaviour of reinforced concrete beams strengthened with carbonf fibre reinforced polymer laminates subjected to corrosion damage. *Canadian Journal of Civil Engineering, 27*(5), 1005 - 1010.

Soudki, K., & Sherwood, T. (2003, August). Bond behaviour of corroded steel reinforcement in concrete wrapped with carbon fibre reinforced polymer sheets. *ASCE Journal of Materials in Civil Engineering, 15*(4), 358 - 370.

Soudki, K., Rteil, A., Al-Hammoud, R., & Topper, T. (2007, March). Fatigue strength of fibre-reinforced-polymer-repaired beams subjected to mild corrosion. *Canadian Journal of Civil Engineering, 34*(3), 414 - 421.

Tachibana, Y., Maeda, K., & Kajikawa, M. (1990). Mechanical behaviour of RC beams damaged by corrosion of reinforcement. *Proceedings: Corrosion of Reinforcement in Concrete Construction, 3rd International Symposium*, (pp. 178 - 187). UK.

Tennyson, R. C., Mufti, A. A., Rizkalla, S., Tadros, G., & Benmokrane, B. (2001). Structural Health Monitoring of innovative Bridges in Canada with Fier Optic Sensors. *Smart Materials and Structures*, 560 - 573.

Uomoto, T., Tsuji, K., & Kakizawa, T. (1984). Deterioration mechanism of concrete structures caused by corrosion of reinforcing bars. *Transactions of japan Concrete Institute, 6*, 163 - 170.

Verna, J., & Stelson, T. (1962, Oct). Failure of small reinforced concrete beams under repeated loads. *ACI Journal, Proceedings, 59*(10), 1489 - 1503.

Wirsching, P., & Yao, J. (1970, June). Statistical methods in structural fatigue. *Journal of the Structural Division: Proceedings of the American Society of Civil Engineers, 96*(ST6), 1201 - 1219.

Yang, Q. (1996). Fatigue test and reliability design of gears. *International Journal of Fatigue, 18*(3), 171 - 177.

Zhang, J., & Mailvaganam, N. (2006). Corrosion Characteristics and key electrochemical factors in patch repair. *Canadian Journal of Civil Engineering, 33*(6), 785 - 793.

Zhou, Z., & Ou, J. (2004). Proceeding of North America Euro-Pacific Workshop "Sensing Issues in Civil Structural Health Monitoring. *Development of FBG Sensors for Structural Health Monitoring in Civil Infrastructures.* Waikiki Beach, Oahu, Hawaii.

Zuo, J., & Darwin, D. (2000). Splice Strength of Conventional and High Relative Rib Area Bars in Nominal and High Strength Concrete. *ACI Structural Journal, 97*, 630 - 641.